



Western Michigan University
ScholarWorks at WMU

Masters Theses

Graduate College

4-2024

Design and Simulation of Flow Channel of Polymer Electrolyte Membrane Fuel Cell (PEMFC)

Rishya Shringhan Ravichandran
Western Michigan University

Follow this and additional works at: https://scholarworks.wmich.edu/masters_theses



Part of the Energy Systems Commons

Recommended Citation

Ravichandran, Rishya Shringhan, "Design and Simulation of Flow Channel of Polymer Electrolyte Membrane Fuel Cell (PEMFC)" (2024). *Masters Theses*. 5410.
https://scholarworks.wmich.edu/masters_theses/5410

This Masters Thesis-Open Access is brought to you for free and open access by the Graduate College at ScholarWorks at WMU. It has been accepted for inclusion in Masters Theses by an authorized administrator of ScholarWorks at WMU. For more information, please contact wmu-scholarworks@wmich.edu.



DESIGN AND SIMULATION OF FLOW CHANNEL OF POLYMER ELECTROLYTE MEMBRANE FUEL CELLS (PEMFC)

Rishya Shringeran Ravichandran, M.S.E

Western Michigan University, 2024

In Polymer Electrolyte Membrane Fuel Cell (PEMFC), flow channel plays an important role on the performance of the cell. This study mainly focuses on the simulation of flow channel under various conditions. A three-dimensional model of PEMFC with 25cm² of active area was employed to simulate the flow channel of PEMFC which has various designs. The flow channel designs such as single serpentine, bi-serpentine and tri-serpentine channels were investigated using ANSYS FLUENT software. Initially, the flow channel width of 2mm was examined. The obtained results were compared to the experimental data to validate the model. Then, the dimension of the flow channel width has been altered to 1mm and 3mm, simulated, and compared with 2mm flow channel width to determine which has the better performance. The pressure distribution, mass fraction of H₂, velocity magnitude and cell Reynolds number were investigated along with the performances of fuel cells. The findings indicated that the tri serpentine flow channel design offers superior performance with power density of 0.6655 W/cm² at 373K while the bi serpentine produced 0.604 W/cm² and single serpentine flow channel yielded 0.5765 W/cm² of power density. Additionally, the findings suggested that increasing the width of the flow channel in PEMFCs enhance the performance due to improved diffusion of reactant gases.

DESIGN AND SIMULATION OF FLOW CHANNEL OF POLYMER ELECTROLYTE MEMBRANE FUEL CELL (PEMFC)

by

Rishya Shringhan Ravichandran

A dissertation submitted to the Graduate College
in partial fulfillment of the requirements
for the degree of Master of Science
Mechanical Engineering
Western Michigan University
April 2024

Thesis Committee:

Dr. Bade Shrestha

Dr. Muralidhar Ghantasala

Dr. Christopher Cho

Copyright by
Rishya Shringhan Ravichandran
2024

ACKNOWLEDGEMENTS

I would like to express my heartfelt gratitude to Dr. Bade Shrestha, Committee Chair, for his immense support and direction throughout the thesis. It would have been an impossible task to finish this thesis without his guidance and constant support. This has helped me to grow as an engineer and widen my portfolio of work. I would also like to thank him for his understanding and patience through the course of this thesis.

I am thankful to Dr. Muralidhar Ghantasala, for his tireless efforts in teaching me various key concepts at the research phase to conduct this research successfully. You went above and beyond your duty to help me with my thesis.

Thirdly, I thank Dr. Christopher Cho for being a part of my thesis committee.

I would like to acknowledge my friends for extending their support in this thesis.

Last, but, not least, I graciously thank my parents, Ravichandran and Chandra Prabha for their continuous support and their confidence in me has been a huge motivation throughout this thesis.

Rishya Shringhan Ravichandran

TABLE OF CONTENTS

ACKNOWLEDGEMENTS.....	ii
LIST OF TABLES.....	vi
LIST OF FIGURES.....	xii
NOMENCLATURE.....	xx
CHAPTER	
1 INTRODUCTION.....	1
1.1 Sustainable Energy.....	1
1.2 Fuel Cells.....	2
1.3 Operating Principle of Fuel Cell.....	2
1.4 Functions of Different Fuel Cell Components.....	4
1.5 Fuel Cell Efficiency.....	5
1.6 Fuel Cell Efficiency Losses.....	6
1.7 Polarization Curve.....	7
1.8 Fuel Cell Classification.....	8
1.9 Thesis Objectives.....	10
1.10 Outline of the Thesis.....	10
2 PROTON EXCHANGE MEMBRANE FUEL CELL (PEMFC).....	12
2.1 Introduction of Proton Exchange Membrane Fuel Cell.....	12
2.2 Components of Proton Exchange Membrane Fuel Cell.....	12
2.3 Automotive Applications of PEM Fuel Cell.....	18
3 LITERATURE SURVEY.....	19
3.1 Literature Survey on Simulation of PEMFC.....	19
3.2 Literature Survey on Flow Channel Design.....	20
3.3 Literature Survey on Operating Conditions.....	37
4 METHODOLOGY.....	39
4.1 Overview.....	39

CHAPTER

Table of Contents - continued

	4.2 Geometry Design.....	39
	4.3 Modeling Assumptions.....	43
	4.4 Governing Equations.....	44
5	COMPARISON WITH EXPERIMENTAL DATA.....	47
	5.1 Model Validation.....	47
	5.2 Description of Experimental Design.....	47
	5.3 Comparison of 0.5V with Simulation Analysis.....	50
	5.4 Comparison of 0.7V with Simulation Analysis.....	53
6	PEMFC SERPENTINE CONFIGURATION RESULTS.....	59
	6.1 Design and Simulation of Flow Channel of Proton Exchange Membrane Fuel Cell (PEMFC).....	59
7	ANALYSIS OF PEMFC.....	75
	7.1 Pressure Distribution of the PEMFC.....	75
	7.2 Velocity Magnitude of the PEMFC.....	88
	7.3 Mass Fraction of the Hydrogen(H ₂).....	100
	7.4 Cell Reynolds Number.....	110
8	COMPARISON AND ANALYSIS OF PEMFC WITH VARYING FLOW CHANNEL WIDTH.....	121
	8.1 1mm and 3mm Flow Channel Width of Single Serpentine Polymer Electrolyte Membrane Fuel Cell (PEMFC).....	123
	8.2 1mm and 3mm Flow Channel Width of Bi Serpentine Polymer Electrolyte Membrane Fuel Cell (PEMFC).....	125
	8.3 1mm and 3mm Flow Channel Width of Tri Serpentine Polymer Electrolyte Membrane Fuel Cell (PEMFC).....	128
	8.4 Pressure Distribution Analysis of 1mm and 3mm Flow Channel Width PEMFC.....	130

CHAPTER

Table of Contents - continued

8.5 Velocity Magnitude Analysis of 1mm and 3mm Flow Channel Width PEMFC.....	140
8.6 Mass Fraction of Hydrogen (H ₂) Analysis of 1mm and 3mm Flow Channel Width PEMFC.....	151
8.7 Cell Reynolds Number Analysis of 1mm and 3mm Flow Channel Width PEMFC.....	160
9 RESULTS AND DISCUSSION.....	172
10 CONCLUSION.....	197
11 FUTURE RESEARCH SCOPE.....	227
BIBLIOGRAPHY.....	230

LIST OF TABLES

4.1 The Characteristic of the Mesh.....	40
4.2 The Geometric Parameters of PEMFC.....	41
4.3 Operating Conditions and Relevant Parameters of the Study.....	41
4.4 The Solving Zones of the Governing Equations.....	44
5.1 Details of the Experimental PEMFC.....	48
5.2 Details of the Various Configuration of Experimental PEMFC.....	49
5.3 Details of the Various Parameters of Experimental Validation Design Simulation of PEMFC.....	57
6.1 Results of PEMFC at 313K and 2 Bar Pressure.....	62
6.2 Results of PEMFC at 323K and 2 Bar Pressure.....	63
6.3 Results of PEMFC at 333K and 2 Bar Pressure.....	65
6.4 Results of PEMFC at 343K and 2 Bar Pressure.....	66
6.5 Results of PEMFC at 353K and 2 Bar Pressure.....	68
6.6 Results of PEMFC at 363K and 2 Bar Pressure.....	69
6.7 Results of PEMFC at 373K and 2 Bar Pressure.....	71
6.8 Experimental Validation Design Simulation and Author's Design Simulation.....	72
8.1 Operating Conditions of the PEM Fuel Cell for Various Flow Channel Ribs.....	121
8.2 Results of Single Serpentine PEMFC at 373K and 2 Bar Pressure.....	125
8.3 Results of Bi Serpentine PEMFC at 373K and 2 Bar Pressure.....	127
8.4 Results of Tri Serpentine PEMFC at 373K and 2 Bar Pressure.....	130
8.5 Results of Pressure Distribution of Single Serpentine PEMFCs at 0.25V(low).....	131
8.6 Results of Pressure Distribution of Single Serpentine PEMFCs at 0.35V (medium).....	131

List of Tables - continued

8.7 Results of Pressure Distribution of Single Serpentine PEMFCs at 0.5V (high).....	132
8.8 Results of Pressure Distribution of Single Serpentine PEMFCs at 0.65V (very high)	132
8.9 Results of Pressure Distribution of Single Serpentine PEMFCs at 0.8V (extreme)	133
8.10 Results of Pressure Distribution of Bi Serpentine PEMFCs at 0.25V(low).	134
8.11 Results of Pressure Distribution of Bi Serpentine PEMFCs at 0.35V (medium)	134
8.12 Results of Pressure Distribution of Bi Serpentine PEMFCs at 0.5V (high)	135
8.13 Results of Pressure Distribution of Bi Serpentine PEMFCs at 0.65V (very high)	136
8.14 Results of Pressure Distribution of Bi Serpentine PEMFCs at 0.8V (extreme)	136
8.15 Results of Pressure Distribution of Tri Serpentine PEMFCs at 0.25V(low).	137
8.16 Results of Pressure Distribution of Tri Serpentine PEMFCs at 0.35V (medium)	138
8.17 Results of Pressure Distribution of Tri Serpentine PEMFCs at 0.5V (high)	138
8.18 Results of Pressure Distribution of Tri Serpentine PEMFCs at 0.65V (very high)	139

List of Tables - continued

8.19 Results of Pressure Distribution of Tri Serpentine PEMFCs at 0.8V (extreme)	140
8.20 Results of Velocity Magnitude of Single Serpentine PEMFCs at 0.25V (low).....	141
8.21 Results of Velocity Magnitude of Single Serpentine PEMFCs at 0.35V (medium)	141
8.22 Results of Velocity Magnitude of Single Serpentine PEMFCs at 0.5V (high)	142
8.23 Results of Velocity Magnitude of Single Serpentine PEMFCs at 0.65V (very high)	143
8.24 Results of Velocity Magnitude of Single Serpentine PEMFCs at 0.8V (extreme)	143
8.25 Results of Velocity Magnitude of Bi Serpentine PEMFCs at 0.25V (low).....	144
8.26 Results of Velocity Magnitude of Bi Serpentine PEMFCs at 0.35V (medium)	144
8.27 Results of Velocity Magnitude of Bi Serpentine PEMFCs at 0.5V (high)	145
8.28 Results of Velocity Magnitude of Bi Serpentine PEMFCs at 0.65V (very high)	146
8.29 Results of Velocity Magnitude of Bi Serpentine PEMFCs at 0.8V (extreme)	146
8.30 Results of Velocity Magnitude of Tri Serpentine PEMFCs at 0.25V (low)	147
8.31 Results of Velocity Magnitude of Tri Serpentine PEMFCs at 0.35V (medium)	148

List of Tables - continued

8.32 Results of Velocity Magnitude of Tri Serpentine PEMFCs at 0.5V (high)	148
8.33 Results of Velocity Magnitude of Tri Serpentine PEMFCs at 0.65V (very high)	149
8.34 Results of Velocity Magnitude of Tri Serpentine PEMFCs at 0.8V (extreme)	150
8.35 Results of Mass Fraction of Hydrogen (H ₂) of Single Serpentine PEMFCs at 0.25V (low)	151
8.36 Results of Mass Fraction of Hydrogen (H ₂) of Single Serpentine PEMFCs at 0.35V (medium)	152
8.37 Results of Mass Fraction of Hydrogen (H ₂) of Single Serpentine PEMFCs at 0.5V (high)	152
8.38 Results of Mass Fraction of Hydrogen (H ₂) of Single Serpentine PEMFCs at 0.65V (very high)	153
8.39 Results of Mass Fraction of Hydrogen (H ₂) of Single Serpentine PEMFCs at 0.8V (extreme)	153
8.40 Results of Mass Fraction of Hydrogen (H ₂) of Bi Serpentine PEMFCs at 0.25V (low)	154
8.41 Results of Mass Fraction of Hydrogen (H ₂) of Bi Serpentine PEMFCs at 0.35V (medium)	155
8.42 Results of Mass Fraction of Hydrogen (H ₂) of Bi Serpentine PEMFCs at 0.5V (high)	155
8.43 Results of Mass Fraction of Hydrogen (H ₂) of Bi Serpentine PEMFCs at 0.65V (very high)	156

List of Tables - continued

8.44 Results of Mass Fraction of Hydrogen (H ₂) of Bi Serpentine PEMFCs at 0.8V (extreme)	156
8.45 Results of Mass Fraction of Hydrogen (H ₂) of Tri Serpentine PEMFCs at 0.25V (low)	157
8.46 Results of Mass Fraction of Hydrogen (H ₂) of Tri Serpentine PEMFCs at 0.35V (medium)	158
8.47 Results of Mass Fraction of Hydrogen (H ₂) of Tri Serpentine PEMFCs at 0.5V (high)	158
8.48 Results of Mass Fraction of Hydrogen (H ₂) of Tri Serpentine PEMFCs at 0.65V (very high)	159
8.49 Results of Mass Fraction of Hydrogen (H ₂) of Tri Serpentine PEMFCs at 0.8V (extreme)	159
8.50 Results of Cell Reynolds Number of Single Serpentine PEMFCs at 0.25V (low)	160
8.51 Results of Cell Reynolds Number of Single Serpentine PEMFCs at 0.35V (medium)	161
8.52 Results of Cell Reynolds Number of Single Serpentine PEMFCs at 0.5V (high)	162
8.53 Results of Cell Reynolds Number of Single Serpentine PEMFCs at 0.65V (very high)	163
8.54 Results of Cell Reynolds Number of Single Serpentine PEMFCs at 0.8V (extreme)	163
8.55 Results of Cell Reynolds Number of Bi Serpentine PEMFCs at 0.25V (low)	164

List of Tables - continued

8.56 Results of Cell Reynolds Number of Bi Serpentine PEMFCs	
at 0.35V (medium)	165
8.57 Results of Cell Reynolds Number of Bi Serpentine PEMFCs	
at 0.5V (high)	166
8.58 Results of Cell Reynolds Number of Bi Serpentine PEMFCs	
at 0.65V (very high)	166
8.59 Results of Cell Reynolds Number of Bi Serpentine PEMFCs	
at 0.8V (extreme)	167
8.60 Results of Cell Reynolds Number of Tri Serpentine PEMFCs	
at 0.25V (low)	168
8.61 Results of Cell Reynolds Number of Tri Serpentine PEMFCs	
at 0.35V (medium)	169
8.62 Results of Cell Reynolds Number of Tri Serpentine PEMFCs	
at 0.5V (high)	169
8.63 Results of Cell Reynolds Number of Tri Serpentine PEMFCs	
at 0.65V (very high)	170
8.64 Results of Cell Reynolds Number of Tri Serpentine PEMFCs	
at 0.8V (extreme)	171

LIST OF FIGURES

1.1 Construction of a fuel cell.....	3
1.2 Polarization curve for PEMFC with activation, ohmic and mass transport polarization region.....	7
2.1 Cross-sectional view of a PEMFC with its components.....	13
3.1 Serpentine flow channel designs of PEMFC.....	20
3.2 Computational mesh of a 14-channel serpentine configuration in a PEMFC.....	21
3.3 Cross sectional view of optimal design.....	22
3.4 Schematic diagram of rib and channel configuration.....	23
3.5 Schematic diagram of the test models of flow fields.....	24
3.6 Serpentine flow channel design in bipolar plates.....	25
3.7 Different channel curvatures.....	25
3.8 Schematic of three dimensional serpentine PEM fuel cell with varying channel heights.....	26
3.9 Schematic illustration of the M-like channel.....	27
3.10 Fractal design of flow field.....	27
3.11 Sinusoidal wavy design of serpentine flow channel.....	28
3.12 Novel leaf shape flow field.....	29
3.13 Schematic representation of the flow field configuration integrated into the bipolar plates.....	30
3.14 Schematic representation of two different bionic flow field (a).symmetric bionic flow channel and (b).asymmetric bionic flow channel.....	31
3.15 Serpentine flow channels featuring different cross-sectional area and slope turns.....	32
3.16 Solitary tapered conduits for fluid flow.....	33

List of Figures - continued

3.17 Wave like PEMFC inspired from cuttle fish fin.....	33
3.18 (a). Parallel design (b). serpentine design (c). compound design.....	34
3.19 Parallel bipolar plate with 25 channels and 24 ribs in land area.....	35
3.20 (a).3-channel serpentine flow field (b). 6-channel flow field (c).13-channel flow field (d). 26-channel flow field (e).26-channel complex flow field.....	36
3.21 All bipolar plate geometries created for the experiment.....	37
5.1 Design of experimental PEMFC.....	49
5.2 Comparison of simulated and experimental data of PEMFC in 368K 0.5V voltage.....	50
5.3 Comparison of simulated and experimental data of PEMFC in 353K 0.5V voltage.....	51
5.4 Comparison of simulated and experimental data of PEMFC in 368K 0.7V voltage.....	53
5.5 Comparison of simulated and experimental data of PEMFC in 353K 0.5V voltage.....	54
6.1 Single serpentine flow channel PEMFC.....	59
6.2 Bi serpentine flow channel PEMFC.....	60
6.3 Tri serpentine flow channel PEMFC.....	60
6.4 Polarization curve of PEMFC at 313K.....	61
6.5 Polarization curve of PEMFC at 323K.....	63
6.6 Polarization curve of PEMFC at 333K.....	64
6.7 Polarization curve of PEMFC at 343K.....	66
6.8 Polarization curve of PEMFC at 353K.....	67
6.9 Polarization curve of PEMFC at 363K.....	69
6.10 Polarization curve of PEMFC at 373K.....	70

List of Figures - continued

7.1 Pressure distribution of 2mm flow channel width of single serpentine PEMFC at 0.25V (low).....	76
7.2 Pressure distribution of 2mm flow channel width of single serpentine PEMFC at 0.35V (medium).....	77
7.3 Pressure distribution of 2mm flow channel width of single serpentine PEMFC at 0.5V (high).....	78
7.4 Pressure distribution of 2mm flow channel width of single serpentine PEMFC at 0.65V (very high).....	79
7.5 Pressure distribution of 2mm flow channel width of single serpentine PEMFC at 0.8V (extreme).....	80
7.6 Pressure distribution of 2mm flow channel width of bi serpentine PEMFC at 0.25V (low).....	81
7.7 Pressure distribution of 2mm flow channel width of bi serpentine PEMFC at 0.35V (medium).....	81
7.8 Pressure distribution of 2mm flow channel width of bi serpentine PEMFC at 0.5V (high).....	82
7.9 Pressure distribution of 2mm flow channel width of bi serpentine PEMFC at 0.65V (very high).....	83
7.10 Pressure distribution of 2mm flow channel width of bi serpentine PEMFC at 0.8V (extreme).....	83
7.11 Pressure distribution of 2mm flow channel width of tri serpentine PEMFC at 0.25V (low).....	84
7.12 Pressure distribution of 2mm flow channel width of tri serpentine PEMFC at 0.35V (medium).....	85
7.13 Pressure distribution of 2mm flow channel width of tri serpentine PEMFC at 0.5V (high).....	85

List of Figures - continued

7.14 Pressure distribution of 2mm flow channel width of tri serpentine PEMFC at 0.65V (very high).....	86
7.15 Pressure distribution of 2mm flow channel width of tri serpentine PEMFC at 0.8V (extreme).....	87
7.16 Velocity magnitude of 2mm flow channel width of single serpentine PEMFC at 0.25V (low).....	89
7.17 Velocity magnitude of 2mm flow channel width of single serpentine PEMFC at 0.35V (medium).....	90
7.18 Velocity magnitude of 2mm flow channel width of single serpentine PEMFC at 0.5V (high).....	90
7.19 Velocity magnitude of 2mm flow channel width of single serpentine PEMFC at 0.65V (very high).....	91
7.20 Velocity magnitude of 2mm flow channel width of single serpentine PEMFC at 0.8V (extreme).....	92
7.21 Velocity magnitude of 2mm flow channel width of bi serpentine PEMFC at 0.25V (low).....	92
7.22 Velocity magnitude of 2mm flow channel width of bi serpentine PEMFC at 0.35V (medium).....	93
7.23 Velocity magnitude of 2mm flow channel width of bi serpentine PEMFC at 0.5V (high).....	94
7.24 Velocity magnitude of 2mm flow channel width of bi serpentine PEMFC at 0.65V (very high).....	94
7.25 Velocity magnitude of 2mm flow channel width of bi serpentine PEMFC at 0.8V (extreme).....	95
7.26 Velocity magnitude of 2mm flow channel width of tri serpentine PEMFC at 0.25V (low).....	96

List of Figures - continued

7.27 Velocity magnitude of 2mm flow channel width of tri serpentine PEMFC at 0.35V (medium).....	96
7.28 Velocity magnitude of 2mm flow channel width of tri serpentine PEMFC at 0.5V (high).....	97
7.29 Velocity magnitude of 2mm flow channel width of tri serpentine PEMFC at 0.65V (very high).....	98
7.30 Velocity magnitude of 2mm flow channel width of tri serpentine PEMFC at 0.8V (extreme).....	98
7.31 Mass fraction of hydrogen in 2mm flow channel width of single serpentine PEMFC at 0.25V (low).....	101
7.32 Mass fraction of hydrogen in 2mm flow channel width of single serpentine PEMFC at 0.35V (medium).....	101
7.33 Mass fraction of hydrogen in 2mm flow channel width of single serpentine PEMFC at 0.5V (high).....	102
7.34 Mass fraction of hydrogen in 2mm flow channel width of single serpentine PEMFC at 0.65V (very high).....	103
7.35 Mass fraction of hydrogen in 2mm flow channel width of single serpentine PEMFC at 0.8V (extreme).....	103
7.36 Mass fraction of hydrogen in 2mm flow channel width of bi serpentine PEMFC at 0.25V (low).....	104
7.37 Mass fraction of hydrogen in 2mm flow channel width of bi serpentine PEMFC at 0.35V (medium).....	104
7.38 Mass fraction of hydrogen in 2mm flow channel width of bi serpentine PEMFC at 0.5V (high).....	105
7.39 Mass fraction of hydrogen in 2mm flow channel width of bi serpentine PEMFC at 0.65V (very high).....	105

List of Figures - continued

7.40 Mass fraction of hydrogen in 2mm flow channel width of bi serpentine PEMFC at 0.8V (extreme).....	106
7.41 Mass fraction of hydrogen in 2mm flow channel width of tri serpentine PEMFC at 0.25V (low).....	106
7.42 Mass fraction of hydrogen in 2mm flow channel width of tri serpentine PEMFC at 0.35V (medium).....	107
7.43 Mass fraction of hydrogen in 2mm flow channel width of tri serpentine PEMFC at 0.55V (high).....	107
7.44 Mass fraction of hydrogen in 2mm flow channel width of tri serpentine PEMFC at 0.65V (very high).....	108
7.45 Mass fraction of hydrogen in 2mm flow channel width of tri serpentine PEMFC at 0.8V (extreme).....	108
7.46 Cell Reynolds number of 2mm flow channel width of single serpentine PEMFC at 0.25V (low).....	111
7.47 Cell Reynolds number of 2mm flow channel width of single serpentine PEMFC at 0.35V (medium).....	111
7.48 Cell Reynolds number of 2mm flow channel width of single serpentine PEMFC at 0.5V (high).....	112
7.49 Cell Reynolds number of 2mm flow channel width of single serpentine PEMFC at 0.65V (very high).....	113
7.50 Cell Reynolds number of 2mm flow channel width of single serpentine PEMFC at 0.8V (extreme).....	113
7.51 Cell Reynolds number of 2mm flow channel width of bi serpentine PEMFC at 0.25V (low).....	114
7.52 Cell Reynolds number of 2mm flow channel width of bi serpentine PEMFC at 0.35V (medium).....	115

List of Figures - continued

7.53 Cell Reynolds number of 2mm flow channel width of bi serpentine PEMFC at 0.5V (high).....	115
7.54 Cell Reynolds number of 2mm flow channel width of bi serpentine PEMFC at 0.65V (very high).....	116
7.55 Cell Reynolds number of 2mm flow channel width of bi serpentine PEMFC at 0.8V (extreme).....	117
7.56 Cell Reynolds number of 2mm flow channel width of tri serpentine PEMFC at 0.25V (low).....	117
7.57 Cell Reynolds number of 2mm flow channel width of tri serpentine PEMFC at 0.35V (medium).....	118
7.58 Cell Reynolds number of 2mm flow channel width of tri serpentine PEMFC at 0.5V (high).....	119
7.59 Cell Reynolds number of 2mm flow channel width of tri serpentine PEMFC at 0.65V (very high).....	119
7.60 Cell Reynolds number of 2mm flow channel width of tri serpentine PEMFC at 0.8V (extreme).....	120
8.1 Single serpentine flow channel PEMFC with 1mm width of flow channel.....	123
8.2 Single serpentine flow channel PEMFC with 3mm width of flow channel.....	124
8.3 Polarization curve of single serpentine PEMFC at 373K and 2 bar pressure.....	124
8.4 Bi serpentine flow channel PEMFC with 1mm width of flow channel.....	126
8.5 Bi serpentine flow channel PEMFC with 3mm width of flow channel.....	126

List of Figures - continued

8.6 Polarization curve of bi serpentine PEMFC at 373K and 2 bar pressure.....	127
8.7 Tri serpentine flow channel PEMFC with 1mm width of flow channel.....	128
8.8 Tri serpentine flow channel PEMFC with 3mm width of flow channel.....	129
8.9 Polarization curve of tri serpentine PEMFC at 373K and 2 bar pressure.....	129
11.1 Naturally inspired design.....	228
11.2 Different fuel cell's flow channel angles.....	228
11.3 Pinned configuration of single serpentine flow channel.....	229

NOMENCLATURE

OCV – Open Circuit Voltage

ΔH_f – Enthalpy of formation of the system

η_{\max} – Maximum efficiency of a fuel cell

ΔG_f – Gibbs free energy

F - Faraday Constant

V – Voltage

K – Kelvin

N_A – Avogadro's Number

E^0 – Ideal equilibrium potential

η_{ohm} – Ohmic losses

η_{act} – activation / charge transfer losses

η_{conc} – concentration/mass transfer losses

ICE – Internal Combustion Engine

FCEV – Fuel Cell Electric Vehicle

BP – Bipolar Plate

GDL - Gas Diffusion Layer

CL – Catalyst Layer

EPA – Environmental Protection Agency

PEMFC – Polymer Electrolyte Membrane Fuel Cell DMFC – Direct Methanol Fuel Cell

SOFC – Solid Oxide Fuel Cell

AFC – Alkaline Fuel Cell

MFC – Molten Carbonate Fuel Cell

PAFC – Phosphoric Acid Fuel Cell

CFD – Computational Fluid Dynamics

RP – Rectangular-channeled Plate

ADS – Anode Down Slanted

CDS – Cathode Down Slanted

AUS – Anode Up Slanted

CUS – Cathode Up Slanted

CHAPTER 1

INTRODUCTION

1.1 Sustainable Energy

According to United Nation Brundtland Commission, sustainability is defined as the “satisfying the requirements of the present without impeding the capacity of future generations to fulfill their own necessities” [1]. Due to the developments that demand for energy, U.S. Energy Information Administration anticipates that the energy usage will raise globally by 50% by 2050 [2]. One of the main reasons for the energy demand is the growth in the world population (currently 7.7 + billion).

Present transportation technologies are harmful as they're environmentally polluting which affects the quality of life. Environmentally friendly, and sustainable technology for transportation requires an alternative change from the Internal Combustion Engine (ICE) powered vehicles. This is a very popular transportation technology that demands around 1.47 billion vehicles worldwide [3]. By being a major contributor to pollution, Internal Combustion Engine emits harmful gases such as carbon monoxide (CO) and nitrogen oxides in the atmosphere with more than 31 billion tons of carbon-di-oxide (CO₂) emissions [2].

To make a better world, sustainable technologies such as solar-powered vehicles, Fuel Cell Electric Vehicles (FCEVs) are developed in order to reduce pollution levels. When compared to other fuel cells, PEMFC's is significantly used in automotive industry. Vehicles like Toyota Mirai, Honda Clarity, Hyundai Nexo, GM Opel rare such good examples that powered by fuel cell systems [4].

In the following section, the technologies related to Fuel Cells along with its working, types and their advantages and disadvantages will be further discussed.

1.2 Fuel Cells

Fuel cells are galvanic device used to generate electricity from chemical energy [5]. It is an important technology for the generation of renewable energy. Fuel Cells use oxidation and reduction (redox) reaction usually occur at anode and cathode respectively. Conventional heat engines generate power by burning fossil fuels resulting in the emission of pollutants in the atmosphere such as oxides of sulphur (S), carbon monoxide (CO), particulates and oxides of nitrogen (NO_x). The Environmental Protection Agency (EPA) declared carbon dioxide (CO₂) as the harmful gas to the atmosphere. Also, there is a rapid decline in the fossil fuel reserves globally. All these factors result in the immediate need to develop energy efficient and environmental friendly power producing devices [6].

In 1839, William Grove demonstrated the very first fuel cell. The practical applications of the fuel cell were demonstrated by the Apollo and Gemini programs [7]. Due to its advantages, several million dollars were invested in development of fuel cells. The primary goal of these kinds of research is to thrive an energy efficient technology that has outstanding features such as fuel flexibility, compact size, lower environmental impact, high performance [5].

1.3 Operating Principle of Fuel Cell

The three main components of a fuel cell are anode, cathode and an electrolyte placed between them. Hydrogen (H₂) is used as a fuel to perform the operation

of a fuel cell. Hydrogen (H₂) and Oxygen (O₂) is supplied to anode and cathode respectively.

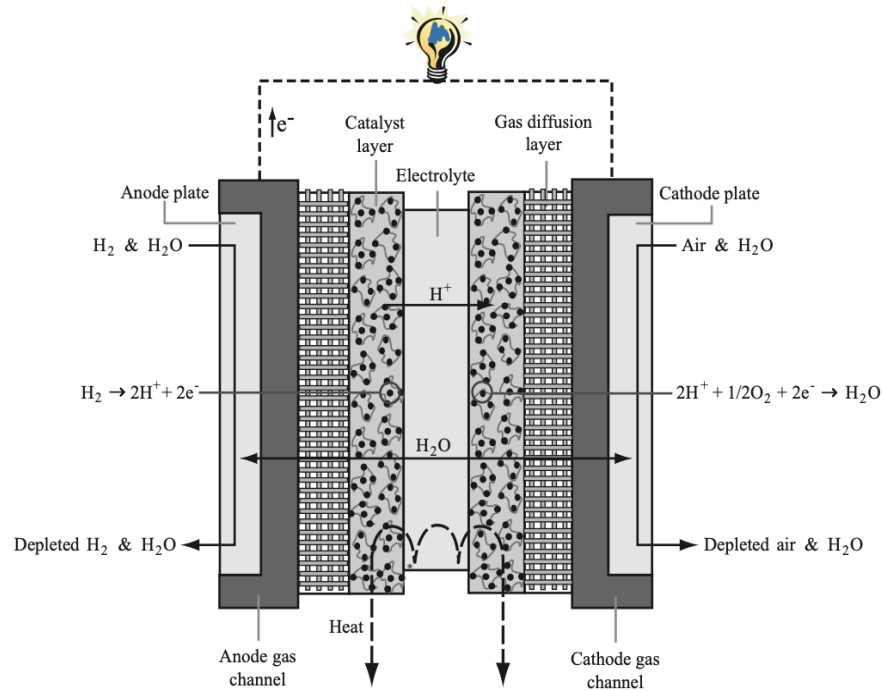


Figure 1.1 - Construction of a Fuel Cell [8]

The reaction at the anode is shown below.



At the anode, hydrogen molecule is oxidized into proton by providing two free electrons. The ion travels through the electrolyte and reaches the cathode. At the cathode, electrons and ion react with the oxygen to form water. The reaction at the cathode is shown below.



At the cathode, the water is formed by combining oxygen with hydrogen. The overall reaction of the cell is shown below in equation 3.



The output of the fuel cell is the electrons going through the external circuit produces electrical energy.

For different types of fuel cells, the equation 1 and 2 may differ according to the type of the fuel cell. For all types of fuel cells, the overall reaction shown in equation 3 remains the same using hydrogen (H₂) as fuel. The thermal management system is required to remove the heat from the fuel cell system.

1.4 Functions of Different Fuel Cell Components

Fuel cell has an integral part consists of two electrodes and an electrolyte which can be a liquid or solid based on the fuel cell type. This integral part is called Electrode Assembly. The functions of electrode assembly are to gather the electrons and deliver a path for the transfer of electrons, and to provide a reaction site for the electrochemical reaction to occur.

The electrodes are in porous form and consists of two regions. The solid region is required for the reaction sites and the hollow region allows the flow of products and reactants. They must be chemically stable and mechanically rigid to resist deformation and must sustain high temperatures. An electrode is made of two subcomponents such as porous region and catalyst region. The porous region is called Gas Diffusion Layer (GDL) where it allows the flow of reactants and products, and the reaction takes place at catalyst region. The function of electrolyte is to act as a barrier to separate the reactants and it has to be a conductor of ions and insulator of electrons.

1.5 Fuel Cell Efficiency

Energy efficiency is an important factor in fuel cell. Generally, the energy efficiency of the fuel cell is between 40% - 60%. As seen in the previous section, in a fuel cell, the chemical energy of the fuel is converted to electrical energy. To evaluate the chemical energy of the fuel, "Gibbs free energy" defined as "availability of energy to perform external work by neglecting any work done by changes in pressure or volume" has to be calculated for the fuel [9]. The change of Gibbs free energy of a system, ΔG_f which is the difference between the Gibbs free energy of the products and reactants as shown in equation 4.

$$\Delta G_f = G_f \text{ of products} - G_f \text{ of reactants} \quad (4)$$

In a fuel cell, the difference between the Gibbs free energy of formation of hydrogen and oxygen and the Gibbs free energy of formation of water is the energy released by the fuel cell. At 25°C (298K), ΔG_f for hydrogen oxygen fuel cell is $-237.2 \text{ KJ mol}^{-1}$ [9]. The negative value denoted that the energy has been released. If there are zero losses, all the Gibbs free energy is converted to electrical energy. One mole of any substance consists of 6.022×10^{23} molecules, atoms, or ions. This number is known as Avogadro's number, denoted by N_A . The charge of one electron is 1.602×10^{-19} Coulombs, represented as "e". Therefore, the charge of 1 mole of electrons is given by $N_A \times e$, which is the Faraday constant, denoted by F , with a value of 96485 Coulombs per mole of electrons. As seen in the equation 1, in a hydrogen fuel cell, there are two free electrons passing through the external circuit for every

mole of hydrogen (H₂) is supplied. Thereby, the charge of two electrons is 2F. The electrical work done by the electrons is given as

$$\text{Electrical work} = \text{charge} \times \text{voltage} = -2FE \quad (5)$$

Under zero losses, the electrical work will be equal to the Gibbs free energy.

$$\Delta G_f = -2FE \quad (6)$$

Hence, the open circuit voltage (OCV) of a fuel cell is given by,

$$E = \frac{-\Delta G_f}{2F} \quad (7)$$

For a cell operating at 25°C (298K), the OCV is given by 237200 J.

$$E = \frac{237200 \text{ J/mol}}{2 \times 96485 \text{ C}} = 1.23 \text{ V} \quad (8)$$

The maximum possible efficiency of a fuel cell is given by

$$\eta_{\max} = \frac{\Delta G_f}{\Delta H_f} * 100\% \quad (9)$$

Where, ΔH_f is the enthalpy of formation of the system.

At 25°C, $\Delta H_f = -285.84 \text{ KJ mol}^{-1}$.

$$\eta_{\max} = \frac{-237.2 \text{ KJ/mol}}{-285.84 \text{ KJ/mol}} * 100\%$$

$$\eta_{\max} = 83\%$$

The maximum possible efficiency for a fuel cell at 25°C (298K) is 83%.

1.6 Fuel Cell Efficiency Losses

There are various losses that reduces the efficiency of a fuel cell. They are [9]:

- **Fuel cross over losses:** There will be few amounts of voltage loss occurs when the electrons and fuel diffuse through the electrolyte.
- **Ohmic losses (ion and electron transport loss):** This type of loss occurs when the resistance offered to the flow of electrons through

the anode and cathode, resistance to the flow of protons and electrons through the electrolyte.

- **Activation Losses:** This loss occurs due to the voltage drop via driving the electrochemical reaction.
- **Concentration Losses (Mass transport loss):** As the fuel is consumed, the change in the concentrations at the surface of the electrodes.

1.7 Polarization Curve

The most standard and fundamental method for assessing the performance of PEMFC is via Polarization Curve. Under steady state or dynamic conditions, the plot of voltage versus current density is recorded. It provides information on the performance losses of the cell such as activation loss, ohmic loss, mass transport loss [10].

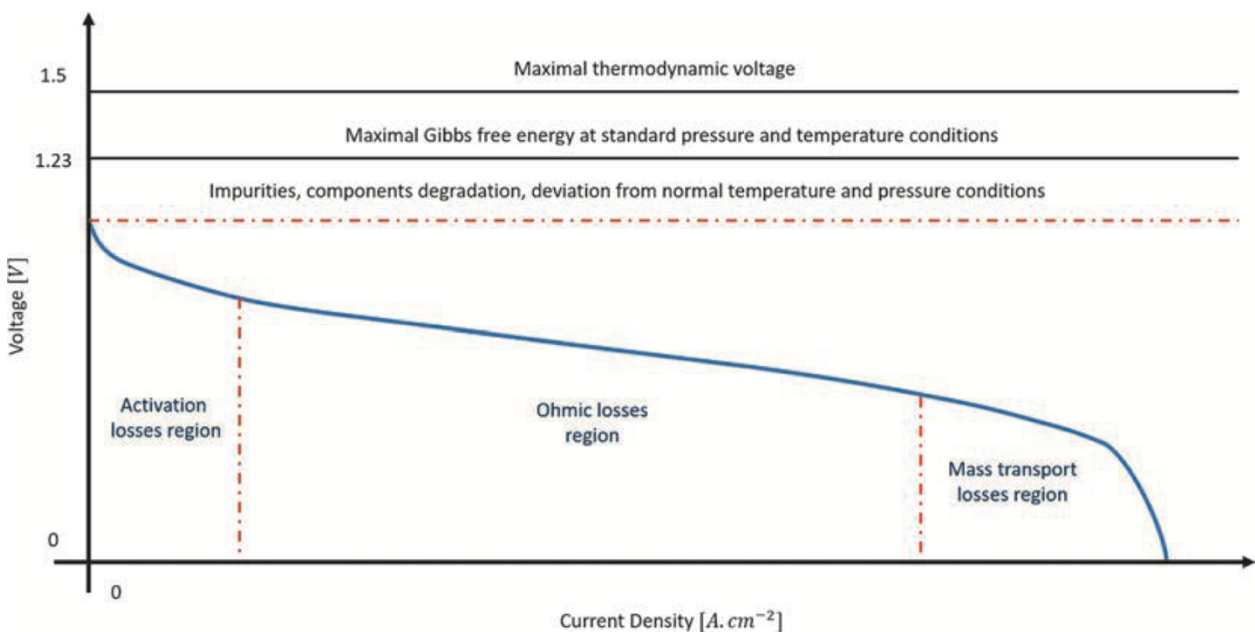


Figure 1.2 Polarization curve for PEMFC with activation, ohmic, and mass transport polarization regions [11]

1.8 Fuel Cell Classification

The classification of fuel cells are generally based on the occurrence of the chemical reaction. Basically, the type of membrane which is used decides the type of fuel cell such as Polymer Electrolyte Membrane Fuel Cells (PEMFC), Alkaline Fuel Cell (AFC), Solid Oxide Fuel Cell (SOFC), Molten Carbonate Fuel Cell (MCFC), Phosphoric Acid Fuel Cell (PAFC), Direct Methanol Fuel Cell (DMFC), etc. These are the most commonly available fuel cells that are discussed below [9,6]

Polymer Electrolyte Membrane Fuel Cell (PEMFC)

Polymer Electrolyte Membrane Fuel Cell is also known as Polymer Exchange Membrane Fuel Cell. The electrolyte of PEMFC is a solid membrane ion conducting polymer. Hydrogen(H_2) is supplied to anode as fuel. The operating temperature of PEMFC ranges between $30^{\circ}C$ to $100^{\circ}C$ ($303K$ to $373K$). This type of fuel cell has a wide range of applications such as mobile, space, stationary and portable power applications. The electrochemical reactions of anode and cathode of a PEMFC are shown in equation 1 and 2. PEMFC has fuel efficiency in the range of 45 to 60%. The working principle, system components and performance are discussed in chapter 2.

Alkaline Fuel Cell (AFC)

The operating temperature of Alkaline fuel cells ranges between $50^{\circ}C$ to $100^{\circ}C$ ($323K$ to $373K$) and for some specific applications the temperature may go up to $200^{\circ}C$ ($473K$). Generally, alkaline solution such as sodium hydroxide or potassium hydroxide in water is used as electrolyte. The application of an AFC is used mobiles and space since it has a life span of 10,000 hours. The fuel efficiency of AFC ranges between 40 to 60%.

Solid Oxide Fuel Cell (SOFC)

In 1937, Baur and Preis developed SOFC [7]. The electrolyte of the SOFC is an oxide ion-conducting ceramic material. The operating temperature of SOFC is between 500 to 1000°C (773K to 1273K). The applications of SOFC are in power plants having power output of few Kilowatts to several Megawatts. The efficiency of SOFC is between 55 to 65%.

Molten Carbonate Fuel Cell (MCFC)

The operating temperature of MCFC is 650°C (923K). The fuel used is hydrogen. At cathode, Carbon-di-oxide (CO_2) needs to be supplied. The electrolyte used in MCFC is molten carbonate salts. The application of MCFC is in medium scale power plants running at few megawatts. The fuel efficiency range between 60 and 65%.

Phosphoric Acid Fuel cell (PAFC)

PAFC was developed to use natural gas as a fuel to produce electricity. PAFC uses phosphoric acid as the electrolyte. The byproduct of the fuel was carbon monoxide (CO), which would reduce the efficiency of anode. In order to remove the carbon monoxide, the fuel cell temperature was increased which eventually increases the rate of the removal process. The typical operating temperature of PAFC is in the range of 220°C (493K). The application of a PAFC is in power plants with power output in the range between 200 to 250KW. The fuel efficiency of PAFC is about 55%.

Direct Methanol Fuel Cells (DMFC)

In DMFC, instead of hydrogen (H_2), methanol (CH_3OH) is used as fuel. The advantage of using Methanol (CH_3OH) is that readily available and is low-cost liquid fuel. The electrolyte used in a DMFC is similar to that of a

PEMFC. The typical operating temperature ranges between 20°C to 90°C (293K to 363K). Its net energy is very high and the main problems associated with DMFC is that the electrochemical reaction results in much lower power output for a given size because it occurs at very slow pace. The applications of DMFC are in portable electronic systems which require low power for its operation. DMFC has fuel efficiency close to 35%.

1.9 Thesis Objectives

The main objective of the study is to evaluate the performance of the PEMFC by varying the dimensions of the flow channel under different operating conditions. In this thesis, a comparison study has been conducted between a published paper results and the simulation results of the author. Then, 3 different types of serpentine flow channel have been designed and simulated under various operating conditions using ANSYS FLUENT module. The pressure distribution, mass fractions of H₂, velocity magnitude, cell Reynolds number were investigated along with the performances of fuel cells. Also, another comparison study has been made by altering the size of flow channel width which tested under various parameters. The results indicate that the tri serpentine provides better performance compared with other designs. This is due to the pressure loss which is lesser in tri serpentine design. Also, the mass fraction of H₂, velocity magnitude and Reynolds number of the cell has been discussed. The PEMFC with narrower width improves on the fuel cell performance due to the reduction in contact resistance losses.

1.10 Outline of the Thesis

After a brief introduction, Chapter 2 discusses about the PEMFC in a detailed manner. Chapter 3 will discuss a detailed review of the design and simulation

of the flow channel to understand the operation of the cell. Chapter 4 discusses the procedures used for different designs and techniques employed to analyze the fuel cell. Chapter 5 deals with the comparison between the experimental data. Then, chapter 6 presents the PEMFC serpentine configurations results. Chapter 7 contains analysis of PEMFC which comprises of pressure distribution, mass fraction of H_2 , velocity magnitude and cell Reynolds number. The comparison and analysis study by altering the flow channel width which tested under various conditions is elaborated in chapter 8. Chapter 9 has results and discussion, and conclusion is documented in chapter 10. Chapter 11 contains the future research scope on the fuel cell flow channel configurations.

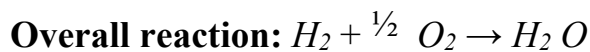
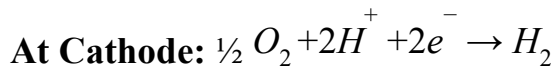
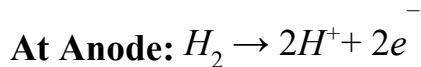
CHAPTER 2

POLYMER EXCHANGE MEMBRANE FUEL CELL (PEMFC)

2.1 Introduction of Polymer Exchange Membrane Fuel Cell (PEMFC)

Among various fuel cells, Polymer Exchange Membrane Fuel Cells (PEMFC) are significant for treating the energy crisis and environmental pollution. PEMFC is employed to power the electric motors in automobiles with zero emission of any harming gases in the atmosphere. It has been widely used in automotive industry compared to other fuel cells. In transportation sector, PEMFC has a greater scope to replace the existing internal combustion engines. In PEMFC, the hydrogen (H_2) passes through the anode splits into protons and electrons. The protons pass to the cathode through the electrolyte of the cell. Meanwhile, the electrons pass through by external circuit. Thus, electricity is generated.

The chemical reaction that takes place within a PEMFC are



2.2 Components and materials of Polymer Exchange Membrane Fuel Cell (PEMFC)

A PEMFC composed of various parts such as current collector, gas diffusion layer (GDL), catalyst layer, and membrane. Each electrode of a cell has gas diffusion layer, catalyst layer and the combination of all these along with membrane is known as Membrane Electrode Assembly (MEA). The design

and composition of these parts can have important effects on the performance of the fuel cell.

The materials of the components used in PEMFC is one of the major factors which decides the performance of the cell [12]. Researchers working on the development of new materials and enhancing the presently using materials to obtain better results.

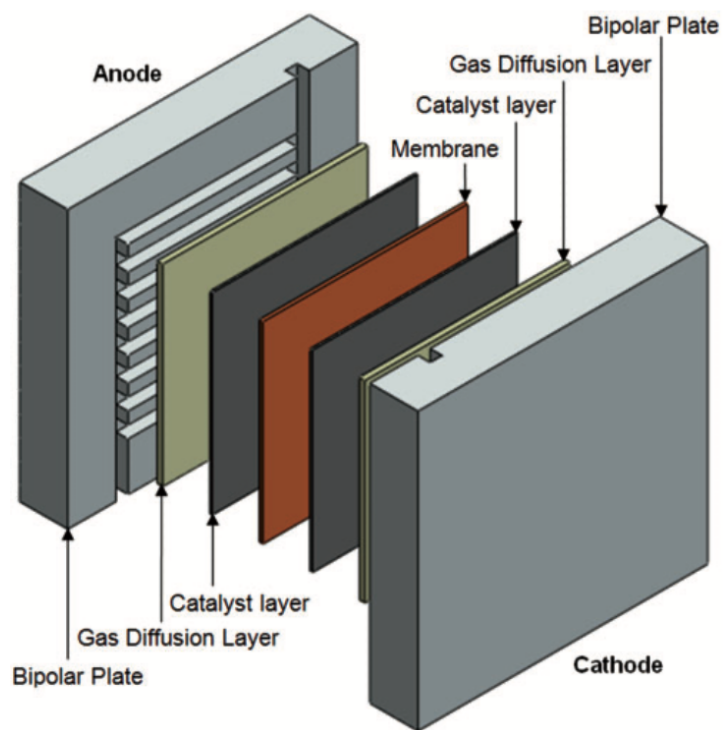


Figure 2.1 - Cross sectional view of a PEMFC with its components [13]

Bipolar Flow Plates

The primary function of the flow plate is to collect the generated current, distribute the fuels to the reactive sites, provide mechanical support and facilitate the water management. An efficient design of the plates offers efficient fuel distribution, enhance water management.

Open Pore Cellular Foam (OPCF) materials have indeed emerged as promising alternatives to traditional flow fields such as interdigitated channels, bio inspired flow field, straight channel, and serpentine channels, in various applications including Polymer Exchange Membrane Fuel Cells (PEMFCs). Researchers [14,15,16,17,18] have highlighted several advantages of Open Pore Cellular Foam (OPCF) materials such as low pressure drop, better gas distribution.

Graphite indeed has been a popular materials choice for flow field applications in Polymer Exchange Membrane Fuel Cells (PEMFCs) due to its advantageous properties such as corrosion resistance, enhanced surface conductivity. However, it does come with certain drawbacks, primarily brittleness and permeability to gases, which can limit its effectiveness in some applications. To address these drawbacks and potentially reduce the usage of graphite in PEMFCs, researchers have been exploring various composites materials and alloys. These alternative materials aim to provide similar or improved performance while overcoming the limitations of graphite. Some of the key considerations in the development of these materials include mechanical strength, has impermeability, conductivity, and compatibility with the operating conditions of PEMFCs.

Researchers observed the corrosion behavior of stainless steel and suggested that the performance of stainless steel depends on the alloying materials like Ni, Mo and Cr [19,20,21,22,23].

Aluminum and its alloys offer several advantages such as cost effectiveness, ease of manufacturing, and low density, they are not as widely used as

stainless steel and titanium in Polymer Exchange Membrane Fuel Cells (PEMFCs) applications [24].

Gas Diffusion Layer (GDL)

The main function of the GDL is to transport the electrons and heat to the current collector and to distribute the reactant gases to the catalyst layer. A good GDL will be electronically & thermally conductive, chemically & mechanically stable, highly porous, lower cost, easy to handle. The GDL acts as a frame for the catalyst layer and responsible for uniform mass transport of reactants. The GDL is made from carbon fibers (6-10 μm diameter) woven into a paper or cloth about 40 – 70% of porosity [25,26]. To accelerate the hydrophobicity and promote water transport, the GDL is treated with 30 wt% of either polytetrafluoroethylene (PTFE) or fluoroethylene propylene [26].

Carbon cloth and carbon fiber paper are the popular materials which fulfils the functions of a good GDL. With internal humidification, carbon cloth provides better performance than carbon fiber paper [27].

In PEMFC, the GDL loses its ability after long term operations. At cold and warm cycles, there are high chances of breaking its fiber [28]. To avoid this problem, the investigation made by F.-Y. Zhang, et al. [29] says that the use of copper, tailored into porous configuration. The material improves the water management due to its pores and minimum thickness.

J. Benziger, et al. [30] investigated the water transport through the various GDL materials coated with PTFE. It was noted that the water flows through

smaller pores at increased hydrostatic pressure. This is due to the hydrophobic nature of PTFE.

Catalyst Layer (CL)

The Catalyst Layers (CLs) are the thin layers attached to both sides of the membrane. The electrochemical reactions take place on the surface of the CLs of a fuel cell. Generally, Platinum based catalyst layers are widely used in PEMFC applications. The performance degradation in Pt catalyst fuel cell arises when hydrogen fuel contains residual mono oxide (CO) which poisons the catalyst layer. To overcome this problem, a platinum-ruthenium catalyst is suggested. It omits the effects of electro-oxidation of CO and improves the performance of the cell. [31,32]

S.M.Haile [33] has indeed explored the use of Pt-Cr alloy as a catalyst on the cathode side has advantages over platinum catalyst.

Membrane

In PEMFC, the membrane is a solid polymer electrolyte. It is an electronic insulator and separates the anode and cathode. It allows protons transport while impermeable to the reactant gases. Thus, the membrane of PEMFC should be good electronic insulation, good separation of hydrogen(H_2) in the anode side and oxygen(O_2) in the cathode side, and high proton conductivity.

A membrane in a PEMFC should have a capability to withstand the operating temperature range between $-30^{\circ}C$ to $200^{\circ}C$. The widely used membrane for a PEMFC is Sulfonated polymers which operates at a temperature $>100^{\circ}C$. NAFION is known as the commercial name of this membrane. The sulfonated

polymers are composed of sulfonated side chains and perfluorinated back bones which are responsible for the hydration, chemical stability.

Gore and Associates introduced [34,35] perfluorinated composite membrane. It is made by reinforcing the perfluorinated membrane by thin polytetrafluoroethene (PTFE). These membranes have very high proton conductivity and mechanical stability.

The investigation by J.Gasa, et al. [36] focused on the fullerene based membrane designed to operate at high temperatures, specifically above 150°C. which improves the performance of the cell.

In order to overcome the hydration problem in Nafion membrane, researchers suggested Nanocomposite membranes. These Nanocomposite membranes are made up of modifying the micron additives with Nafion membrane. This additive provides high water retention capabilities are TiSiO_4 [37], TiO_2 [38], ZrO_2 [39]. In addition, the additives offer improved physical properties like tensile strength, elastic modulus.

K. Kaneko, et al. [40] suggested the hydrocarbon polymers like sulfonated hydrocarbons for the applications of PEMFC. The advantages of this materials are cheap, operates at high temperature, eco-friendly. The disadvantages are poor proton conductivity, low chemical stability.

2.3 Automobile Applications of PEM Fuel Cell

In general, there are two types of PEMFCs based on temperature: High temperature PEMFC (HTPEMFC) and low temperature PEMFC (LTPEMFC). LTPEMFCs has increased efficiency, low operating temperature, and suitability to automobiles. Because of these advantages, Fuel Cell Electric Vehicles (FCEVs) utilizes LTPEMFCs. To run a FCEV, PEMFC provides efficiency up to 60% of electrical output by converting the chemical energy of the fuel. FCEV is an eco-friendly technology which is capable of replacing Internal Combustion Engines (ICEs). There are several advantages of FCEV such as high-power densities, zero NO_x or CO₂ emissions, silent and safe operation. Vehicles such as forklifts, cars, boats, trains, trucks, motorcycles are powered by PEM fuel cell is an evidence that the utilization of fuel cells is increasing in industries [41].

Due to high electrical efficiencies, zero emission of gases, low operating noise and temperature PEMFC is the most applicable fuel cell for automotive applications. Toyota Mirai was one of the fuel cell cars in the automotive market currently that runs on hydrogen as a fuel. The cost of the car is around \$49,500 [42] which is much higher than the average price of an IC Engine powered vehicle (\$37,000) [43].

CHAPTER 3

LITERATURE SURVEY

There has been a significant amount of research conducted in the field of fuel cells over the past few decades. Numerous researchers have dedicated their efforts to studying the performance of Polymer Exchange Membrane Fuel Cells (PEMFCs) under diverse operating and system parameters. A plethora of research articles have been published, detailing simulations of PEMFCs and analyzing their performance characteristics.

3.1 Literature Survey on Simulation of PEMFC

Due to the complexity of the design, the experimental implementation is expensive for fuel cells [44,45]. Consequently, simulation models generated by software have become instrumental in fuel cell research and development. Modelling and Simulation to scrutinize the performance of PEMFC has become a major development due to its rapid growth because of its wide range of applications in automotive, stationary, and portable applications. This method of study facilitated the identification of parameters that influence fuel cell functionality, offering researchers valuable insights. Simulation models offer a cost-effective alternative to experimental implementation, significantly reducing costs associated with prototyping and testing makes it easier for researchers to identify the parameters that influence the functioning of a fuel cell. Fabricating a whole fuel cell system and studying parameters would consume more time, expensive and complex. To avoid that, the simulation software helps one to study all the parameters easily [46]. Eker and Taymaz [47] utilized the Fluent module to simulate the PEMFCs to examine the flow channel width and operating temperature. The result revealed that the

performance of the battery impacted when the operating temperature decreases with increase in flow channel width.

The performance of the PEMFC depends on the various design and operating parameters revealed from the various literature survey given below.

3.2 Literature Survey on Flow Channel Design

A Polymer Exchange Membrane Fuel Cells (PEMFCs) offer numerous advantages including null emissions, low temperature, high power density. Enhancing the performance of PEMFC involves optimizing the flow channel's geometry is one of the most crucial aspect [48].

Liu et al. [49] created a computational model to optimize current collector dimensions and cross-sectional area of the flow channel dimensions. The figure 3.1 illustrates the various designs of serpentine flow channel. The findings reported that the power output of PEMFC is increased by reducing the flow channel total width and the rib-to- total width ratio.

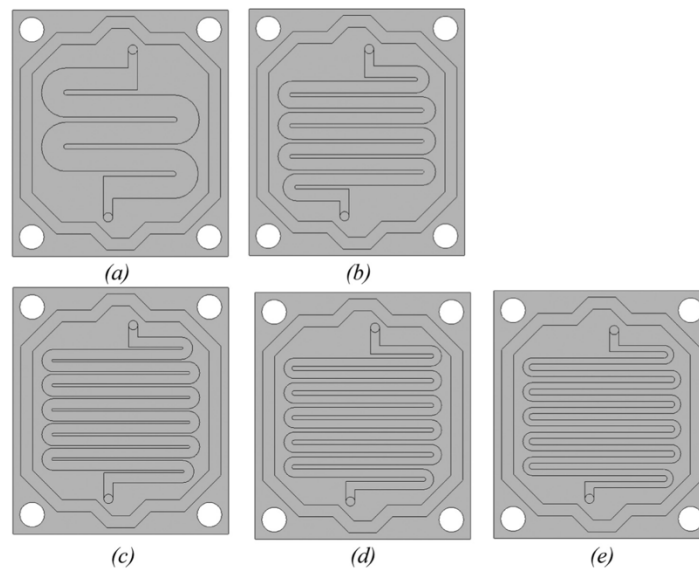


Figure 3.1 – Serpentine flow channel designs of PEMFC [49]

The effects of flow channel dimensions have been investigated by Mohammad and Behzad on the fuel cell performance. The simulation results revealed that the increase in the flow channel width enhances the limiting current density [50].

Khazaei et al. [51] explored the performance of triangular channel geometry of PEMFC under various operating parameters like cell operating pressure, temperature, and reactants on anode and cathode flow rate. The results demonstrated that the PEMFC performance can be enhanced by increasing the inlet pressure, inlet temperature of reactants and cell temperature.

In the study by Carcada et al. [52], the influence of channel cross sectional area and the serpentine channel patterns illustrated in figure 3.2. The findings shows that the current density enhanced up to 7% for the smallest depth and provides better humidification.

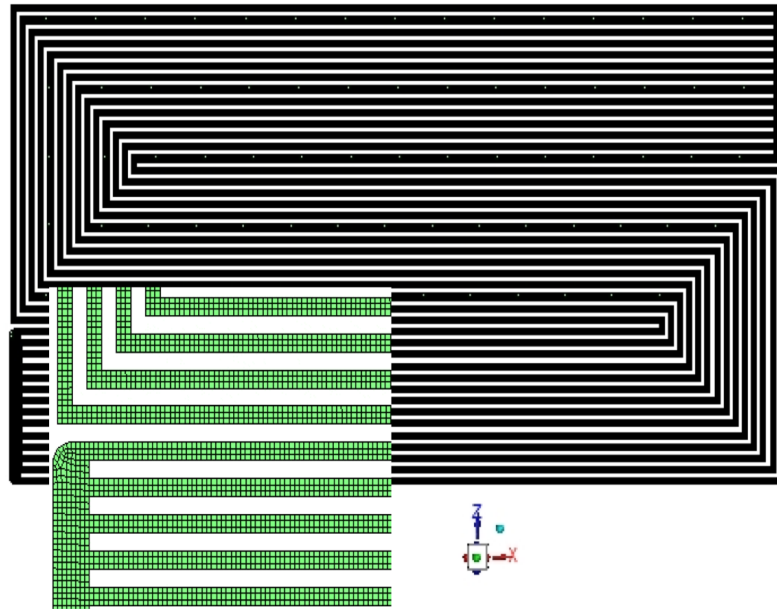


Figure 3.2 – Computational mesh of a 14-channel serpentine configuration in a PEMFC [52]

In the study by Sukkee and Wang [53], a three-dimensional interplay of straight and interdigitated flow field channels using Computational Fluid Dynamics (CFD). The results shows that the interdigitated flow effectively removes water from catalyst layer compared to straight channel. The performance of Polymer Exchange Membrane Fuel Cells (PEMFCs) with serpentine and straight flow fields was investigated by Hashemi et al. [54]. The findings indicated that serpentine flow field exhibits a superior distribution of current density and temperature.

The results of X.Zeng et al. [55] shows that at 0.5 V, the power output of the tapered design was 3.25% higher than the original design. This is due to reducing the width of the channel in the direction of flow as shown in figure 3.3 quickens the movement of the reactant gas, strengthens the electrochemical reaction, and directs the reactant into the Gas Diffusion Layer (GDL), thereby boosting the overall performance of the cell.

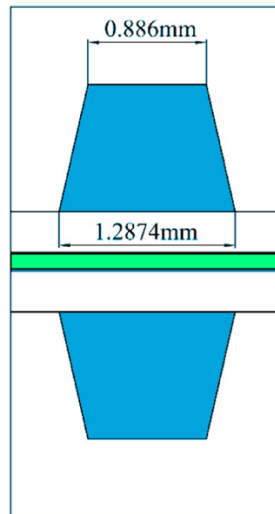


Figure 3.3 - Cross sectional view of optimal design [55]

Young-Gi Yoon et al. [56] investigated the effects of channel and rib widths of flow field plates which are adjusted from 0.5 to 3mm as shown in figure

3.4. It's observed that a narrower rib width correlates with improved cell performance. These findings suggest that gas diffusion plays a more significant role than electric conduction in influencing the cell's overall performance.

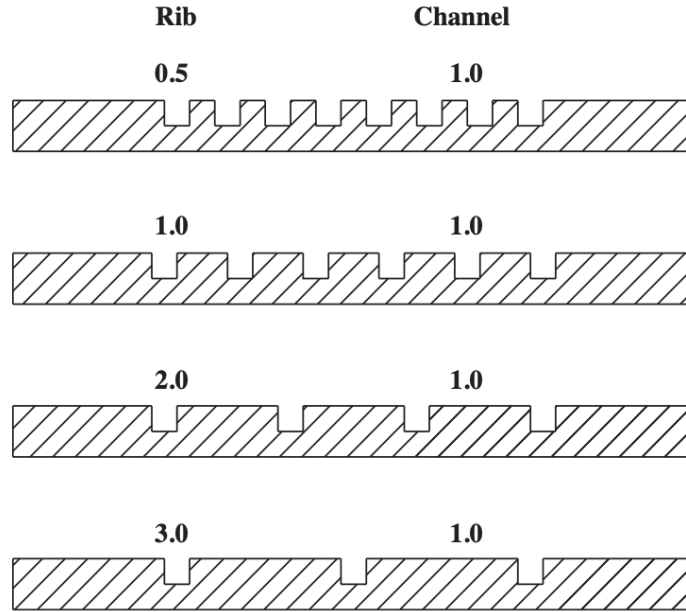


Figure 3.4 – Schematic diagram of rib and channel configurations [56]

Santamaria et al. [57] conducted tests comparing gas distribution variations in channels with length varies from 5cm to 25cm. The results shows that the longer channel performs better than the shorter ones.

Researcher Wei-Mon Yan et al. [58] investigated the impact of interdigitated flow channel design on the performance of PEMFC. The figure 3.5 illustrates the test models of the flow field. The findings suggested that the power output of the interdigitated flow field yields 1.4 times higher than the conventional flow field. This is due to the inlet flow rate and cathode humidification temperature at the interdigitated flow design improves cell performance.

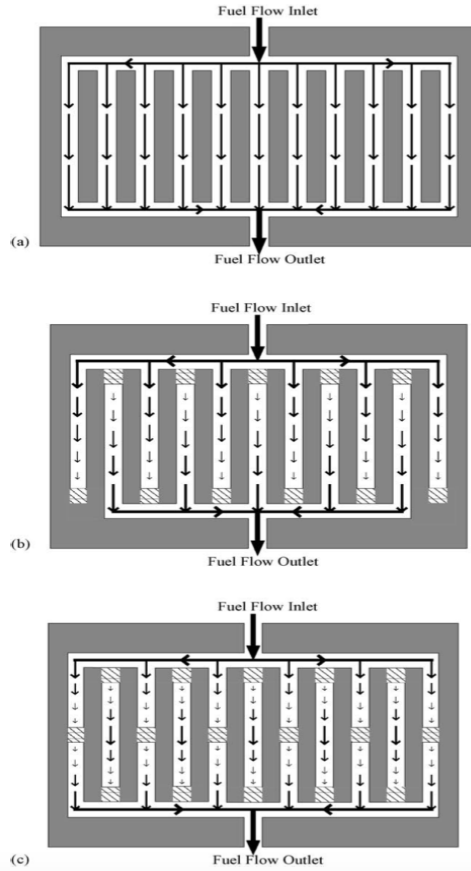


Figure 3.5 – Schematic diagram of the test models of flow fields [58]

Atul Kumar et al. [59] focused on the optimization of the flow channel shape and dimensions in the end plates of flow field in a serpentine flow field design. The figure 3.6 shows the serpentine flow channel design in bipolar plate. The increase in the performance of the PEMFC can be influenced by the excess hydrogen (H_2) consumption in anode side by 9%.

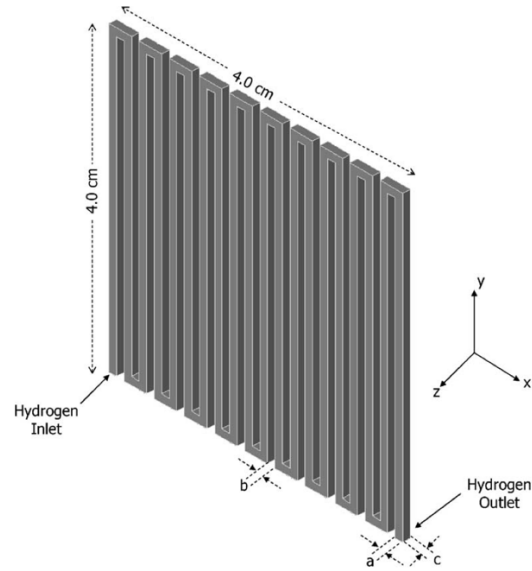


Figure 3.6 – Serpentine flow channel design in bipolar plates [59]

Jaruwasupant & Khunatorn [60] investigated the effects of serpentine flow channel curvature and length, pressure drop, velocity distribution on the performance of PEMFC using a three-dimensional computational fluid dynamics (CFD) model. The channel curvatures are depicted in figure 3.7. The result shows that the best configuration was the sharp curve because this yields 25% better performance than other channels. Also, this can provide a non- uniform flow distribution with high pressure drop and low velocity during the reactant flow.

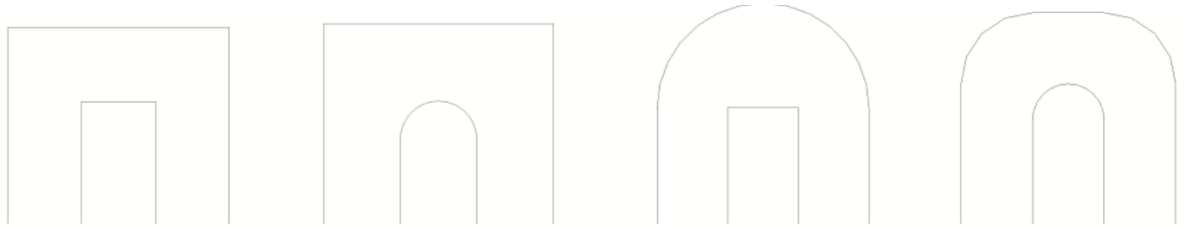


Figure 3.7 – Different channel curvatures [60]

A serpentine flow field design with five channels, each having different heights from channel 2 (H_1) to channel 5 (H_4) as depicted in Figure 3.8, was utilized to optimize the flow field [61]. The outcomes demonstrated enhanced flow in the main channel, leading to increased rates of oxygen transport and current density. Compared to straight channels, the proposed serpentine flow channel design boosted the power density of the fuel cell by 11.9%. Additionally, a diverging final channel was incorporated to minimize reactant leakage to the outlet.

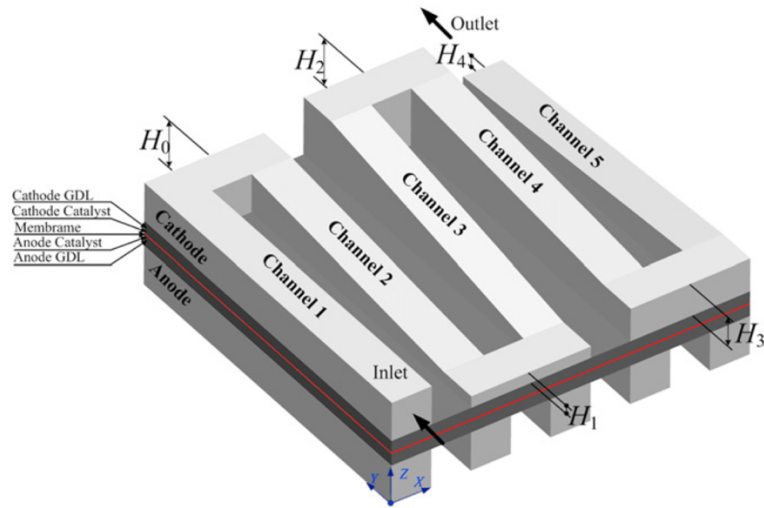


Figure 3.8 – Schematic of three dimensional serpentine PEM fuel cell with varying channel heights [61]

Zhongmin Wan et al. [62] worked on the optimal design of a novel M-like channel in bipolar plates of PEMFC as shown in figure 3.9. The results revealed that M-shaped channels, increasing the height of obstacles and the thickness of blockages enhanced the flow of reactants in the direction of the wall, resulting in higher rates of heat and mass transfer. This wavy design yielded a high power density by 21.3 % while maintaining same amount of pumping energy.

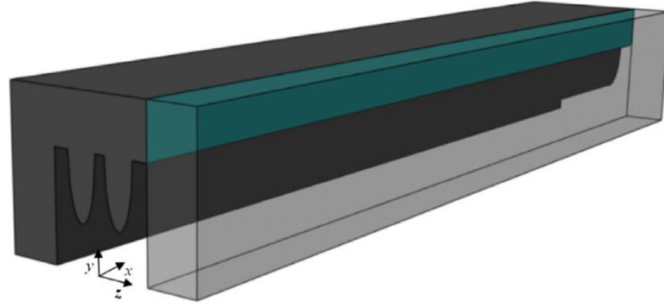


Figure 3.9 – Schematic illustration of the M-like channel [62]

The researcher K.Tuber et al. [63] designed a fractal structures featuring a multi-ramified network of flow channels in PEMFC as illustrated in Figure 3.10. A computer algorithm was developed to optimize for minimal pressure drop and uniform fluid distribution. This novel fractal configurations was evaluated and contrasted with serpentine and parallel configurations. The findings indicated that while the fractal configuration performed almost identically to the parallel configuration, the serpentine configuration yielded the highest and most consistent power output.

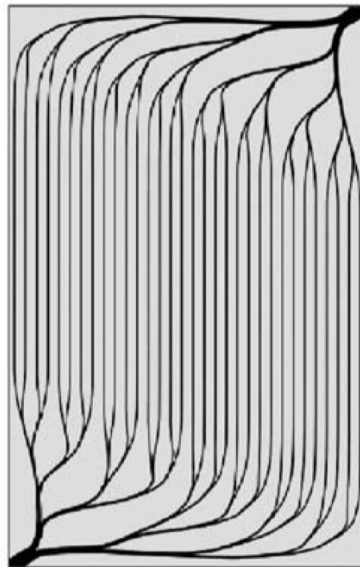


Figure 3.10 – Fractal design of flow fields [63]

Chowdary et al. [64] designed four different flow fields by changing the channel depth and observed that decreasing the channel depth improved species diffusion within the PEMFC. Ahmed & Sung [65] investigated the performance of PEMFCs with different flow fields (rectangular, trapezoidal, parallelogram) using computational fluid dynamics (CFD). The results exhibits that a rectangular flow field yielded better cell voltages compared to parallelogram and trapezoidal flow fields. However, the trapezoidal flow field enhanced current density, reactant diffusion and uniform reactant flow over the reacting area, results in lower cathode over potential of the fuel cell.

Performance prediction of PEM fuel cell with wavy serpentine flow channel was studied by Mehmet Seyhan et al. [66]. In the study, three different amplitudes (0.25 mm, 0.5 mm, 0.75mm) were employed for a sinusoidal wavy design with a consistent wavelength of 6.28mm. Comparing these configurations, the results indicated that the sinusoidal wavy configurations with a 0.25mm amplitude outperformed the conventional configuration by 20.15%. This configuration demonstrated improved performance, enhancing both diffusion and flow rates.

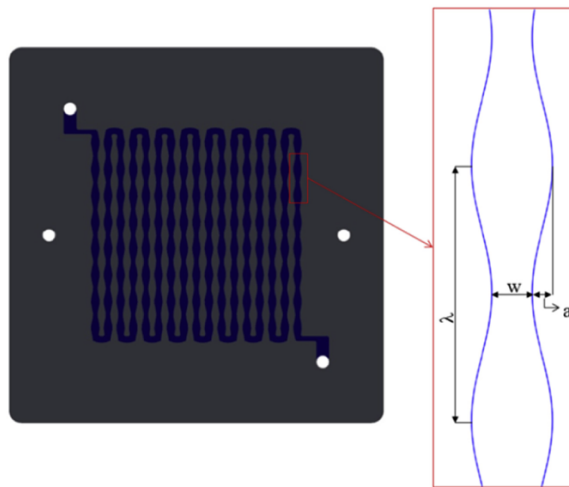


Figure 3.11 – Sinusoidal Wavy design of serpentine flow channel [66]

Roshandel.R et al. [67] focused on the simulation of an innovative flow field design based on a bio inspired pattern for PEM fuel cells. The analysis of the novel leaf-shaped flow field design depicted in figure 3.12 was conducted. The findings indicated that the distributions of oxygen concentration, pressure, and velocity were more uniform compared to traditional designs. Furthermore, there were observed increases of 26% and 56% in current density compared to serpentine and parallel flow fields, respectively.

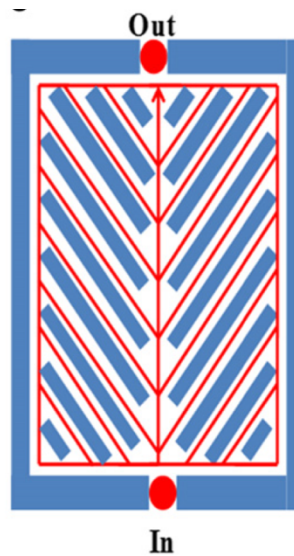


Figure 3.12 – Novel leaf shape flow field [67]

Lorenzini-Gutierrez D et al. [68] simulated the tree shaped flow channel PEMFC to study the performance of the cell. The suggested flow fields featured radial designs connecting the central flow entrance to the circumference of the plate, as illustrated in figure 3.11. Three types of tree shaped flow fields with varying levels of bifurcation (three levels, two levels, and one level) were employed in the numerical simulation. Cell performance was assessed by comparing tree-shaped channels with parallel and serpentine flow channels using power and polarization curves. The results indicated that the tree shaped design reduced pressure drop and achieved uniform flow

distribution. Furthermore, increasing the number of bifurcation levels resulted in a larger active area utilization, leading to higher current and power densities.

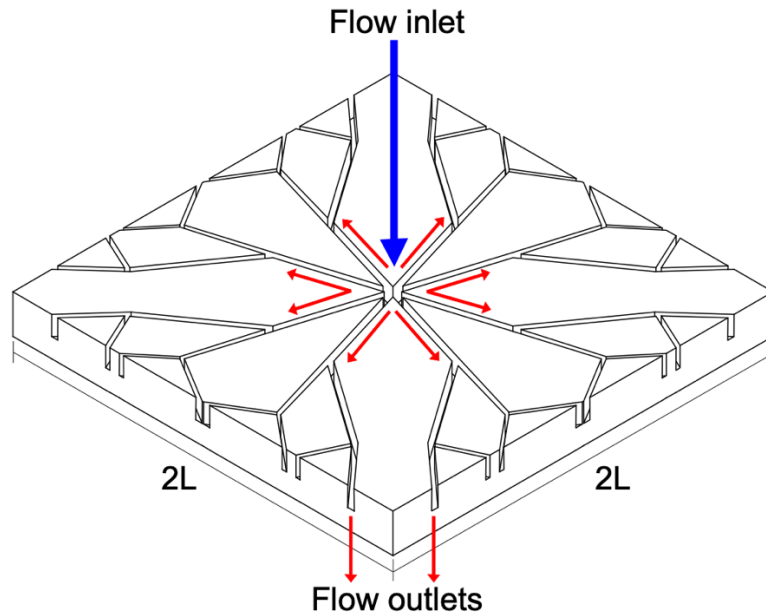


Figure 3.13 – Schematic representation of the flow field configuration integrated into the bipolar plates [68]

The impact of bionic configuration on fuel cell performance under gravity was investigated by Liu, S et al. [69]. Both asymmetrical and symmetrical bionic flow channels were utilized in visualization and simulation, as depicted in figure 3.12. The results from these experiments showed significant differences in performance between symmetric bionic flow channels. Specifically, fuel cells with an asymmetric configuration of bionic flow channels exhibited the best performance.

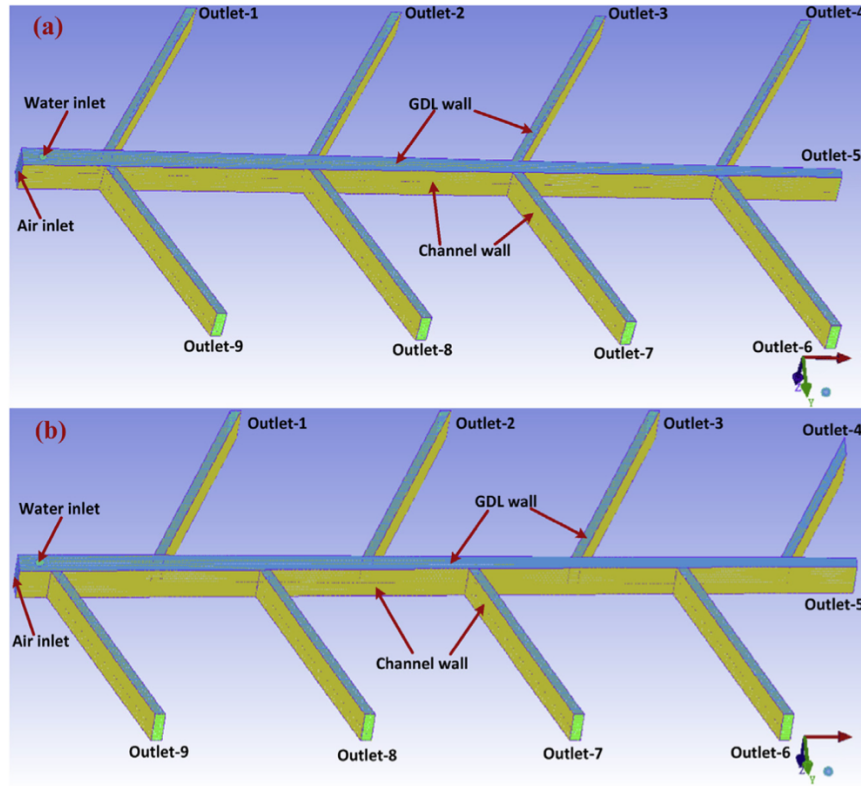


Figure 3.14 – Schematic representation of two different bionic flow field (a). symmetric bionic flow channel and (b). asymmetric bionic flow channel [69]

Investigations were conducted by Liu H et al. [70] on the serpentine flow channel performance in large, small, and normal sectional areas with and without slope turns, as shown in figure 3.13. The results indicated that to prevent droplets from rebounding from the bottom of the flow channel to the top surface (MEA), the slope angle must be sufficiently large. However, excessively large slope angles resulted in increased pressure drop and reduced water removal capacity. Improved water removal was observed at slope angles of 120° and 160° , along with corresponding contact angles under similar conditions.

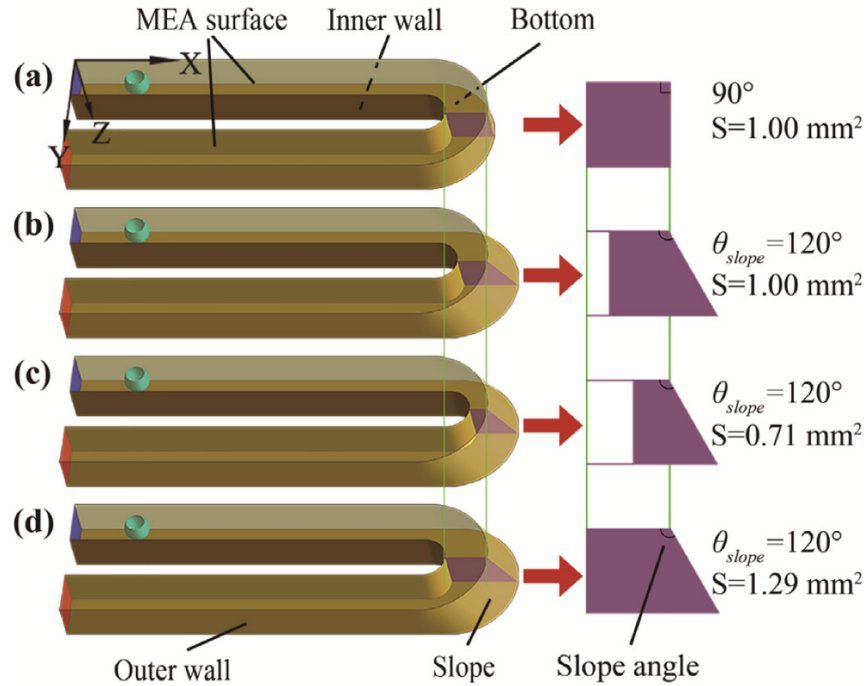


Figure 3.15 – serpentine flow channels featuring different cross-sectional areas and slope turns [70]

Eliton Fontana et al. [71] conducted a study on the influence of channel depth on PEMFC performance. Three angles of flow channel inclination (0° , 0.5° , and 0.75°) were examined, as depicted in figure 3.14. The findings revealed that a 0.75° inclination of the flow channel notably enhanced power and current densities by 8% and 9.5%, respectively. However, the main drawback of employing non-uniform channels (tapered channels) was the significant increase in pressure drop, which rose by 3.5 times for the 0.75° inclination and by 2 times for the 0.5° inclination.

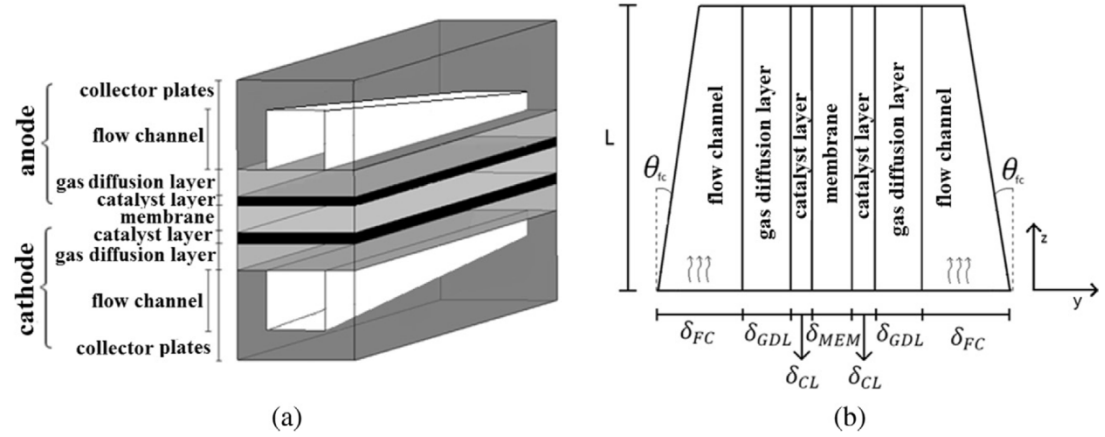


Figure 3.16 – Solitary tapered conduits for fluid flow [71]

The conventional wave shape was altered by G. Cai et al. [72] by implementing a bio-inspired wave shape within the channels, drawing inspiration from a cuttlefish fin as shown in figure 3.15. In comparison to straight channels, the performance of wavy channels is typically enhanced owing to reduced resistance to reactant flow. Moreover, a bio-inspired wave channel exhibits higher efficiency and lower flow resistance when contrasted with a regular wave channel. The optimized dimensions for the wave channel, which can enhance power density by 2.2%, are determined to be 3.52 wave cycles.

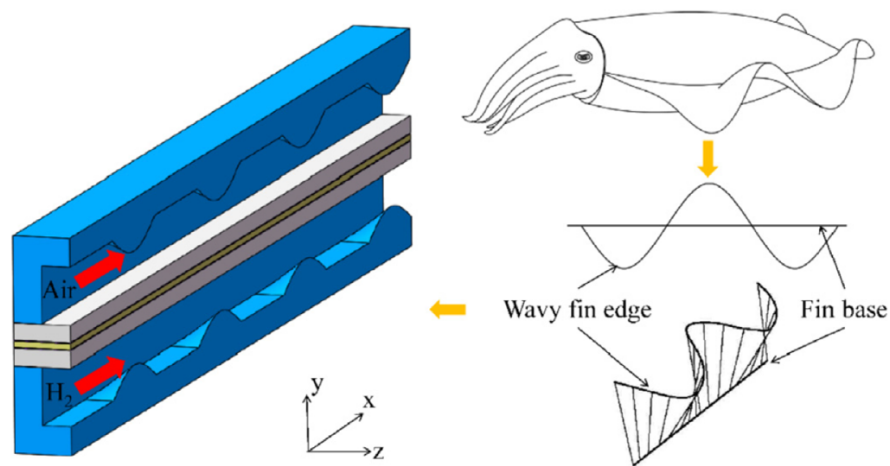


Figure 3.17 –wave like PEMFC inspired from cuttle fish fin [72]

Mahammad et al. [73] observed that the PEMFC performance is influenced by the channel dimension. They concluded that the optimum rib thickness provides a better performance.

The work of Yousef et al. [74] on how a novel flow channel design affect the PEMFC performance by CFD approach which resulted that the performance of this design is better than the conventional design. The figure shows the various flow channel design

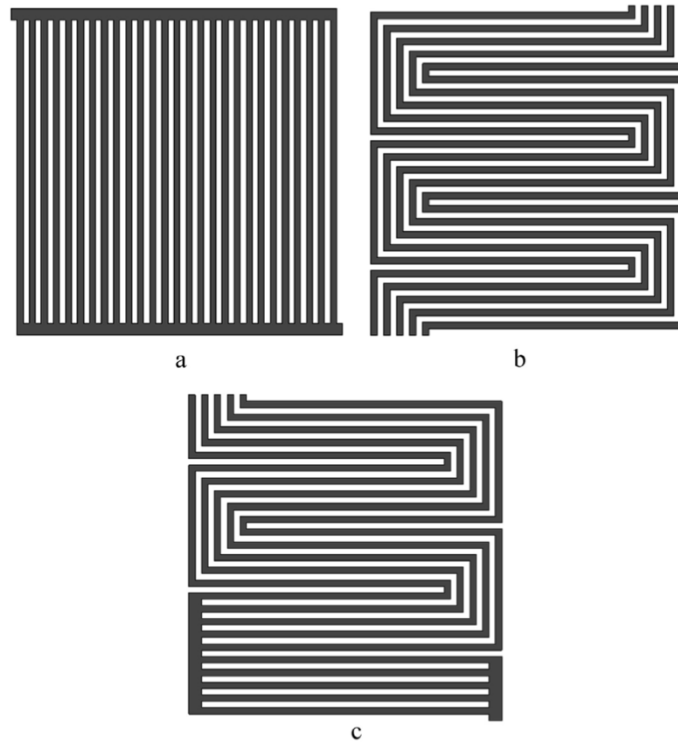


Figure 3.18 – (a).parallel design (b).serpentine design (c).compound design [75]

Liu et al. [75] investigated the effect of gas flow fields on fuel cell performance with the various flow channel designs like pin type, single and multiple channel serpentine, multiple channels parallel, spiral, and interdigitated type flow channel with 23.5 cm² effective area of the PEMFC.

The results exhibited that the best performance provided by the single serpentine flow channel design amongst all the flow channel design that exist.

Iranzo et al. [76] explored a Computational Fluid Dynamics (CFD) model of Polymer Exchange Membrane Fuel Cells (PEMFCs) featuring both parallel and serpentine flow fields, utilizing the Ansys fluent software. The parallel bipolar plate with 25 channels and 24 ribs in land area is illustrated in figure 3.17. The study emphasized the superior performance of serpentine flow fields compared to parallel ones. The serpentine flow field exhibited the most outstanding performance when the fuel cell operated with pure oxygen (O_2) and full humidification. This configuration led to enhanced exchange current density and minimized concentration polarization, contributing to improved overall performance.

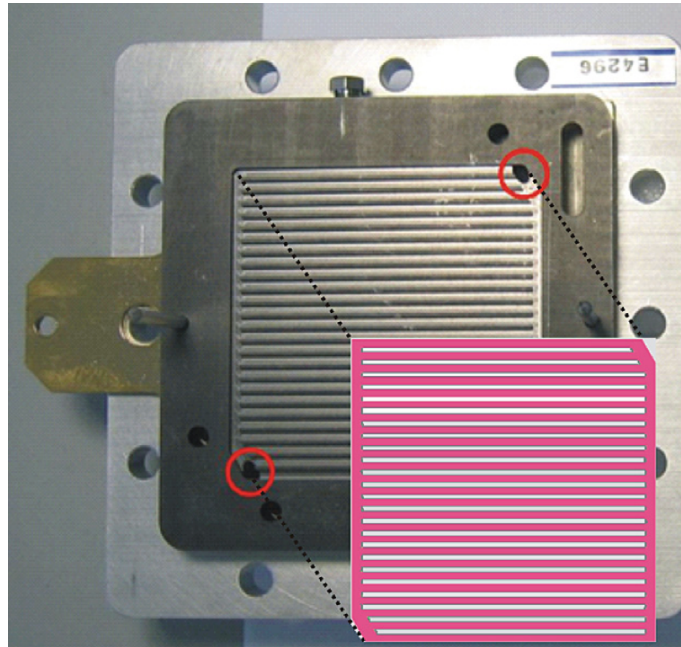


Figure 3.19 – Parallel bipolar plate with 25 channels and 24 ribs in land area [76]

Geneva et al. [77] concluded that excessive flow field length causes pressure loss can lead to water flooding and reduced performance of PEMFC. Shimpalee et al. [78] discussed about the comparison on the performance of a PEMFC with active area of 200 cm^2 which had various number of Straight Flow Field (SFF) channels as shown in the figure 3.18. The researcher concluded that the cell provides better performance when with 13 straight channels.

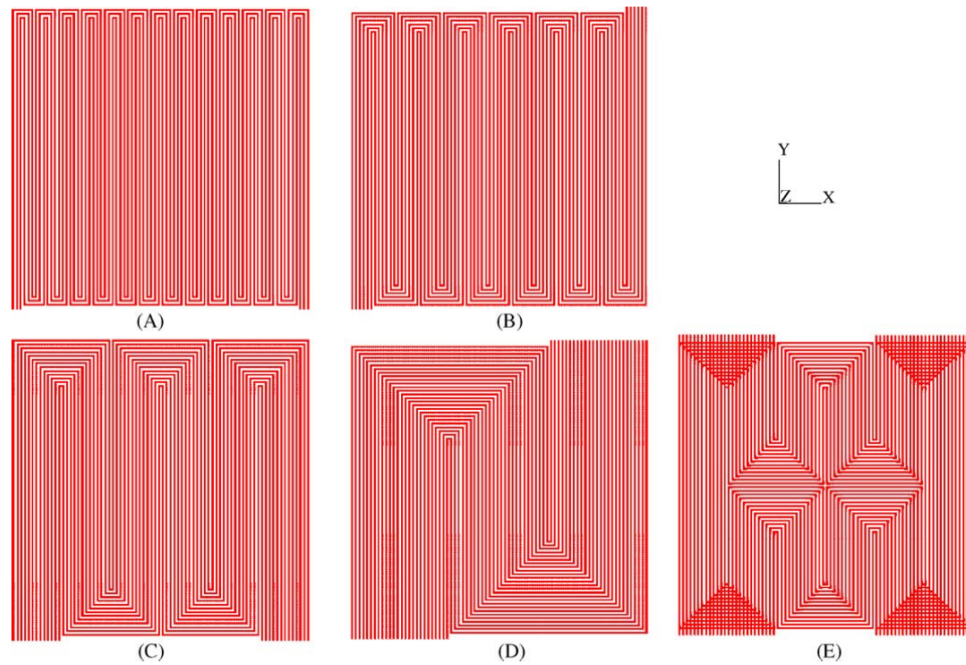


Figure 3.20 – (a).3-channel serpentine flow field (b). 6-channel flow field (c). 13-channel flow field (d). 26-channel flow field (e).26-channel complex flow field [78]

Cooper et al. [79] studied the impact of modifying channel width on the performance of PEMFC and concluded that flow field width has a significant effect on the power and current density. The results shows that 15% of the variability in limiting current density was attributed to channel and land width due to the improved distribution of the reactants resulting from a greater

number of channels. In addition, the channel depth accounted for 11.5% of the variability in limiting current density. The figure 3.19 shows the various bipolar plates created for the experiment.

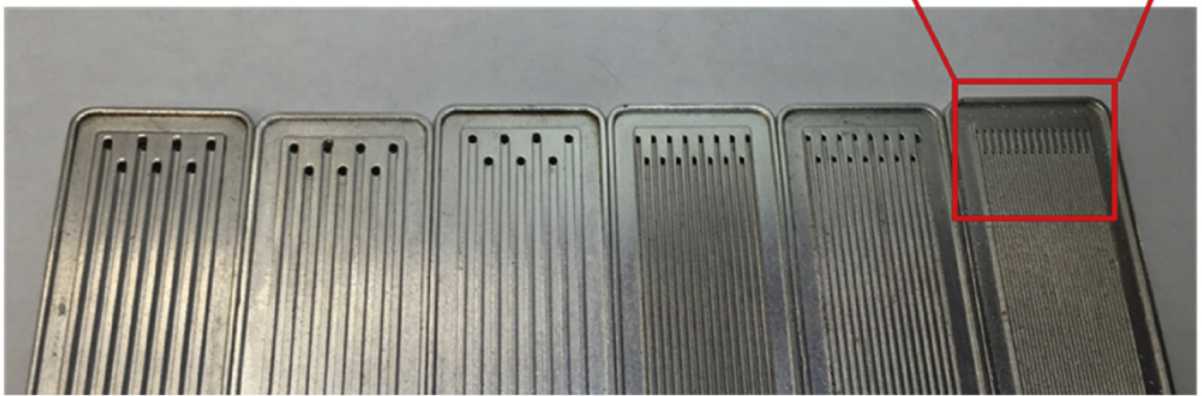


Figure 3.21 – All bipolar plate geometries created for the experiment [79]

3.3 Literature Survey on Operating Conditions

The characterization of the behavior of a PEMFC effective area of 25cm^2 with several operating parameters like cell temperature, reactant pressure, the anode and the cathode flow temperature in saturation and dry conditions has been discussed by Santarelli & Torchio [80]. The results indicated that the performance of PEMFC improves with increase of temperature, reactant pressure, and humidification, particularly at high cell temperatures.

Venkateswarlu et al. [81] analyzed three types of flow channels and observed that the triple serpentine flow field performs better at higher flow rates, while the single serpentine flow field exhibits best performance at low flow rates. Mahmoudimehr and Daryadel [82] examined the effect of flow channel width and height under various operating conditions. It observed that the optimum channel sizes vary depending on the specific operating conditions.

Freire et al. [83] studied the effect of operational parameters on the performance of PEMFC using a serpentine flow field having different cross section shapes (rectangular & trapezoidal). The result exhibited that the reactant humidification temperature has a significant impact on the effect of serpentine flow channels with trapezoidal cross-section on cell performance.

Amirinejad et al. [84] investigated the performance of PEMFC with an active area of 5cm^2 under various operating conditions, including temperature, pressures, and humidity of reactant gases. The results demonstrated that increasing the cell temperature and operating pressure enhances the performance of PEMFC. Additionally, the anode humidification has a considerable effect on the performance of PEMFC.

CHAPTER 4

METHODOLOGY

4.1 Overview

The 3D model of the PEMFC is designed using Solidworks and the study is conducted with ANSYS software. The simulation starts with creating the CAD drawing of the PEMFC geometry, follows by meshing generation, boundary conditions application, and running of the simulation by utilizing appropriate models. The voltage generated from the fuel cell model was recorded to plot the polarization curve. The polarization curve of the PEMFC was studied to indicate the fuel cell model performance.

4.2 Geometry Design

The geometry model was created using SOLIDWORKS 2022 software. Subsequently, the geometry, along with relevant zones like current collectors, flow field channels, gas diffusion layers, catalyst layers and membrane, generated within the software, as depicted in Figure 2.1. Afterwards, the grid was exported to ANSYS FLUENT 2022 R2 licensed software for meshing, followed by solving the complete set of the module within ANSYS. The models were read into the FLUENT application, then various specifications and boundary conditions were set for each zone. This numerical model domain is a single cell geometry. In this model, the reactant gases are humidified hydrogen and air. The operating temperature was 313 K / 323 K / 333 K / 343 K / 353 K / 363 K / 373 K while the operating pressure was 2 bar respectively. The open circuit voltage ranges between 0.1 V to 1 V. The active area for the model is $5 \times 5 \text{ cm}^2$. The width and depth of flow channels are 2mm. Then, the width has been modified to 1mm and 3mm to compare the

results of the channel with 2mm. Tables 4.2 and 4.3 shows the geometry properties and parameters for the simulation. Also, the characteristic of the mesh is given in table 4.1. The nodes and elements of the mesh is maintained in all the designs.

Table 4.1 - The characteristics of the mesh

S.no	DESCRIPTION	VALUE
1	Nodes	1008943
2	Elements	1109348

Within the ANSYS software suite, the Fluent add-on module is employed. This module encompasses a range of parameters crucial for detailed simulations, including but not limited to:

1. Joule heating
2. Electrochemistry
3. Membrane water transport
4. Multiphase phenomena
5. Multi component diffusion
6. Anisotropic e-conductivity in porous electrode
7. Butler-Volmer rate

These parameters enable comprehensive analysis and modeling of various electrochemical processes within the system.

The software configuration involved selecting specific modules essential for the analysis. The flow module facilitated species transport based on predefined boundary conditions such as pressure, temperature, and mass flow rate. Meanwhile, the species transport module managed chemical reactions by utilizing the provided diffusivity matrix. The current distribution module quantified the generated current density corresponding to the ongoing

reactions. Consequently, a coupled analysis integrating these three modules was executed within the software framework, culminating in the derivation of power density from the polarization curve.

Table 4.2 - The geometric parameters of PEMFC [85]

PART NAME	LENGTH (mm)	WIDTH (mm)	THICKNESS (mm)	MATERIAL
Anode and Cathode Flow Plate	80	80	10	Bipolar graphite
Anode and Cathode Catalyst	80	80	0.08	Carbon 0.5 mg/cm ² platinum
Anode and Cathode GDL	80	80	0.3	Tetra fluoro polyethylene
Membrane	80	80	0.127	nafion

Table 4.2 shows the details of the design of PEMFC and materials used for each components of the cell.

Table 4.3 - Operating conditions and relevant parameters of the study

PARAMETERS	VALUES	REF
Cell temperature (K)	313/323/333/343/353/363/373	Estimated
Mass flow rate of Hydrogen (H ₂) at Anode (Kg/s)	4.33E-07	[85]

Table 4.3 - continued

Mass flow rate of Oxygen (O ₂) at Cathode (Kg/s)	3.33E-06	[85]
Anode inlet temperature (K)	313/323/333/343/353/363/373	Estimated
Cathode inlet temperature (K)	313/323/333/343/353/363/373	Estimated
Operating pressure (Bar)	2	[85]
Open Circuit Voltage (V)	0.1, 0.15, 0.2, 0.25... to 1 V	Estimated
Porosity of GDL	0.4	Assumed
Porosity of CL	0.5	Assumed

The table 4.3 provides a comprehensive overview of the operating conditions and pertinent parameters utilized in simulating the PEMFC. Some of the operating conditions were considered from [85] and are used in this study as well. Cell temperatures, as well as anode and cathode inlet temperatures, range from 313 to 373 Kelvin. Anode and cathode mass flow rates are specified accordingly. The operating pressure is set at 2bar, while the Open Circuit Voltage (OCV) spans from 0.1V to 1V in increments. Additionally, the porosity of the Gas Diffusion Layer (GDL) and Catalyst Layer (CL) are defined as 0.4 and 0.5, respectively.

4.3 Modeling Assumptions

The simulated 3-D fuel cell includes three distinct channel configurations such as single serpentine, bi serpentine, and tri serpentine straight channels, as depicted in figures 6.1, 6.2, and 6.3, respectively. Detailed dimensions for each configuration are provided in table 4.2. To conduct the simulations, relevant parameters and operating conditions are utilized, as outlined in the table 4.3.

The model is developed based on specific assumptions to accurately represent the behavior and performance of the fuel cell under investigation. These assumptions provide a foundation for the simulation setup and enable the analysis of various design configurations and operating scenarios.

- The PEMFC is operating under steady state condition and its temperature is maintained at the operating temperature.
- The pure form of hydrogen and air is used for the simulation, and these gasses follow the ideal gas law.
- Both the reactant gasses flow in the laminar region in flow channels.
- Catalyst layers, GDLs, and membrane are homogeneous and isotropic materials.
- The membrane is impermeable to gasses, i.e, there is no leakage current.
- The mass flow rate is constant at the inlet of the channel, and channel outlet is at constant pressure.

4.4 Governing Equations

For the PEMFC module, we used the Fuel Cell and Electrolysis Model in ANSYS Fluent 2022 R2. Table lists the solving zones of the governing equations.

Table 4.4 - The solving zones of the governing equations

S.NO	CONSERVATION EQUATIONS	SOLVED ZONES
1	Mass conservation equation	Channels, GDLs, CLs
2	Momentum conservation equation	Channels, GDLs, CLs
3	Gas species equation	Channels, GDLs, CLs
4	Liquid water equation	GDLs, CLs
5	Electronic charge equation	BPs, GDLs, CLs
6	Ionic charge equation	CLs, Membrane
7	Energy conservation equation	BPs, Channels, GDLs, CLs, Membrane

The governing equations are as follows

Mass conservation equation

$$\frac{\partial(\varepsilon\rho)}{\partial t} + \nabla \cdot (\varepsilon\rho\vec{u}) = S_m \quad (1)$$

ε – porosity of porous media

ρ – fluid density

\vec{u} – fluid velocity vector

S_m – quality source term

t – time

Momentum conservation equation

$$\frac{1}{\varepsilon^2} \nabla \cdot (\rho \vec{u} \vec{u}) = -\nabla p + \frac{1}{\varepsilon} \nabla (\mu \nabla \vec{u}) + S_u \quad (2)$$

μ – kinetic viscocity

S_u – momentum source term

\vec{u} – fluid velocity vector

ε – porosity of porous media

ρ – fluid density

p – fluid pressure

Energy conservation equation

$$\frac{\partial(\varepsilon \rho c_p T)}{\partial t} + \nabla \cdot (\varepsilon \rho c_p \vec{u} T) = \nabla \cdot (k^{eff} \nabla T) + S_h \quad (3)$$

c_p – specific heat capacity

T – temperature

S_h – energy source term

ρ – fluid density

ε – porosity of porous media

\vec{u} – fluid velocity vector

t – time

k^{eff} – effective thermal conductivity

Where the effective thermal conductivity is expressed as

$$k^{eff} = \varepsilon k^f + (1-\varepsilon) k^s$$

k^f – thermal conductivity of fluid

k^s – thermal conductivity of solid

Species transport equation

$$\frac{\partial(\varepsilon c_i)}{\partial t} + \nabla (\varepsilon \vec{u} c_i) = \nabla (D_i^{eff} \nabla c_i) + S_i \quad (4)$$

ε – porosity of porous media

t – time

c_i – volume fraction of species

D_i^{eff} – effective species diffusivity

S_i – species source term

\vec{u} – fluid velocity vector

Water saturation equation

$$\frac{\partial(\varepsilon \rho_l s)}{\partial t} + \nabla \left[\rho_l \frac{K s^\gamma}{\mu} \frac{dp_c}{ds} \nabla s \right] = r_w \quad (5)$$

ε – porosity of porous media

t – time

s – water saturation

ρ_l – density of liquid water

μ – viscosity of liquid water

r_w – condensation rate

K – absolute permeability

p_c – capillary pressure

CHAPTER 5

COMPARISON WITH EXPERIMENTAL DATA

5.1 Model Validation

Validation is indeed a critical aspect of Computational Fluid Dynamics (CFD) analysis, ensuring the accuracy and reliability of simulation results. This process involves comparing simulated data with existing results or experimental data obtained from real-world experiments. This comparison serves to assess the performance of the simulation model by evaluating its ability to accurately predict physical phenomena and replicate experimental observations.

By comparing simulated data with experimental data, discrepancies, and similarities between the two datasets can be identified. Any differences observed can provide valuable insights into the accuracy of the simulation model and highlight areas for improvement or further refinement. Additionally, successful validation strengthens confidence in the simulation results and enhances their credibility for use in engineering design, optimization, and decision-making process.

Overall validation plays a crucial role in ensuring the reliability and validity of CFD simulations, ultimately contributing to the development of robust and accurate computational models for various engineering applications.

5.2 Description of Experimental Design

In this design, five different arrangements of the flow channels are considered, incorporating both rectangular and slanted channels. These configurations are tabulated in the table 5.2. To validate these models, experimental data from

Wawdee P, et al [86] is utilized for comparison. The dimensions and details of the experimental PEMFC are outlined in the table 5.1.

Table 5.1 - Details of the experimental PEMFC [86]

PART NAME	LENGTH (mm)	WIDTH (mm)	THICKNESS (mm)	ZONE TYPE
Anode and Cathode Flow Plate	200	200	10	Solid
Anode and Cathode Catalyst	173.4	86.5	0.4	Fluid
Anode and Cathode GDL	173.4	86.5	0.4	Fluid
Membrane	173.4	86.5	0.4	Fluid

The active area of the fuel cell is 150cm². The flow channel plate is designed with parallel serpentine configuration featuring primary grooved channels. Rectangular cross-sectional channels measuring 1.5mm in width and 1mm in depth are grooved on the conventional graphite flow field. In the modified assisted flow field, each channel is slanted at an angle of 35°. The stoichiometry of hydrogen and air flow rates is set at 1.7 and 2.2 respectively, with a pressure 1.5 bar.

In the data of Wawdee P, the experiment was done under two different voltages and temperatures: 353K (80°C) and 368K (95°C) at 0.5 and 0.7 V. These parameters are chosen to evaluate the performance of the fuel cell under varying operating conditions and flow channel configurations at two different

voltages 0.5V and 0.7V. The figure 5.1 shows the design of experimental PEMFC.

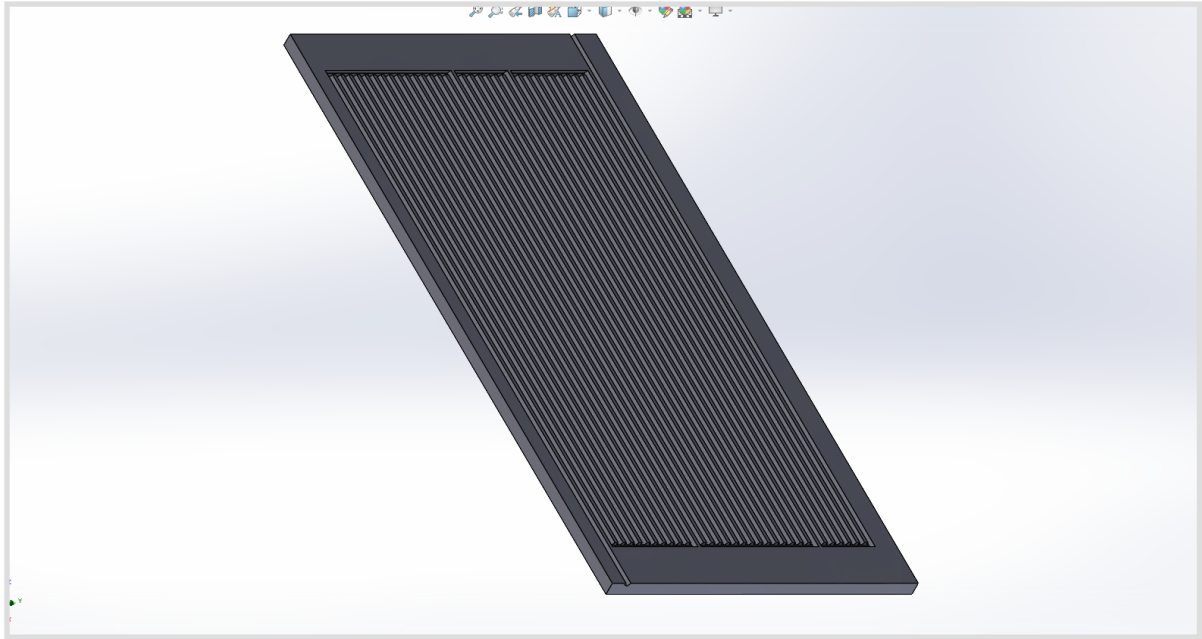


Figure 5.1 - Design of Experimental PEMFC [86]

Table 5.2 - Details of the various configuration of experimental PEMFC

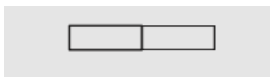
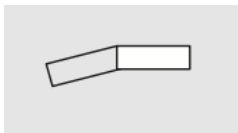
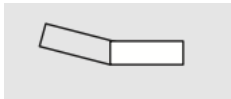
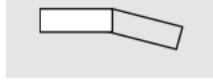
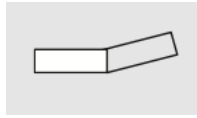
RUN	ANODE	CONFIGURATION	CATHODE
1	Rectangular Channel Plate (RP)		Rectangular Channel Plate (RP)
2	Down-slanted (ADS)		Rectangular Channel Plate (RP)
3	Up-Slanted(AUS)		Rectangular Channel Plate (RP)

Table 5.2 - continued

4	Rectangular Channel Plate (RP)		Down-slanted (CDS)
5	Rectangular Channel Plate (RP)		Up-Slanted (CUS)

The simulation data obtained was compared with experimental data, uncovering slight variations between the two sets of results. These differences can be ascribed to several factors, including variations in parameters and data, along with disparities in the software versions utilized for simulation. In chapter 5.3, comparison of 0.5V with simulation analysis were done whereas the chapter 5.4 comprises of comparison of 0.7 V with simulation analysis was shown.

5.3 Comparison of 0.5 V with Simulation Analysis

Below is a comparison of data analysis conducted at temperatures of 368K (95°C) and 353K (80°C), both at a voltage of 0.5V, across difference configurations.

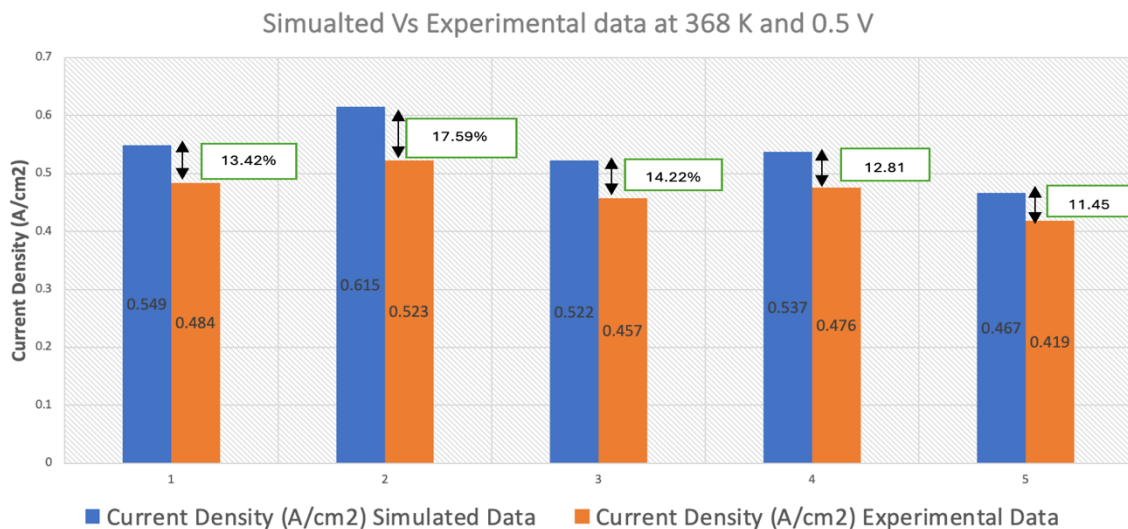


Figure 5.2 - Comparison of simulated and experimental data of PEMFC in 368K temperature at 0.5V voltage

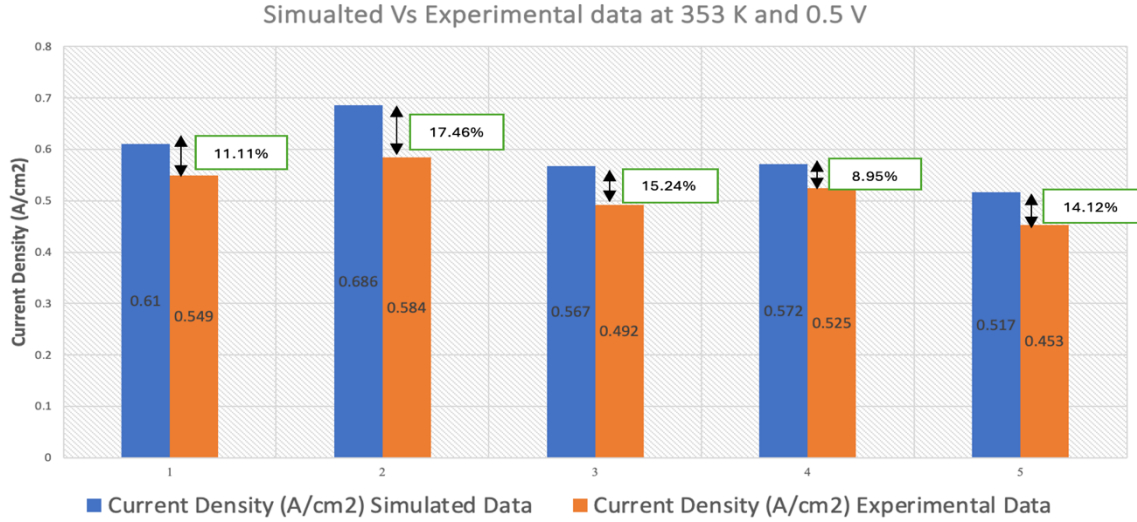


Figure 5.3 - Comparison of simulated and experimental data of PEMFC in 353K temperature at 0.5V voltage

Figures 5.2 and 5.3 depict the comparison between simulated and experimental results for all five configurations. The results for each configuration are provided and discussed below.

Figure 5.2 presents the data results at 0.5V and 368K (95°C) for different configurations:

1. **Configuration 1 (RP & RP):** The simulated current density is 0.549 A/cm², while the experimental current density is 0.484 A/cm². The percentile error between the simulated and experimental current density is 13.42%.
2. **Configuration 2 (ADS & RP):** The simulated current density is 0.615 A/cm², while the experimental current density is 0.523 A/cm². The percentage error between the simulated and experimental current density is 17.59%
3. **Configuration 3 (AUS & RP):** The simulated current density is 0.522 A/cm², while the experimental current density is 0.457 A/cm².

The percentage error between the simulated and experimental current density is 14.22%

4. **Configuration 4 (RP & CDS):** The simulated current density is 0.537 A/cm², while the experimental current density is 0.476 A/cm². The percentage error between the simulated and experimental current density is 12.81%
5. **Configuration 5 (RP & CUS):** The simulated current density is 0.467 A/cm², while the experimental current density is 0.419 A/cm². The percentage error between the simulated and experimental current density is 11.45%

Figure 5.3 presents the data results at 0.5V and 353K (80°C) for different configurations:

6. **Configuration 1 (RP & RP):** The simulated current density is 0.61 A/cm², while the experimental current density is 0.549 A/cm². The percentage error between the simulated and experimental current density is 11.11%.
7. **Configuration 2 (ADS & RP):** The simulated current density is 0.686 A/cm², while the experimental current density is 0.584 A/cm². The percentage error between the simulated and experimental current density is 17.46%
8. **Configuration 3 (AUS & RP):** The simulated current density is 0.567 A/cm², while the experimental current density is 0.492 A/cm². The percentage error between the simulated and experimental current density is 15.24%
9. **Configuration 4 (RP & CDS):** The simulated current density is 0.572 A/cm², while the experimental current density is 0.525 A/cm².

The percentage error between the simulated and experimental current density is 8.95%

10.Configuration 5 (RP & CUS): The simulated current density is 0.517 A/cm², while the experimental current density is 0.453 A/cm². The percentage error between the simulated and experimental current density is 14.12%

5.4 Comparison of 0.7 V with Simulation Analysis

The following presents a comparative analysis of data obtained at 368K (95°C) and 353K (80°C), specifically at 0.7V across different configurations.

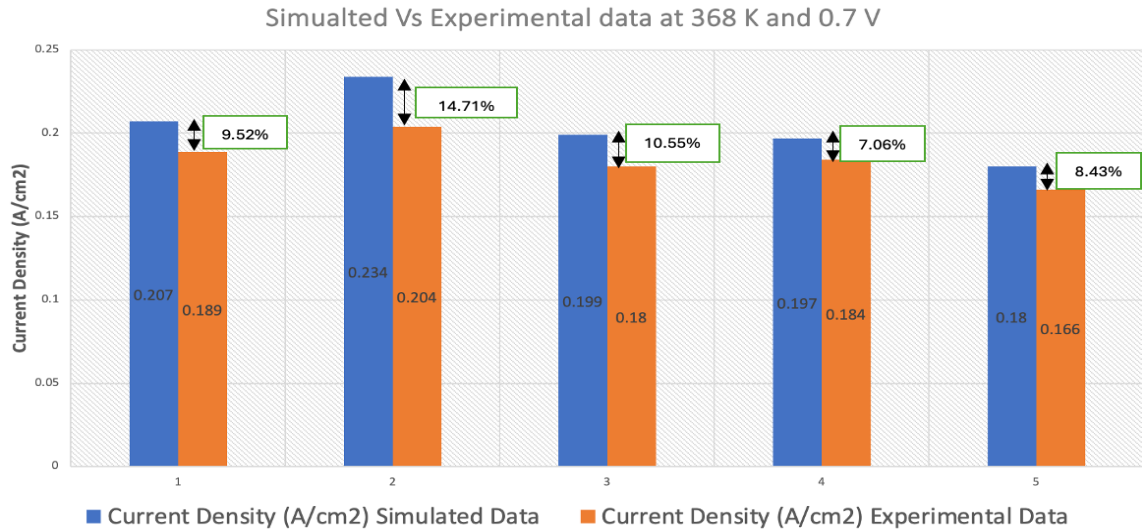


Figure 5.4 - Comparison of simulated and experimental data of PEMFC in 368K temperature 0.7 V voltage

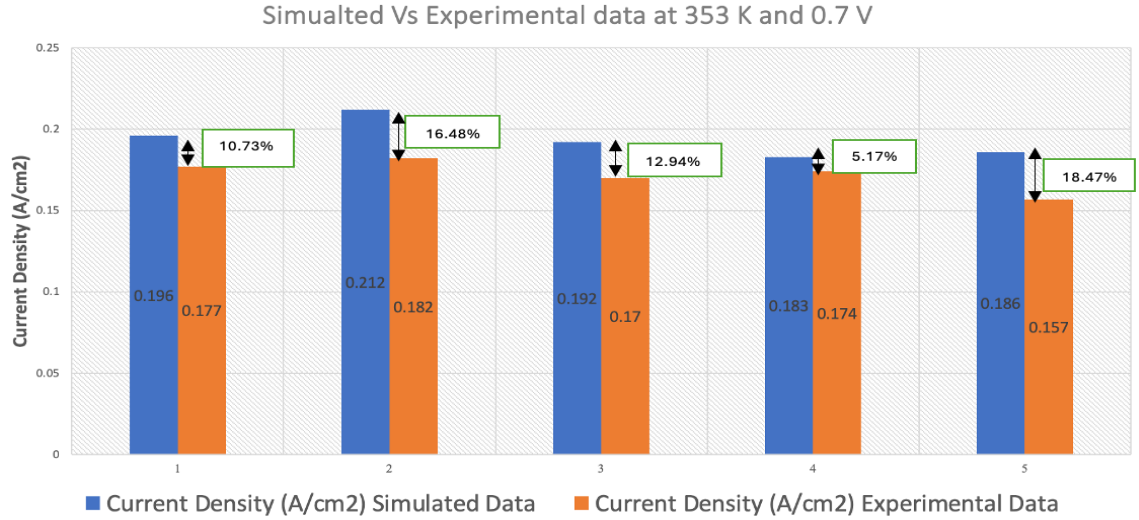


Figure 5.5 - Comparison of simulated and experimental data of PEMFC in 353K temperature at 0.7 V voltage

Figures 5.4 and 5.5 depict the comparison between simulated and experimental results for all five configurations. The results for each configuration are provided and discussed below.

Figure 5.4 presents the data results at 0.7V and 368K (95°C) for different configurations:

11.Configuration 1 (RP & RP): The simulated current density is 0.207 A/cm², while the experimental current density is 0.189 A/cm². The percentage error between the simulated and experimental current density is 9.52%.

12.Configuration 2 (ADS & RP): The simulated current density is 0.234 A/cm², while the experimental current density is 0.204 A/cm². The percentage error between the simulated and experimental current density is 14.71%

13.Configuration 3 (AUS & RP): The simulated current density is 0.199 A/cm², while the experimental current density is 0.18 A/cm².

The percentage error between the simulated and experimental current density is 10.55%

14. Configuration 4 (RP & CDS): The simulated current density is 0.197 A/cm², while the experimental current density is 0.184 A/cm². The percentage error between the simulated and experimental current density is 7.06%

15. Configuration 5 (RP & CUS): The simulated current density is 0.18 A/cm², while the experimental current density is 0.166 A/cm². The percentage error between the simulated and experimental current density is 8.43%

Figure 5.5 presents the data results at 0.7V and 353K (80°C) for different configurations:

- 1. Configuration 1 (RP & RP):** The simulated current density is 0.196 A/cm², while the experimental current density is 0.177 A/cm². The percentage error between the simulated and experimental current density is 10.73%.
- 2. Configuration 2 (ADS & RP):** The simulated current density is 0.212 A/cm², while the experimental current density is 0.182 A/cm². The percentage error between the simulated and experimental current density is 16.48%
- 3. Configuration 3 (AUS & RP):** The simulated current density is 0.192 A/cm², while the experimental current density is 0.17 A/cm². The percentage error between the simulated and experimental current density is 12.94%
- 4. Configuration 4 (RP & CDS):** The simulated current density is 0.183 A/cm², while the experimental current density is 0.174 A/cm².

The percentage error between the simulated and experimental current density is 5.17%

5. **Configuration 5 (RP & CUS):** The simulated current density is 0.186 A/cm², while the experimental current density is 0.157 A/cm². The percentage error between the simulated and experimental current density is 18.47%

These results indicate the percentage errors between the simulated and experimental current densities for each configuration at the specified operating conditions. The results indicates that the current density is inversely proportional to the voltage drop in the circuit, given other factors remain constant.

The variation between the simulated and experimental results can be attributed to several factors, including assumptions made in the model, such as neglecting leakage and acculturation of rounding off errors. Despite these challenges, the study presented results within a reasonable range of expectations for PEM fuel cells and achieved a good agreement between the simulated and experimental results. This indicated that the model effectively captured the underlying behavior of the system, contributing to a comprehensive understanding of the performance of PEM fuel cells under different configurations and operating conditions.

The details of the various parameters of the experimental validation design simulation of the PEMFC has been provided in the table 5.3.

Table 5.3 - Details of the various parameters of experimental validation design simulation of PEMFC

S.No	Categories / Factors	Experimental – Validation Simulation
1	Active Area of the Cell	150 cm ²
2	Material of Anode and Cathode Flow Plate	Bipolar Graphite
3	Material of Anode and Cathode Catalyst Layer	0.4mg/cm ² platinum
4	Material of Anode and Cathode GDL	GDL 10 BA
5	Material of Membrane	Nafion 112
6	Stoichiometry of Hydrogen (H ₂) at Anode	1.7
7	Stoichiometry of Air at Cathode	2.2
8	Voltage (V)	0.5 and 0.7
9	Temperature (K)	353 and 368
10	Operating Pressure (Bar)	1.5
11	Porosity of GDL	0.6
12	Porosity of Catalyst Layer	0.6
13	Electric Potential	1.5
14	Water Content	1.5
15	Protonic Potential	1.5
16	Momentum	0.7

Table 5.3 - continued

17	Pressure	0.3
18	Water Saturation	1.5

The simulation of the experimental – validation phase is driven by several crucial factors. This demonstrates that the model is captured the inherent behavior of the system, leading to a holistic grasp of PEM fuel cell performance across diverse configurations and operational conditions. Next, the chapter 6 deals with the simulation of the three serpentine configurations and polarization curves results are explained.

CHAPTER 6

PEMFC SERPENTINE CONFIGURATION RESULTS

With the satisfactory validation of simulated results against experimental data, this chapter presents the simulation outcomes for all three serpentine configurations. The polarization curve results are summarized below, with detailing findings elaborated in chapter 9.

6.1 Design and Simulation of Flow Channel of PEMFC

Three different fuel cells equipped with varying flow channels designs are described below. Each fuel cell is distinguished by the dimension of its flow channel. They are single serpentine flow channel, bi serpentine flow channel and tri serpentine flow channel. Each of these fuel cells presents unique characteristics and performance attributes based on their respective flow channel designs, offering insights into the impact of flow channel dimension on fuel cell behavior. The design details of the PEMFC's are outlined in table 4.2.

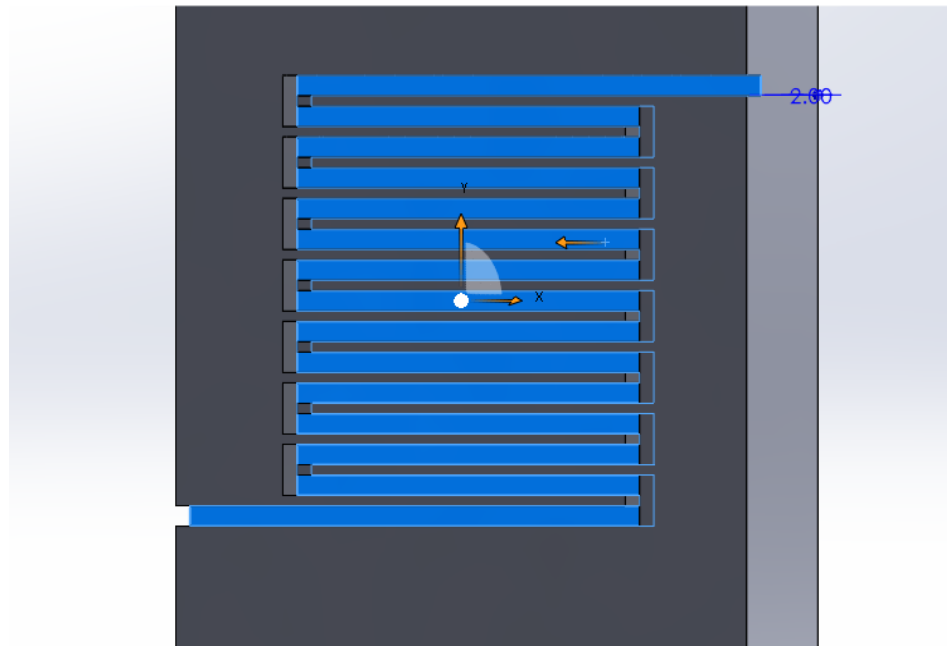


Figure 6.1- 2mm flow channel width of single serpentine PEMFC

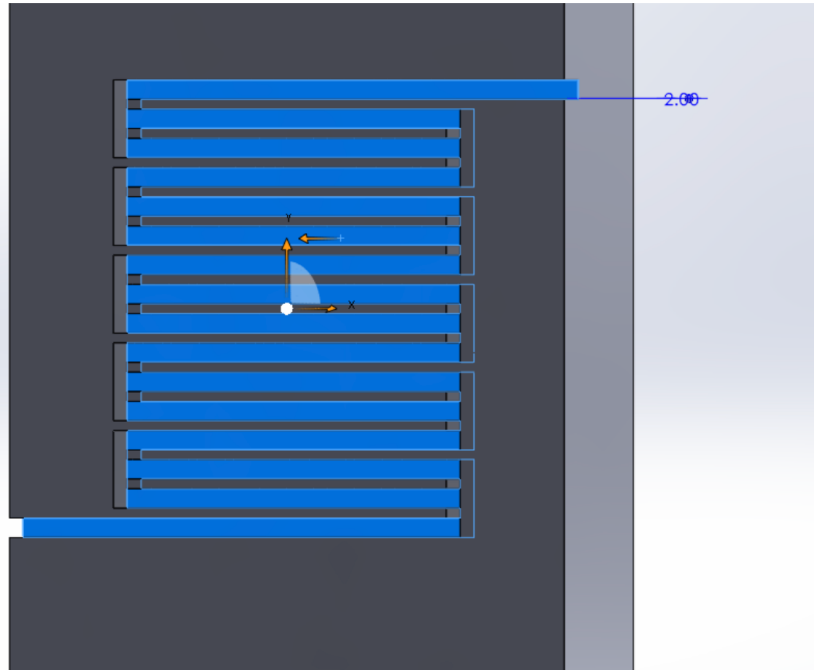


Figure 6.2 - 2mm flow channel width of bi-serpentine flow channel PEMFC

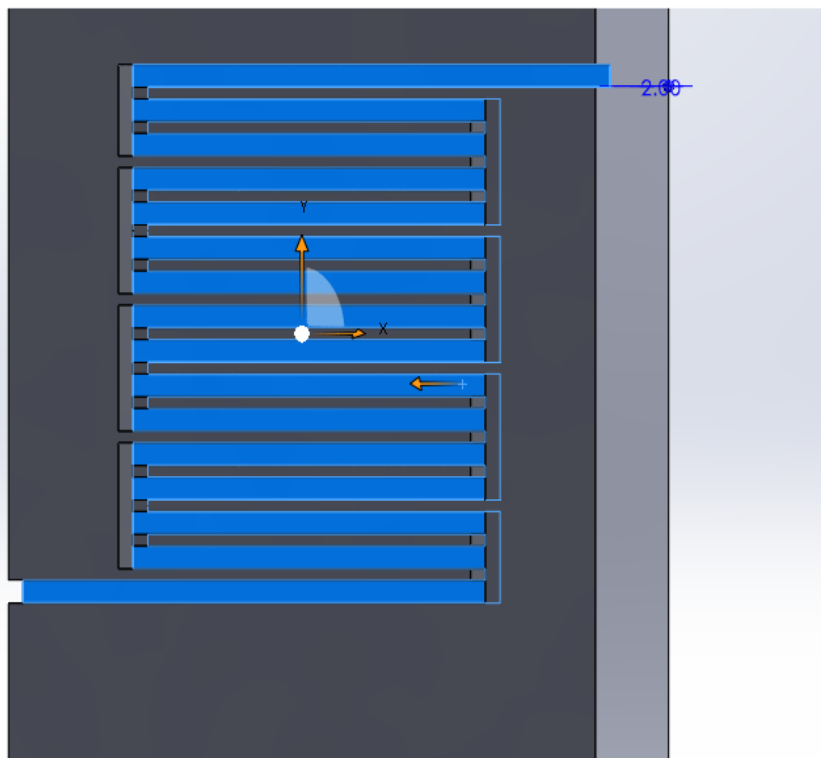


Figure 6.3 - 2mm flow channel width of tri-serpentine flow channel PEMFC

All PEMFCs are simulated with active area of 25cm^2 , employing various parameters as outlined in the table 4.3. The polarization curve graph illustrates Voltage (V) on the primary Y-axis, Power Density (W/cm^2) on the secondary Y-axis, with Current Density (A/cm^2) represented on the X-axis. This graph features Voltage-Current (V-I) and Power-Current (P-I) curves for single, bi, and tri serpentine flow channel configurations of PEMFCs.

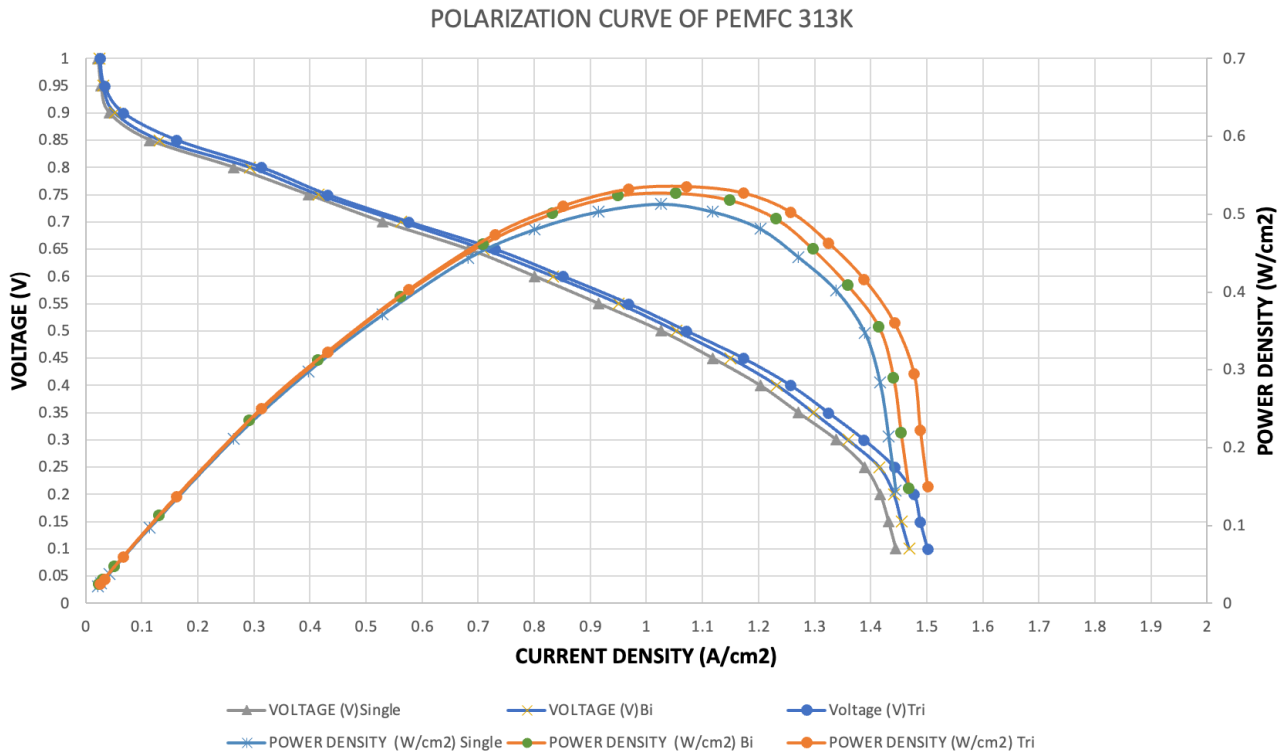


Figure 6.4 - Polarization curve of PEMFC at 313K and 2 bar pressure

Table 6.1 - Results of PEMFC at 313K and 2 bar pressure

Temperature (K)	Flow Channel Pattern	Voltage (V)	Current Density (A/cm ²)	Peak Power Density (W/cm ²)
313K (40°C)	Single Serpentine	0.5	1.026	0.513
313K (40°C)	Bi Serpentine	0.5	1.053	0.5265
313K (40°C)	Tri Serpentine	0.5	1.071	0.5355

Figure 6.4 displays the polarization curve of the PEMFC at 313K and 2 bar pressure, while table 6.1 presents the corresponding results. In the single serpentine flow channel, the maximum current density is measured at 1.026 A/cm², yielding a corresponding power density of 0.513 W/cm² at 0.5 V. Similarly, in the bi serpentine flow channel, the maximum current density is recorded as 1.053 A/cm², resulting in a power density of 0.5265 W/cm² at 0.5 V. Lastly, in the tri serpentine flow channel, the maximum current density is determined to be 1.071 A/cm², corresponding to a power density is 0.5355 W/cm² at 0.5 V.

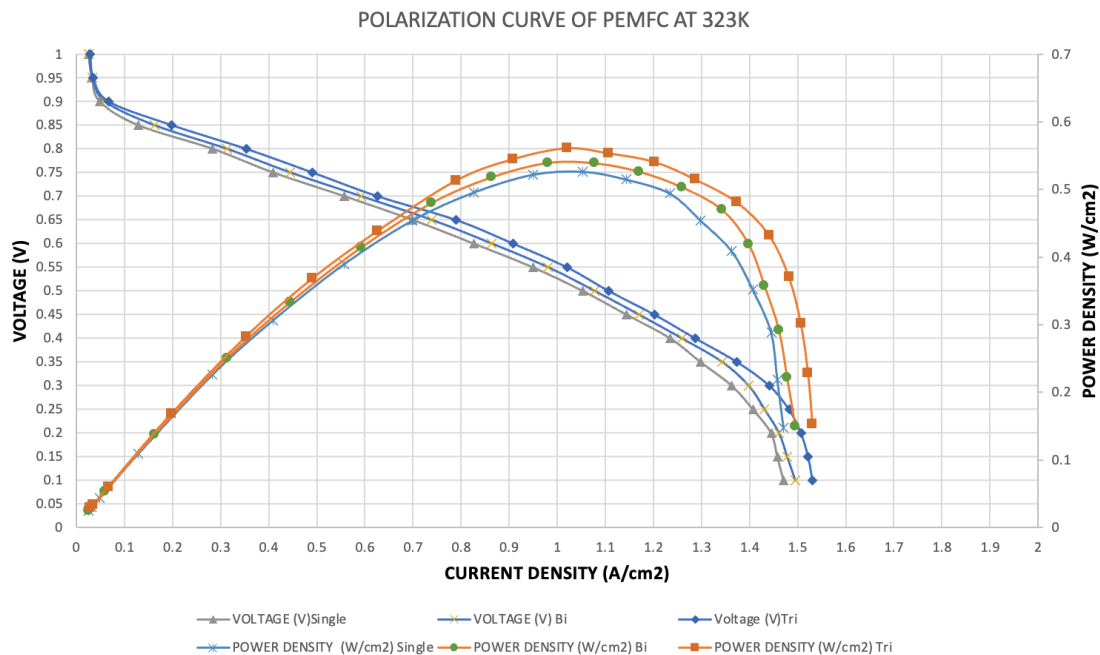


Figure 6.5 - Polarization curve of PEMFC at 323K and 2 bar pressure

Table 6.2 - Results of PEMFC at 323K and 2 bar pressure

Temperature (K)	Flow Channel Pattern	Voltage (V)	Current Density (A/cm ²)	Peak Power Density (W/cm ²)
323K (50°C)	Single Serpentine	0.5	1.053	0.526
323K (50°C)	Bi Serpentine	0.5	0.981	0.539
323K (50°C)	Tri Serpentine	0.55	1.02	0.55

Figure 6.5 displays the polarization curve of the PEMFC at 323K and 2 bar pressure, while table 6.2 presents the corresponding results. In the single serpentine flow channel, the maximum current density is measured at 1.053

A/cm², yielding a corresponding power density of 0.526 W/cm² at 0.5 V. Similarly, in the bi serpentine flow channel, the maximum current density is recorded as 0.981 A/cm², resulting in a power density of 0.539 W/cm² at 0.5 V. Lastly, in the tri serpentine flow channel, the maximum current density is determined to be 1.02 A/cm², corresponding to a power density is 0.55 W/cm² at 0.55 V.

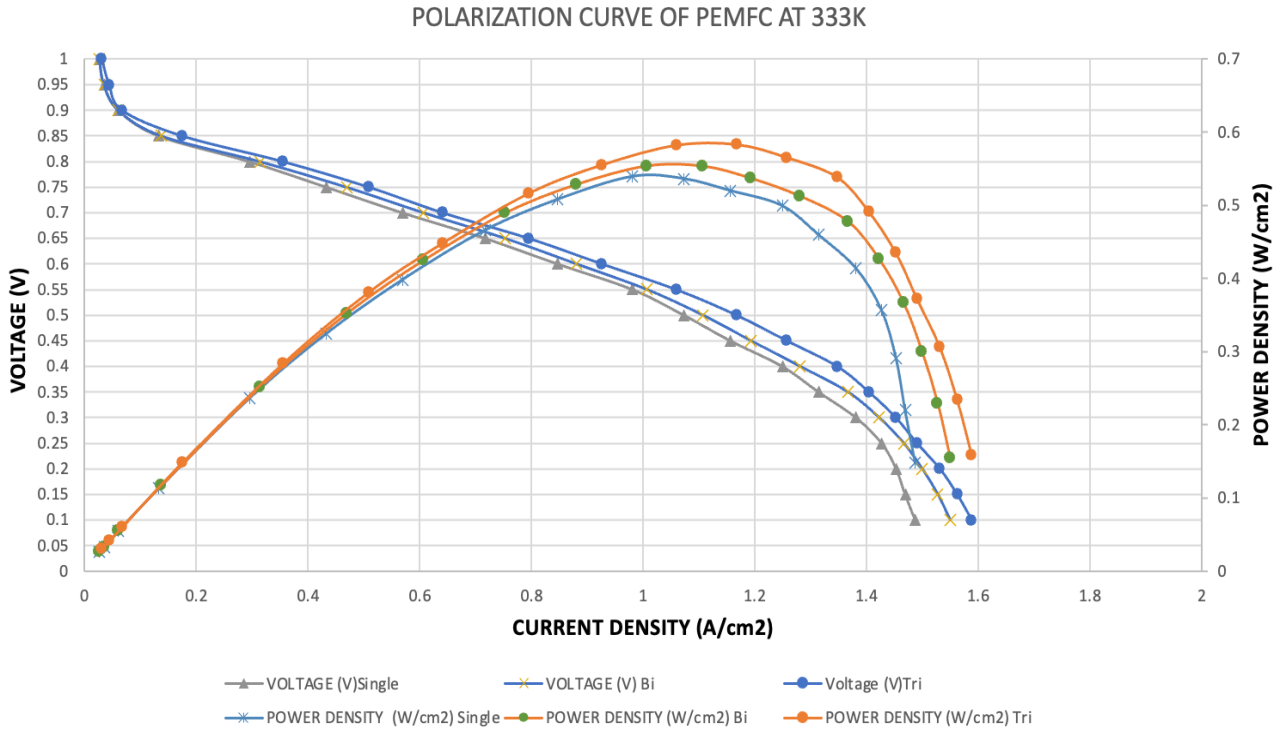


Figure 6.6 - Polarization curve of PEMFC at 333K and 2 bar pressure

Table 6.3 - Results of PEMFC at 333K and 2 bar pressure

Temperature (K)	Flow Channel Pattern	Voltage (V)	Current Density (A/cm ²)	Peak Power Density (W/cm ²)
333K (60°C)	Single Serpentine	0.55	0.982	0.54
333K (60°C)	Bi Serpentine	0.55	1.007	0.554
333K (60°C)	Tri Serpentine	0.5	1.167	0.583

Figure 6.6 displays the polarization curve of the PEMFC at 333K and 2 bar pressure, while table 6.3 presents the corresponding results. In the single serpentine flow channel, the maximum current density is measured at 0.982 A/cm², yielding a corresponding power density of 0.54 W/cm² at 0.55 V. Similarly, in the bi serpentine flow channel, the maximum current density is recorded as 1.007 A/cm², resulting in a power density of 0.554 W/cm² at 0.55 V. Lastly, in the tri serpentine flow channel, the maximum current density is determined to be 1.167 A/cm², corresponding to a power density is 0.583 W/cm² at 0.5 V.

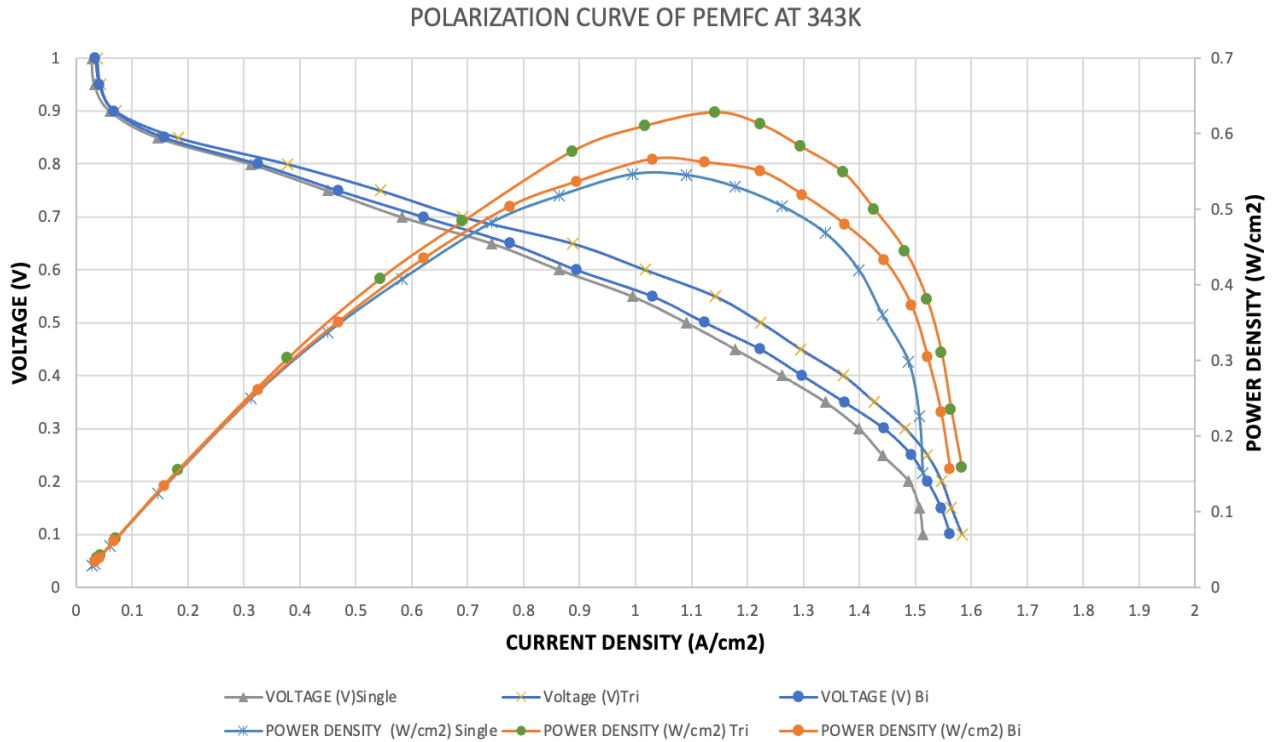


Figure 6.7 - Polarization curve of PEMFC at 343K and 2 bar pressure

Table 6.4 - Results of PEMFC at 343K and 2 bar pressure

Temperature (K)	Flow Channel Pattern	Voltage (V)	Current Density (A/cm ²)	Peak Power Density (W/cm ²)
343K (70°C)	Single Serpentine	0.55	0.994	0.5467
343K (70°C)	Bi Serpentine	0.55	1.03	0.5665
343K (70°C)	Tri Serpentine	0.55	1.142	0.6281

Figure 6.7 displays the polarization curve of the PEMFC at 343K and 2 bar pressure, while table 6.4 presents the corresponding results. In the single

serpentine flow channel, the maximum current density is measured at 0.994 A/cm², yielding a corresponding power density of 0.5467 W/cm² at 0.55 V. Similarly, in the bi serpentine flow channel, the maximum current density is recorded as 1.03 A/cm², resulting in a power density of 0.5665 W/cm² at 0.55 V. Lastly, in the tri serpentine flow channel, the maximum current density is determined to be 1.142 A/cm², corresponding to a power density is 0.6281 W/cm² at 0.55 V.

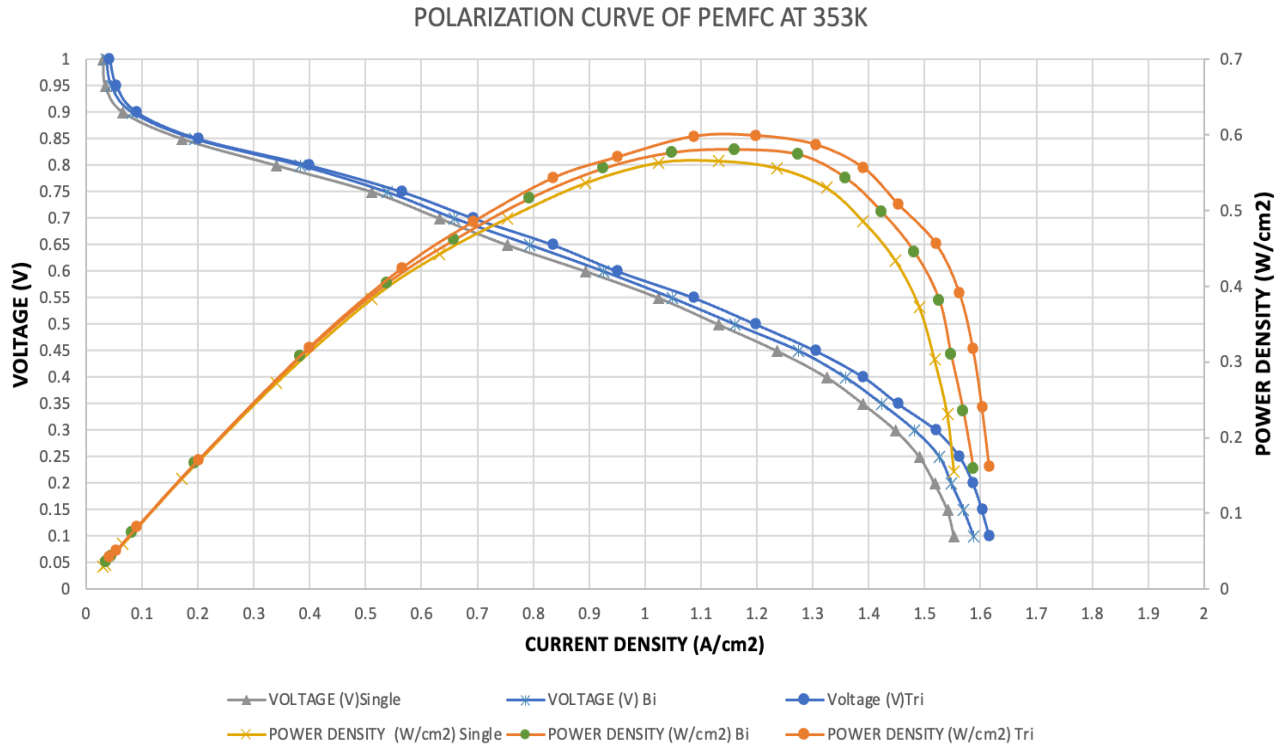


Figure 6.8 - Polarization curve of PEMFC at 353K and 2 bar pressure

Table 6.5 - Results of PEMFC at 353K and 2 bar pressure

Temperature (K)	Flow Channel Pattern	Voltage (V)	Current Density (A/cm ²)	Peak Power Density (W/cm ²)
353K (80°C)	Single Serpentine	0.5	1.131	0.5655
353K (80°C)	Bi Serpentine	0.5	1.161	0.5805
353K (80°C)	Tri Serpentine	0.5	1.198	0.599

Figure 6.8 displays the polarization curve of the PEMFC at 353K and 2 bar pressure, while table 6.5 presents the corresponding results. In the single serpentine flow channel, the maximum current density is measured at 1.131 A/cm², yielding a corresponding power density of 0.5655 W/cm² at 0.5 V. Similarly, in the bi serpentine flow channel, the maximum current density is recorded as 1.161 A/cm², resulting in a power density of 0.5805 W/cm² at 0.5 V. Lastly, in the tri serpentine flow channel, the maximum current density is determined to be 1.198 A/cm², corresponding to a power density is 0.599 W/cm² at 0.5 V.

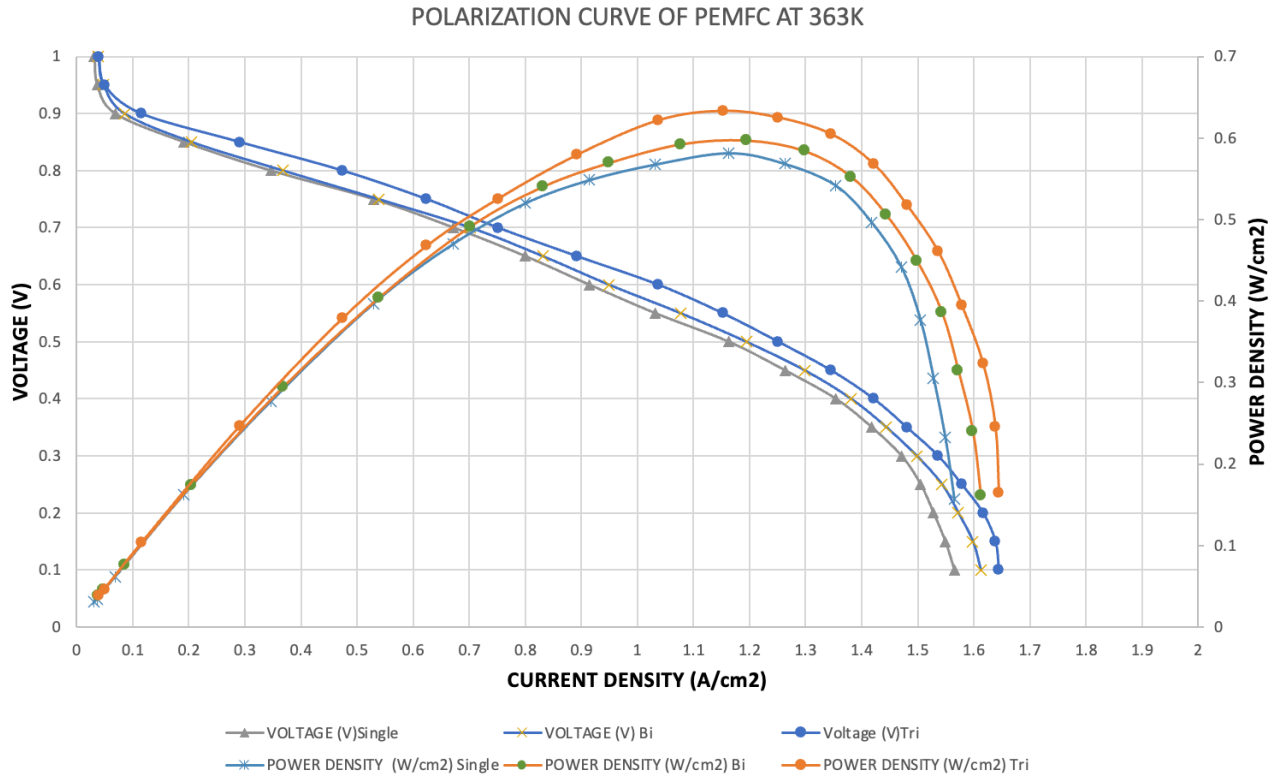


Figure 6.9 - Polarization curve of PEMFC at 363K and 2 bar pressure

Table 6.6 - Results of PEMFC at 363K and 2 bar pressure

Temperature (K)	Flow Channel Pattern	Voltage (V)	Current Density (A/cm ²)	Peak Power Density (W/cm ²)
363K (90°C)	Single Serpentine	0.5	1.163	0.5815
363K (90°C)	Bi Serpentine	0.5	1.194	0.597
363K (90°C)	Tri Serpentine	0.55	1.152	0.6336

Figure 6.9 displays the polarization curve of the PEMFC at 363K and 2 bar pressure, while table 6.6 presents the corresponding results. In the single serpentine flow channel, the maximum current density is measured at 1.163 A/cm², yielding a corresponding power density of 0.5815 W/cm² at 0.5 V. Similarly, in the bi serpentine flow channel, the maximum current density is recorded as 1.194 A/cm², resulting in a power density of 0.597 W/cm² at 0.5 V. Lastly, in the tri serpentine flow channel, the maximum current density is determined to be 1.152 A/cm², corresponding to a power density is 0.6336 W/cm² at 0.55 V.

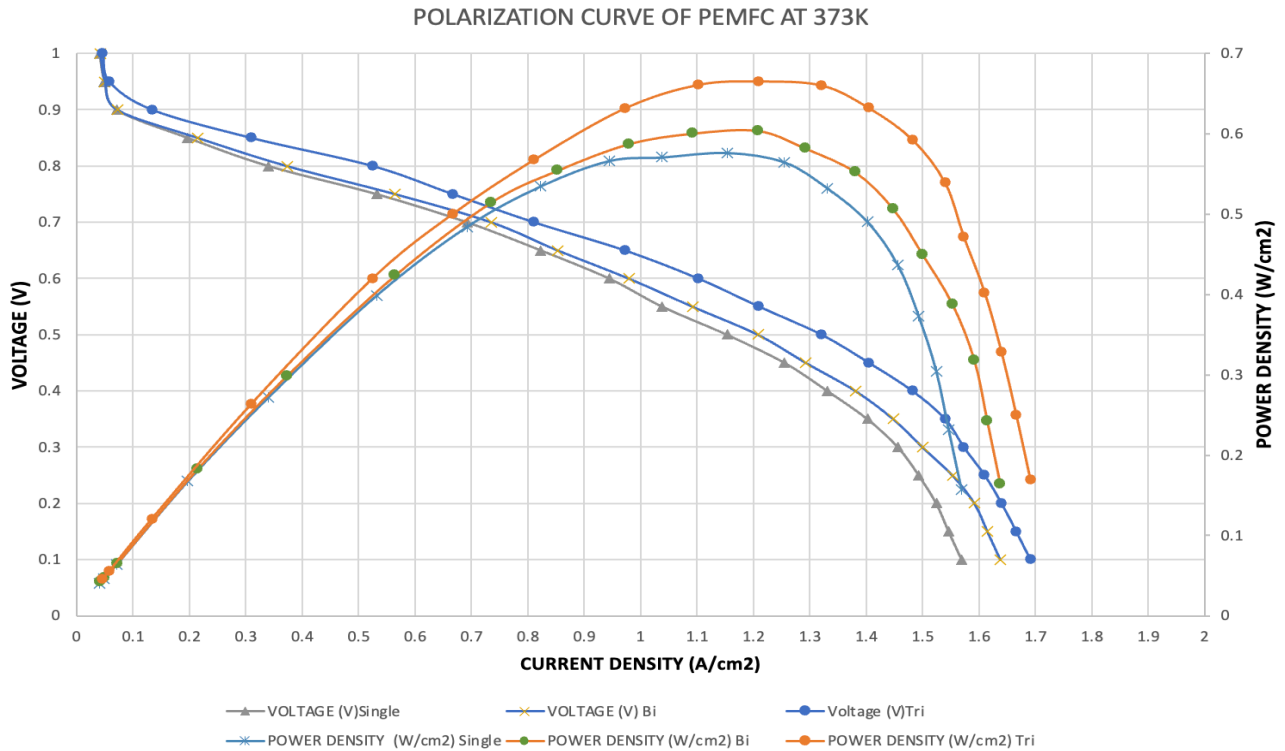


Figure 6.10 – Polarization curve of PEMFC at 373K and 2 bar pressure

Table 6.7 - Results of PEMFC at 373K and 2 bar pressure

Temperature (K)	Flow Channel Pattern	Voltage (V)	Current Density (A/cm ²)	Peak Power Density (W/cm ²)
373K (100°C)	Single Serpentine	0.5	1.153	0.5765
373K (100°C)	Bi Serpentine	0.5	1.208	0.604
373K (100°C)	Tri Serpentine	0.55	1.12	0.6655

Figure 6.10 displays the polarization curve of the PEMFC at 373K and 2 bar pressure, while table 6.7 presents the corresponding results. In the single serpentine flow channel, the maximum current density is measured at 1.153 A/cm², yielding a corresponding power density of 0.5765 W/cm² at 0.5 V. Similarly, in the bi serpentine flow channel, the maximum current density is recorded as 1.208 A/cm², resulting in a power density of 0.604 W/cm² at 0.5 V. Lastly, in the tri serpentine flow channel, the maximum current density is determined to be 1.12 A/cm², corresponding to a power density is 0.6655 W/cm² at 0.55 V.

These results provide insights into the performance characteristics of different flow channel configurations in the PEMFC at the specified temperature.

Chapter 5 delves into the validation phase, offering a detailed comparison between experimental and simulation data. Notably, the author's design

simulations exhibit distinct differences within their respective categories, influenced by a range of factors elucidated in the provided table 6.8.

Table 6.8 – Experimental validation design simulation and author’s design simulation

S.No	Categories / Factors	Experimental – Validation Design Simulation	Author’s Design Simulation
1	Active Area of the Cell	150 cm ²	25 cm ²
2	Anode and Cathode Flow Plate Dimension (L X W X T)	200 X 200 X 10 mm	80 X 80 X 10 mm
3	Anode and Cathode Catalyst Dimension (L X W X T)	173.4 X 86.5 X 0.4 mm	80 X 80 X 0.08 mm
4	Anode and Cathode GDL Dimension (L X W X T)	173.4 X 86.5 X 0.4 mm	80 X 80 X 0.3 mm
5	Membrane Dimension (L X W X T)	173.4 X 86.5 X 0.4 mm	80 X 80 X 0.127 mm
6	Flow Channel Width	1.5 mm	2 mm
7	Material of Anode and Cathode Flow Plate	Bipolar Graphite	Bipolar Graphite

Table 6.8 - continued

8	Material of Anode and Cathode Catalyst Layer	0.4mg/cm ² platinum	Carbon 0.5 mg/cm ² platinum
9	Material of Anode and Cathode GDL	GDL 10 BA	Tetra Fluoro Polyethylene
10	Material of Membrane	Nafion 112	Nafion
11	Mass flow rate / Stoichiometry of Hydrogen (H ₂) Anode	1.7	4.33 e ⁻⁰⁷ (Kg/s)
12	Mass flow rate of Oxygen (O ₂) and Stoichiometry of Air at Cathode	2.2	3.33 e ⁻⁰⁶ (Kg/s)
13	Voltage (V)	0.5 and 0.7	0.1, 0.15, 0.2, 0.25,1
14	Temperature (K)	353 and 368	313, 323, 333, 343, 353, 363, 373
15	Operating Pressure (Bar)	1.5	2
16	Porosity of GDL	0.6	0.4
17	Porosity of Catalyst Layer	0.6	0.5
18	Electric Potential	1.5	0.75
19	Water Content	1.5	0.75
20	Protonic Potential	1.5	0.75
21	Momentum	0.7	0.3

Table 6.8 - continued

22	Pressure	0.3	0.7
23	Water Saturation	1.5	0.75

The differences between the validation design simulation and the author's design simulation lie in various factors: geometric dimensions, material properties, operating conditions, and user defined specifications, each having distinct values. These differences in parameters contribute to the variations in results between the two simulations.

In evaluating the performance of three different flow channel patterns, it becomes evident that the tri serpentine flow channel produces the higher power density than single and bi serpentine. By comparing all the flow channels, tri serpentine flow channel emerges the highest power density, followed by bi serpentine and single serpentine flow channel. This is due to the various factors such as pressure distribution, velocity, mass fraction of the reactant etc. The analysis of the PEMFC is discussed in detail at chapter 7.

CHAPTER 7

ANALYSIS OF PEMFC

In this chapter, the primary focus is on the simulation and analysis of various parameters crucial for fuel cell performance. Specifically, the pressure distribution, mass fraction of hydrogen (H_2), velocity magnitude and cell Reynolds number. All the analysis has been done at 2 bar pressure and 373K (100°C) temperature. Notably, the stoichiometric ratio at the anode is set at 1.5 ensure optimal operating conditions. The study encompasses an examination of three distinct flow channel designs to comprehensively understand their impact on fuel cell behavior and efficiency. Additionally, the study's analysis was conducted across distinct stages: low (0.25V), medium (0.35V), and high (0.5V), very high (0.65V) and extreme (0.8V) in order to compare the outcomes at each level.

7.1 Pressure Distribution of the PEMFC

To enhance performance, optimizing pressure distribution is a crucial factor. The simulation is carried out across all the three designs of flow channel of PEMFC to understand their impact on pressure distribution. The primary aim is to identify the strategies for improving fuel cell performance through effective pressure management.

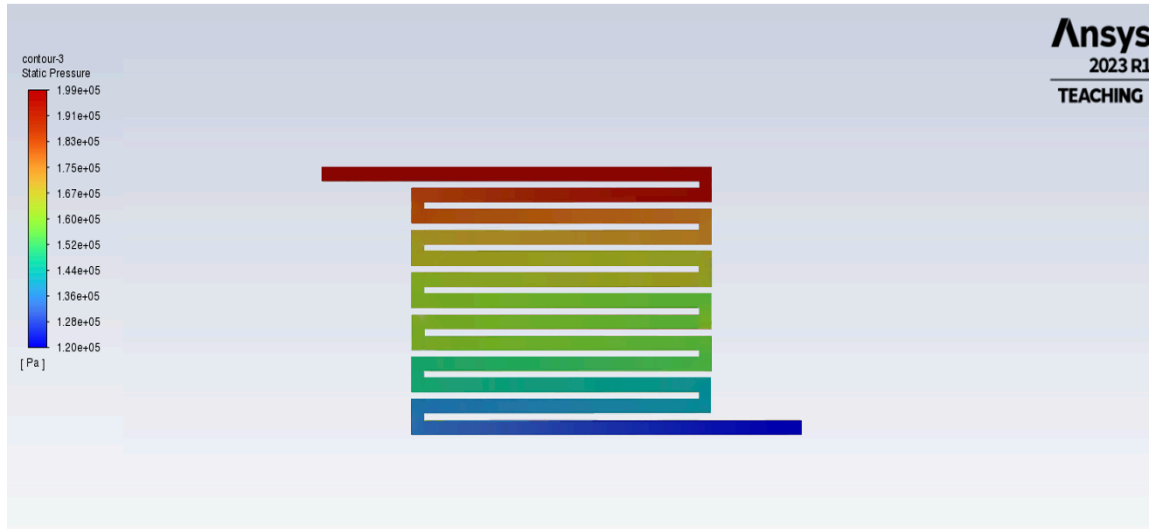


Figure 7.1 - Pressure distribution of 2mm flow channel width of single serpentine PEMFC at 0.25V (low)

Figure 7.1 illustrates the pressure distribution of 2mm flow channel width of the single serpentine PEMFC at 0.25V. At the flow channel inlet, the initial pressure is recorded as 199KPa, while at the outlet, the pressure is measured at 120KPa. Consequently, the pressure drop at the single serpentine flow channel is calculated to be 79KPa. The corresponding current density and power density for figure 7.1 is 1.513 (A/Cm²) and 0.3782 (W/Cm²) respectively.

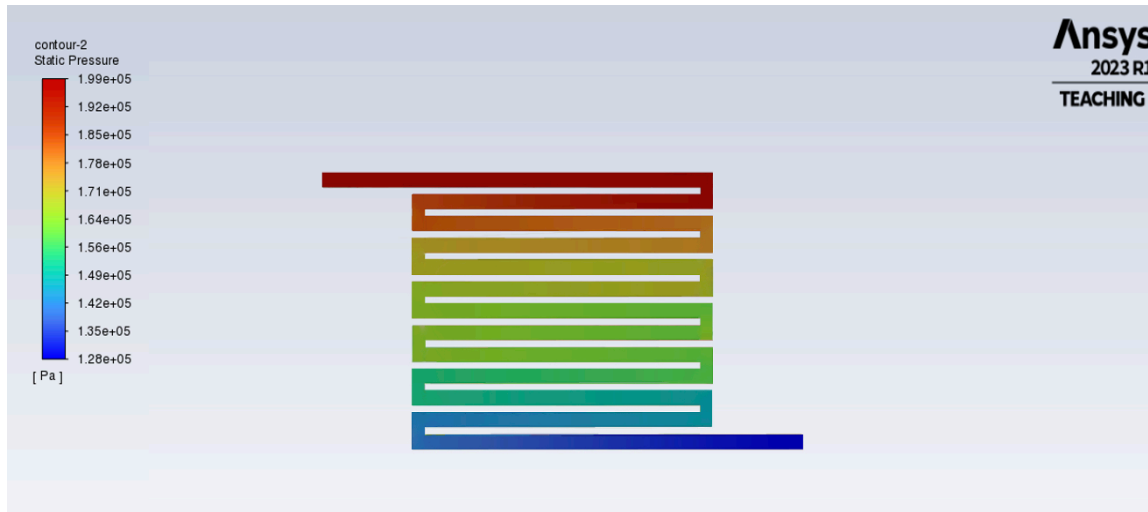


Figure 7.2 - Pressure distribution of 2mm flow channel width of single serpentine PEMFC at 0.35V (medium)

Figure 7.2 illustrates the pressure distribution of 2mm flow channel width of the single serpentine PEMFC at 0.35 V. At the flow channel inlet, the initial pressure is recorded as 199KPa, while at the outlet, the pressure is measured at 128KPa. Consequently, the pressure drop at the single serpentine flow channel is calculated to be 71KPa. The corresponding current density and power density for figure 7.2 is 1.432 (A/Cm²) and 0.5012 (W/ Cm²) respectively.

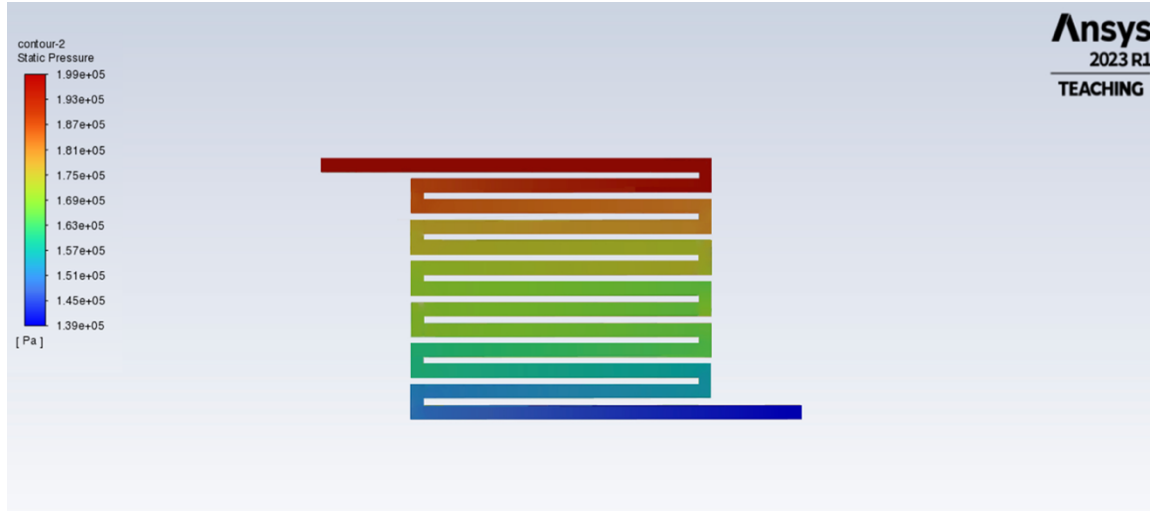


Figure 7.3 - Pressure distribution of 2mm flow channel width of single serpentine PEMFC at 0.5V (high)

Figure 7.3 illustrates the pressure distribution of 2mm flow channel width of the single serpentine PEMFC at 0.5 V. At the flow channel inlet, the initial pressure is recorded as 199KPa, while at the outlet, the pressure is measured at 139KPa. Consequently, the pressure drop at the single serpentine flow channel is calculated to be 60KPa. The corresponding current density and power density for figure 7.3 is 1.173 (A/Cm²) and 0.5865 (W/ Cm²) respectively.

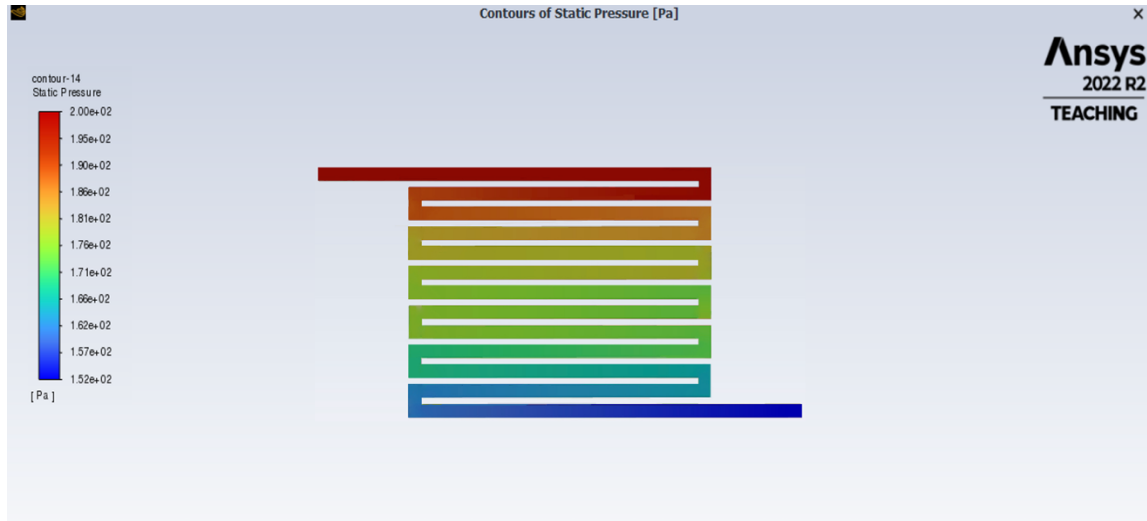


Figure 7.4 - Pressure distribution of 2mm flow channel width of single serpentine PEMFC at 0.65 V (very high)

Figure 7.4 illustrates the pressure distribution of 2mm flow channel width of the single serpentine PEMFC at 0.65 V. At the flow channel inlet, the initial pressure is recorded as 200KPa, while at the outlet, the pressure is measured at 152KPa. Consequently, the pressure drop at the single serpentine flow channel is calculated to be 48KPa. The corresponding current density and power density for figure 7.4 is 0.833 (A/Cm²) and 0.5414 (W/Cm²) respectively.

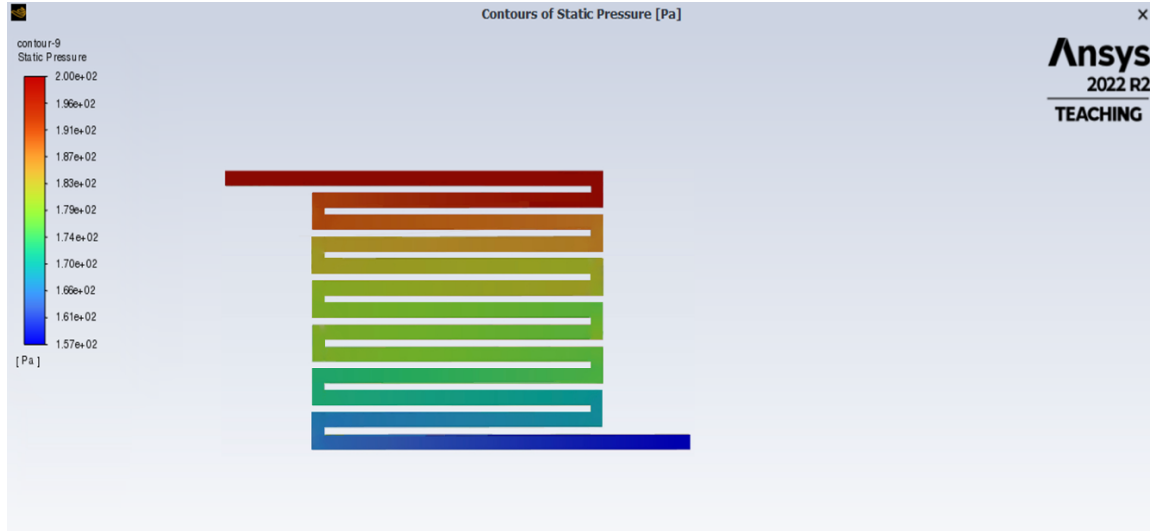


Figure 7.5 - Pressure distribution of 2mm flow channel width of single serpentine PEMFC at 0.8 V (extreme)

Figure 7.5 illustrates the pressure distribution of 2mm flow channel width of the single serpentine PEMFC at 0.8 V. At the flow channel inlet, the initial pressure is recorded as 200KPa, while at the outlet, the pressure is measured at 157KPa. Consequently, the pressure drop at the single serpentine flow channel is calculated to be 43KPa. The corresponding current density and power density for figure 7.5 is 0.34 (A/Cm²) and 0.272 (W/Cm²) respectively.

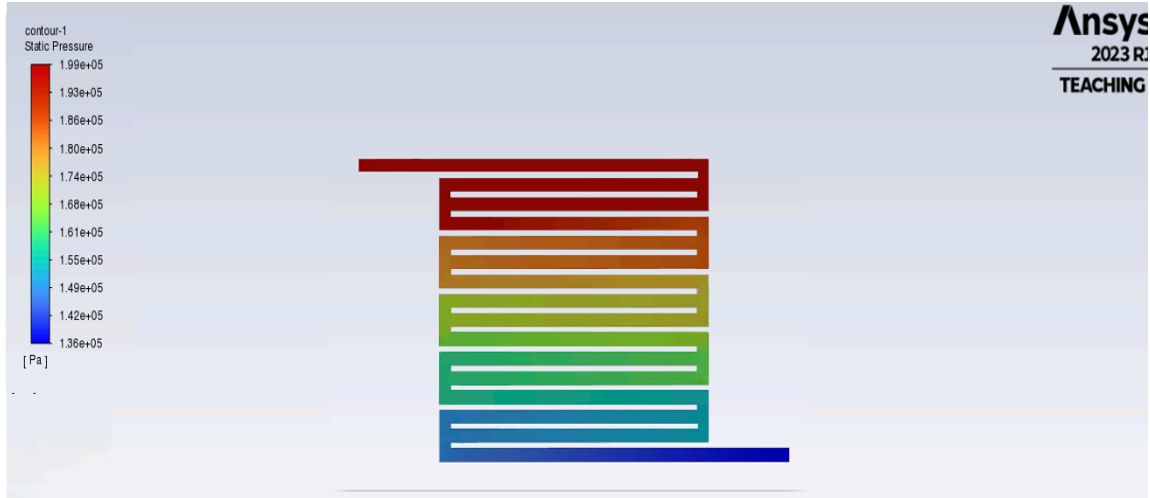


Figure 7.6 - Pressure distribution of 2mm flow channel width of bi serpentine PEMFC at 0.25 V (low)

Figure 7.6 illustrates the pressure distribution of 2mm flow channel width of bi serpentine PEMFC at 0.25 V. At the flow channel inlet, the initial pressure is recorded as 199KPa, while at the outlet, the pressure is measured at 136KPa. Consequently, the pressure drop at the bii serpentine flow channel is calculated to be 63KPa. The corresponding current density and power density for figure 7.6 is 1.553 (A/Cm²) and 0.388 (W/Cm²) respectively.

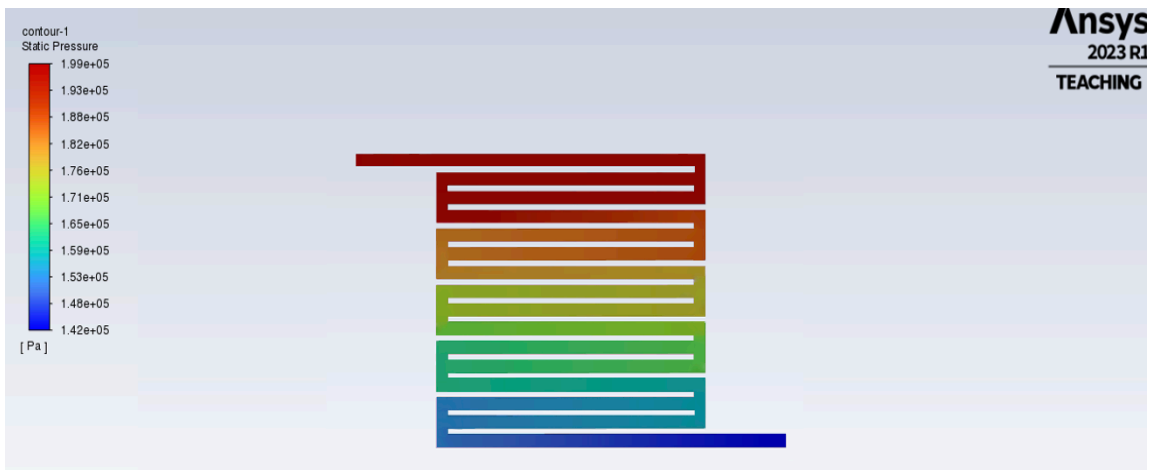


Figure 7.7 - Pressure distribution of 2mm flow channel width of bi serpentine flow channel at 0.35V (medium)

Figure 7.7 illustrates the pressure distribution of 2mm flow channel width of the bi serpentine PEMFC at 0.35 V. At the flow channel inlet, the initial pressure is recorded as 199KPa, while at the outlet, the pressure is measured at 142KPa. Consequently, the pressure drop at the bi serpentine flow channel is calculated to be 57KPa. The corresponding current density and power density for figure 7.7 is 1.448 (A/Cm²) and 0.5068 (W/Cm²) respectively.

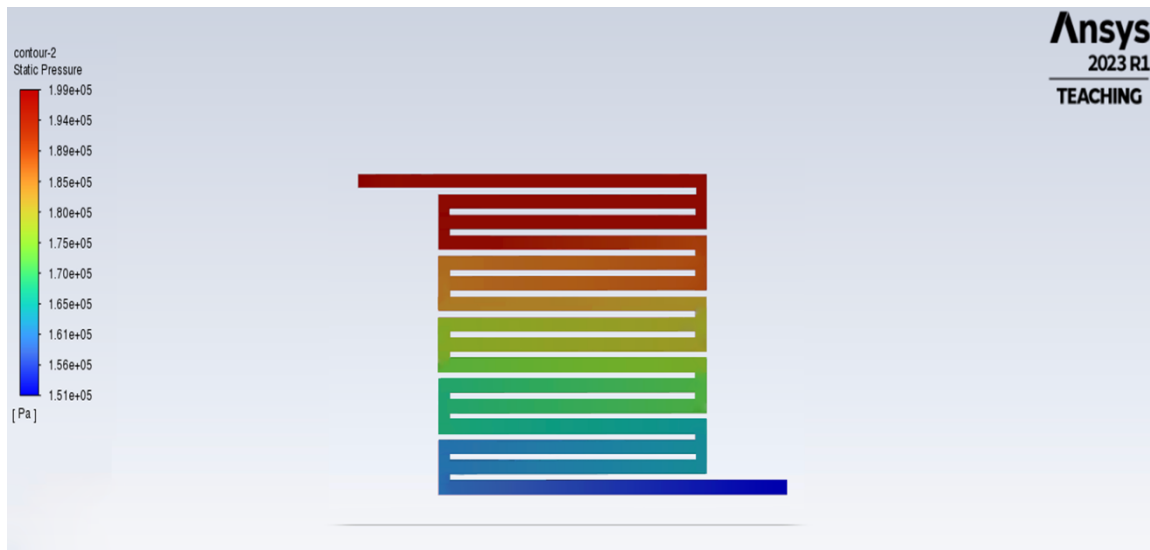


Figure 7.8- Pressure distribution of 2mm flow channel width of bi serpentine PEMFC at 0.5V (high)

Figure 7.8 illustrates the pressure distribution of 2mm flow channel width of bi serpentine PEMFC at 0.5V. At the flow channel inlet, the initial pressure is recorded as 199KPa, while at the outlet, the pressure is measured at 151KPa. Consequently, the pressure drop at the bi serpentine flow channel is calculated to be 48KPa. The corresponding current density and power density for figure 7.8 is 1.208 (A/Cm²) and 0.604 (W/Cm²) respectively.

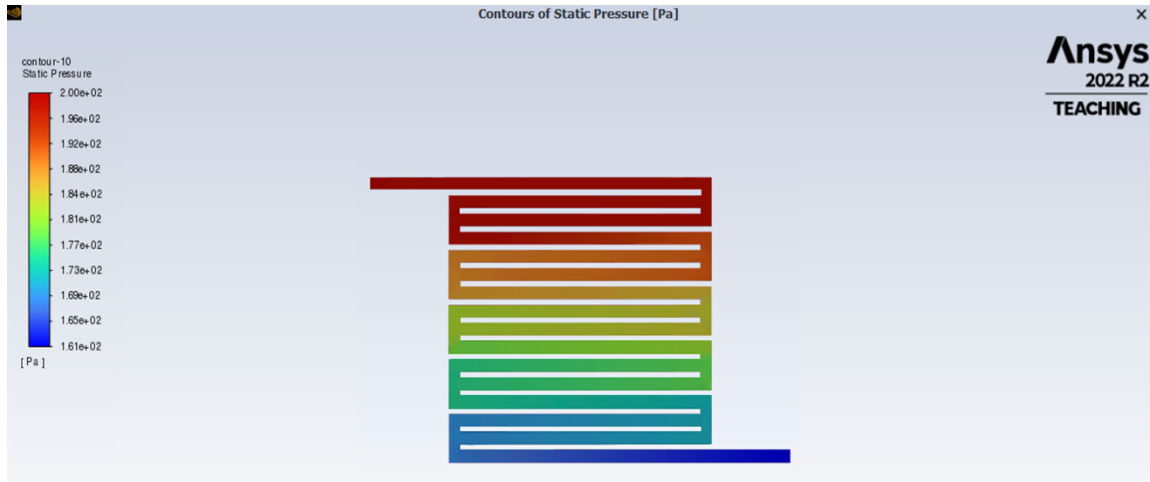


Figure 7.9- Pressure distribution of 2mm flow channel width of bi serpentine PEMFC at 0.65V (very high)

Figure 7.9 illustrates the pressure distribution of 2mm flow channel width of bi serpentine PEMFC at 0.65V. At the flow channel inlet, the initial pressure is recorded as 200KPa, while at the outlet, the pressure is measured at 161KPa. Consequently, the pressure drop at the bi serpentine flow channel is calculated to be 39KPa. The corresponding current density and power density for figure 7.9 is 0.853 (A/Cm²) and 0.5544 (W/Cm²) respectively.

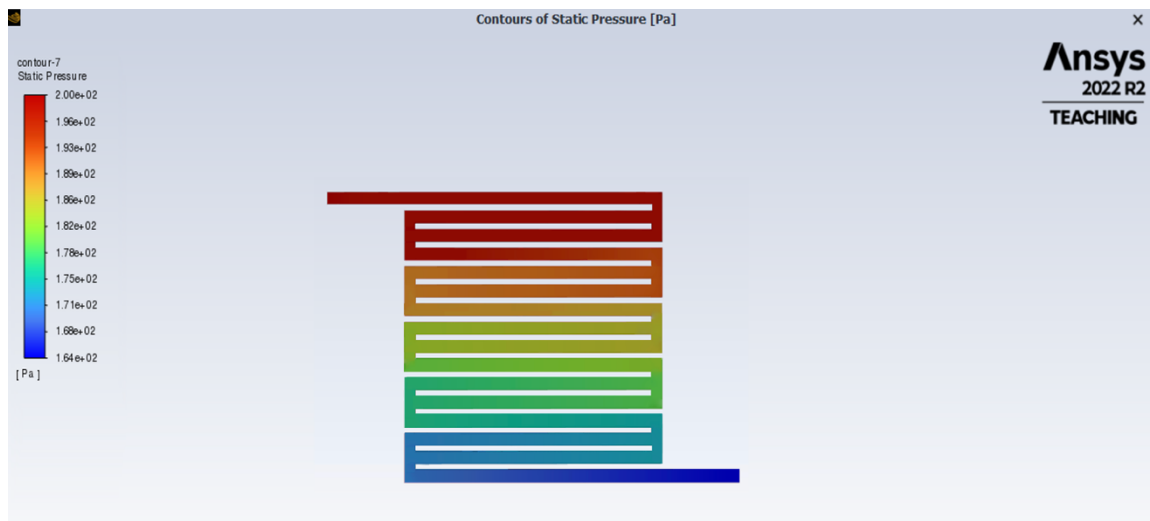


Figure 7.10- Pressure distribution of 2mm flow channel width of bi serpentine PEMFC at 0.8V (extreme)

Figure 7.10 illustrates the pressure distribution of 2mm flow channel width of bi serpentine PEMFC at 0.8V. At the flow channel inlet, the initial pressure is recorded as 200KPa, while at the outlet, the pressure is measured at 164KPa. Consequently, the pressure drop at the bi serpentine flow channel is calculated to be 36KPa. The corresponding current density and power density for figure 7.10 is 0.373 (A/Cm²) and 0.298 (W/Cm²) respectively.

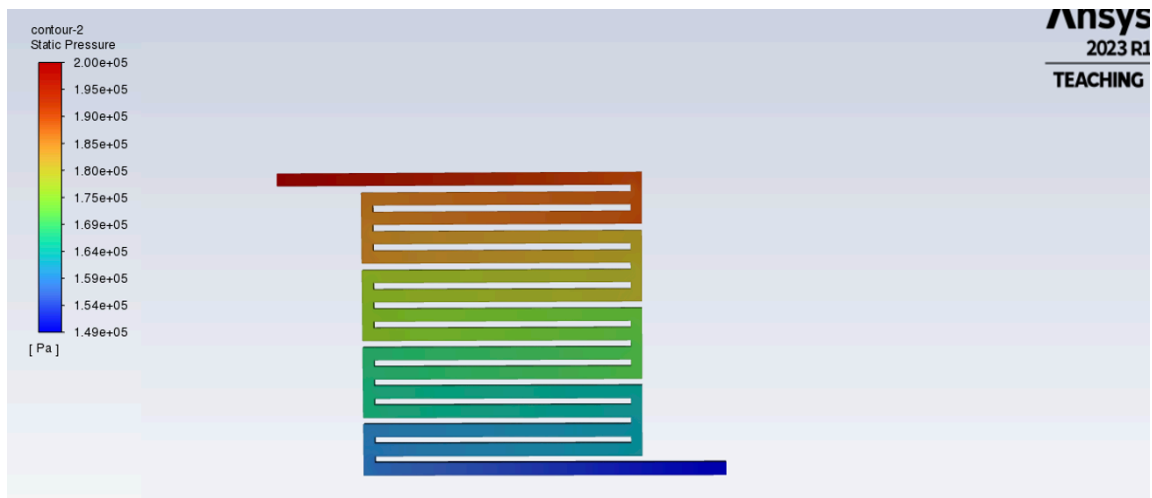


Figure 7.11 - Pressure distribution of 2mm flow channel width of tri serpentine PEMFC at 0.25V (low)

Figure 7.11 illustrates the pressure distribution of 2mm flow channel width of the tri serpentine PEMFC at 0.25 V. At the flow channel inlet, the initial pressure is recorded as 200KPa, while at the outlet, the pressure is measured at 149KPa. Consequently, the pressure drop at the tri serpentine flow channel is calculated to be 51KPa. The corresponding current density and power density for figure 7.11 is 1.61 (A/Cm²) and 0.402 (W/Cm²) respectively.

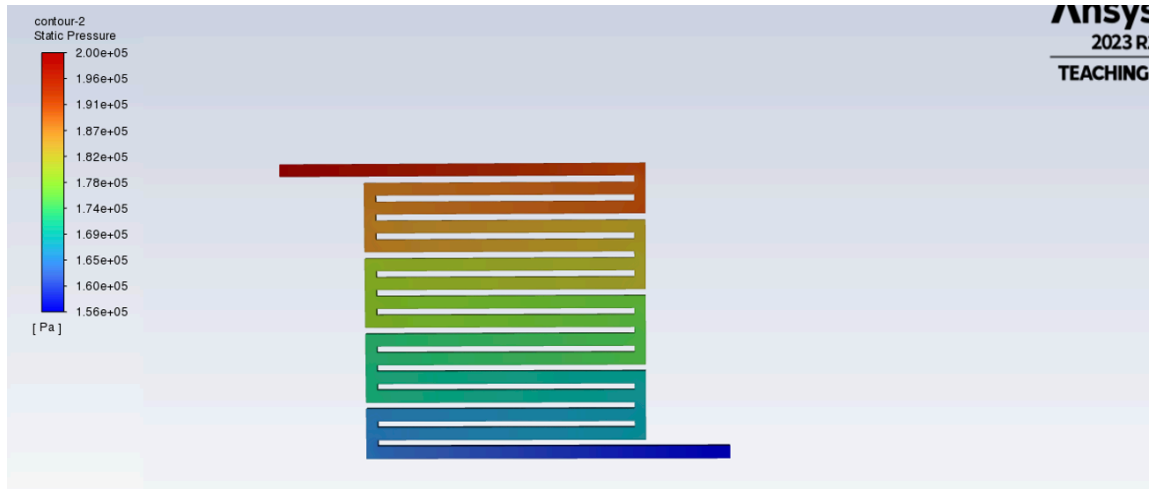


Figure 7.12 - Pressure distribution of 2mm flow channel width of tri serpentine PEMFC at 0.35 V (medium)

Figure 7.12 illustrates the pressure distribution of 2mm flow channel width of the tri serpentine PEMFC at 0.35 V. At the flow channel inlet, the initial pressure is recorded as 200KPa, while at the outlet, the pressure is measured at 156KPa. Consequently, the pressure drop at the tri serpentine flow channel is calculated to be 44KPa. The corresponding current density and power density for figure 7.12 is 1.54 (A/Cm²) and 0.539 (W/Cm²) respectively.

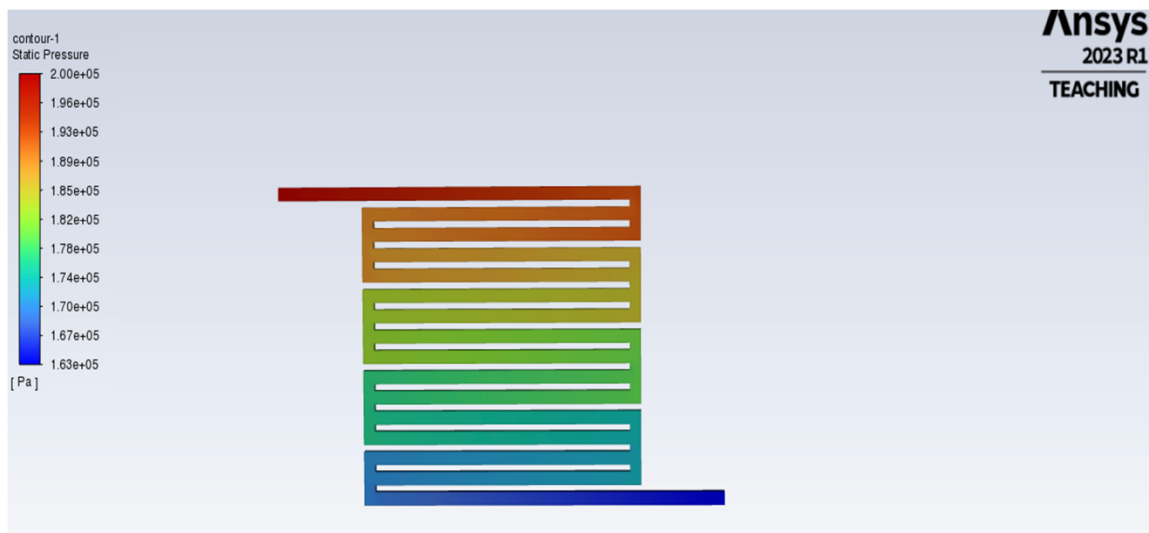


Figure 7.13- Pressure distribution of 2mm flow channel width of tri serpentine PEMFC at 0.55V (high)

Figure 7.13 illustrates the pressure distribution of 2mm flow channel width of the tri serpentine flow channel at 0.55 V. At the flow channel inlet, the initial pressure is recorded as 200KPa, while at the outlet, the pressure is measured at 163KPa. Consequently, the pressure drop at the tri serpentine flow channel is calculated to be 37KPa. The corresponding current density and power density for figure 7.13 is 1.21 (A/Cm²) and 0.6655 (W/Cm²) respectively.

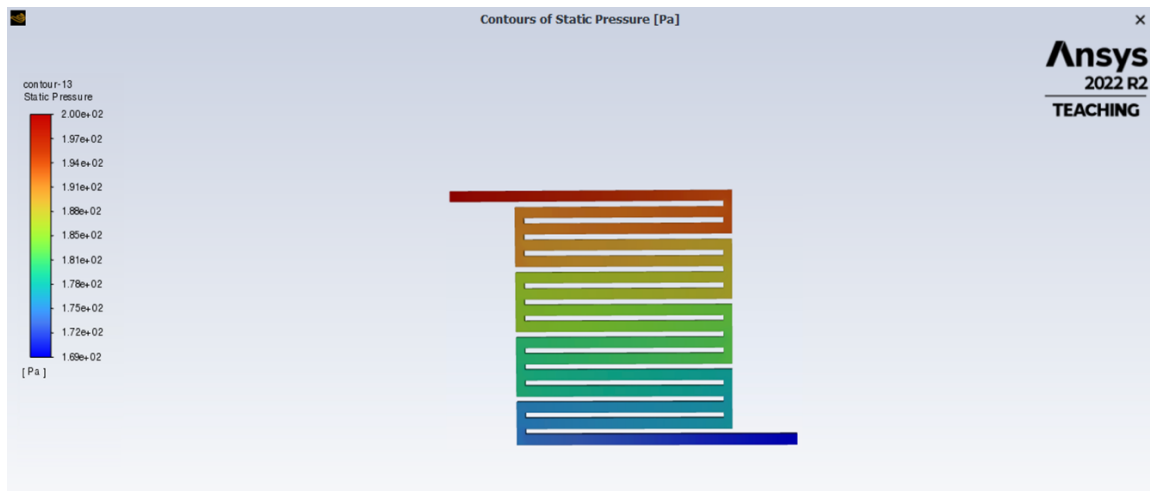


Figure 7.14- Pressure distribution of 2mm flow channel width of tri serpentine PEMFC at 0.65V(very high)

Figure 7.14 illustrates the pressure distribution of 2mm flow channel width of the tri serpentine flow channel at 0.65 V. At the flow channel inlet, the initial pressure is recorded as 200KPa, while at the outlet, the pressure is measured at 169KPa. Consequently, the pressure drop at the tri serpentine flow channel is calculated to be 31KPa. The corresponding current density and power density for figure 7.14 is 0.972 (A/Cm²) and 0.6318 (W/Cm²) respectively.

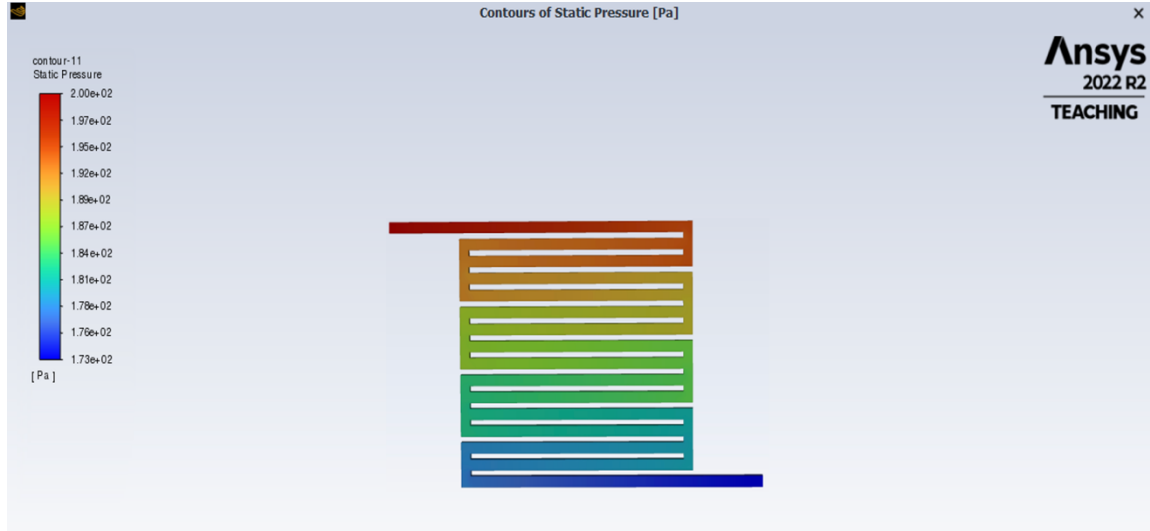


Figure 7.15- Pressure distribution of 2mm flow channel width of tri serpentine PEMFC at 0.8V (extreme)

Figure 7.15 illustrates the pressure distribution of 2mm flow channel width of the tri serpentine flow channel at 0.8 V. At the flow channel inlet, the initial pressure is recorded as 200KPa, while at the outlet, the pressure is measured at 173KPa. Consequently, the pressure drop at the tri serpentine flow channel is calculated to be 27KPa. The corresponding current density and power density for figure 7.15 is 0.525 (A/Cm²) and 0.42 (W/Cm²) respectively.

The pressure variation across different flow channel designs is depicted on low (0.25V), medium (0.35V), high (0.5V), very high (0.65V) and extreme (0.8V) stages for the single, bi and tri serpentine flow channels respectively.

In 0.25V, the static pressure drop at the 2mm flow channel width of the single serpentine PEMFC is measured as 79KPa while the bi serpentine flow channel, it is 63KPa and, in the tri, serpentine flow channel, it is 51KPa.

In 0.35V, the static pressure drop at 2mm flow channel width of the single serpentine PEMFC is measured as 71KPa while the bi serpentine flow channel, it is 57KPa and in the tri serpentine flow channel, it is 44KPa.

In 0.5V, it is noted that the pressure drop at 2mm flow channel width of the single serpentine PEMFC is measured to be 60KPa while the bi serpentine flow channel, it is 48KPa. At 0.55V, the tri serpentine flow channel's pressure loss is calculated to be 37KPa.

In 0.65V, it is noted that the pressure drop at 2mm flow channel width of the single serpentine PEMFC is measured to be 48KPa while the bi serpentine flow channel, it is 39KPa. The tri serpentine flow channel's pressure loss is calculated to be 31KPa.

In 0.8V, it is noted that the pressure drop at 2mm flow channel width of the single serpentine PEMFC is measured to be 43KPa while the bi serpentine flow channel, it is 36KPa. The tri serpentine flow channel's pressure loss is calculated to be 27KPa.

Despite the variations in pressure drop, it is observed that the pressure is distributed evenly across all designs. The higher pressure drop in the single serpentine flow channel can be attributed to the presence of more bends in its design, leading to increased resistance and consequent pressure drop. Conversely, the tri serpentine design exhibits the minimum pressure drop due to its fewer bends, ultimately contributing to improved cell performance.

7.2 Velocity Magnitude of the PEMFC

Velocity magnitude is indeed a crucial parameter for assessing the performance of PEMFCs. Below, the velocity magnitude of various types of flow an important parameter to know the performance of the PEMFC. The

velocity magnitude of all the different types of flow channels are discussed below.

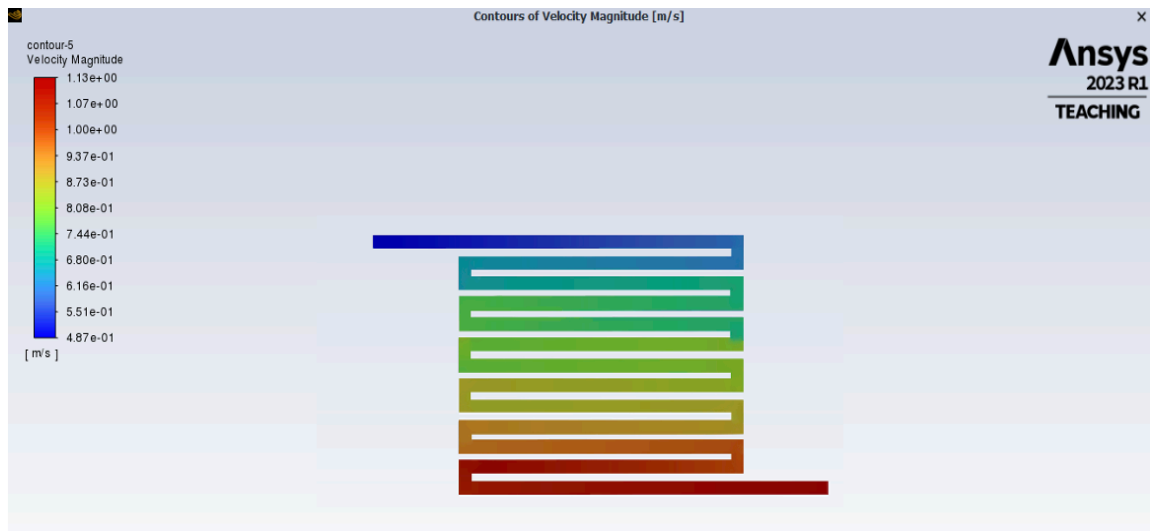


Figure 7.16- Velocity magnitude of 2mm flow channel width of single serpentine PEMFC at 0.25V (low)

In figure 7.16, the velocity profile of 2mm flow channel width of the single serpentine PEMFC at 0.25 V is depicted. Specifically, the velocity at the inlet of the flow channel is measured at 0.487 m/s, while at the outlet, it increases to 1.13 m/s. Consequently, the difference in velocity magnitude from the inlet to the outlet of the single serpentine flow channel is calculated to 0.643 m/s.

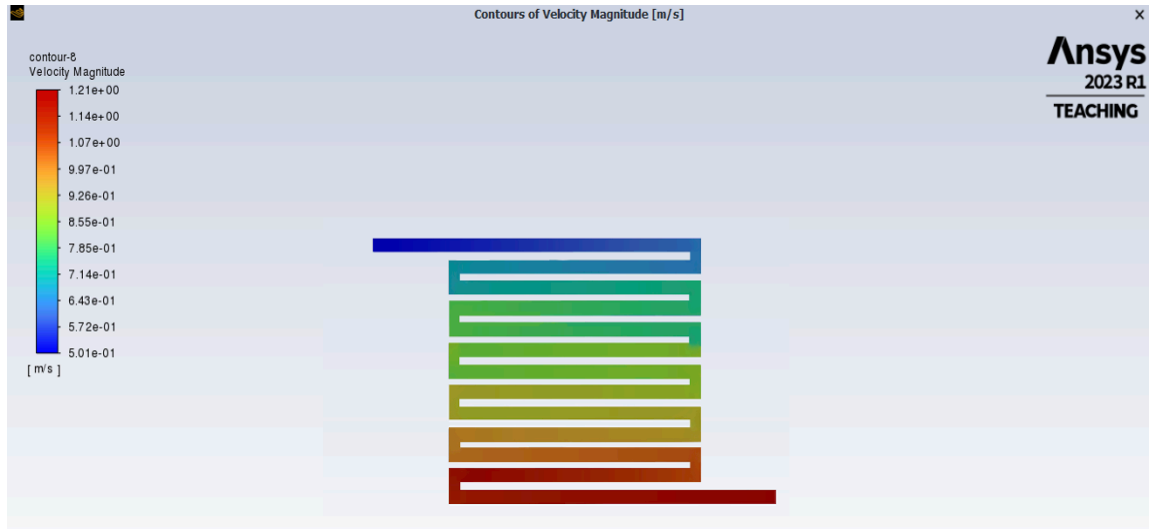


Figure 7.17- Velocity magnitude of 2mm flow channel width of single serpentine PEMFC at 0.35V (medium)

In figure 7.17, the velocity profile of 2mm flow channel width of the single serpentine PEMFC at 0.35V is depicted. Specifically, the velocity at the inlet of the flow channel is measured at 0.501 m/s, while at the outlet, it increases to 1.21 m/s. Consequently, the difference in velocity magnitude from the inlet to the outlet of the single serpentine flow channel is calculated to 0.709 m/s.

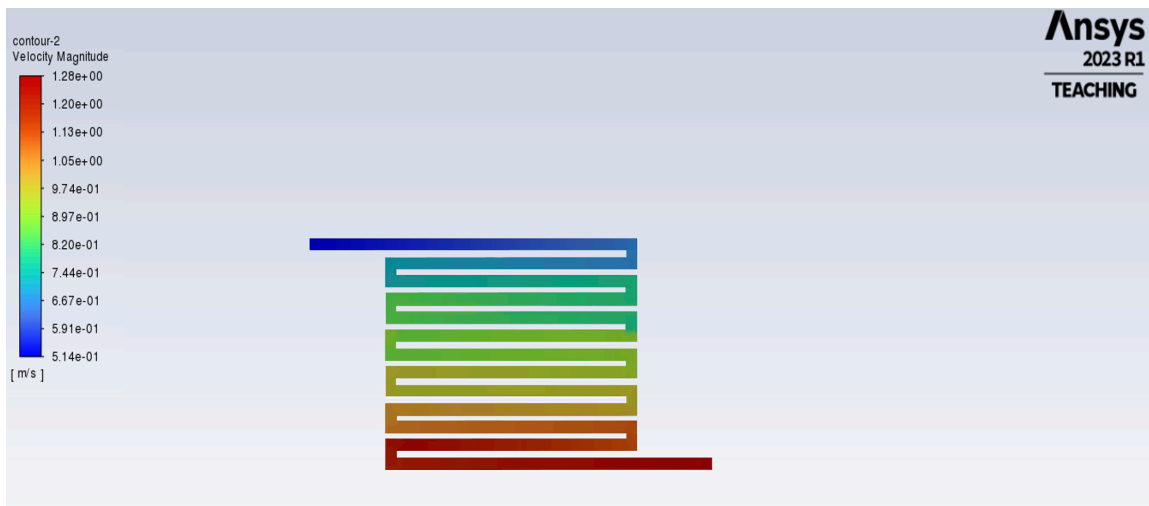


Figure 7.18- Velocity magnitude of 2mm flow channel width of single serpentine PEMFC at 0.5V (high)

In figure 7.18, the velocity profile of 2mm flow channel width of the single serpentine PEMFC at 0.5V is depicted. Specifically, the velocity at the inlet of the flow channel is measured at 0.514 m/s, while at the outlet, it increases to 1.28 m/s. Consequently, the difference in velocity magnitude from the inlet to the outlet of the single serpentine flow channel is calculated to 0.766 m/s.

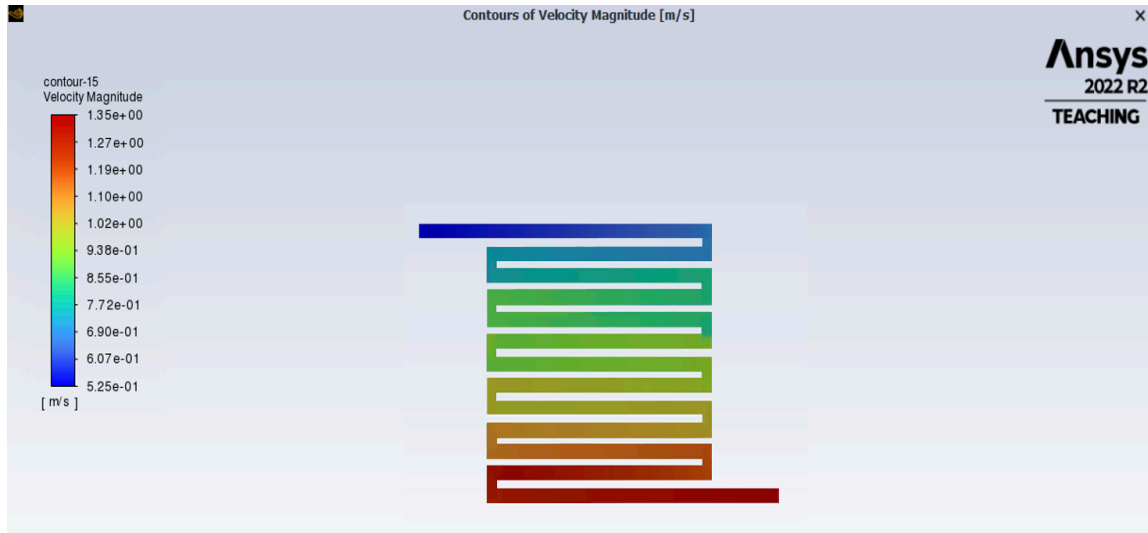


Figure 7.19- Velocity magnitude of 2mm flow channel width of single serpentine PEMFC at 0.65V (very high)

In figure 7.19, the velocity profile of 2mm flow channel width of the single serpentine PEMFC at 0.65V is depicted. Specifically, the velocity at the inlet of the flow channel is measured at 0.525 m/s, while at the outlet, it increases to 1.35 m/s. Consequently, the difference in velocity magnitude from the inlet to the outlet of the single serpentine flow channel is calculated to 0.825 m/s.

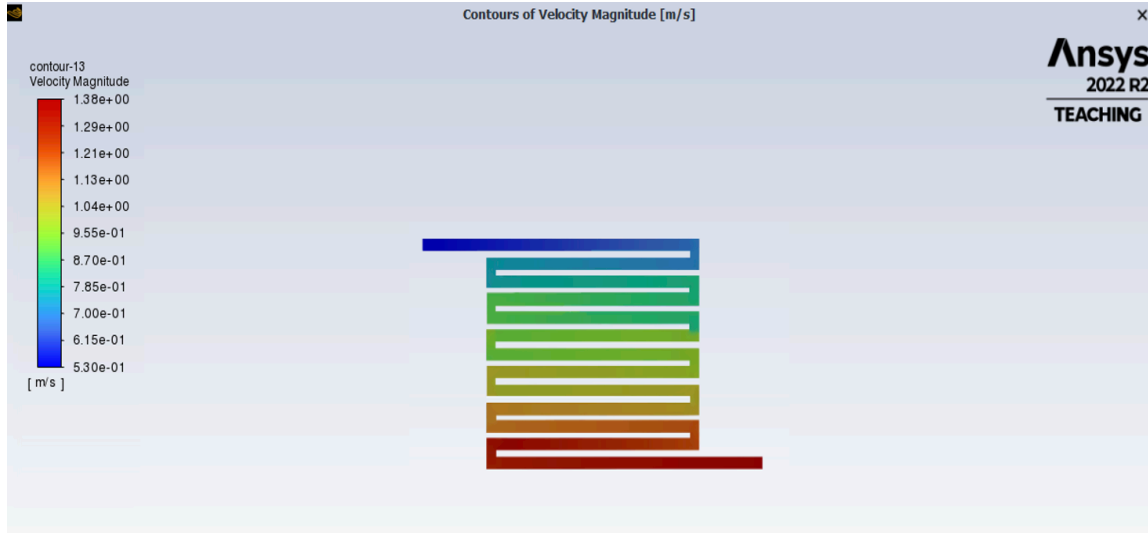


Figure 7.20- Velocity magnitude of 2mm flow channel width of single serpentine PEMFC at 0.8V (high)

In figure 7.20, the velocity profile of 2mm flow channel width of the single serpentine PEMFC at 0.8V is depicted. Specifically, the velocity at the inlet of the flow channel is measured at 0.530 m/s, while at the outlet, it increases to 1.38 m/s. Consequently, the difference in velocity magnitude from the inlet to the outlet of the single serpentine flow channel is calculated to 0.85 m/s.

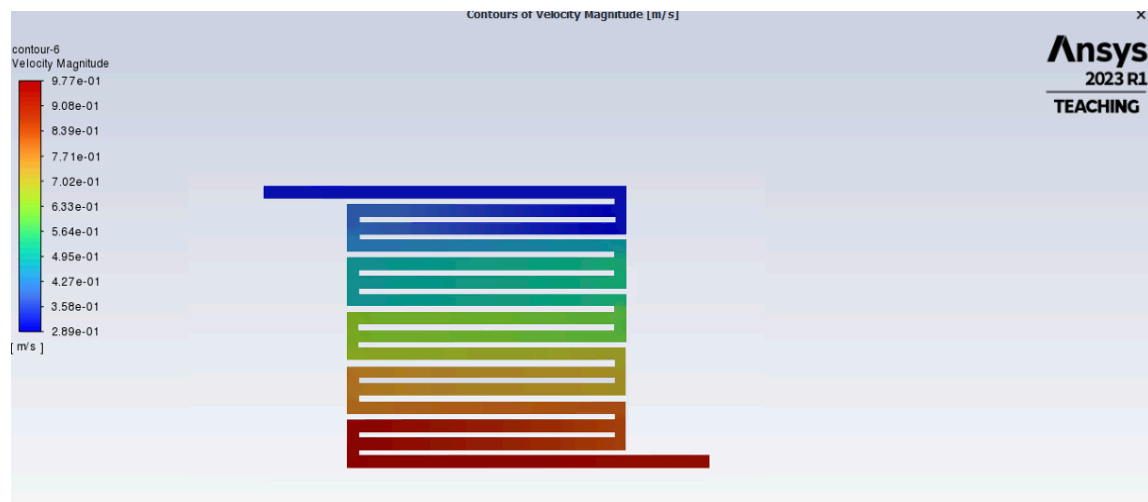


Figure 7.21- Velocity magnitude of 2mm flow channel width of bi serpentine PEMFC at 0.25V (low)

In figure 7.21, the velocity of 2mm flow channel width of bi serpentine PEMFC at 0.25V is depicted. Specifically, the velocity at the inlet of the flow channel is measured at 0.289 m/s while at the outlet, it increases to 0.977 m/s. Consequently, the difference in velocity magnitude from the inlet to the outlet of the bi serpentine flow channel is calculated to be 0.688 m/s.

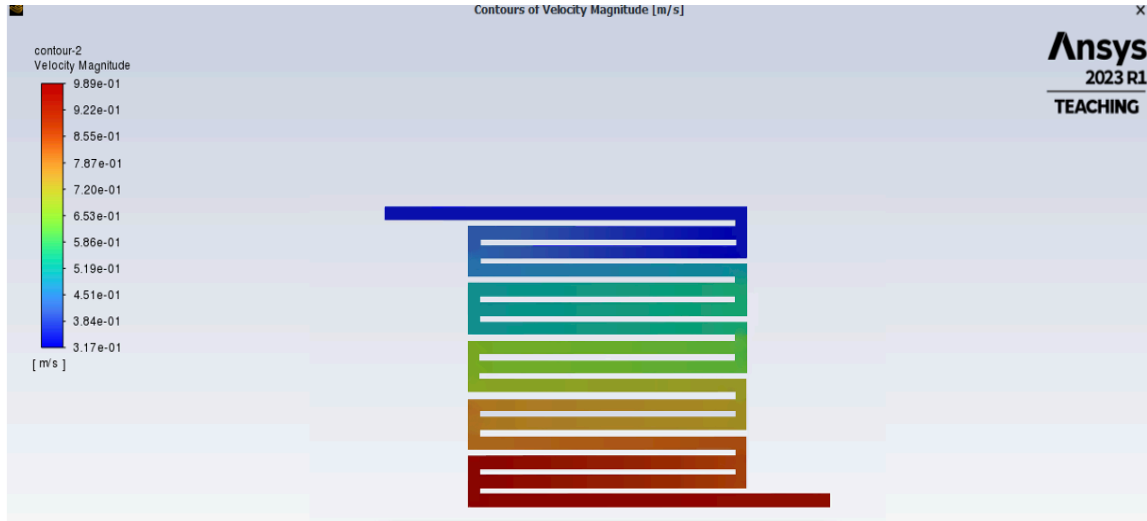


Figure 7.22- Velocity magnitude of 2mm flow channel width of bi serpentine PEMFC at 0.35V (medium)

In figure 7.22, the velocity of 2mm flow channel width of bi serpentine PEMFC at 0.35V is depicted. Specifically, the velocity at the inlet of the flow channel is measured at 0.317 m/s while at the outlet, it increases to 0.989 m/s. Consequently, the difference in velocity magnitude from the inlet to the outlet of the bi serpentine flow channel is calculated to be 0.672 m/s.

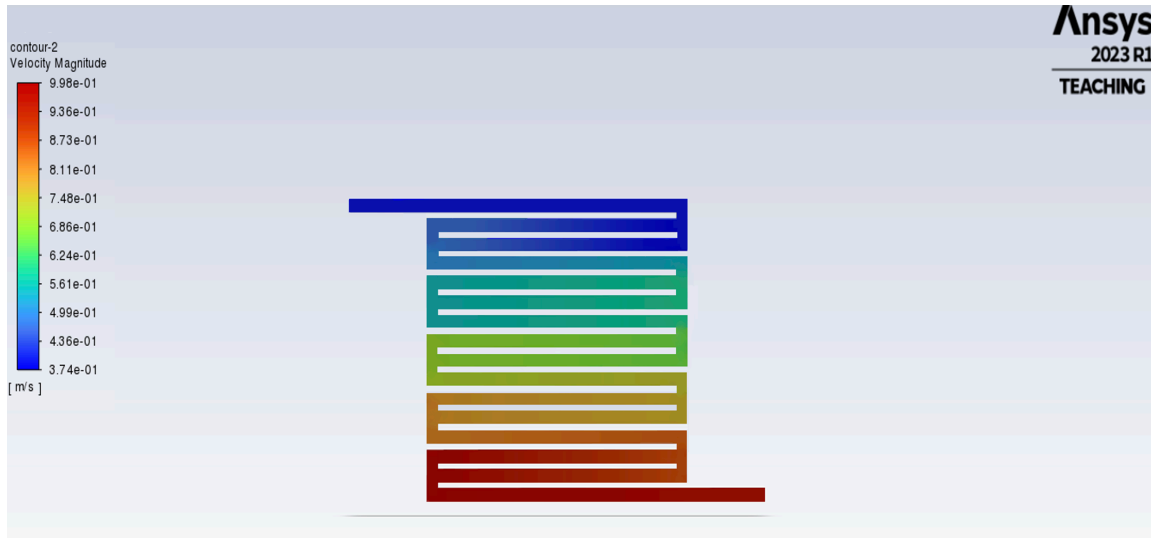


Figure 7.23- Velocity magnitude of 2mm flow channel width of bi serpentine PEMFC at 0.5V (high)

In figure 7.23, the velocity of 2mm flow channel width of bi serpentine PEMFC at 0.5V is depicted. Specifically, the velocity at the inlet of the flow channel is measured at 0.374 m/s while at the outlet, it increases to 0.998 m/s. Consequently, the difference in velocity magnitude from the inlet to the outlet of the bi serpentine flow channel is calculated to be 0.624 m/s.

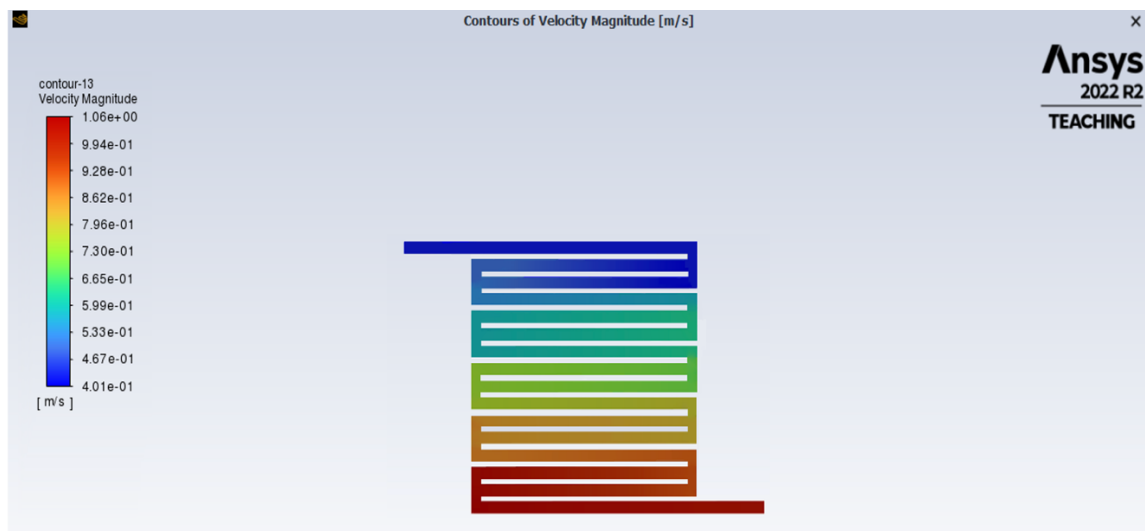


Figure 7.24- Velocity magnitude of 2mm flow channel width of bi serpentine PEMFC at 0.65V (very high)

In figure 7.24, the velocity of 2mm flow channel width of bi serpentine PEMFC at 0.65V is depicted. Specifically, the velocity at the inlet of the flow channel is measured at 0.401 m/s while at the outlet, it increases to 1.06 m/s. Consequently, the difference in velocity magnitude from the inlet to the outlet of the bi serpentine flow channel is calculated to be 0.659 m/s.

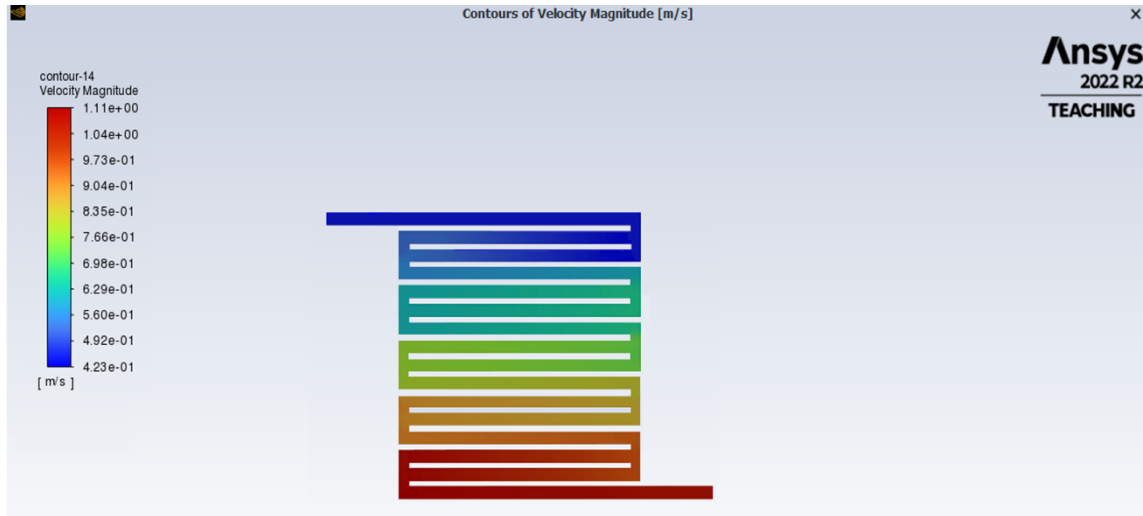


Figure 7.25- Velocity magnitude of 2mm flow channel width of bi serpentine PEMFC at 0.8V (extreme)

In figure 7.25, the velocity of 2mm flow channel width of bi serpentine PEMFC at 0.8V is depicted. Specifically, the velocity at the inlet of the flow channel is measured at 0.423 m/s while at the outlet, it increases to 1.11 m/s. Consequently, the difference in velocity magnitude from the inlet to the outlet of the bi serpentine flow channel is calculated to be 0.677 m/s.

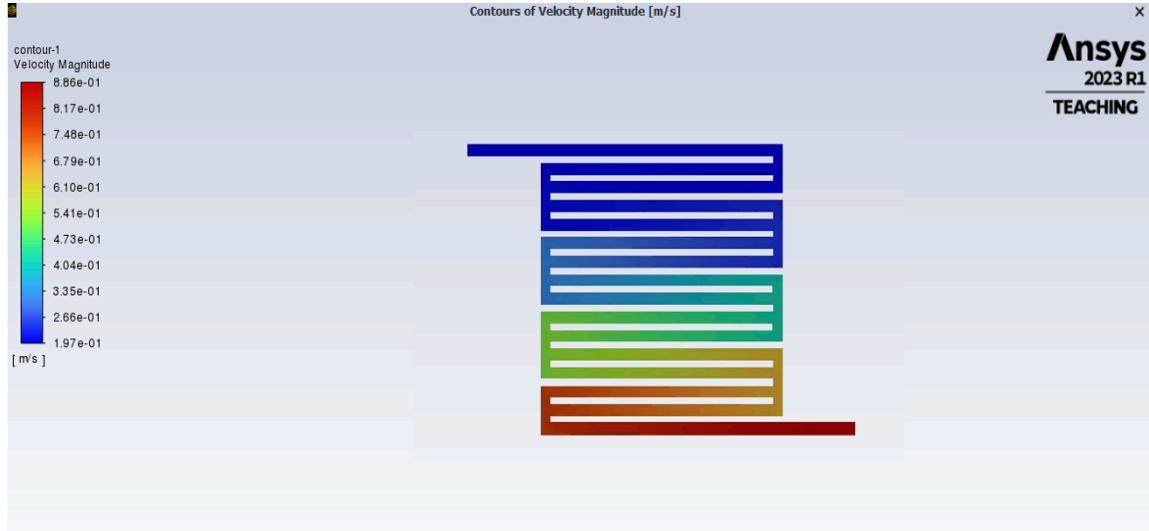


Figure 7.26- Velocity magnitude of 2mm flow channel width of tri serpentine PEMFC at 0.25V (low)

In figure 7.26, the velocity profile of 2mm flow channel width of the tri serpentine PEMFC at 0.25 V is depicted. Specifically, the velocity at the inlet of the flow channel is measured at 0.197 m/s while at the outlet, it increases to 0.886 m/s. Consequently, the difference in velocity magnitude from the inlet to the outlet of the tri serpentine flow channel is calculated to be 0.689 m/s.

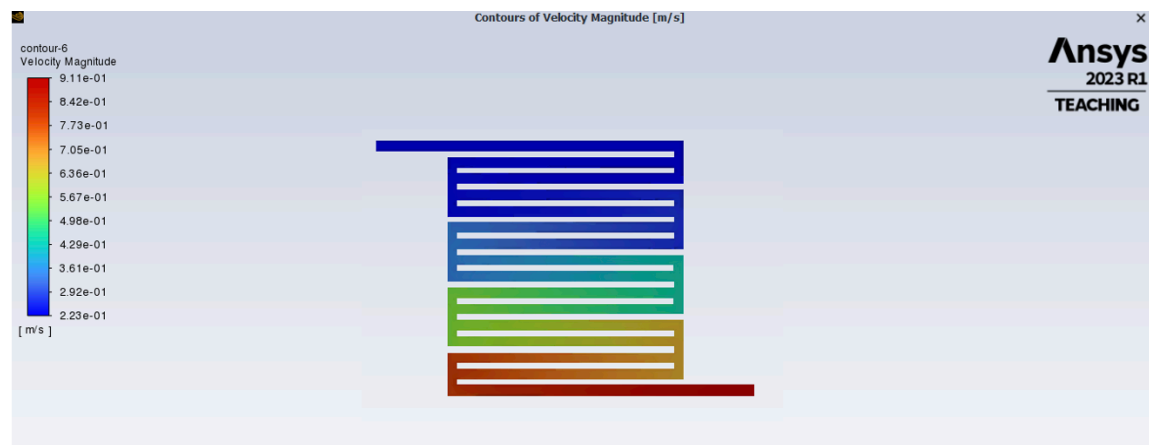


Figure 7.27- Velocity magnitude of 2mm flow channel width of tri serpentine PEMFC at 0.35V (medium)

In figure 7.27, the velocity profile of 2mm flow channel width of the tri serpentine PEMFC at 0.35 V is depicted. Specifically, the velocity at the inlet of the flow channel is measured at 0.223 m/s while at the outlet, it increases to 0.911 m/s. Consequently, the difference in velocity magnitude from the inlet to the outlet of the tri serpentine flow channel is calculated to be 0.688 m/s.

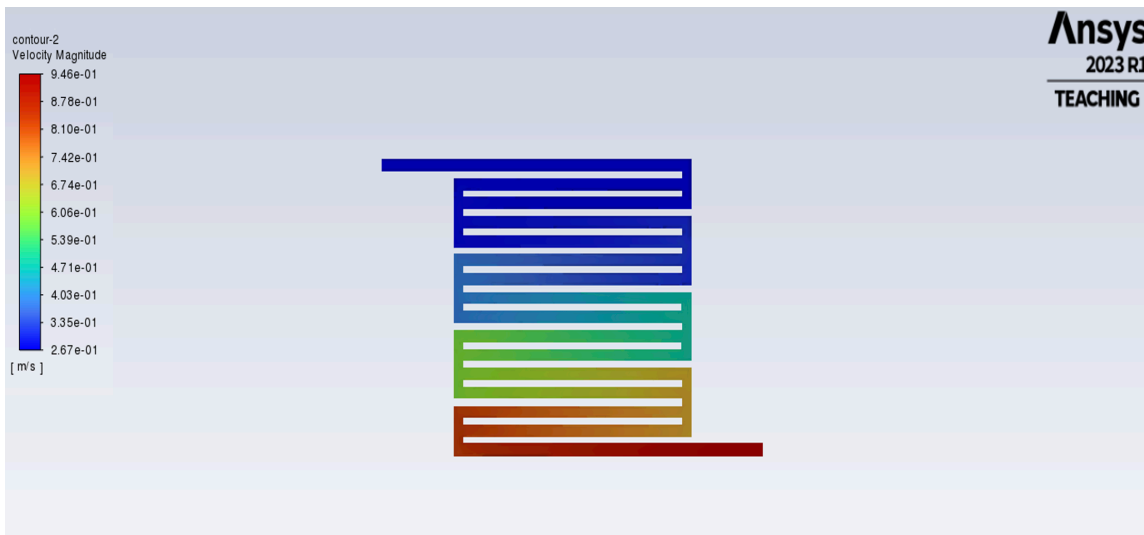


Figure 7.28- Velocity magnitude of 2mm flow channel width of tri serpentine PEMFC at 0.55V (high)

In figure 7.28, the velocity profile of 2mm flow channel width of the tri serpentine PEMFC at 0.55 V is depicted. Specifically, the velocity at the inlet of the flow channel is measured at 0.267 m/s while at the outlet, it increases to 0.946 m/s. Consequently, the difference in velocity magnitude from the inlet to the outlet of the tri serpentine flow channel is calculated to be 0.679 m/s.

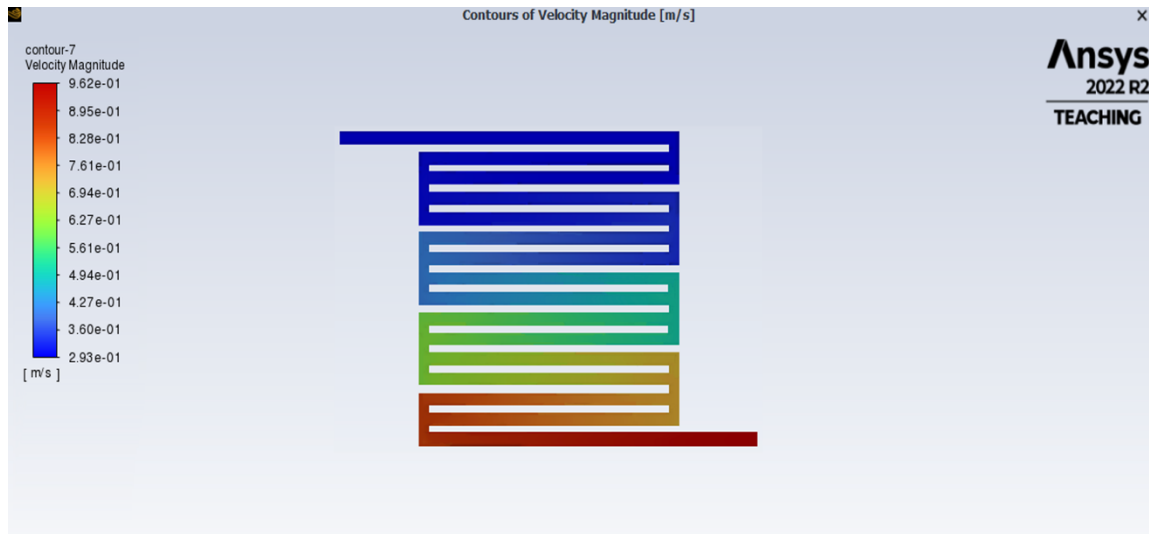


Figure 7.29- Velocity magnitude of 2mm flow channel width of tri serpentine PEMFC at 0.65V (very high)

In figure 7.29, the velocity profile of 2mm flow channel width of the tri serpentine PEMFC at 0.65 V is depicted. Specifically, the velocity at the inlet of the flow channel is measured at 0.293 m/s while at the outlet, it increases to 0.962 m/s. Consequently, the difference in velocity magnitude from the inlet to the outlet of the tri serpentine flow channel is calculated to be 0.669 m/s.

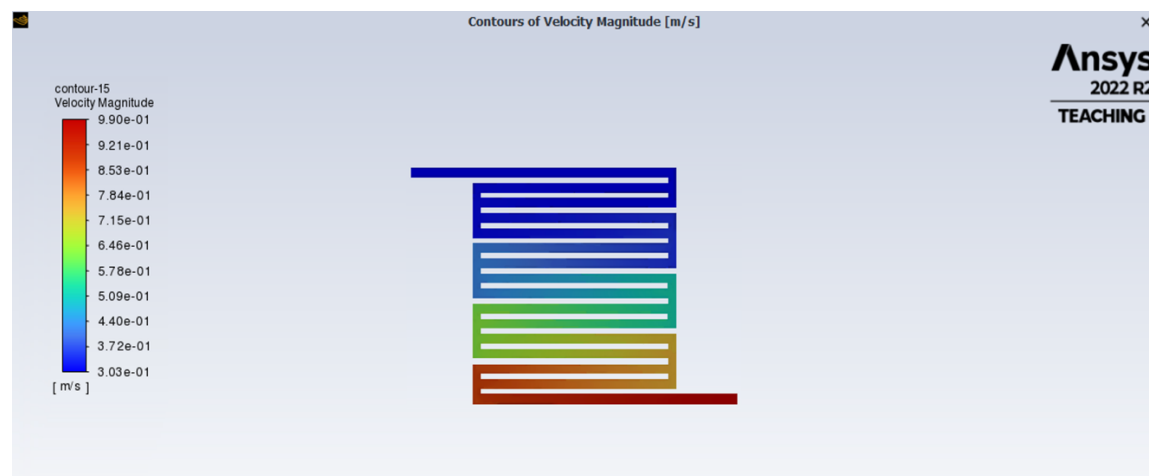


Figure 7.30- Velocity magnitude of 2mm flow channel width of tri serpentine PEMFC at 0.8V (extreme)

In figure 7.30, the velocity profile of 2mm flow channel width of the tri serpentine PEMFC at 0.8 V is depicted. Specifically, the velocity at the inlet of the flow channel is measured at 0.303 m/s while at the outlet, it increases to 0.990 m/s. Consequently, the difference in velocity magnitude from the inlet to the outlet of the tri serpentine flow channel is calculated to be 0.687 m/s.

The velocity magnitude of the 2mm flow channel width of single serpentine PEMFC is illustrated in figure 7.10, 7.11 and 7.12 while the bi serpentine flow channel is depicted in figure 7.13, 7.14, 7.15 and tri serpentine flow channels are depicted in figures 7.16, 7.17 and 7.18, respectively.

At 0.25V, it is observed that the velocity increases in the 2mm flow channel width of single serpentine PEMFC is measured at 0.643 m/s, while for the bi serpentine flow channel, it is 0.688 m/s, and for the tri serpentine flow channel, it is 0.689 m/s.

At 0.35V, it is noted that the velocity increases in the 2mm flow channel width of single serpentine PEMFC is measured at 0.709 m/s , while for the bi serpentine flow channel, it is 0.672 m/s, and for the tri serpentine flow channel, it is 0.688 m/s.

At 0.5V, it is perceived that the velocity increases in the 2mm flow channel width of single serpentine PEMFC is measured at 0.766 m/s , while for the bi serpentine flow channel, it is 0.624 m/s. At 0.55V, the tri serpentine velocity increase is calculated to be 0.679 m/s.

At 0.65V, it is perceived that the velocity increases in the 2mm flow channel width of single serpentine PEMFC is measured at 0.825 m/s, while for the bi serpentine flow channel, it is 0.657 m/s. The tri serpentine velocity increase is calculated to be 0.669 m/s.

At 0.8V, it is perceived that the velocity increases in the 2mm flow channel width of single serpentine PEMFC is measured at 0.85 m/s, while for the bi serpentine flow channel, it is 0.677 m/s. The tri serpentine velocity increase is calculated to be 0.687 m/s.

The velocity magnitude in the single serpentine flow channel is typically higher due to its straighter design, allowing for more direct flow. This configuration often results in efficient transport of reactants and better performance. In the bi serpentine flow channel, the velocity magnitude is slightly lower compared to the single serpentine design. This is due to the presence of additional bends in the flow path, which may cause some resistance and reduce overall velocity. The velocity magnitude in the tri serpentine flow channel is generally lower than both the single and bi serpentine designs. While this configuration offers increased surface area for reactant contact, the presence of more bends and turns can lead to higher resistance and lower velocity. Furthermore, it is observed that the velocity is evenly distributed throughout the flow channel, confirming uniform flow distribution across occurs all the regions of the channel.

7.3 Mass Fraction of the Hydrogen (H₂)

The mass fraction of the hydrogen (H₂) is visualized for the single serpentine, bi serpentine, and tri serpentine flow channel. Understanding the transportation of hydrogen (H₂) along the anode side is crucial for improving the performance of the cell. The distribution of hydrogen (H₂) in y-z plane is depicted, showcasing varying concentrations across the channels. In all three serpentine designs, hydrogen concentrations are discussed, with reactants being consumed in the active area of the gas diffusion layer (GDL).

Concentration is highest at the inlet of the channels and gradually decreases towards the outlet.

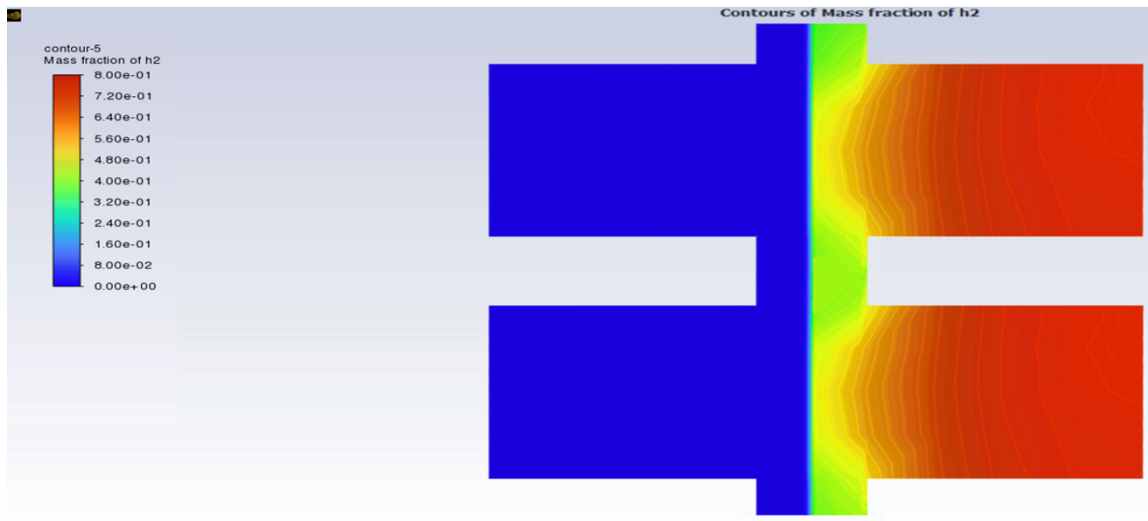


Figure 7.31- Mass fraction of hydrogen in 2mm flow channel width of of single-serpentine PEMFC at 0.25V (low)

In the figure 7.31, the consumption rate of the mass fraction of hydrogen (H_2) at the gas diffusion lay (GDL) in the 2mm flow channel width of single serpentine PEMFC at 0.25 V is measured at 0.541.

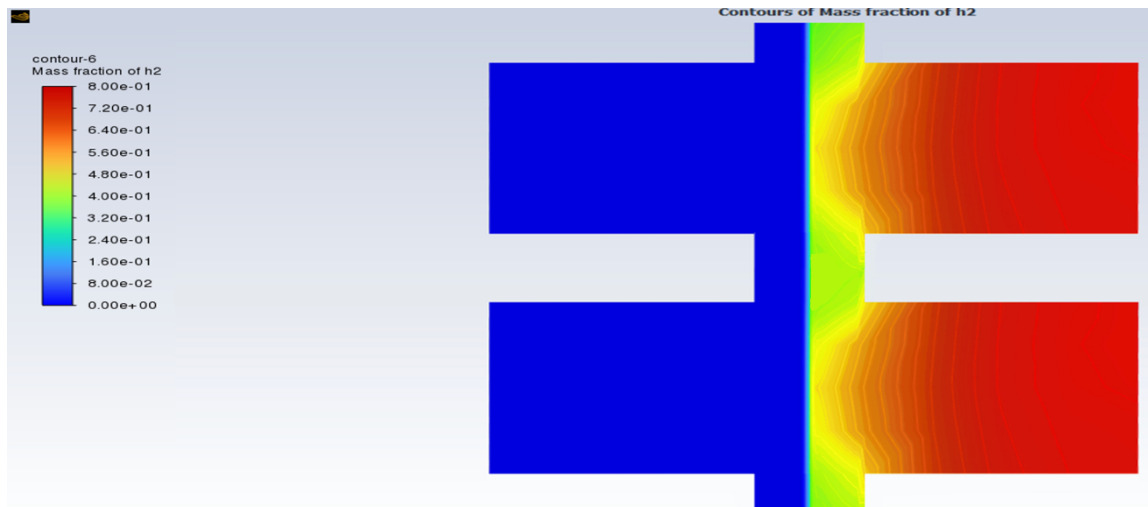


Figure 7.32- Mass fraction of hydrogen in 2mm flow channel width of single-serpentine PEMFC at 0.35V (medium)

In the figure 7.32, the consumption rate of the mass fraction of hydrogen (H_2) at the gas diffusion lay (GDL) in the 2mm flow channel width of single serpentine PEMFC at 0.35 V is measured at 0.587.

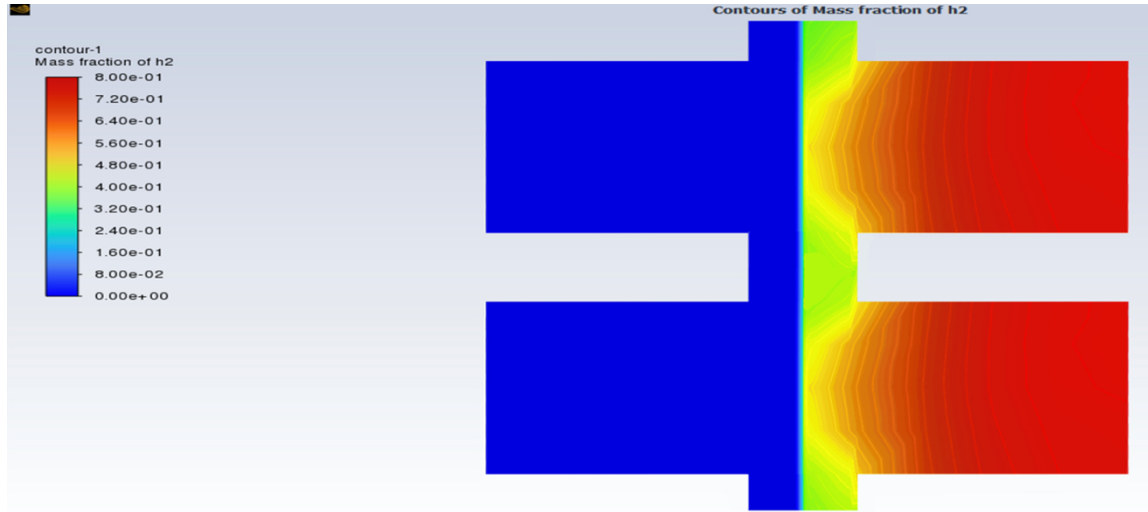


Figure 7.33- Mass fraction of hydrogen in 2mm flow channel width of single-serpentine PEMFC at 0.5V (high)

In the figure 7.33, the consumption rate of the mass fraction of hydrogen (H_2) at the gas diffusion lay (GDL) in the 2mm flow channel width of single serpentine PEMFC at 0.5 V is measured at 0.630.

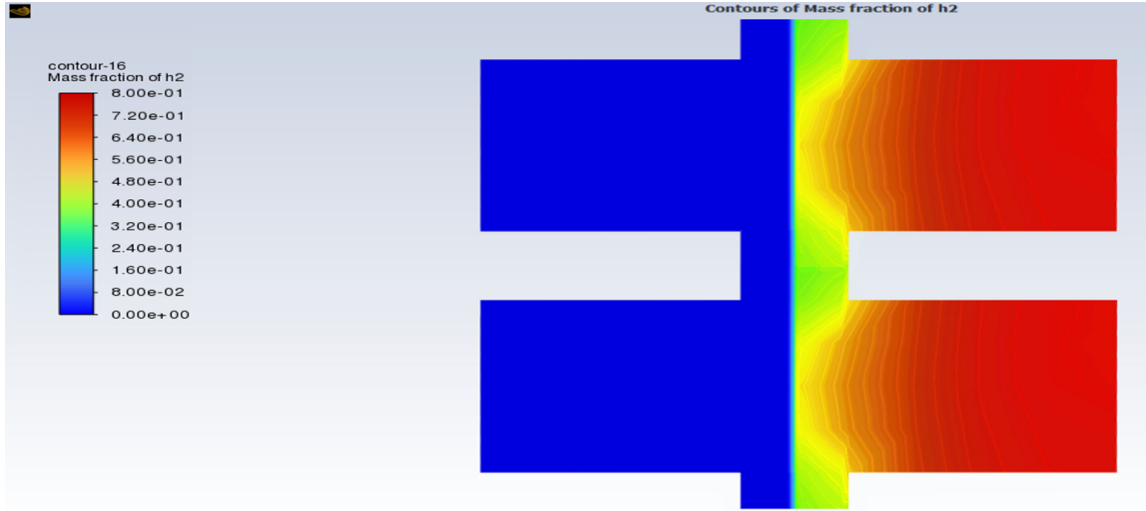


Figure 7.34- Mass fraction of hydrogen in 2mm flow channel width of single-serpentine PEMFC at 0.65V (very high)

In the figure 7.34, the consumption rate of the mass fraction of hydrogen (H_2) at the gas diffusion lay (GDL) in the 2mm flow channel width of single serpentine PEMFC at 0.65 V is measured at 0.683.

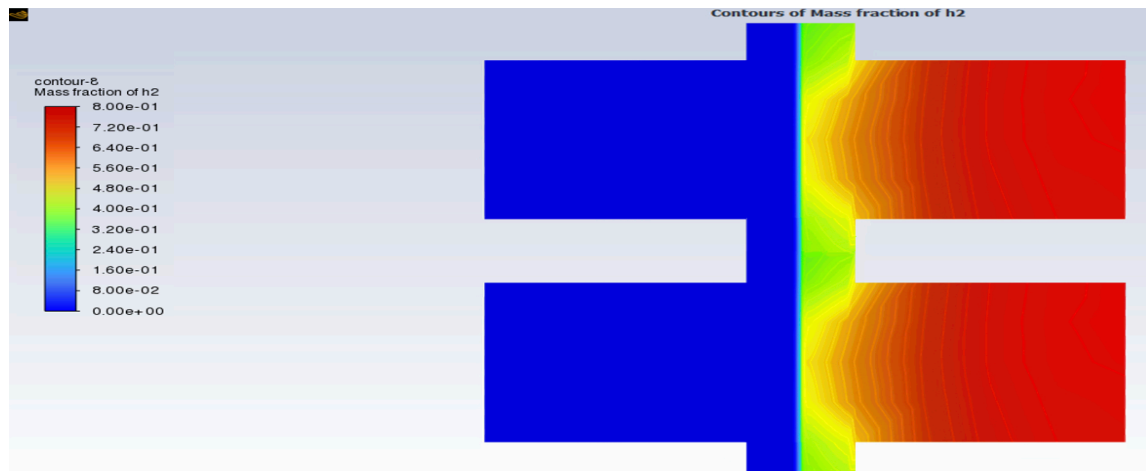


Figure 7.35- Mass fraction of hydrogen in 2mm flow channel width of single-serpentine PEMFC at 0.8V (extreme)

In the figure 7.35, the consumption rate of the mass fraction of hydrogen (H_2) at the gas diffusion lay (GDL) in the 2mm flow channel width of single serpentine PEMFC at 0.8 V is measured at 0.709.

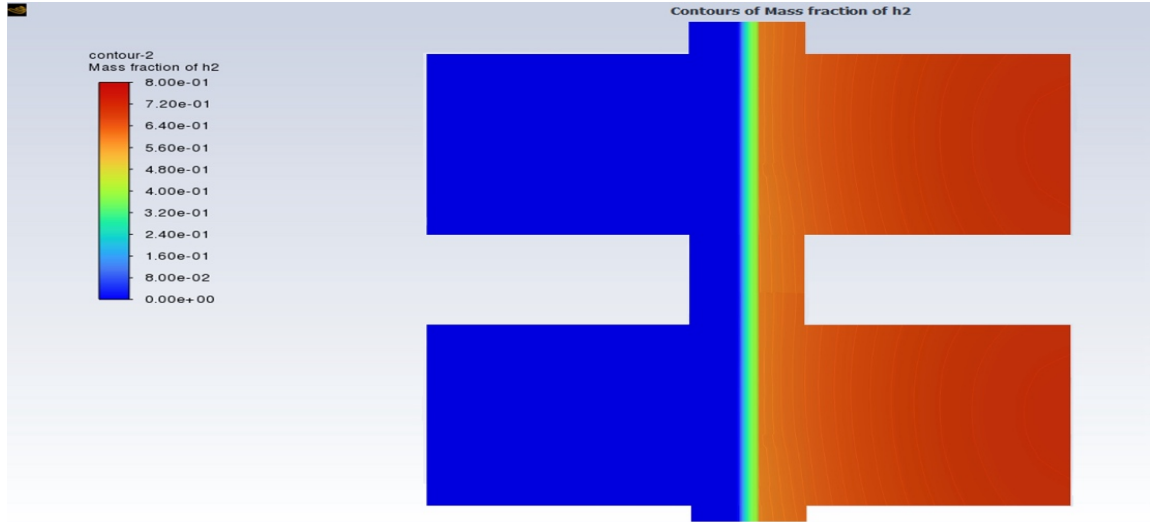


Figure 7.36- Mass fraction of hydrogen in 2mm flow channel width of bi serpentine PEMFC at 0.25V (low)

In the figure 7.36, the consumption rate of the mass fraction of hydrogen (H_2) at the gas diffusion lay (GDL) in the 2mm flow channel width of bi serpentine PEMFC at 0.25 V is measured at 0.601.

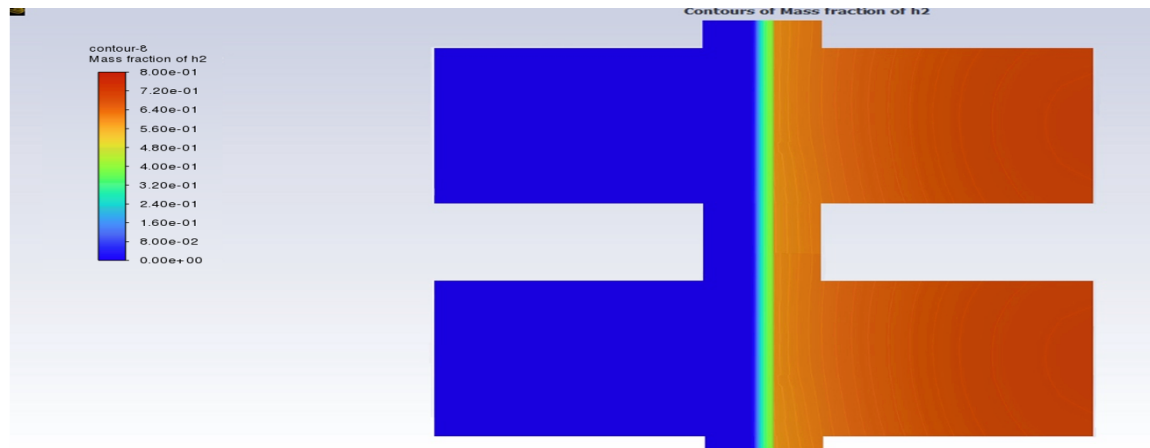


Figure 7.37- Mass fraction of hydrogen in 2mm flow channel width of bi serpentine PEMFC at 0.35V (medium)

In the figure 7.37, the consumption rate of the mass fraction of hydrogen (H_2) at the gas diffusion layer (GDL) in the 2mm flow channel width of bi serpentine PEMFC at 0.35 V is measured at 0.625.

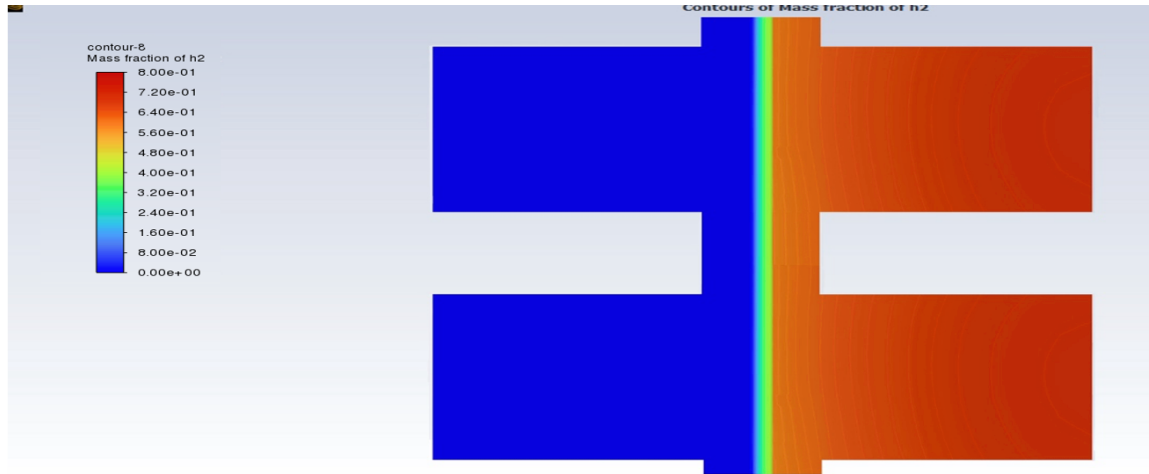


Figure 7.38- Mass fraction of hydrogen in 2mm flow channel width of bi-serpentine PEMFC at 0.5V (high)

In figure 7.38, the consumption rate of the mass fraction of hydrogen (H_2) at the gas diffusion layer (GDL) in the 2mm flow channel width of tri serpentine flow channel at 0.5 V is measured at 0.662.

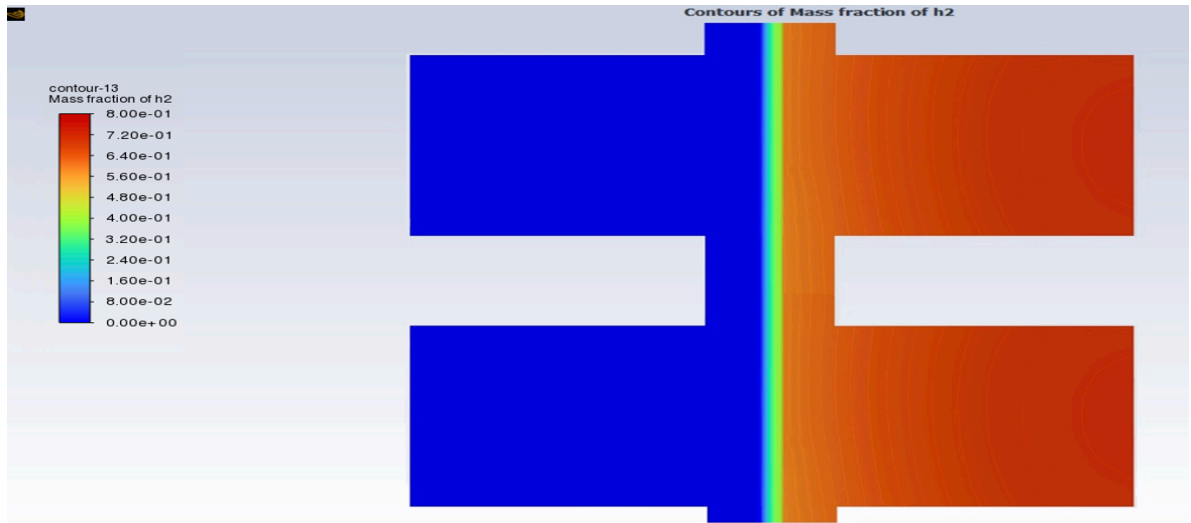


Figure 7.39- Mass fraction of hydrogen in 2mm flow channel width of bi-serpentine PEMFC at 0.65V (very high)

In figure 7.39, the consumption rate of the mass fraction of hydrogen (H_2) at the gas diffusion layer (GDL) in the 2mm flow channel width of tri serpentine flow channel at 0.65 V is measured at 0.707.

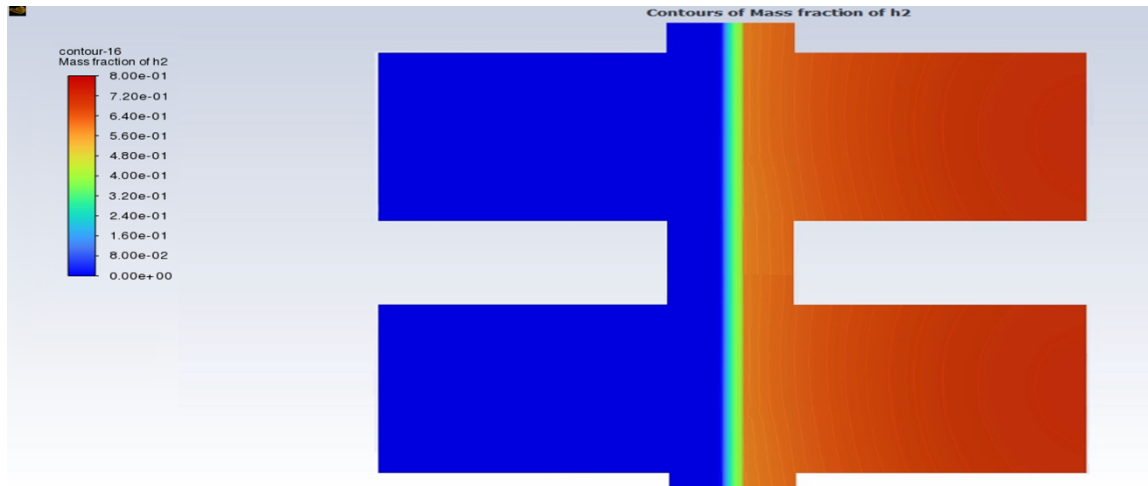


Figure 7.40- Mass fraction of hydrogen in 2mm flow channel width of bi-serpentine PEMFC at 0.8V (extreme)

In figure 7.40, the consumption rate of the mass fraction of hydrogen (H_2) at the gas diffusion layer (GDL) in the 2mm flow channel width of tri serpentine flow channel at 0.8 V is measured at 0.734.

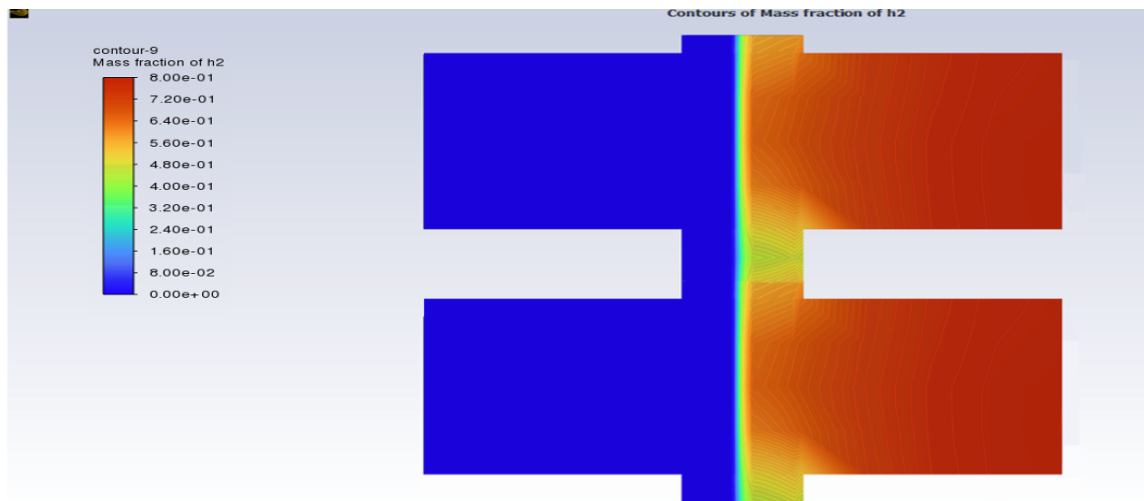


Figure 7.41- Mass fraction of hydrogen in 2mm flow channel width of tri serpentine PEMFC at 0.25 V (low)

In figure 7.41, the consumption rate of the mass fraction of hydrogen (H_2) at the gas diffusion layer (GDL) in the 2mm flow channel width of tri serpentine flow channel at 0.25 V is measured at 0.642.

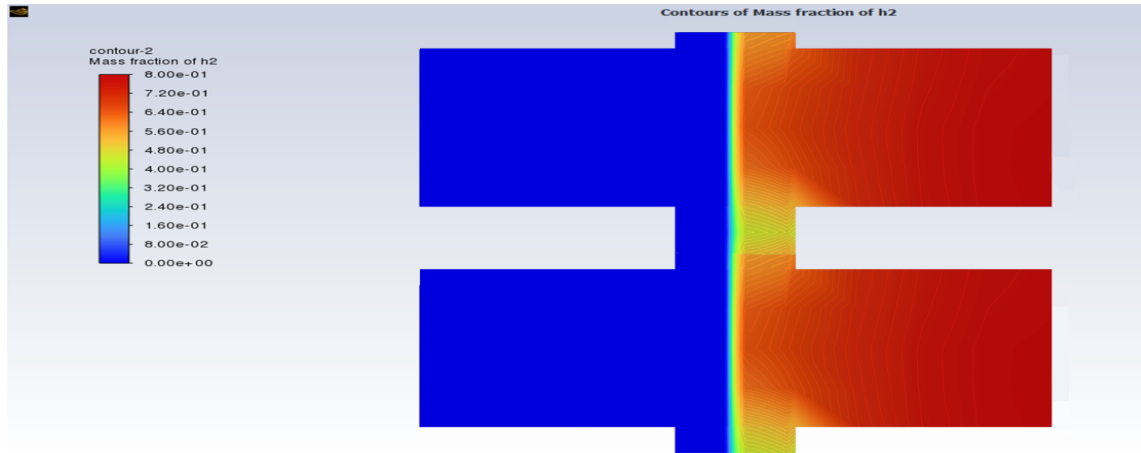


Figure 7.42- Mass fraction of hydrogen in 2mm flow channel width of tri serpentine PEMFC at 0.35V (medium)

In figure 7.42, the consumption rate of the mass fraction of hydrogen (H_2) at the gas diffusion layer (GDL) in the 2mm flow channel width of tri serpentine flow channel at 0.35V is measured at 0.676.

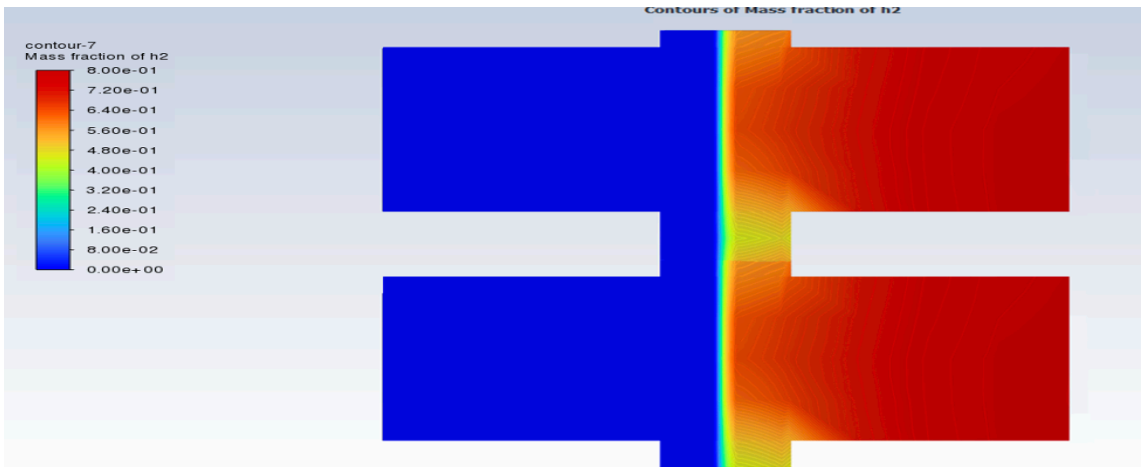


Figure 7.43- Mass fraction of hydrogen in 2mm flow channel width of tri-serpentine PEMFC at 0.55V (high)

In figure 7.43, the consumption rate of the mass fraction of hydrogen (H_2) at the gas diffusion layer (GDL) at 0.55V tri serpentine flow channel is measured at 0.719.

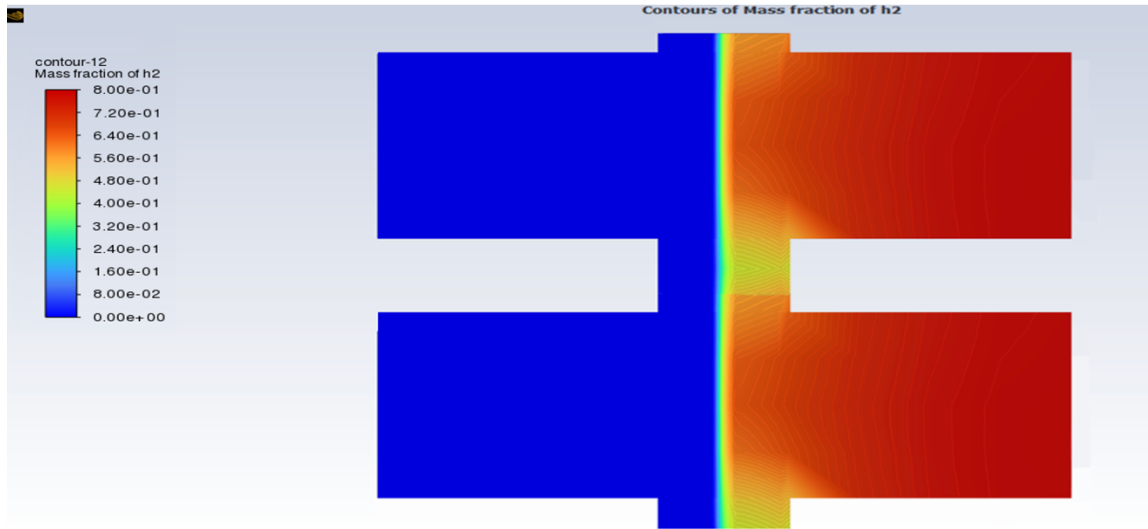


Figure 7.44- Mass fraction of hydrogen in 2mm flow channel width of tri-serpentine PEMFC at 0.65V (very high)

In figure 7.44, the consumption rate of the mass fraction of hydrogen (H_2) at the gas diffusion layer (GDL) at 0.65V tri serpentine flow channel is measured at 0.765.

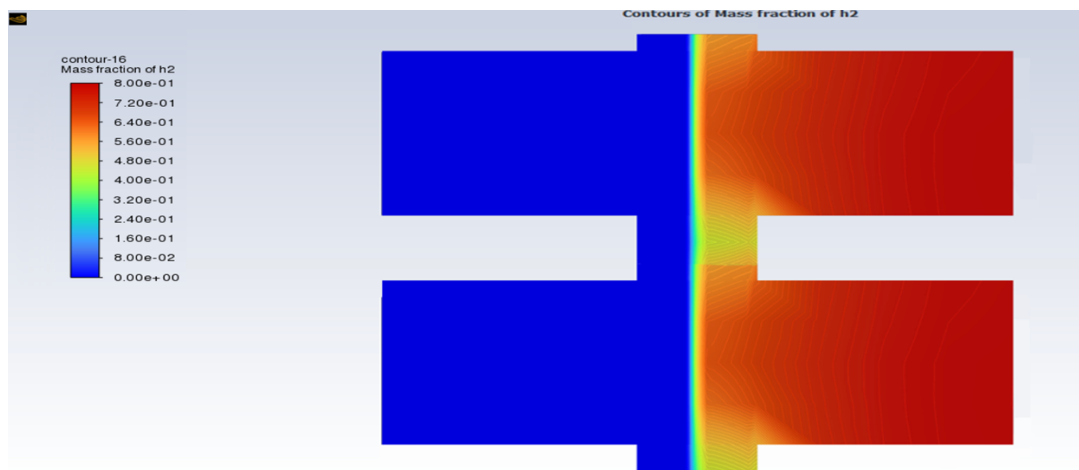


Figure 7.45- Mass fraction of hydrogen in 2mm flow channel width of tri-serpentine PEMFC at 0.8V (extreme)

In figure 7.45, the consumption rate of the mass fraction of hydrogen (H_2) at the gas diffusion layer (GDL) at 0.8V tri serpentine flow channel is measured at 0.796.

At 0.25V, it is noted that the 2mm flow channel width of single serpentine PEMFC exhibited the hydrogen (H_2) consumption rate of 0.541 while the bi serpentine flow channel, it is 0.601 and, in the tri, serpentine flow channel, it is 0.642.

At 0.35V, it is noted that the 2mm flow channel width of single serpentine PEMFC exhibited the hydrogen (H_2) consumption rate of 0.587 while the bi serpentine flow channel, it is 0.625 and, in the tri, serpentine flow channel, it is 0.676.

At 0.5V, it is noted that the 2mm flow channel width of single serpentine PEMFC exhibited the hydrogen (H_2) consumption rate of 0.630 while the bi serpentine flow channel, it is 0.662. At 0.55V, the tri serpentine flow channel has a hydrogen (H_2) consumption rate of 0.719.

At 0.65V, it is noted that the 2mm flow channel width of single serpentine PEMFC exhibited the hydrogen (H_2) consumption rate of 0.683 while the bi serpentine flow channel, it is 0.707. The tri serpentine flow channel has a hydrogen (H_2) consumption rate of 0.765.

At 0.8 V, it is noted that the 2mm flow channel width of single serpentine PEMFC exhibited the hydrogen (H_2) consumption rate of 0.709 while the bi serpentine flow channel, it is 0.734. The tri serpentine flow channel has a hydrogen (H_2) consumption rate of 0.796.

From the analysis of mass fraction of hydrogen (H_2) across all flow channels, it was observed that the hydrogen distribution is uniform. Notably, the tri

serpentine flow channel exhibited the highest hydrogen (H₂) consumption rate compared to the single and bi serpentine flow channels. The higher consumption rate in tri serpentine flow channel contributed to the generation of higher current. Furthermore, ensuring gas is evenly spread leads to longer lifespan and enhanced functionality of the cell. The high diffusibility of hydrogen (H₂) stems from its status as the lightest element worldwide.

7.4 Cell Reynolds Number

The Reynolds number is a parameter used to determine the flow pattern, whether it is laminar, turbulent or in transition. In this study, the author initially assumed laminar flow pattern in the software. The simulation is conducted to verify whether this assumption aligns with the actual flow behavior. Typically, the Reynolds number is influenced by the velocity of the flow. It is calculated using the following equation.

$$Re = \frac{\rho V D}{\mu}$$

where, V = velocity of the fluid (m/s)

ρ = density of the fluid (kg/m³)

D = diameter of the pipe (m)

μ = dynamic viscosity of the fluid (kg/ms)

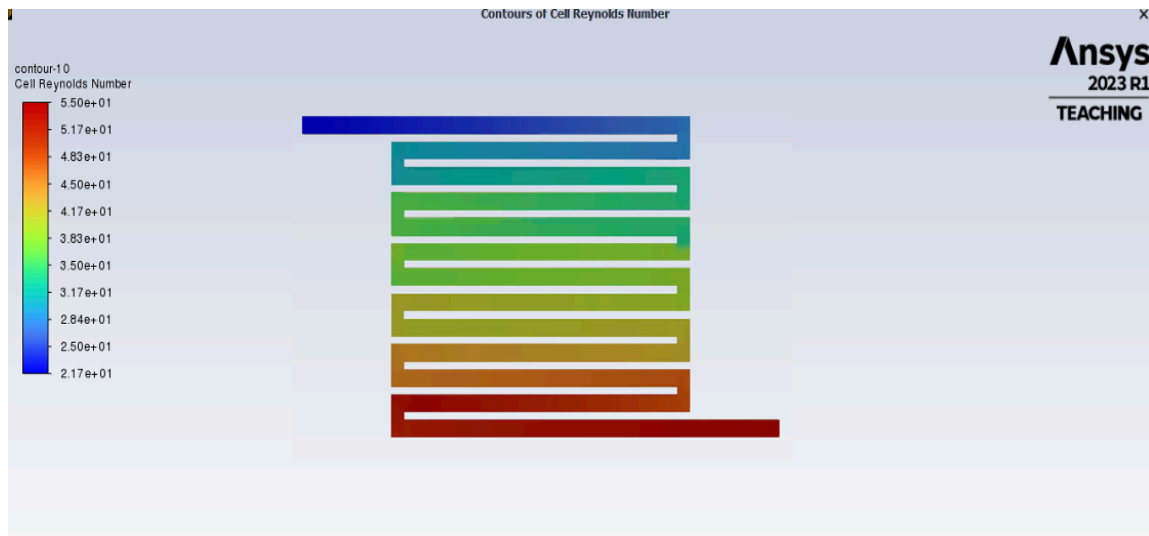


Figure 7.46 – Cell Reynolds Number of 2mm flow channel width of single serpentine PEMFC at 0.25V (low)

The figure 7.46 illustrated the variation in Cell Reynolds number along the 2mm flow channel width of single serpentine PEMFC at 0.25 V. Specifically, the Reynolds number at the inlet of the single serpentine PEMFC is measured to be 21.7, while at the outlet, it is 55.

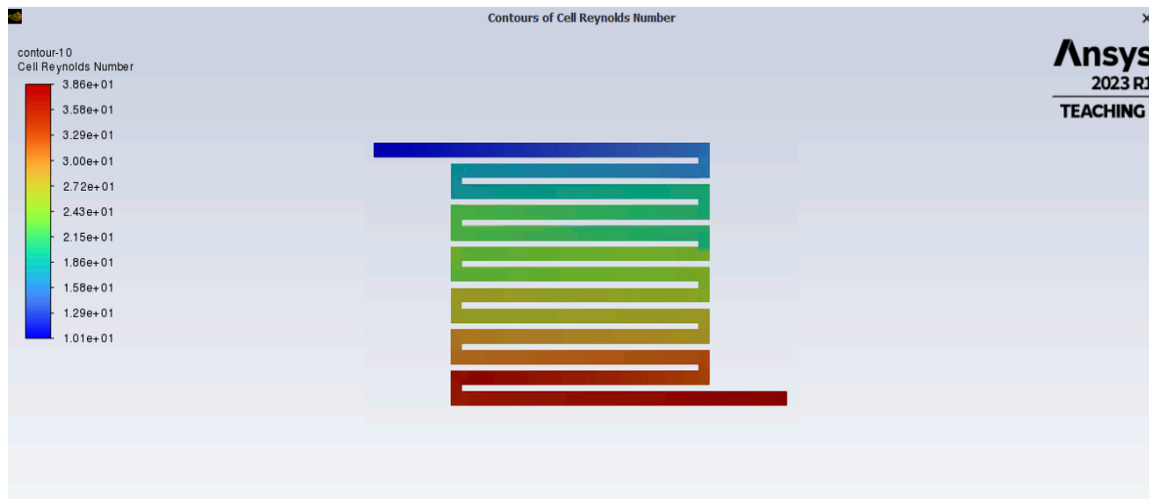


Figure 7.47 – Cell Reynolds Number of 2mm flow channel width of single serpentine PEMFC at 0.35V (medium)

The figure 7.47 illustrated the variation in Cell Reynolds number along 2mm flow channel width of single serpentine PEMFC at 0.35 V. Specifically, the Reynolds number at the inlet of the single serpentine PEMFC is measured to be 28.8, while at the outlet, it is 60.9.

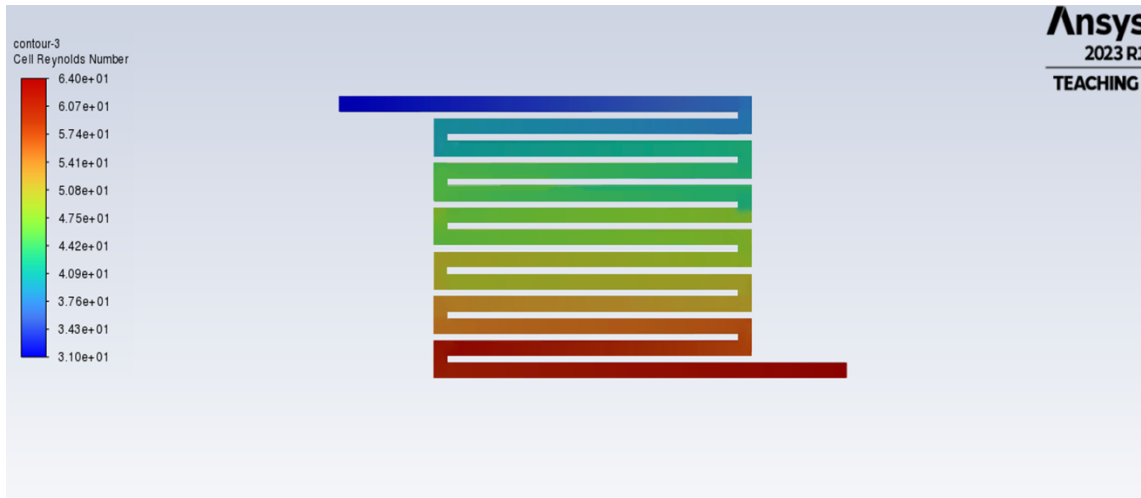


Figure 7.48 – Cell Reynolds Number of 2mm flow channel width of single serpentine PEMFC at 0.5V (high)

The figure 7.48 illustrated the variation in Cell Reynolds number along 2mm flow channel width of single serpentine PEMFC at 0.5 V. Specifically, the Reynolds number at the inlet of the single serpentine PEMFC is measured to be 31, while at the outlet, it is 64.

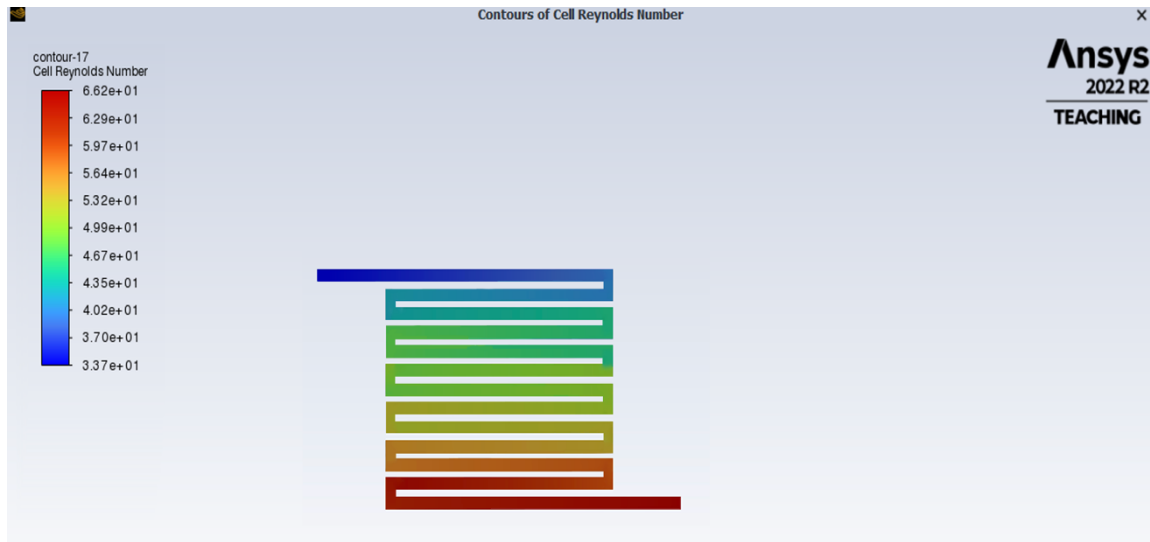


Figure 7.49 – Cell Reynolds Number of 2mm flow channel width of single serpentine PEMFC at 0.65V (very high)

The figure 7.49 illustrated the variation in Cell Reynolds number along 2mm flow channel width of single serpentine PEMFC at 0.65 V. Specifically, the Reynolds number at the inlet of the single serpentine PEMFC is measured to be 33.7, while at the outlet, it is 66.2.

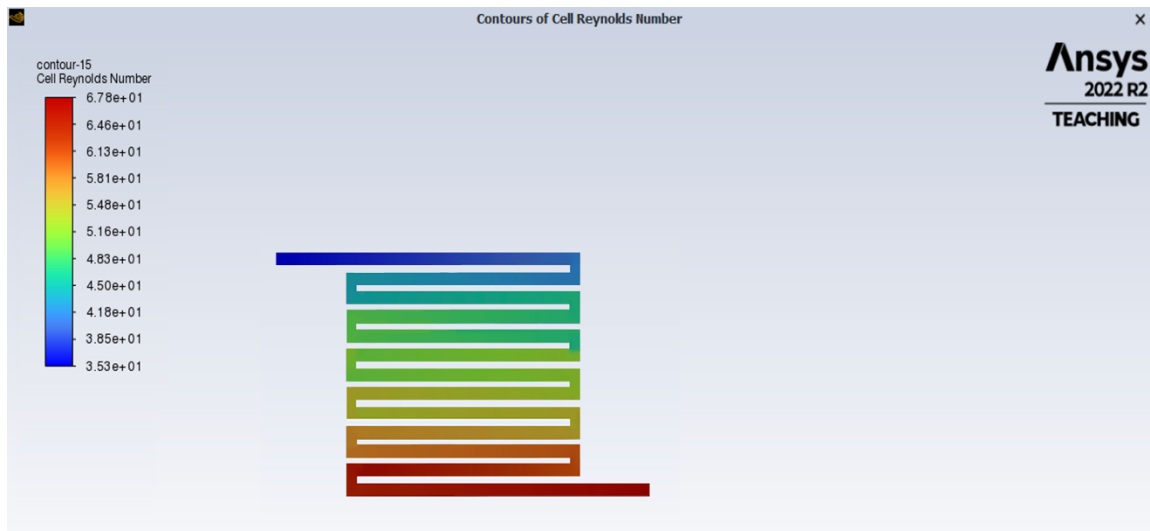


Figure 7.50 – Cell Reynolds Number of 2mm flow channel width of single serpentine PEMFC at 0.8V (extreme)

The figure 7.50 illustrated the variation in Cell Reynolds number along 2mm flow channel width of single serpentine PEMFC at 0.8 V. Specifically, the Reynolds number at the inlet of the single serpentine PEMFC is measured to be 35.3, while at the outlet, it is 67.8.

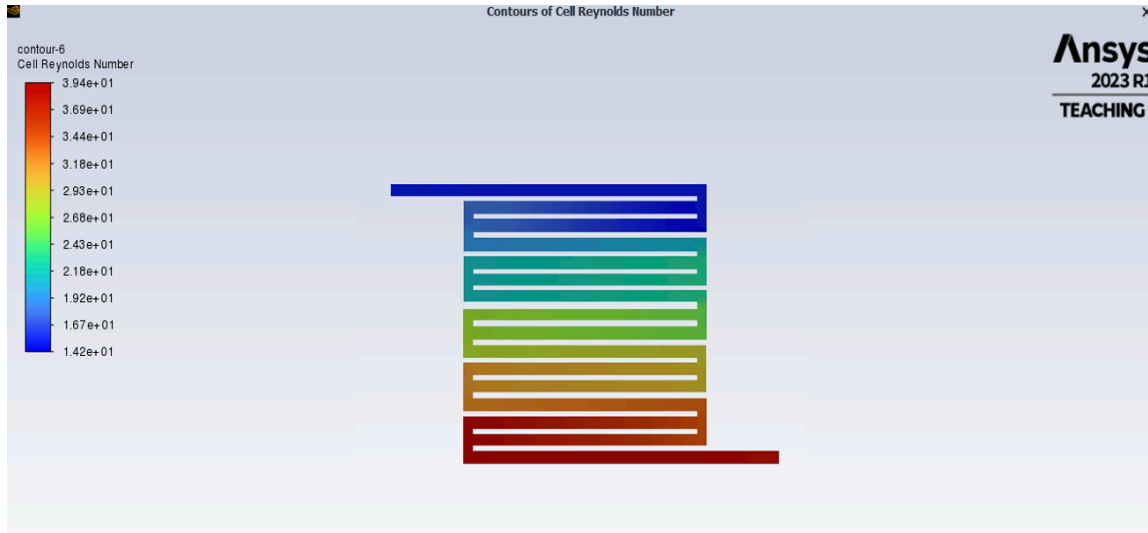


Figure 7.51– Cell Reynolds Number of 2mm flow channel width of bi serpentine PEMFC at 0.25 (low)

The figure 7.51 illustrated the variation in Cell Reynolds number along 2mm flow channel width of bi serpentine PEMFC at 0.25 V. Specifically, the Reynolds number at the inlet of the bi serpentine PEMFC is measured to be 14.2, while at the outlet, it is 39.4.

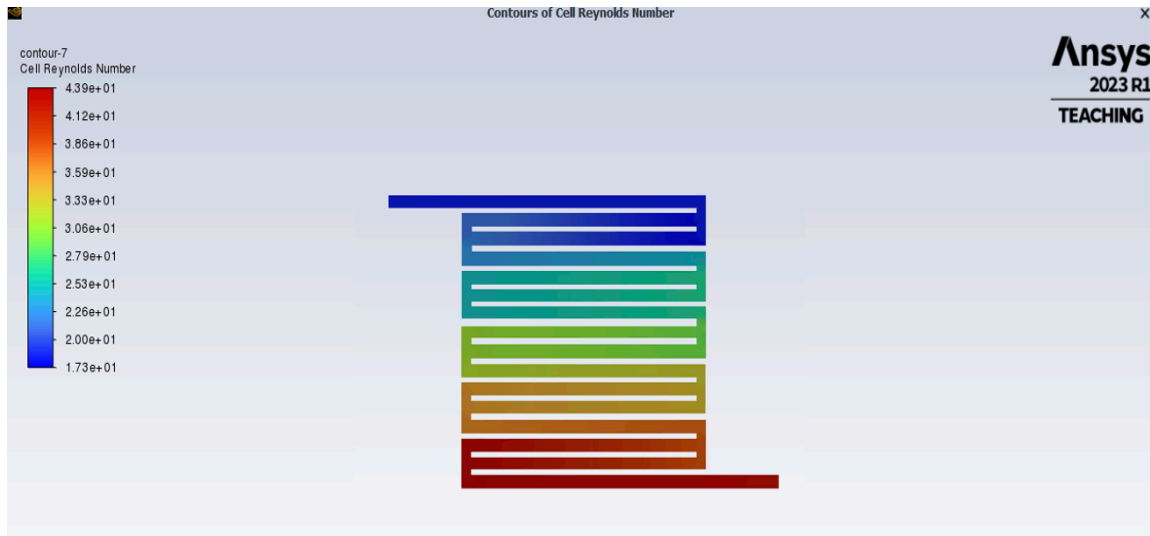


Figure 7.52– Cell Reynolds Number of 2mm flow channel width of bi serpentine PEMFC at 0.35 V (medium)

The figure 7.52 illustrated the variation in Cell Reynolds number along 2mm flow channel width of bi serpentine PEMFC at 0.35 V. Specifically, the Reynolds number at the inlet of the bi serpentine PEMFC is measured to be 17.3, while at the outlet, it is 43.9.

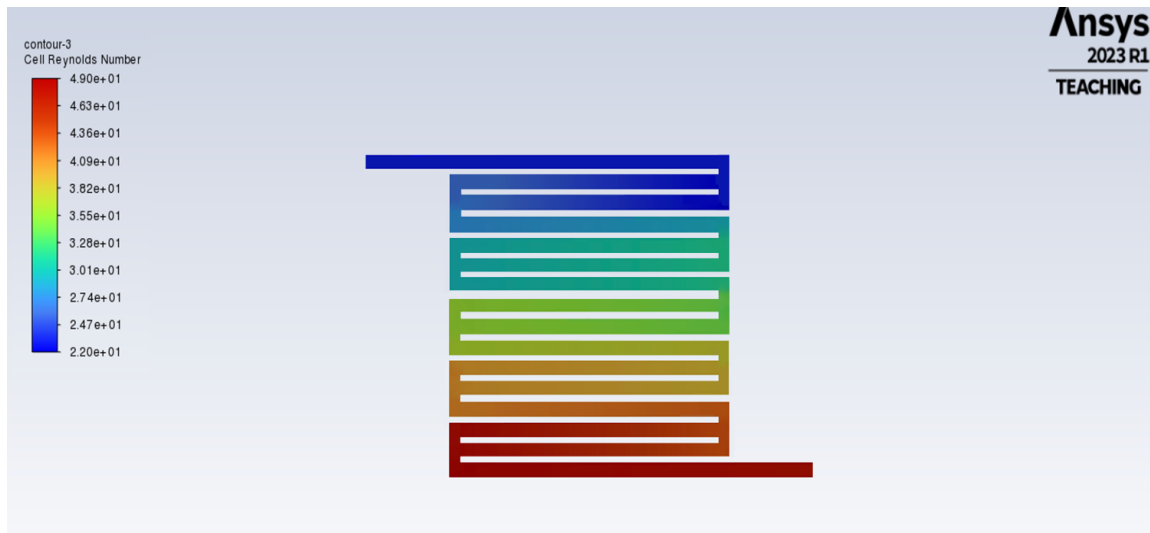


Figure 7.53– Cell Reynolds Number of 2mm flow channel width of bi serpentine PEMFC at 0.5V (high)

The figure 7.53 illustrated the variation in Cell Reynolds number along 2mm flow channel width of bi serpentine PEMFC at 0.5 V. Specifically, the Reynolds number at the inlet of the bi serpentine PEMFC is measured to be 22, while at the outlet, it is 49.

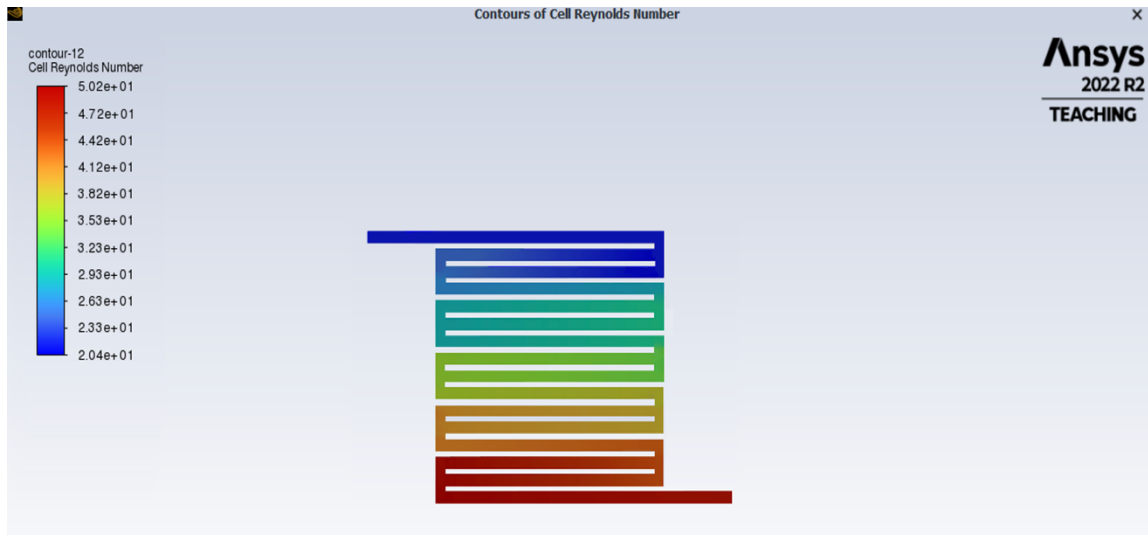


Figure 7.54– Cell Reynolds Number of 2mm flow channel width of bi serpentine PEMFC at 0.65V (very high)

The figure 7.54 illustrated the variation in Cell Reynolds number along 2mm flow channel width of bi serpentine PEMFC at 0.65 V. Specifically, the Reynolds number at the inlet of the bi serpentine PEMFC is measured to be 23.7, while at the outlet, it is 50.5.

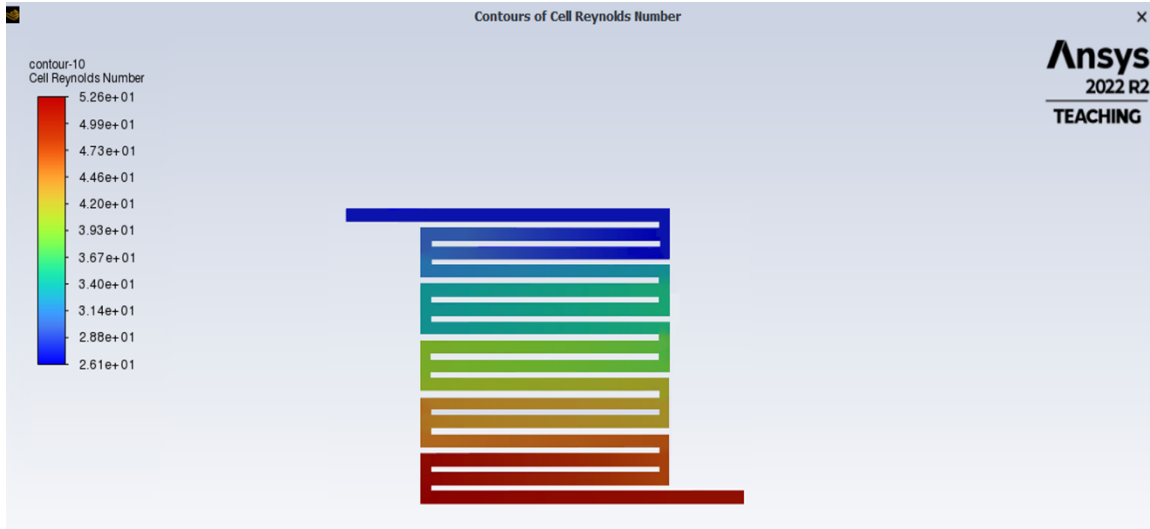


Figure 7.55– Cell Reynolds Number of 2mm flow channel width of bi serpentine PEMFC at 0.8V (extreme)

The figure 7.55 illustrated the variation in Cell Reynolds number along 2mm flow channel width of bi serpentine PEMFC at 0.8 V. Specifically, the Reynolds number at the inlet of the bi serpentine PEMFC is measured to be 26.1, while at the outlet, it is 52.6.

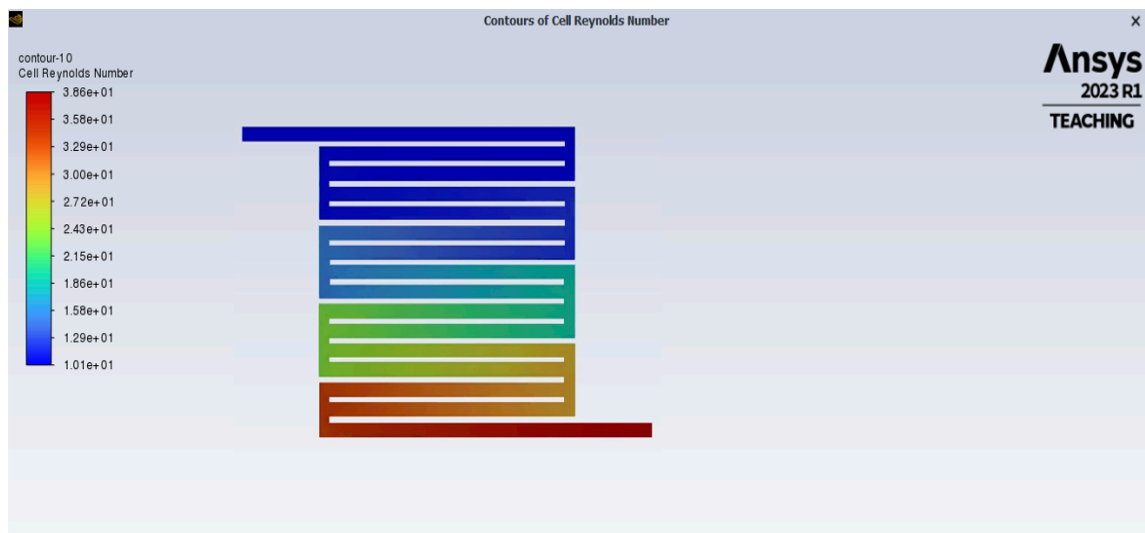


Figure 7.56– Cell Reynolds Number of 2mm flow channel width of tri serpentine PEMFC at 0.25V (low)

The figure 7.56 illustrates the variation in Cell Reynolds number along 2mm flow channel width of the tri serpentine PEMFC at 0.25 V. Specifically, the Reynolds number at the inlet of the tri serpentine PEMFC is measured to be 10.1, while at the outlet, it is 38.6.

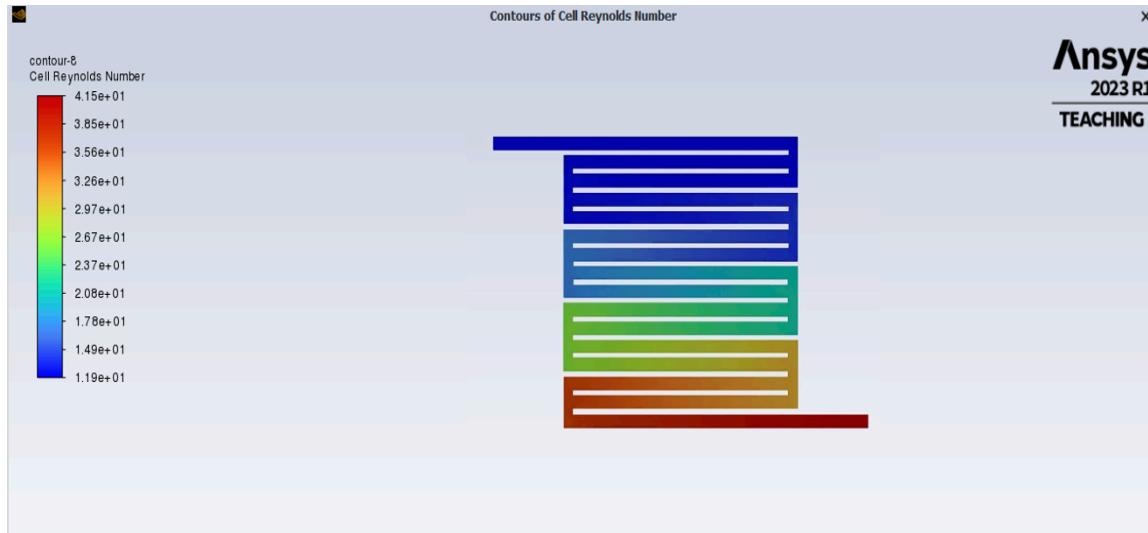


Figure 7.57– Cell Reynolds Number of 2mm flow channel width of tri serpentine PEMFC at 0.35V (medium)

The figure 7.57 illustrates the variation in Cell Reynolds number along 2mm flow channel width of the tri serpentine PEMFC at 0.35 V. Specifically, the Reynolds number at the inlet of the tri serpentine PEMFC is measured to be 11.9, while at the outlet, it is 41.5.

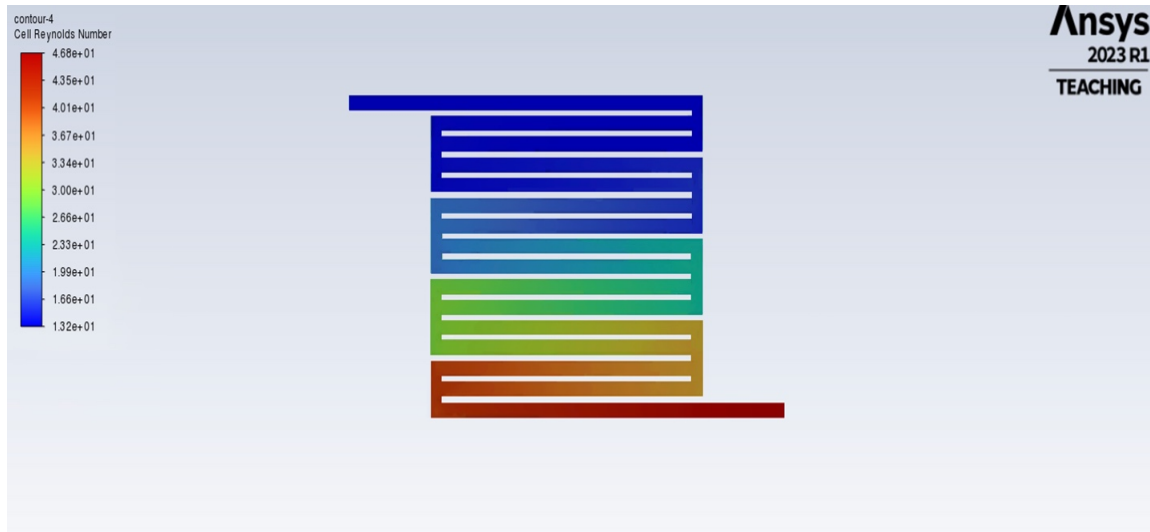


Figure 7.58 – Cell Reynolds Number of 2mm flow channel width of tri serpentine PEMFC at 0.55V (high)

The figure 7.58 illustrates the variation in Cell Reynolds number along 2mm flow channel width of the tri serpentine PEMFC at 0.55 V. Specifically, the Reynolds number at the inlet of the tri serpentine PEMFC is measured to be 13.2, while at the outlet, it is 46.8.

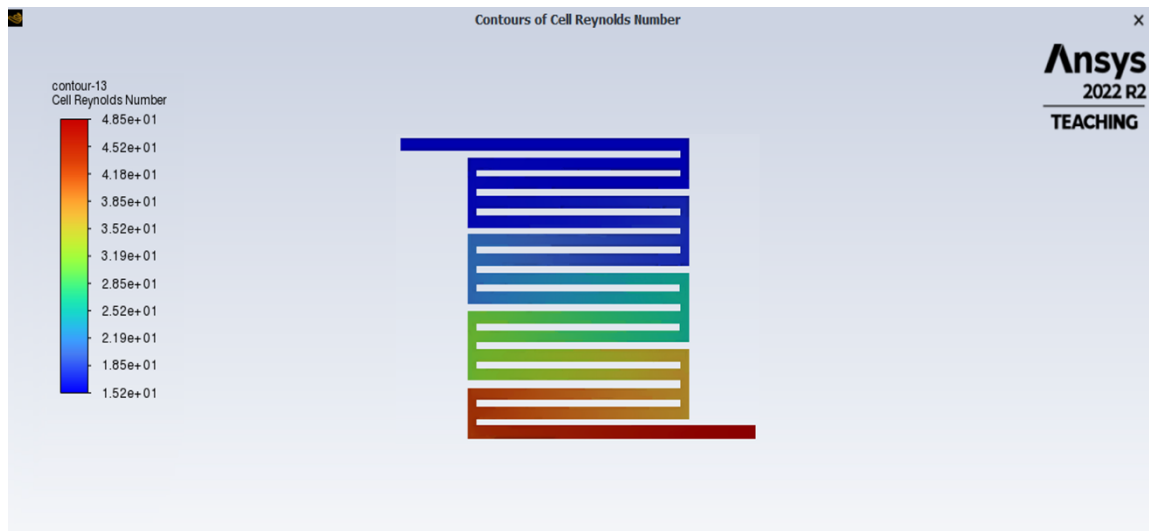


Figure 7.59 – Cell Reynolds Number of 2mm flow channel width of tri serpentine PEMFC at 0.65V (very high)

The figure 7.59 illustrates the variation in Cell Reynolds number along 2mm flow channel width of the tri serpentine PEMFC at 0.65 V. Specifically, the Reynolds number at the inlet of the tri serpentine PEMFC is measured to be 15.1, while at the outlet, it is 48.4.

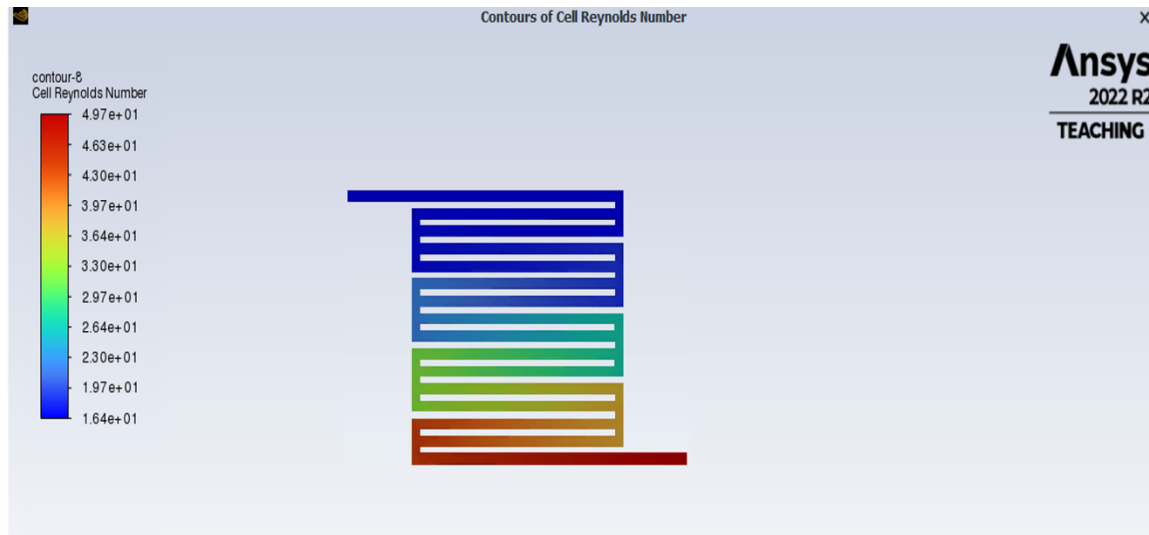


Figure 7.60 – Cell Reynolds Number of 2mm flow channel width of tri serpentine PEMFC at 0.8V (extreme)

The figure 7.60 illustrates the variation in Cell Reynolds number along 2mm flow channel width of the tri serpentine PEMFC at 0.8 V. Specifically, the Reynolds number at the inlet of the tri serpentine PEMFC is measured to be 16.4, while at the outlet, it is 49.6.

The observed Reynolds numbers for all the three flow channels ranges from 10.1 to 67.8 for all the three flow channels.

At all the low (0.25V), medium (0.35V), high (0.5V), very high (0.65V) and extreme (0.8V) range of voltage, the Cell Reynolds number values fall within the laminar flow regime, confirming that the flow is indeed laminar and aligning with the initial assumption.

CHAPTER 8

COMPARISON AND ANALYSIS OF PEMFC WITH VARYING FLOW CHANNEL WIDTH

This chapter delves into the adjustment of flow channel widths in the PEMFC, specifically focusing on dimensions of 1mm and 3mm. Previous discussions in Chapter 6 have covered the 2mm flow channel width. The primary objective of this research is to conduct a comparative analysis of flow channel performance across single, bi, and tri serpentine configurations with varying width dimensions. The specifications for the dimensions and materials of the components are detailed in the table 4.2. The simulations for all models are conducted based on the operating conditions outlined in table 8.1. Additionally, the study delves into the analysis of three different flow channel designs with width of 1mm and 3mm to gain a comprehensive understanding of their impact on fuel cell behavior and efficiency.

Table 8.1 - Operating conditions of the PEMFC for various flow channel width

Cell temperature (K)	373 (100°C)	Estimated
Mass flow rate at Anode (Kg/s)	4.33E-07	[85]
Mass flow rate at Cathode (Kg/s)	3.33E-06	[85]

Table 8.1 - continued

Anode inlet temperature (K)	373 (100°C)	Estimated
Cathode inlet temperature (K)	373 (100°C)	Estimated
Operating pressure (Bar)	2	[85]
Open Circuit Voltage (V)	0.1V, 0.15V, 0.2V, 0.25V,...1V	Estimated
Porosity of GDL	0.4	Assumed
Porosity of CL	0.5	Assumed

The table 8.1 provides a comprehensive overview of the operating conditions and pertinent parameters utilized in simulating the PEMFC. Some of the operating conditions were considered from [85]. Cell temperatures, as well as anode and cathode inlet temperatures are 373 Kelvin. Anode and cathode mass flow rates are specified accordingly. The operating pressure is set at 2bar, while the Open Circuit Voltage (OCV) spans from 0.1V to 1V in increments. Additionally, the porosity of the Gas Diffusion Layer (GDL) and Catalyst Layer (CL) are defined as 0.4 and 0.5, respectively.

In the forthcoming sections, adjustments to the flow channel widths of single serpentine, bi serpentine, and tri serpentine PEMFCs to dimensions of 1mm and 3mm will be discussed. These modifications will be compared to

investigate their impact on cell performance. It is important to note that all PEMFCs under examination maintain an identical active area.

8.1 1mm and 3mm Flow Channel Width of Single Serpentine PEMFC

This section covers the design and simulation of single serpentine PEMFC with flow channel widths of 1mm and 3mm. It delves into the specifics of designing and simulating these configurations to investigate their performance.

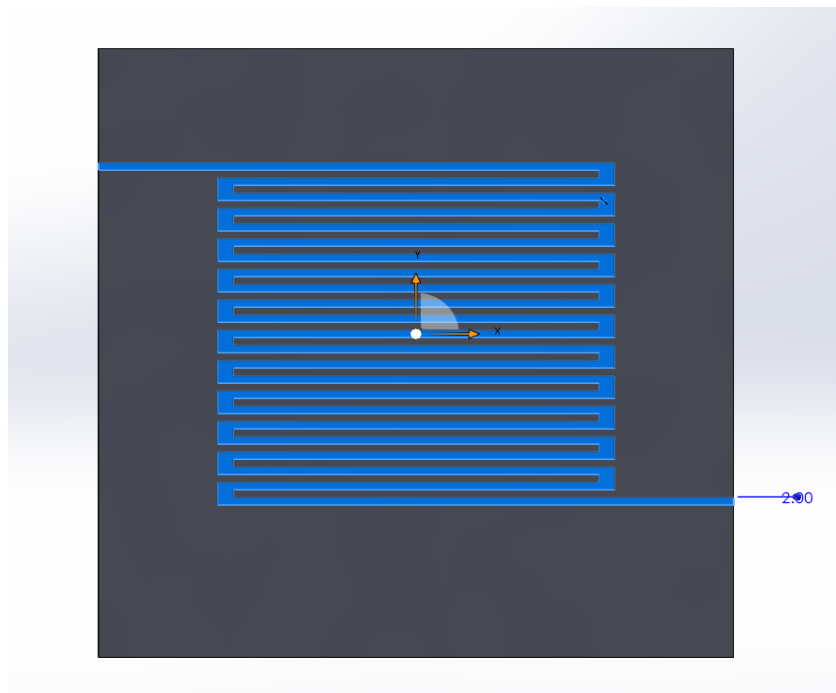


Figure 8.1 - Single serpentine PEMFC of 1mm width of flow channel

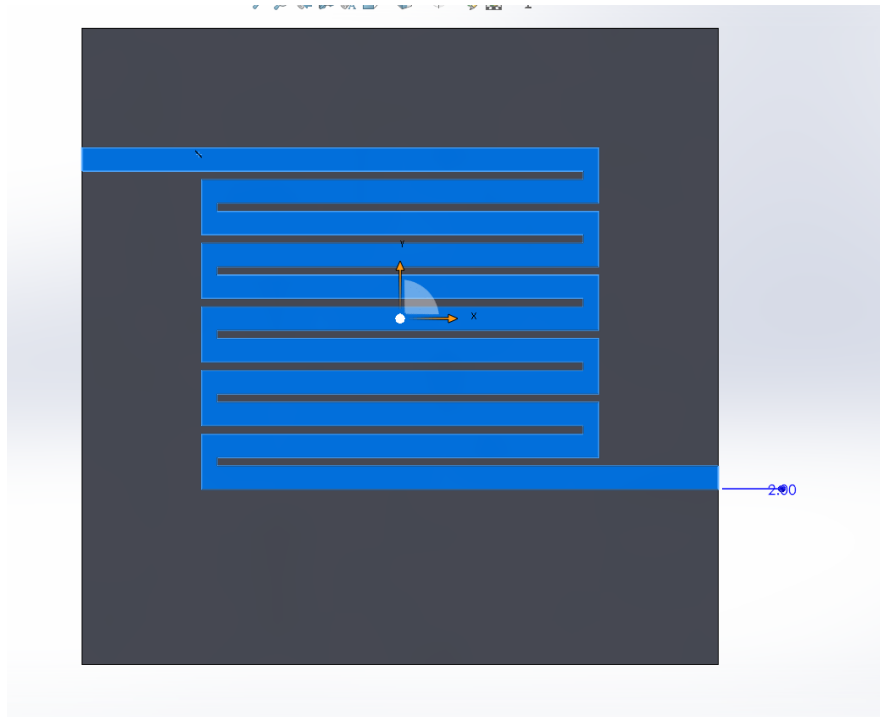


Figure 8.2 - Single serpentine PEMFC of 3mm width of flow channel

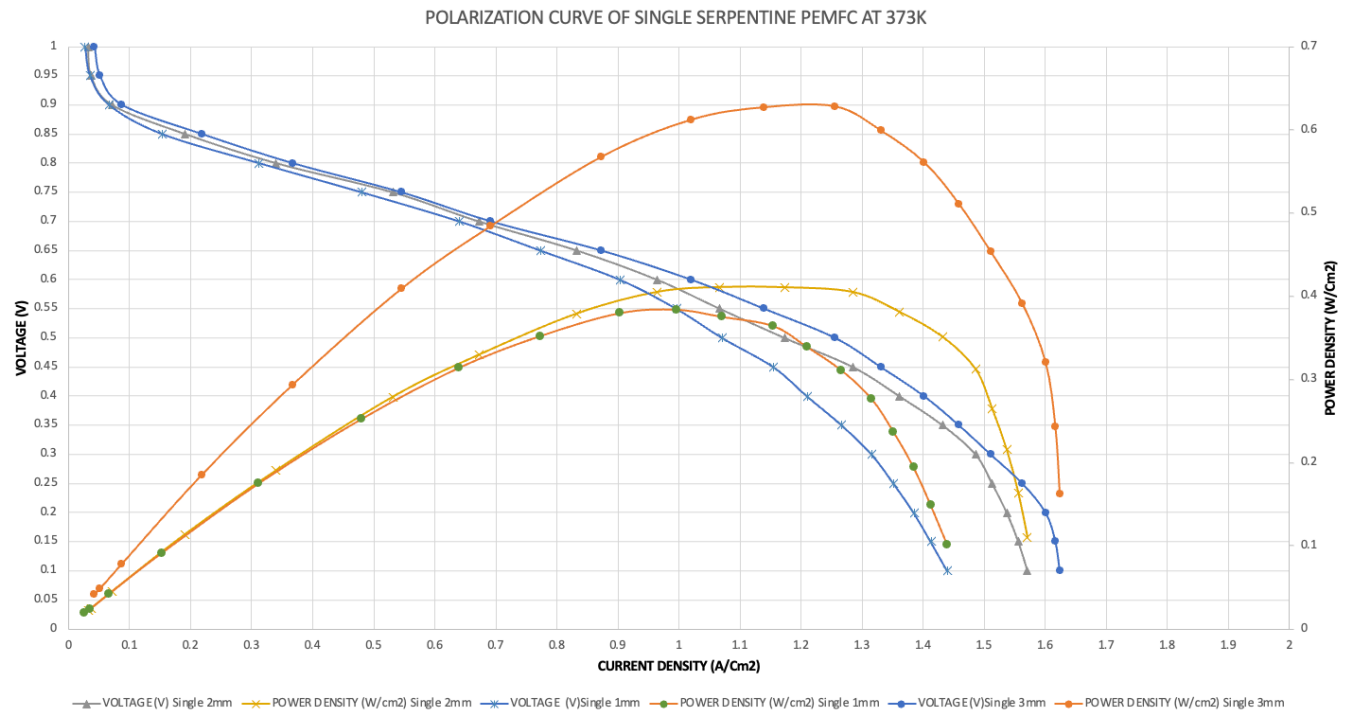


Figure 8.3 – Polarization curve of single serpentine PEMFC at 373K and 2 bar pressure

Table 8.2 - Results of single serpentine PEMFC at 373K and 2 bar pressure

Temperature (K)	Flow Channel Width (mm)	Voltage (V)	Current Density (A/cm ²)	Peak Power Density (W/cm ²)
373 (100°C)	1	0.55	0.981	0.539
373 (100°C)	2	0.55	1.067	0.5868
373 (100°C)	3	0.5	1.284	0.642

Figure 8.3 illustrates the polarization curve of single serpentine PEMFC at 373K and 2 bar pressure. Table 8.2 presents the corresponding results for the same conditions. Within the single serpentine flow channel, the current density for a 1mm width is recorded as 0.981 A/cm² with an associated power density of 0.539 W/cm² at 0.55V. For a 2mm width, the current density is slightly higher at 1.067 A/cm², resulting in a power density of 0.5868 W/cm² at 0.55V. Lastly, for a 3mm width, the current density increases to 1.284 A/cm², yielding a power density of 0.642 W/cm² at 0.5V.

8.2 1mm and 3mm Flow Channel Width of Bi Serpentine PEMFC

In this section, the design and simulation of bi serpentine PEMFC with flow channel width has been discussed. The design has 1mm and 3mm flow channel width of bi serpentine PEMFC.

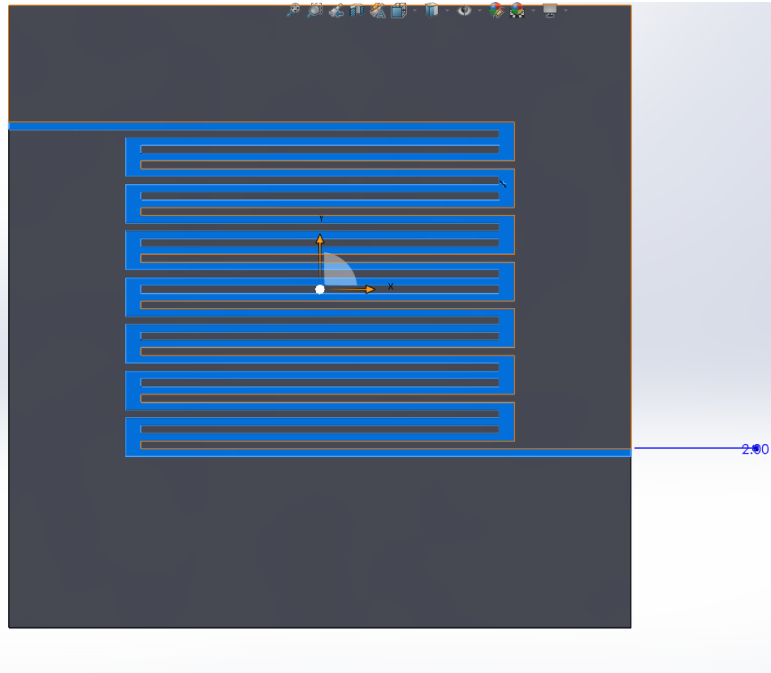


Figure 8.4 - Bi serpentine flow channel PEMFC with 1mm width of flow channel

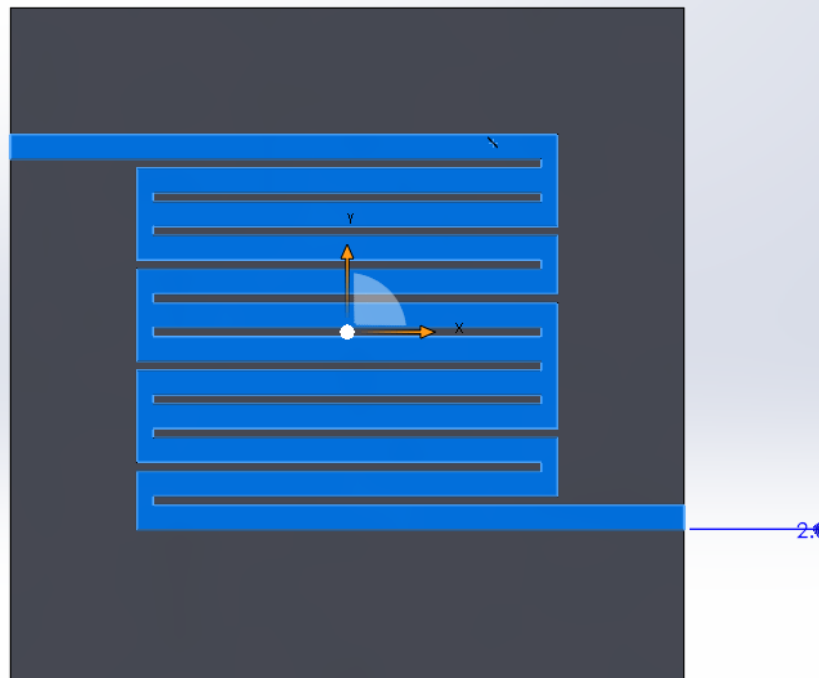


Figure 8.5 - Bi serpentine flow channel PEMFC with 3mm width of flow channel

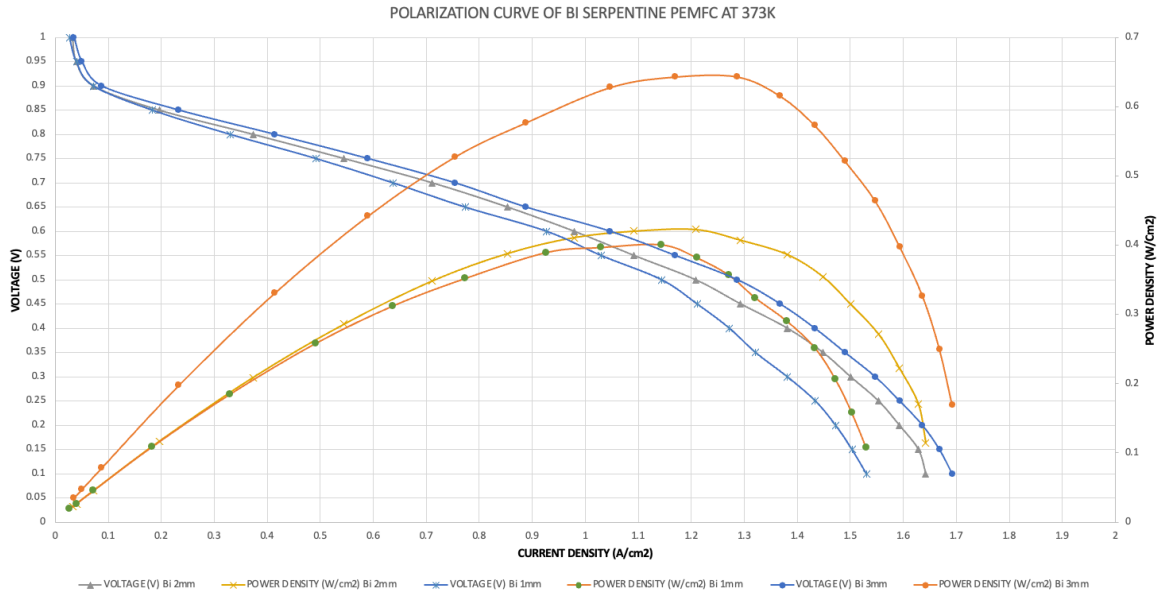


Figure 8.6 – Polarization curve of bi serpentine PEMFC at 373K and 2 bar pressure

Table 8.3 - Results of bi serpentine PEMFC at 373K and 2 bar pressure

Temperature (K)	Flow Channel Width (mm)	Voltage (V)	Current Density (A/cm ²)	Peak Power Density (W/cm ²)
373 (100°C)	1	0.5	1.15	0.575
373 (100°C)	2	0.5	1.208	0.604
373 (100°C)	3	0.5	1.293	0.6465

Figure 8.6 illustrated the polarization curve of the bi serpentine PEMFC at 373K and 2 bar pressure, while table 8.3 presents the results of bi serpentine PEMFC at 373K. Within the bi serpentine flow channel, the current density for a 1mm width is recorded as 1.15 A/cm² with an associated power density

of 0.575 W/cm^2 at 0.5 V . For a 2mm width, the current density is slightly higher at 1.208 A/cm^2 , resulting in a power density of 0.604 W/cm^2 at 0.5 V . Lastly, for a 3mm width, the current density increases to 1.293 A/cm^2 , yielding a power density of 0.6464 W/cm^2 at 0.5 V .

8.3 1mm and 3mm Flow Channel Width of Tri Serpentine PEMFC

This section covers the design and simulation of tri serpentine PEMFC with flow channel widths of 1mm and 3mm . It delves into the specifics of designing and simulating these configurations to investigate their performance.

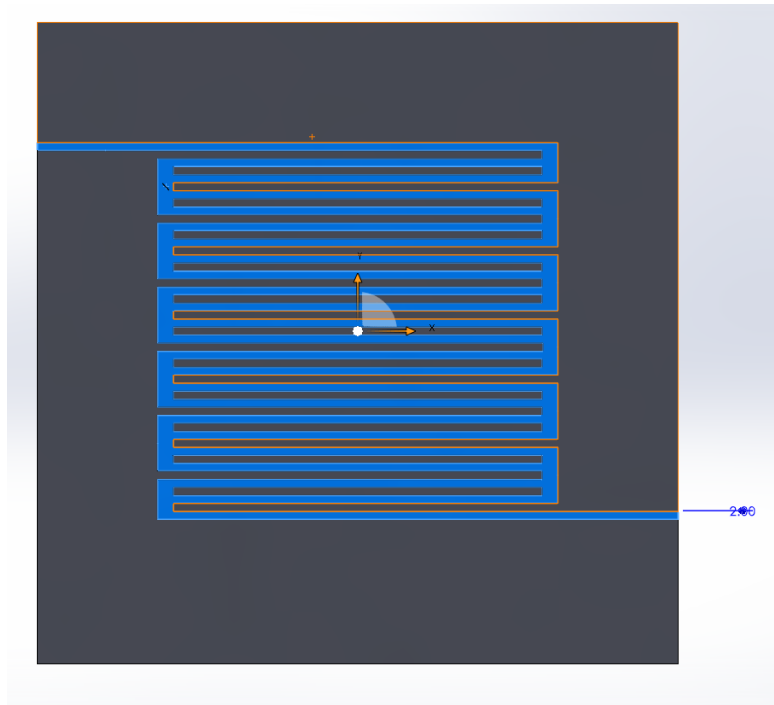


Figure 8.7 - Tri serpentine flow channel PEMFC with 1mm width of flow channel

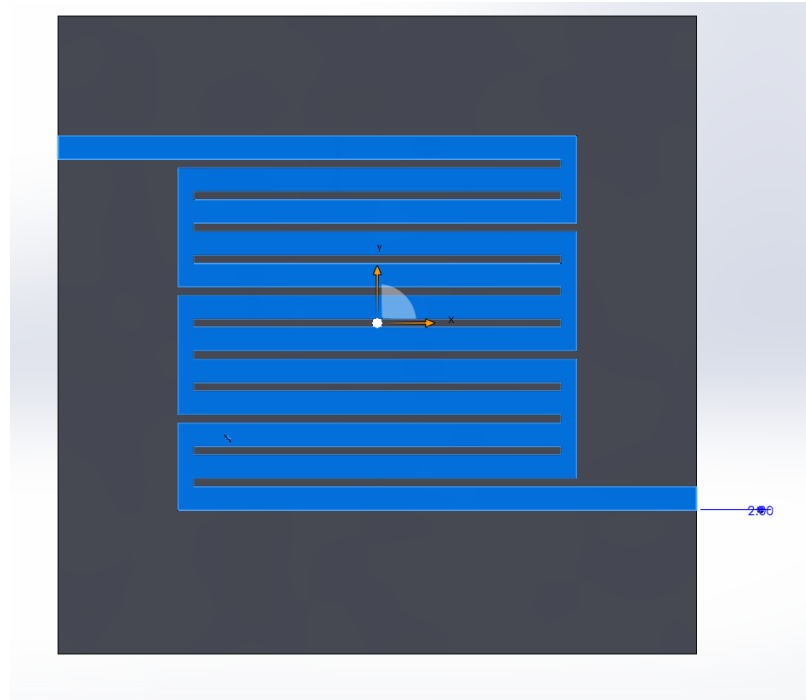


Figure 8.8 - Tri serpentine flow channel PEMFC with 3mm width of flow channel

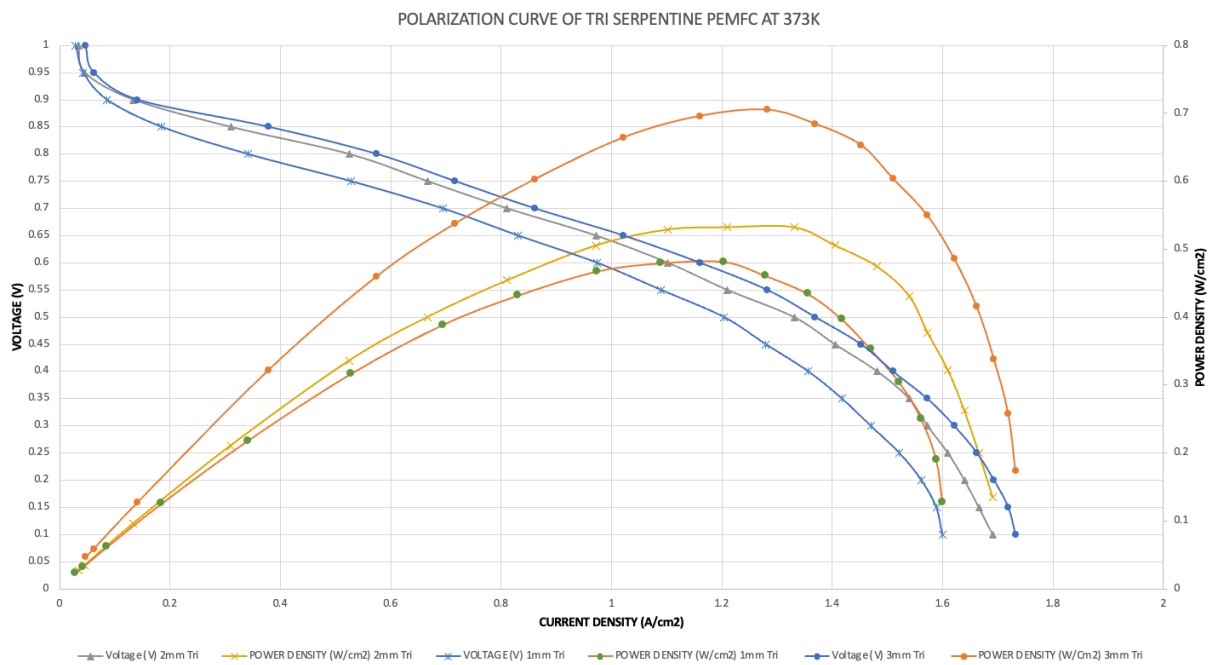


Figure 8.9 – Polarization curve of tri serpentine PEMFC at 373K and 2 bar pressure

Table 8.4 - Results of tri serpentine PEMFC at 373K and 2 bar pressure

Temperature (K)	Flow Channel Width (mm)	Voltage (V)	Current Density (A/cm ²)	Peak Power Density (W/cm ²)
373 (100°C)	1	0.5	1.2	0.6
373 (100°C)	2	0.55	1.21	0.6655
373 (100°C)	3	0.55	1.3	0.715

Figure 8.9 illustrates the polarization curve of the tri serpentine PEMFC at 373K and 2 bar pressure, while table 8.4 presents the corresponding results for the same conditions. Within the tri serpentine flow channel, the current density for a 1mm width is recorded as 1.2 A/cm² with an associated power density of 0.6 W/cm² at 0.5V. For a 2mm width, the current density slightly higher at 1.21 A/cm², resulting in a corresponding power density of 0.6655 W/cm² at 0.55V. Lastly, for a 3mm width, the current density increases to 1.3 A/cm², yielding a power density of 0.715W/cm² at 0.55V.

8.4 Pressure Distribution Analysis of 1mm and 3mm Flow Channel Width PEMFC

Optimizing pressure distribution is essential for improving performance, and its crucial in analyzing the impact of different designs having 1mm and 3mm flow channel width on pressure distribution in PEMFC. The main goal is to identify effective pressure management strategies for enhancing fuel cell performance. In this analysis, the pressure distribution of 2mm flow channel width also included to compare with 1mm and 3mm flow channel width.

Table 8.5 - Results of pressure distribution of single serpentine PEMFCs at 0.25V (low)

S.No	Flow Channel Width (mm)	Voltage (V)	Current Density (A/cm ²)	Inlet Pressure (KPa)	Outlet Pressure (KPa)	Pressure loss (KPa)
1	1	0.25	1.352	200	117	83
2	2	0.25	1.513	199	120	79
3	3	0.25	1.563	200	127	73

Table 8.5 illustrates the results of pressure distribution of single serpentine PEMFC at 0.25 V. For the 1mm, the pressure drops across the channel is 83KPa, while the 2mm has a pressure drop of 79KPa, and the pressure loss of 3mm channel width is found to be 73KPa.

Table 8.6 - Results of pressure distribution of single serpentine PEMFCs at 0.35V (medium)

S.No	Flow Channel Width (mm)	Voltage (V)	Current Density (A/cm ²)	Inlet Pressure (KPa)	Outlet Pressure (KPa)	Pressure loss (KPa)
1	1	0.35	1.267	200	127	73
2	2	0.35	1.432	199	128	71
3	3	0.35	1.459	200	135	65

Table 8.6 presents the pressure distribution results for a single serpentine PEMFC at 0.35V. The 1mm channel exhibits a pressure drop of 73KPa, while the 2mm channel experiences a pressure drops of 71KPa. Additionally, the 3mm channel width shows a pressure drop of 65KPa.

Table 8.7 - Results of pressure distribution of single serpentine PEMFCs at 0.5V (high)

S.No	Flow Channel Width (mm)	Voltage (V)	Current Density (A/cm ²)	Inlet Pressure (KPa)	Outlet Pressure (KPa)	Pressure loss (KPa)
1	1	0.5	1.071	200	138	62
2	2	0.5	1.173	199	139	60
3	3	0.5	1.256	200	146	54

Table 8.7 displays the pressure distribution findings for a single serpentine PEMFC operating at 0.5V. The pressure drops across the 1mm channel is 62KPa, while the 2mm channel experiences a pressure drops of 60KPa. Similarly, the 3mm channel width shows a pressure drop of 54 KPa.

Table 8.8 - Results of pressure distribution of single serpentine PEMFCs at 0.65V (very high)

S.No	Flow Channel Width (mm)	Voltage (V)	Current Density (A/cm ²)	Inlet Pressure (KPa)	Outlet Pressure (KPa)	Pressure loss (KPa)
1	1	0.65	0.773	200	144	56

Table 8.8 - continued

2	2	0.65	0.833	200	152	48
3	3	0.65	0.873	200	159	41

Table 8.8 illustrates the results of pressure distribution of single serpentine PEMFC at 0.65 V. For the 1mm, the pressure drops across the channel is 56KPa, while the 2mm has a pressure drop of 48KPa, and the pressure loss of 3mm channel width is found to be 41KPa.

Table 8.9 - Results of pressure distribution of single serpentine PEMFCs at 0.8V (extreme)

S.No	Flow Channel Width (mm)	Voltage (V)	Current Density (A/cm ²)	Inlet Pressure (KPa)	Outlet Pressure (KPa)	Pressure loss (KPa)
1	1	0.8	0.312	200	153	47
2	2	0.8	0.34	200	157	43
3	3	0.8	0.367	200	163	37

Table 8.9 illustrates the results of pressure distribution of single serpentine PEMFC at 0.25 V. For the 1mm, the pressure drops across the channel is 47KPa, while the 2mm has a pressure drop of 43KPa, and the pressure loss of 3mm channel width is found to be 37KPa.

Table 8.10 - Results of pressure distribution of bi serpentine PEMFCs at 0.25V (low)

S.No	Flow Channel Width (mm)	Voltage (V)	Current Density (A/cm ²)	Inlet Pressure (KPa)	Outlet Pressure (KPa)	Pressure loss (KPa)
1	1	0.25	1.434	200	133	67
2	2	0.25	1.553	199	136	63
3	3	0.25	1.593	200	142	58

Table 8.10 illustrates the results of pressure distribution of bi serpentine PEMFC at 0.25 V. For the 1mm, the pressure drops across the channel is 67KPa, while the 2mm has a pressure drop of 63KPa, and the pressure loss of 3mm channel width is found to be 58KPa.

Table 8.11 - Results of pressure distribution of bi serpentine PEMFCs at 0.35V (medium)

S.No	Flow Channel Width (mm)	Voltage (V)	Current Density (A/cm ²)	Inlet Pressure (KPa)	Outlet Pressure (KPa)	Pressure loss (KPa)
1	1	0.35	1.321	200	140	60
2	2	0.35	1.448	199	142	57
3	3	0.35	1.49	200	149	51

Table 8.11 presents the pressure distribution results for a bi serpentine PEMFC at 0.35V. The 1mm channel exhibits a pressure drop of 60KPa, while the 2mm channel experiences a pressure drops of 57KPa. Additionally, the 3mm channel width shows a pressure drop of 51KPa.

Table 8.12 - Results of pressure distribution of bi serpentine PEMFCs at 0.5V (high)

S.No	Flow Channel Width (mm)	Voltage (V)	Current Density (A/cm ²)	Inlet Pressure (KPa)	Outlet Pressure (KPa)	Pressure loss (KPa)
1	1	0.5	1.144	200	149	51
2	2	0.5	1.208	199	151	48
3	3	0.5	1.287	200	155	45

Table 8.12 displays the pressure distribution findings for a bi serpentine PEMFC operating at 0.5V. The pressure drops across the 1mm channel is 51KPa, while the 2mm channel experiences a pressure drops of 48KPa. Similarly, the 3mm channel width shows a pressure drop of 45 KPa.

Table 8.13 - Results of pressure distribution of bi serpentine PEMFCs at 0.65V (very high)

S.No	Flow Channel Width (mm)	Voltage (V)	Current Density (A/cm ²)	Inlet Pressure (KPa)	Outlet Pressure (KPa)	Pressure loss (KPa)
1	1	0.65	0.773	200	156	44
2	2	0.65	0.853	200	161	39
3	3	0.65	0.888	200	165	35

Table 8.13 displays the pressure distribution findings for a bi serpentine PEMFC operating at 0.65V. The pressure drops across the 1mm channel is 44KPa, while the 2mm channel experiences a pressure drops of 39KPa. Similarly, the 3mm channel width shows a pressure drop of 35KPa.

Table 8.14 - Results of pressure distribution of bi serpentine PEMFCs at 0.8V (extreme)

S.No	Flow Channel Width (mm)	Voltage (V)	Current Density (A/cm ²)	Inlet Pressure (KPa)	Outlet Pressure (KPa)	Pressure loss (KPa)
1	1	0.8	0.33	200	160	40
2	2	0.8	0.373	200	164	36
3	3	0.8	0.414	200	170	30

Table 8.14 displays the pressure distribution findings for a bi serpentine PEMFC operating at 0.8V. The pressure drops across the 1mm channel is 40KPa, while the 2mm channel experiences a pressure drops of 36KPa. Similarly, the 3mm channel width shows a pressure drop of 30KPa

Table 8.15 - Results of pressure distribution of tri serpentine PEMFCs at 0.25V (low)

S.No	Flow Channel Width (mm)	Voltage (V)	Current Density (A/cm ²)	Inlet Pressure (KPa)	Outlet Pressure (KPa)	Pressure loss (KPa)
1	1	0.25	1.522	200	148	52
2	2	0.25	1.61	200	149	51
3	3	0.25	1.662	200	151	49

Table 8.15 illustrates the results of pressure distribution of tri serpentine PEMFC at 0.25 V. For the 1mm, the pressure drops across the channel is 52KPa, while the 2mm has a pressure drop of 51KPa, and the pressure loss of 3mm channel width is found to be 49KPa.

Table 8.16 - Results of pressure distribution of tri serpentine PEMFCs at 0.35V (medium)

S.No	Flow Channel Width (mm)	Voltage (V)	Current Density (A/cm ²)	Inlet Pressure (KPa)	Outlet Pressure (KPa)	Pressure loss (KPa)
1	1	0.35	1.418	200	153	47
2	2	0.35	1.54	200	156	44
3	3	0.35	1.572	200	160	40

Table 8.16 presents the pressure distribution results for a tri serpentine PEMFC at 0.35V. The 1mm channel exhibits a pressure drop of 47KPa, while the 2mm channel experiences a pressure drops of 44KPa. Additionally, the 3mm channel width shows a pressure drop of 40KPa.

Table 8.17 - Results of pressure distribution of tri serpentine PEMFCs at 0.5V (high)

S.No	Flow Channel Width (mm)	Voltage (V)	Current Density (A/cm ²)	Inlet Pressure (KPa)	Outlet Pressure (KPa)	Pressure loss (KPa)
1	1	0.5	1.204	200	161	39
2	2	0.5	1.331	200	163	37
3	3	0.5	1.369	200	167	33

Table 8.17 displays the pressure distribution findings for a tri serpentine PEMFC operating at 0.5V. The pressure drops across the 1mm channel is 39KPa, while the 2mm channel experiences a pressure drops of 37KPa. Similarly, the 3mm channel width shows a pressure drop of 33 KPa.

Table 8.18 - Results of pressure distribution of tri serpentine PEMFCs at 0.65V (very high)

S.No	Flow Channel Width (mm)	Voltage (V)	Current Density (A/cm ²)	Inlet Pressure (KPa)	Outlet Pressure (KPa)	Pressure loss (KPa)
1	1	0.65	0.831	200	162	38
2	2	0.65	0.972	200	169	31
3	3	0.65	1.022	200	174	26

Table 8.18 displays the pressure distribution findings for a tri serpentine PEMFC operating at 0.65V. The pressure drops across the 1mm channel is 38KPa, while the 2mm channel experiences a pressure drops of 31KPa. Similarly, the 3mm channel width shows a pressure drop of 26KPa.

Table 8.19 - Results of pressure distribution of tri serpentine PEMFCs at 0.8V (extreme)

S.No	Flow Channel Width (mm)	Voltage (V)	Power Density	Inlet Pressure (KPa)	Outlet Pressure (KPa)	Pressure loss (KPa)
1	1	0.8	0.341	200	167	33
2	2	0.8	0.525	200	173	27
3	3	0.8	0.575	200	178	22

Table 8.19 displays the pressure distribution findings for a tri serpentine PEMFC operating at 0.8V. The pressure drops across the 1mm channel is 33KPa, while the 2mm channel experiences a pressure drops of 27KPa. Similarly, the 3mm channel width shows a pressure drop of 22KPa.

The results indicate that as the flow channel width increases, the pressure drop decreases across three different voltage settings. Specifically, the 3mm channel width exhibits the lowest pressure drop among the rested widths. There is a distinct variation in pressure drop between all channel, with the 2mm channel width positioned between the other two, demonstrating a gradual decrease in pressure drop from 1mm to 3mm.

8.5 Velocity Magnitude Analysis of 1mm and 3mm Flow Channel Width PEMFC

Assessing PEMFC performance hinges on understanding the velocity magnitude. Knowing the velocity magnitude across different flow types is key

to evaluating PEMFC performance. The discussion below covers the velocity magnitude of 1mm and 3mm flow channel width along with 2mm channel width to compare the results.

Table 8.20 - Results of velocity magnitude of single serpentine PEMFCs at 0.25V(low)

S.No	Flow Channel Width (mm)	Voltage (V)	Inlet Velocity Magnitude (m/s)	Outlet Velocity Magnitude (m/s)	Velocity Difference (m/s)
1	1	0.25	0.477	1.10	0.63
2	2	0.25	0.487	1.13	0.643
3	3	0.25	0.505	1.27	0.765

Table 8.20 represents the results of velocity magnitude of single serpentine PEMFCs at 0.25V. The 1mm flow channel width exhibited a velocity magnitude difference of 0.63, while the 2mm flow channel experiences a velocity difference of 0.643. Additionally, the velocity difference for the 3mm flow channel was measured at 0.765.

Table 8.21 - Results of velocity magnitude of single serpentine PEMFCs at 0.35V(medium)

S.No	Flow Channel Width (mm)	Voltage (V)	Inlet Velocity Magnitude (m/s)	Outlet Velocity Magnitude (m/s)	Velocity Difference (m/s)

Table 8.21 - continued

1	1	0.35	0.493	1.18	0.691
2	2	0.35	0.501	1.21	0.709
3	3	0.35	0.519	1.31	0.821

In table 8.21, the velocity magnitudes of single serpentine PEMFCs at 0.35V are presented. The 1mm flow channel width showed a velocity magnitude difference of 0.691, while the 2mm flow channel exhibited a velocity difference of 0.709. Similarly, the velocity difference for the 3mm flow channel was recorded at 0.821.

Table 8.22 - Results of velocity magnitude of single serpentine PEMFCs at 0.5V(high)

S.No	Flow Channel Width (mm)	Voltage (V)	Inlet Velocity Magnitude (m/s)	Outlet Velocity Magnitude (m/s)	Velocity Difference (m/s)
1	1	0.5	0.503	1.24	0.741
2	2	0.5	0.514	1.28	0.766
3	3	0.5	0.526	1.4	0.874

Table 8.22 displays the velocity magnitudes of single serpentine PEMFCs at 0.5V. The 1mm channel width demonstrated a velocity magnitude change of 0.741, the 2mm channel showed a velocity difference of 0.766 and the 3mm channel had a velocity difference of 0.874.

Table 8.23 - Results of velocity magnitude of single serpentine PEMFCs at 0.65V (very high)

S.No	Flow Channel Width (mm)	Voltage (V)	Inlet Velocity Magnitude (m/s)	Outlet Velocity Magnitude (m/s)	Velocity Difference (m/s)
1	1	0.65	0.519	1.33	0.811
2	2	0.65	0.533	1.40	0.867
3	3	0.65	0.561	1.48	0.919

Table 8.23 displays the velocity magnitudes of single serpentine PEMFCs at 0.65V. The 1mm channel width demonstrated a velocity magnitude change of 0.811, the 2mm channel showed a velocity difference of 0.867 and the 3mm channel had a velocity difference of 0.919.

Table 8.24 - Results of velocity magnitude of single serpentine PEMFCs at 0.8V (extreme)

S.No	Flow Channel Width (mm)	Voltage (V)	Inlet Velocity Magnitude (m/s)	Outlet Velocity Magnitude (m/s)	Velocity Difference (m/s)
1	1	0.8	0.53	1.43	0.9
2	2	0.8	0.542	1.51	0.968
3	3	0.8	0.5	1.59	1.09

Table 8.24 displays the velocity magnitudes of single serpentine PEMFCs at 0.8V. The 1mm channel width demonstrated a velocity magnitude change of 0.9, the 2mm channel showed a velocity difference of 0.968 and the 3mm channel had a velocity difference of 1.09.

Table 8.25 - Results of velocity magnitude of bi serpentine PEMFCs at 0.25V(low)

S.No	Flow Channel Width (mm)	Voltage (V)	Inlet Velocity Magnitude (m/s)	Outlet Velocity Magnitude (m/s)	Velocity Difference (m/s)
1	1	0.25	0.283	0.957	0.674
2	2	0.25	0.289	0.977	0.688
3	3	0.25	0.341	1.03	0.689

Table 8.25 represents the results of velocity magnitude of bi serpentine PEMFCs at 0.25V. The 1mm flow channel width exhibited a velocity magnitude difference of 0.674, while the 2mm flow channel experiences a velocity difference of 0.688. Additionally, the velocity difference for the 3mm flow channel was measured at 0.689.

Table 8.26 - Results of velocity magnitude of bi serpentine PEMFCs at 0.35V(medium)

S.No	Flow Channel Width (mm)	Voltage (V)	Inlet Velocity Magnitude (m/s)	Outlet Velocity Magnitude (m/s)	Velocity Difference (m/s)

Table 8.26 - continued

1	1	0.35	0.311	0.974	0.663
2	2	0.35	0.317	0.989	0.672
3	3	0.35	0.322	1.07	7.48

In table 8.26, the velocity magnitudes of bi serpentine PEMFCs at 0.35V are presented. The 1mm flow channel width showed a velocity magnitude difference of 0.663, while the 2mm flow channel exhibited a velocity difference of 0.672. Similarly, the velocity difference for the 3mm flow channel was recorded at 0.748.

Table 8.27 - Results of velocity magnitude of bi serpentine PEMFCs at 0.5V(high)

S.No	Flow Channel Width (mm)	Voltage (V)	Inlet Velocity Magnitude (m/s)	Outlet Velocity Magnitude (m/s)	Velocity Difference (m/s)
1	1	0.5	0.369	0.985	0.616
2	2	0.5	0.374	0.998	0.624
3	3	0.5	0.399	1.11	0.711

Table 8.27 displays the velocity magnitudes of bi serpentine PEMFCs at 0.5V. The 1mm channel width demonstrated a velocity magnitude change of 0.616, the 2mm channel showed a velocity difference of 0.624 and the 3mm channel had a velocity difference of 0.711.

Table 8.28 - Results of velocity magnitude of bi serpentine PEMFCs at 0.65V(very high)

S.No	Flow Channel Width (mm)	Voltage (V)	Inlet Velocity Magnitude (m/s)	Outlet Velocity Magnitude (m/s)	Velocity Difference (m/s)
1	1	0.65	0.38	0.997	0.617
2	2	0.65	0.392	1.06	0.668
3	3	0.65	0.407	1.18	0.773

Table 8.28 displays the velocity magnitudes of bi serpentine PEMFCs at 0.65V. The 1mm channel width demonstrated a velocity magnitude change of 0.617, the 2mm channel showed a velocity difference of 0.668 and the 3mm channel had a velocity difference of 0.773.

Table 8.29 - Results of velocity magnitude of bi serpentine PEMFCs at 0.8V(extreme)

S.No	Flow Channel Width (mm)	Voltage (V)	Inlet Velocity Magnitude (m/s)	Outlet Velocity Magnitude (m/s)	Velocity Difference (m/s)
1	1	0.8	0.4	1.12	0.72
2	2	0.8	0.413	1.18	0.767
3	3	0.8	0.419	1.25	0.831

Table 8.29 displays the velocity magnitudes of bi serpentine PEMFCs at 0.8V. The 1mm channel width demonstrated a velocity magnitude change of 0.72, the 2mm channel showed a velocity difference of 0.767 and the 3mm channel had a velocity difference of 0.831.

Table 8.30 - Results of velocity magnitude of tri serpentine PEMFCs at 0.25V (low)

S.No	Flow Channel Width (mm)	Voltage (V)	Inlet Velocity Magnitude (m/s)	Outlet Velocity Magnitude (m/s)	Velocity Difference (m/s)
1	1	0.25	0.191	0.861	0.67
2	2	0.25	0.197	0.886	0.689
3	3	0.25	0.231	0.917	0.686

Table 8.30 represents the results of velocity magnitude of tri serpentine PEMFCs at 0.25V. The 1mm flow channel width exhibited a velocity magnitude difference of 0.67, while the 2mm flow channel experiences a velocity difference of 0.689. Additionally, the velocity difference for the 3mm flow channel was measured at 0.686.

Table 8.31 - Results of velocity magnitude of tri serpentine PEMFCs at 0.35V (medium)

S.No	Flow Channel Width (mm)	Voltage (V)	Inlet Velocity Magnitude (m/s)	Outlet Velocity Magnitude (m/s)	Velocity Difference (m/s)
1	1	0.35	0.216	0.882	0.666
2	2	0.35	0.223	0.911	0.688
3	3	0.35	0.244	0.924	0.68

In table 8.31, the velocity magnitudes of tri serpentine PEMFCs at 0.35V are presented. The 1mm flow channel width showed a velocity magnitude difference of 0.666, while the 2mm flow channel exhibited a velocity difference of 0.688. Similarly, the velocity difference for the 3mm flow channel was recorded at 0.68.

Table 8.32 - Results of velocity magnitude of tri serpentine PEMFCs at 0.5V(high)

S.No	Flow Channel Width (mm)	Voltage (V)	Inlet Velocity Magnitude (m/s)	Outlet Velocity Magnitude (m/s)	Velocity Difference (m/s)
1	1	0.5	0.26	0.921	0.661
2	2	0.5	0.267	0.946	0.679

Table 8.32 - continued

3	3	0.5	0.271	0.948	0.677
---	---	-----	-------	-------	-------

Table 8.32 displays the velocity magnitudes of tri serpentine PEMFCs at 0.5V. The 1mm channel width demonstrated a velocity magnitude change of 0.661, the 2mm channel showed a velocity difference of 0.679 and the 3mm channel had a velocity difference of 0.677.

Table 8.33 - Results of velocity magnitude of tri serpentine PEMFCs at 0.65V(very high)

S.No	Flow Channel Width (mm)	Voltage (V)	Inlet Velocity Magnitude (m/s)	Outlet Velocity Magnitude (m/s)	Velocity Difference (m/s)
1	1	0.65	0.282	0.937	0.655
2	2	0.65	0.297	0.952	0.655
3	3	0.65	0.306	0.958	0.652

Table 8.33 displays the velocity magnitudes of tri serpentine PEMFCs at 0.65V. The 1mm channel width demonstrated a velocity magnitude change of 0.655, the 2mm channel showed a velocity difference of 0.655 and the 3mm channel had a velocity difference of 0.652.

Table 8.34 - Results of velocity magnitude of tri serpentine PEMFCs at 0.8V(extreme)

S.No	Flow Channel Width (mm)	Voltage (V)	Inlet Velocity Magnitude (m/s)	Outlet Velocity Magnitude (m/s)	Velocity Difference (m/s)
1	1	0.8	0.296	0.945	0.649
2	2	0.8	0.308	0.966	0.658
3	3	0.8	0.315	0.974	0.659

Table 8.34 displays the velocity magnitudes of tri serpentine PEMFCs at 0.8V. The 1mm channel width demonstrated a velocity magnitude change of 0.649, the 2mm channel showed a velocity difference of 0.658 and the 3mm channel had a velocity difference of 0.659.

The results suggest that as the following flow channel with increases, the velocity magnitude difference also increases. The 1mm flow channel has the lowest velocity magnitude difference indicating relatively smaller variations in flow velocity compared to wider channels. The 2mm flow channel has slightly higher velocity difference showing a gradual increase in velocity magnitude difference. This trend indicates that wider channels may experience greater variation in velocity magnitude within the channel these findings are important for understanding flow dynamics and optimizing channel designs for improved performance in PEMFCs operating at 0.35V. This variability in velocity magnitude highlights the importance of channel

width in influencing flow dynamics and the distribution of fluid velocities within PEMFCs.

8.6 Mass Fraction of Hydrogen (H₂) Analysis of 1mm and 3mm Flow Channel Width PEMFC

The mass fraction of hydrogen (H₂) is a critical factor in evaluating PEMFC performance. Improving cell performance is closely tied to understanding the transportation of hydrogen (H₂) along the anode side. The forthcoming discourse focuses on analyzing the mass fraction of hydrogen (H₂) in flow channels of 1mm and 3mm along with 2mm flow channel width to compare the results.

Table 8.35 - Results of mass fraction of hydrogen (H₂) of single serpentine PEMFCs at 0.25V(low)

S.No	Flow Channel Width (mm)	Voltage (V)	Mass Fraction of Hydrogen (H ₂)
1	1	0.25	0.536
2	2	0.25	0.541
3	3	0.25	0.555

The mass fraction of hydrogen (H₂) in single serpentine PEMFC at 0.25V is detailed in Table 8.35. Consumption rates of hydrogen mass fraction at the Gas Diffusion Layer (GDL) are indicated as 0.536 for the 1mm channel width, 0.541 for the 2mm channel width, and 0.555 for the 3mm channel width.

Table 8.36 - Results of mass fraction of hydrogen (H₂) of single serpentine PEMFCs at 0.35V(medium)

S.No	Flow Channel Width (mm)	Voltage (V)	Mass Fraction of Hydrogen (H ₂)
1	1	0.35	0.574
2	2	0.35	0.587
3	3	0.35	0.599

In table 8.36, the mass fraction of hydrogen (H₂) in single serpentine PEMFC at 0.35V is presented. The consumption rate of hydrogen (H₂) mass fraction at the gas diffusion layer (GDL) is measured as 0.574 for the 1mm channel width, 0.587 for the 2mm channel width and 0.599 for the 3mm channel width.

Table 8.37 - Results of mass fraction of hydrogen (H₂) of single serpentine PEMFCs at 0.5V(high)

S.No	Flow Channel Width (mm)	Voltage (V)	Mass Fraction of Hydrogen (H ₂)
1	1	0.5	0.622
2	2	0.5	0.63
3	3	0.5	0.639

Table 8.37 presents the mass fraction of hydrogen (H₂) in single serpentine PEMFCs at 0.5V. The consumption rate of hydrogen (H₂) mass fraction at the gas diffusion layer (GDL) for the 1mm channel width is measured to be 0.622,

while the 2mm channel shows a consumption rate of 0.63 at GDL. Similarly, the 3mm flow channel width exhibits a hydrogen (H₂) consumption rate of 0.639.

Table 8.38 - Results of mass fraction of hydrogen (H₂) of single serpentine PEMFCs at 0.65V(very high)

S.No	Flow Channel Width (mm)	Voltage (V)	Mass Fraction of Hydrogen (H ₂)
1	1	0.65	0.669
2	2	0.65	0.676
3	3	0.65	0.691

Table 8.38 presents the mass fraction of hydrogen (H₂) in single serpentine PEMFCs at 0.65V. The consumption rate of hydrogen (H₂) mass fraction at the gas diffusion layer (GDL) for the 1mm channel width is measured to be 0.669, while the 2mm channel shows a consumption rate of 0.676 at GDL. Similarly, the 3mm flow channel width exhibits a hydrogen (H₂) consumption rate of 0.691.

Table 8.39 - Results of mass fraction of hydrogen (H₂) of single serpentine PEMFCs at 0.8V(extreme)

S.No	Flow Channel Width (mm)	Voltage (V)	Mass Fraction of Hydrogen (H ₂)
1	1	0.8	0.682
2	2	0.8	0.69

Table 8.39 - continued

3	3	0.8	0.712
---	---	-----	-------

Table 8.39 presents the mass fraction of hydrogen (H_2) in single serpentine PEMFCs at 0.8V. The consumption rate of hydrogen (H_2) mass fraction at the gas diffusion layer (GDL) for the 1mm channel width is measured to be 0.682, while the 2mm channel shows a consumption rate of 0.69 at GDL. Similarly, the 3mm flow channel width exhibits a hydrogen (H_2) consumption rate of 0.712.

Table 8.40 - Results of mass fraction of hydrogen (H_2) of bi serpentine PEMFCs at 0.25V(low)

S.No	Flow Channel Width (mm)	Voltage (V)	Mass Fraction of Hydrogen (H_2)
1	1	0.25	58.3
2	2	0.25	60.1
3	3	0.25	61.1

The mass fraction of hydrogen (H_2) in bi serpentine PEMFC at 0.25V is detailed in Table 8.40. Consumption rates of hydrogen mass fraction at the Gas Diffusion Layer (GDL) are indicated as 58.3 for the 1mm channel width, 60.1 for the 2mm channel width, and 61.1 for the 3mm channel width.

Table 8.41 - Results of mass fraction of hydrogen (H₂) of bi serpentine PEMFCs at 0.35V(medium)

S.No	Flow Channel Width (mm)	Voltage (V)	Mass Fraction of Hydrogen (H ₂)
1	1	0.35	61.6
2	2	0.35	62.5
3	3	0.35	63.2

In table 8.41, the mass fraction of hydrogen (H₂) in bi serpentine PEMFC at 0.35V is presented. The consumption rate of hydrogen (H₂) mass fraction at the gas diffusion layer (GDL) is measured as 61.6 for the 1mm channel width, 62.5 for the 2mm channel width and 63.2 for the 3mm channel width.

Table 8.42 - Results of mass fraction of hydrogen (H₂) of bi serpentine PEMFCs at 0.5V(high)

S.No	Flow Channel Width (mm)	Voltage (V)	Mass Fraction of Hydrogen (H ₂)
1	1	0.5	64.9
2	2	0.5	66.2
3	3	0.5	67.1

Table 8.42 presents the mass fraction of hydrogen (H₂) in bi serpentine PEMFCs at 0.5V. The consumption rate of hydrogen (H₂) mass fraction at the gas diffusion layer (GDL) for the 1mm channel width is measured to be 64.9,

while the 2mm channel shows a consumption rate of 66.2 at GDL. Similarly, the 3mm flow channel width exhibits a hydrogen (H₂) consumption rate of 67.1.

Table 8.43 - Results of mass fraction of hydrogen (H₂) of bi serpentine PEMFCs at 0.65V(very high)

S.No	Flow Channel Width (mm)	Voltage (V)	Mass Fraction of Hydrogen (H ₂)
1	1	0.65	0.665
2	2	0.65	0.678
3	3	0.65	0.693

Table 8.43 presents the mass fraction of hydrogen (H₂) in bi serpentine PEMFCs at 0.65V. The consumption rate of hydrogen (H₂) mass fraction at the gas diffusion layer (GDL) for the 1mm channel width is measured to be 0.665, while the 2mm channel shows a consumption rate of 0.678 at GDL. Similarly, the 3mm flow channel width exhibits a hydrogen (H₂) consumption rate of 0.693.

Table 8.44 - Results of mass fraction of hydrogen (H₂) of bi serpentine PEMFCs at 0.8V(extreme)

S.No	Flow Channel Width (mm)	Voltage (V)	Mass Fraction of Hydrogen (H ₂)
1	1	0.8	0.679
2	2	0.8	0.686

Table 8.44 - continued

3	3	0.8	0.708
---	---	-----	-------

Table 8.44 presents the mass fraction of hydrogen (H_2) in bi serpentine PEMFCs at 0.8V. The consumption rate of hydrogen (H_2) mass fraction at the gas diffusion layer (GDL) for the 1mm channel width is measured to be 0.679, while the 2mm channel shows a consumption rate of 0.686 at GDL. Similarly, the 3mm flow channel width exhibits a hydrogen (H_2) consumption rate of 0.708.

Table 8.45 - Results of mass fraction of hydrogen (H_2) of tri serpentine PEMFCs at 0.25V(low)

S.No	Flow Channel Width (mm)	Voltage (V)	Mass Fraction of Hydrogen (H_2)
1	1	0.25	0.633
2	2	0.25	0.642
3	3	0.25	0.661

The mass fraction of hydrogen (H_2) in tri serpentine PEMFC at 0.25V is detailed in Table 8.45. Consumption rates of hydrogen mass fraction at the Gas Diffusion Layer (GDL) are indicated as 0.633 for the 1mm channel width, 0.642 for the 2mm channel width, and 0.661 for the 3mm channel width.

Table 8.46 - Results of mass fraction of hydrogen (H₂) of tri serpentine PEMFCs at 0.35V(medium)

S.No	Flow Channel Width (mm)	Voltage (V)	Mass Fraction of Hydrogen (H ₂)
1	1	0.35	0.670
2	2	0.35	0.676
3	3	0.35	0.693

In table 8.46, the mass fraction of hydrogen (H₂) in tri serpentine PEMFC at 0.35V is presented. The consumption rate of hydrogen (H₂) mass fraction at the gas diffusion layer (GDL) is measured as 0.67 for the 1mm channel width, 0.676 for the 2mm channel width and 0.693 for the 3mm channel width.

Table 8.47 - Results of mass fraction of hydrogen (H₂) of tri serpentine PEMFCs at 0.5V(high)

S.No	Flow Channel Width (mm)	Voltage (V)	Mass Fraction of Hydrogen (H ₂)
1	1	0.5	0.696
2	2	0.5	0.719
3	3	0.5	0.727

Table 8.47 presents the mass fraction of hydrogen (H₂) in tri serpentine PEMFCs at 0.5V. The consumption rate of hydrogen (H₂) mass fraction at the gas diffusion layer (GDL) for the 1mm channel width is measured to be 0.696, while the 2mm channel shows a consumption rate of 0.719 at GDL. Similarly,

the 3mm flow channel width exhibits a hydrogen (H₂) consumption rate of 0.727.

Table 8.48 - Results of mass fraction of hydrogen (H₂) of tri serpentine PEMFCs at 0.65V(very high)

S.No	Flow Channel Width (mm)	Voltage (V)	Mass Fraction of Hydrogen (H ₂)
1	1	0.65	0.701
2	2	0.65	0.721
3	3	0.65	0.730

Table 8.48 presents the mass fraction of hydrogen (H₂) in tri serpentine PEMFCs at 0.65V. The consumption rate of hydrogen (H₂) mass fraction at the gas diffusion layer (GDL) for the 1mm channel width is measured to be 0.701, while the 2mm channel shows a consumption rate of 0.721 at GDL. Similarly, the 3mm flow channel width exhibits a hydrogen (H₂) consumption rate of 0.730.

Table 8.49 - Results of mass fraction of hydrogen (H₂) of tri serpentine PEMFCs at 0.8V(extreme)

S.No	Flow Channel Width (mm)	Voltage (V)	Mass Fraction of Hydrogen (H ₂)
1	1	0.8	0.710
2	2	0.8	0.726
3	3	0.8	0.735

Table 8.49 presents the mass fraction of hydrogen (H_2) in tri serpentine PEMFCs at 0.8V. The consumption rate of hydrogen (H_2) mass fraction at the gas diffusion layer (GDL) for the 1mm channel width is measured to be 0.710, while the 2mm channel shows a consumption rate of 0.726 at GDL. Similarly, the 3mm flow channel width exhibits a hydrogen (H_2) consumption rate of 0.735.

The results suggested that wider channels lead to higher consumption rate of hydrogen mass fraction in PEMFC. These findings highlight the importance of optimizing channel width to achieve optimal hydrogen utilization efficiency in PEMFC with wider channels generally leading to higher efficiency in hydrogen utilization. There are noticeable variations in mass fraction consumption rates among the three channels, indicating different rates of hydrogen usage.

8.7 Cell Reynolds Number Analysis of 1mm and 3mm Flow Channel Width PEMFC

The Cell Reynolds number simulation is aimed at determining if this assumption accurately represents the flow behavior. In the ensuing discussion, the Cell Reynolds Number across flow channels of 1mm and 3mm along with 2mm to compare the results.

Table 8.50 - Results of cell reynolds number of single serpentine PEMFCs at 0.25V (low)

S.No	Flow Channel Width (mm)	Voltage (V)	Cell Reynolds Number at Channel Inlet	Cell Reynolds Number at Channel Outlet

Table 8.50 - continued

1	1	0.25	20.9	54.1
2	2	0.25	21.7	55
3	3	0.25	23.9	58.1

The Table 8.50 illustrates the variation in cell Reynolds number of single serpentine flow channel at 0.25 V. In 1mm channel PEMFC, the Reynolds number at the inlet is measured to be 20.9, while at the outlet, it is 54.1. For the 2mm channel PEMFC, the Reynolds number at the inlet is 21.7, and at the outlet, it is 55. In 3mm channel PEMFC, the Reynolds number at the inlet is 23.9, and at the outlet, it is 58.1.

Table 8.51 - Results of cell Reynolds number of single serpentine PEMFCs at 0.35V (medium)

S.No	Flow Channel Width (mm)	Voltage (V)	Cell Reynolds Number at Channel Inlet	Cell Reynolds Number at Channel Outlet
1	1	0.35	28.1	59.4
2	2	0.35	28.8	60.9
3	3	0.35	29.6	63

Table 8.51 presents the variation in cell Reynolds numbers for a single serpentine flow channel operating at 0.35 V. In the 1mm channel PEMFC, the Reynolds number is 28.1 at the inlet and 59.4 at the outlet. Similarly, for the 2mm channel PEMFC, the Reynolds number is 28.8^{at} the inlet and 60.9 outlet.

In the 3mm channel PEMFC, the Reynolds number is 29.6 at the inlet and 63 at the outlet.

Table 8.52 - Results of cell Reynolds number of single serpentine PEMFCs at 0.5V (high)

S.No	Flow Channel Width (mm)	Voltage (V)	Cell Reynolds Number at Channel Inlet	Cell Reynolds Number at Channel Outlet
1	1	0.5	30.3	63.1
2	2	0.5	31	64
3	3	0.5	31.7	65.5

Table 8.52 showcases the variation in cell Reynolds numbers for a single serpentine flow channel operating at 0.5V. In the 1mm channel PEMFC, the Reynolds number is 30.3 at the inlet and 63.1 at the outlet. Likewise, for the 2mm channel PEMFC, the Reynolds number is 31 at the inlet and 64 at the outlet. In the 3mm channel PEMFC, the Reynolds number is 31.7 at the inlet and 65.5 at the outlet.

Table 8.53 - Results of cell Reynolds number of single serpentine PEMFCs at 0.65V (very high)

S.No	Flow Channel Width (mm)	Voltage (V)	Cell Reynolds Number at Channel Inlet	Cell Reynolds Number at Channel Outlet
1	1	0.65	34.5	67.3
2	2	0.65	39.8	72.4
3	3	0.65	42.6	77.3

Table 8.53 showcases the variation in cell Reynolds numbers for a single serpentine flow channel operating at 0.65V. In the 1mm channel PEMFC, the Reynolds number is 34.5 at the inlet and 67.3 at the outlet. Likewise, for the 2mm channel PEMFC, the Reynolds number is 39.8 at the inlet and 72.4 at the outlet. In the 3mm channel PEMFC, the Reynolds number is 42.6 at the inlet and 77.3 at the outlet.

Table 8.54 - Results of cell Reynolds number of single serpentine PEMFCs at 0.8V (extreme)

S.No	Flow Channel Width (mm)	Voltage (V)	Cell Reynolds Number at Channel Inlet	Cell Reynolds Number at Channel Outlet
1	1	0.8	38.9	70.4
2	2	0.8	43.6	79.3

Table 8.54 - continued

3	3	0.8	47	85.6
---	---	-----	----	------

Table 8.54 showcases the variation in cell Reynolds numbers for a single serpentine flow channel operating at 0.8V. In the 1mm channel PEMFC, the Reynolds number is 38.9 at the inlet and 70.4 at the outlet. Likewise, for the 2mm channel PEMFC, the Reynolds number is 43.6 at the inlet and 79.3 at the outlet. In the 3mm channel PEMFC, the Reynolds number is 47 at the inlet and 85.6 at the outlet.

Table 8.55 - Results of cell Reynolds number of bi serpentine PEMFCs at 0.25V (low)

S.No	Flow Channel Width (mm)	Voltage (V)	Cell Reynolds Number at Channel Inlet	Cell Reynolds Number at Channel Outlet
1	1	0.25	13.7	38.5
2	2	0.25	14.2	39.4
3	3	0.25	14.9	40.5

The Table 8.55 illustrates the variation in cell Reynolds number of bi serpentine flow channel at 0.25 V. In 1mm channel PEMFC, the Reynolds number at the inlet is measured to be 13.7, while at the outlet, it is 38.5. For the 2mm channel PEMFC, the Reynolds number at the inlet is 14.2, and at the

outlet, it is 39.4. In 3mm channel PEMFC, the Reynolds number at the inlet is 14.9, and at the outlet, it is 40.5.

Table 8.56 - Results of cell Reynolds number of bi serpentine PEMFCs at 0.35V (medium)

S.No	Flow Channel Width (mm)	Voltage (V)	Cell Reynolds Number at Channel Inlet	Cell Reynolds Number at Channel Outlet
1	1	0.35	16.6	4.33
2	2	0.35	17.3	4.39
3	3	0.35	18.1	4.51

Table 8.56 presents the variation in cell Reynolds numbers for a bi serpentine flow channel operating at 0.35 V. In the 1mm channel PEMFC, the Reynolds number is 16.6 at the inlet and 43.3 at the outlet. Similarly, for the 2mm channel PEMFC, the Reynolds number is 17.3 at the inlet and 43.9 outlet. In the 3mm channel PEMFC, the Reynolds number is 18.1 at the inlet and 45.1 at the outlet.

Table 8.57 - Results of cell Reynolds number of bi serpentine PEMFCs at 0.5V (high)

S.No	Flow Channel Width (mm)	Voltage (V)	Cell Reynolds Number at Channel Inlet	Cell Reynolds Number at Channel Outlet
1	1	0.5	21.2	48.3
2	2	0.5	22	49
3	3	0.5	23.1	51.7

Table 8.57 showcases the variation in cell Reynolds numbers for a bi serpentine flow channel operating at 0.5V. In the 1mm channel PEMFC, the Reynolds number is 21.2 at the inlet and 48.3 at the outlet. Likewise, for the 2mm channel PEMFC, the Reynolds number is 22 at the inlet and 49 at the outlet. In the 3mm channel PEMFC, the Reynolds number is 23.1 at the inlet and 51.7 at the outlet.

Table 8.58 - Results of cell Reynolds number of bi serpentine PEMFCs at 0.65V (very high)

S.No	Flow Channel Width (mm)	Voltage (V)	Cell Reynolds Number at Channel Inlet	Cell Reynolds Number at Channel Outlet
1	1	0.65	24.3	52.3

Table 8.58 - continued

2	2	0.65	27.8	53.6
3	3	0.65	28.4	55.7

Table 8.58 showcases the variation in cell Reynolds numbers for a bi serpentine flow channel operating at 0.65V. In the 1mm channel PEMFC, the Reynolds number is 24.3 at the inlet and 52.3 at the outlet. Likewise, for the 2mm channel PEMFC, the Reynolds number is 27.8 at the inlet and 53.6 at the outlet. In the 3mm channel PEMFC, the Reynolds number is 28.4 at the inlet and 55.7 at the outlet.

Table 8.59 - Results of cell Reynolds number of bi serpentine PEMFCs at 0.8V (extreme)

S.No	Flow Channel Width (mm)	Voltage (V)	Cell Reynolds Number at Channel Inlet	Cell Reynolds Number at Channel Outlet
1	1	0.8	26.2	53.4
2	2	0.8	29	57.2
3	3	0.8	31.2	60.6

Table 8.59 showcases the variation in cell Reynolds numbers for a bi serpentine flow channel operating at 0.8V. In the 1mm channel PEMFC, the Reynolds number is 26.2 at the inlet and 53.4 at the outlet. Likewise, for the 2mm channel PEMFC, the Reynolds number is 29 at the inlet and 57.2 at the

outlet. In the 3mm channel PEMFC, the Reynolds number is 31.2 at the inlet and 60.6 at the outlet.

Table 8.60 - Results of cell Reynolds number of tri serpentine PEMFCs at 0.25V (low)

S.No	Flow Channel Width (mm)	Voltage (V)	Cell Reynolds Number at Channel Inlet	Cell Reynolds Number at Channel Outlet
1	1	0.25	9.7	37.8
2	2	0.25	10.1	38.6
3	3	0.25	10.8	40.1

The Table 8.60 illustrates the variation in cell Reynolds number of tri serpentine flow channel at 0.25 V. In 1mm channel PEMFC, the Reynolds number at the inlet is measured to be 9.7, while at the outlet, it is 37.8. For the 2mm channel PEMFC, the Reynolds number at the inlet is 10.1, and at the outlet, it is 38.6. In 3mm channel PEMFC, the Reynolds number at the inlet is 10.8, and at the outlet, it is 40.1.

Table 8.61 - Results of cell Reynolds number of tri serpentine PEMFCs at 0.35V (medium)

S.No	Flow Channel Width (mm)	Voltage (V)	Cell Reynolds Number at Channel Inlet	Cell Reynolds Number at Channel Outlet
1	1	0.35	11.7	41.1
2	2	0.35	11.9	41.5
3	3	0.35	12.5	42.7

Table 8.61 presents the variation in cell Reynolds numbers for a tri serpentine flow channel operating at 0.35 V. In the 1mm channel PEMFC, the Reynolds number is 11.7 at the inlet and 41.1 at the outlet. Similarly, for the 2mm channel PEMFC, the Reynolds number is 11.9 at the inlet and 41.5 outlet. In the 3mm channel PEMFC, the Reynolds number is 12.5 at the inlet and 42.7 at the outlet.

Table 8.62 - Results of cell Reynolds number of tri serpentine PEMFCs at 0.5V (high)

S.No	Flow Channel Width (mm)	Voltage (V)	Cell Reynolds Number at Channel Inlet	Cell Reynolds Number at Channel Outlet
1	1	0.5	12.9	43.9
2	2	0.5	13.2	46.8

Table 8.62 - continued

3	3	0.5	13.9	48.5
---	---	-----	------	------

The Table 8.62 illustrates the variation in cell Reynolds number of tri serpentine flow channel at 0.5 V. In 1mm channel PEMFC, the Reynolds number at the inlet is measured to be 12.9, while at the outlet, it is 43.9. For the 2mm channel PEMFC, the Reynolds number at the inlet is 13.2, and at the outlet, it is 46.8. In 3mm channel PEMFC, the Reynolds number at the inlet is 13.9, and at the outlet, it is 48.5.

Table 8.63 - Results of cell Reynolds number of tri serpentine PEMFCs at 0.65V (very high)

S.No	Flow Channel Width (mm)	Voltage (V)	Cell Reynolds Number at Channel Inlet	Cell Reynolds Number at Channel Outlet
1	1	0.65	13.7	45.2
2	2	0.65	14.4	47.8
3	3	0.65	15.3	51.1

The Table 8.63 illustrates the variation in cell Reynolds number of tri serpentine flow channel at 0.5 V. In 1mm channel PEMFC, the Reynolds number at the inlet is measured to be 13.7, while at the outlet, it is 45.2. For the 2mm channel PEMFC, the Reynolds number at the inlet is 14.4, and at the outlet, it is 47.8. In 3mm channel PEMFC, the Reynolds number at the inlet is 15.3, and at the outlet, it is 51.1.

Table 8.64 - Results of cell Reynolds number of tri serpentine PEMFCs at 0.8V (extreme)

S.No	Flow Channel Width (mm)	Voltage (V)	Cell Reynolds Number at Channel Inlet	Cell Reynolds Number at Channel Outlet
1	1	0.8	14.5	47.7
2	2	0.8	16.1	50.6
3	3	0.8	17.9	54.5

The Table 8.64 illustrates the variation in cell Reynolds number of tri serpentine flow channel at 0.8 V. In 1mm channel PEMFC, the Reynolds number at the inlet is measured to be 14.5, while at the outlet, it is 47.7. For the 2mm channel PEMFC, the Reynolds number at the inlet is 16.1, and at the outlet, it is 50.6. In 3mm channel PEMFC, the Reynolds number at the inlet is 17.9, and at the outlet, it is 54.5.

The results show that wider flow channels exhibit higher Reynolds numbers at both inlet and outlet points, indicating increased flow velocities and potentially improved fluid dynamics. This can be advantages for optimizing performance and efficiency in PEMFCs. Additionally, there is a gradual increase in the inlet and outlet points, Reynolds number from the 1mm channel to the 3mm channel, reflecting higher flow velocities at the channel inlets with increasing channel width.

CHAPTER 9

RESULTS AND DISCUSSION

The three models of PEMFC, each consisting of seven layers including anode and cathode flow channels, anode, and cathode gas diffusion layers GDL, anode and cathode catalyst layers, and membrane, were simulated at various cell temperatures under a pressure of 2 bar.

All the designs of PEMFC, at various cell temperatures of 313K (40°C), 323K (50°C), 333K (60°C), 343K (70°C), 353K(80°C), 363K (90°C), 373K (100°C) have been analyzed under the operating conditions outlined in chapter 6.

At 313K (40°C) and 2 bar pressure, the single serpentine flow channel achieved a maximum current density of 1.026 A/cm² and a corresponding power density of 0.513 W/cm² at 0.5 V. Subsequently, in the bi serpentine PEMFC simulation, the maximum current density produced by bi serpentine flow channel is 1.053 A/cm² with a corresponding power density of 0.5265 W/cm² at 0.5 V. Lastly, in the analysis of the tri-serpentine flow channel, the maximum current density obtained is 1.071 A/cm² with a corresponding power density of 0.5355 W/cm² at 0.5 V.

At 323K (50°C) and 2 bar pressure, the single serpentine flow channel achieved a maximum current density of 1.053 A/cm² and a corresponding power density of 0.526 W/cm² at 0.5 V. Subsequently, in the bi serpentine PEMFC simulation, the maximum current density produced by bi serpentine flow channel is 0.981 A/cm² with a corresponding power density of 0.539 W/cm² at 0.5 V. Lastly, in the analysis of the tri serpentine flow channel, the

maximum current density obtained is 1.02 A/cm^2 with a corresponding power density of 0.55 W/cm^2 at 0.55 V .

At 333K (60°C) and 2 bar pressure, the single serpentine flow channel achieved a maximum current density of 0.982 A/cm^2 and a corresponding power density of 0.54 W/cm^2 at 0.55 V . Subsequently, in the bi-serpentine PEMFC simulation, the maximum current density produced by bi serpentine flow channel is 1.007 A/cm^2 with a corresponding power density of 0.554 W/cm^2 at 0.55 V . Lastly, in the analysis of the tri serpentine flow channel, the maximum current density obtained is 1.167 A/cm^2 with a corresponding power density of 0.583 W/cm^2 at 0.5 V .

At 343K (70°C) and 2 bar pressure, the single serpentine flow channel achieved a maximum current density of 0.994 A/cm^2 and a corresponding power density of 0.5467 W/cm^2 at 0.55 V . Subsequently, in the bi-serpentine PEMFC simulation, the maximum current density produced by bi serpentine flow channel is 1.03 A/cm^2 with a corresponding power density of 0.5665 W/cm^2 at 0.55 V . Lastly, in the analysis of the tri serpentine flow channel, the maximum current density obtained is 1.142 A/cm^2 with a corresponding power density of 0.6281 W/cm^2 at 0.55 V .

At 353K (80°C) and 2 bar pressure, the single serpentine flow channel achieved a maximum current density of 1.131 A/cm^2 and a corresponding power density of 0.5655 W/cm^2 at 0.5 V . Subsequently, in the bi serpentine PEMFC simulation, the maximum current density produced by bi serpentine flow channel is 1.161 A/cm^2 with a corresponding power density of 0.5805 W/cm^2 at 0.5 V . Lastly, in the analysis tri serpentine flow channel, the maximum current density obtained is 1.198 A/cm^2 with a corresponding power density of 0.599 W/cm^2 at 0.5 V .

At 363K (90°C) and 2 bar pressure, the single serpentine flow channel achieved a maximum current density of 1.163 A/cm² and a corresponding power density of 0.5815 W/cm² at 0.5 V. Subsequently, in the bi serpentine PEMFC simulation, the maximum current density produced by bi serpentine flow channel is 1.194 A/cm² with a corresponding power density of 0.597 W/cm² at 0.5 V. Lastly, in the analysis of tri serpentine flow channel, the maximum current density obtained is 1.152 A/cm² with a corresponding power density of 0.6336 W/cm² at 0.55 V.

At 373K (100°C) and 2 bar pressure, the single serpentine flow channel achieved a maximum current density of 1.153 A/cm² and a corresponding power density of 0.5765 W/cm² at 0.5 V. Subsequently, in the bi serpentine PEMFC simulation, the maximum current density produced by bi serpentine flow channel is 1.208 A/cm² with a corresponding power density of 0.604 W/cm² at 0.5 V. Lastly, in the analysis of tri serpentine flow channel, the maximum current density obtained is 1.12 A/cm² with a corresponding power density of 0.6655 W/cm² at 0.55 V.

The results clearly indicate that the tri serpentine flow channel achieves a higher power density compared to both single and bi serpentine flow channels. Upon comparing all the flow channels, it is evident that the tri serpentine flow channel consistently exhibits the highest power density, followed by bi serpentine and single serpentine flow channel.

Chapter 7 contains the analysis work of PEMFC which comprises of pressure distribution, velocity magnitude, mass fraction of the hydrogen (H₂), and Reynolds number of the cell.

In the pressure distribution of the PEMFC at 0.25V (low), the initial pressure at the inlet of the single serpentine flow channel is 199 KPa, and at the outlet, it is 129 KPa. Therefore, the pressure drops across the single serpentine flow channel is 79 KPa. Next, the bi-serpentine PEMFC was simulated, with the initial pressure at the inlet of the bi serpentine flow channel being 199 KPa, and at the outlet, it is 136 KPa. Consequently, the pressure drops across the bi serpentine flow channel is 63 KPa. Lastly, the tri-serpentine configuration was analyzed, revealing an initial pressure at the inlet of 200 KPa, and at the outlet, it is 149 KPa. Therefore, the pressure drops across the tri serpentine flow channel is 51 KPa.

In the pressure distribution of the PEMFC at 0.35V (medium), the initial pressure at the inlet of the single serpentine flow channel is 199 KPa, and at the outlet, it is 128 KPa. Therefore, the pressure drops across the single serpentine flow channel is 71 KPa. Next, the bi-serpentine PEMFC was simulated, with the initial pressure at the inlet of the bi serpentine flow channel being 199 KPa, and at the outlet, it is 142 KPa. Consequently, the pressure drops across the bi serpentine flow channel is 57 KPa. Lastly, the tri-serpentine configuration was analyzed, revealing an initial pressure at the inlet of 200 KPa, and at the outlet, it is 163 KPa. Therefore, the pressure drops across the tri serpentine flow channel is 37 KPa.

In the pressure distribution of the PEMFC at 0.5V (high), the initial pressure at the inlet of the single serpentine flow channel is 199 KPa, and at the outlet, it is 139 KPa. Therefore, the pressure drops across the single serpentine flow channel is 60 KPa. Next, the bi-serpentine PEMFC was simulated, with the initial pressure at the inlet of the bi serpentine flow channel being 199 KPa, and at the outlet, it is 150 KPa. Consequently, the pressure drops across the bi

serpentine flow channel is 48 KPa. Lastly, the tri-serpentine configuration was analyzed, revealing an initial pressure at the inlet of 200 KPa, and at the outlet, it is 156 KPa at 0.55V. Therefore, the pressure drops across the tri serpentine flow channel is 44 KPa.

In the pressure distribution of the PEMFC at 0.65V (very high), the initial pressure at the inlet of the single serpentine flow channel is 200 KPa, and at the outlet, it is 152 KPa. Therefore, the pressure drops across the single serpentine flow channel is 48 KPa. Next, the bi-serpentine PEMFC was simulated, with the initial pressure at the inlet of the bi serpentine flow channel being 200 KPa, and at the outlet, it is 161 KPa. Consequently, the pressure drops across the bi serpentine flow channel is 39 KPa. Lastly, the tri-serpentine configuration was analyzed, revealing an initial pressure at the inlet of 200 KPa, and at the outlet, it is 169 KPa. Therefore, the pressure drop across the tri serpentine flow channel is 31 KPa.

In the pressure distribution of the PEMFC at 0.8V (extreme), the initial pressure at the inlet of the single serpentine flow channel is 200 KPa, and at the outlet, it is 157 KPa. Therefore, the pressure drops across the single serpentine flow channel is 43 KPa. Next, the bi-serpentine PEMFC was simulated, with the initial pressure at the inlet of the bi serpentine flow channel being 200 KPa, and at the outlet, it is 164 KPa. Consequently, the pressure drops across the bi serpentine flow channel is 36 KPa. Lastly, the tri-serpentine configuration was analyzed, revealing an initial pressure at the inlet of 200 KPa, and at the outlet, it is 173 KPa. Therefore, the pressure drops across the tri serpentine flow channel is 27 KPa.

By comparing the pressure distributions across all the flow channels at different voltages, it is observed that the pressure drop is higher in the single

serpentine flow channel than in the other flow channels. This can be attributed to the greater number of bends in the single serpentine flow channel. Conversely, the tri serpentine design exhibits the minimum pressure drop due to its fewer bends, resulting in improved performance of the cell.

In velocity magnitude of PEMFC at 0.25V (low), the velocity at the inlet and outlet of the single serpentine flow channel is 0.487 m/s and 1.13 m/s respectively. The difference in velocity magnitude from the inlet to the outlet of the single serpentine flow channel is 0.643 m/s. Next, the bi-serpentine PEMFC was simulated, with the velocities at the inlet and outlet of 0.289 m/s and 0.977 m/s respectively. The difference in velocity magnitude from the inlet to the outlet of the bi serpentine flow channel is 0.688 m/s. Lastly, the tri-serpentine was analyzed, revealing velocities at the inlet and outlet of 0.197 m/s and 0.886 m/s respectively. The difference in velocity magnitude from the inlet to the outlet of the tri serpentine flow channel is 0.689 m/s.

In velocity magnitude of PEMFC at 0.35V (medium), the velocity at the inlet and outlet of the single serpentine flow channel is 0.501 m/s and 1.21 m/s respectively. The difference in velocity magnitude from the inlet to the outlet of the single serpentine flow channel is 0.709 m/s. Next, the bi-serpentine PEMFC was simulated, with the velocities at the inlet and outlet of 0.317 m/s and 0.989 m/s respectively. The difference in velocity magnitude from the inlet to the outlet of the bi serpentine flow channel is 0.672 m/s. Lastly, the tri-serpentine was analyzed, revealing velocities at the inlet and outlet of 0.223 m/s and 0.911 m/s respectively. The difference in velocity magnitude from the inlet to the outlet of the tri serpentine flow channel is 0.688 m/s.

In velocity magnitude of PEMFC at 0.5V (high), the velocity at the inlet and outlet of the single serpentine flow channel is 0.514 m/s and 1.28 m/s

respectively. The difference in velocity magnitude from the inlet to the outlet of the single serpentine flow channel is 0.766 m/s. Next, the bi-serpentine PEMFC was simulated, with the velocities at the inlet and outlet of 0.374 m/s and 0.998 m/s respectively. The difference in velocity magnitude from the inlet to the outlet of the bi serpentine flow channel is 0.624 m/s. Lastly, the tri-serpentine was analyzed at 0.55V, revealing velocities at the inlet and outlet of 0.267 m/s and 0.946 m/s respectively. The difference in velocity magnitude from the inlet to the outlet of the tri serpentine flow channel is 0.679 m/s.

In velocity magnitude of PEMFC at 0.65V (very high), the velocity at the inlet and outlet of the single serpentine flow channel is 0.525 m/s and 1.35 m/s respectively. The difference in velocity magnitude from the inlet to the outlet of the single serpentine flow channel is 0.825 m/s. Next, the bi-serpentine PEMFC was simulated, with the velocities at the inlet and outlet of 0.401 m/s and 1.06 m/s respectively. The difference in velocity magnitude from the inlet to the outlet of the bi serpentine flow channel is 0.659 m/s. Lastly, the tri-serpentine was analyzed, revealing velocities at the inlet and outlet of 0.293 m/s and 0.962 m/s respectively. The difference in velocity magnitude from the inlet to the outlet of the tri serpentine flow channel is 0.669 m/s.

In velocity magnitude of PEMFC at 0.8V (extreme), the velocity at the inlet and outlet of the single serpentine flow channel is 0.530 m/s and 1.38 m/s respectively. The difference in velocity magnitude from the inlet to the outlet of the single serpentine flow channel is 0.85 m/s. Next, the bi-serpentine PEMFC was simulated, with the velocities at the inlet and outlet of 0.423 m/s and 1.11 m/s respectively. The difference in velocity magnitude from the inlet to the outlet of the bi serpentine flow channel is 0.677 m/s. Lastly, the tri-

serpentine was analyzed, revealing velocities at the inlet and outlet of 0.303 m/s and 0.990 m/s respectively. The difference in velocity magnitude from the inlet to the outlet of the tri serpentine flow channel is 0.687 m/s.

By comparing the velocity magnitude across all the flow channels, the velocity is high at single serpentine flow channel followed by bi and tri serpentine flow channel. The higher velocity at the outlet is attributed to the stoichiometric ratio of the anode.

In the mass fraction of hydrogen (H_2) at 0.25V (low), the consumption rate of hydrogen (H_2) at the single serpentine flow channel is 0.541. Next, the bi-serpentine PEMFC was simulated, showing a hydrogen (H_2) consumption rate of 0.601. Lastly, the tri-serpentine configuration was analyzed, revealing a hydrogen (H_2) consumption rate of 0.642.

In the mass fraction of hydrogen (H_2) at 0.35V (medium), the consumption rate of hydrogen (H_2) at the single serpentine flow channel is 0.587. Next, the bi-serpentine PEMFC was simulated, showing a hydrogen (H_2) consumption rate of 0.625. Lastly, the tri-serpentine configuration was analyzed, revealing a hydrogen (H_2) consumption rate of 0.676.

In the mass fraction of hydrogen (H_2) at 0.5V (high), the consumption rate of hydrogen (H_2) at the single serpentine flow channel is 0.63. Next, the bi-serpentine PEMFC was simulated, showing a hydrogen (H_2) consumption rate of 0.662. Lastly, the tri-serpentine configuration was analyzed at 0.5V, revealing a hydrogen (H_2) consumption rate of 0.719.

In the mass fraction of hydrogen (H_2) at 0.65V (very high), the consumption rate of hydrogen (H_2) at the single serpentine flow channel is 0.683. Next, the bi-serpentine PEMFC was simulated, showing a hydrogen (H_2) consumption

rate of 0.707. Lastly, the tri-serpentine configuration was analyzed, revealing a hydrogen (H_2) consumption rate of 0.765.

In the mass fraction of hydrogen (H_2) at 0.8V (extreme), the consumption rate of hydrogen (H_2) at the single serpentine flow channel is 0.709. Next, the bi-serpentine PEMFC was simulated, showing a hydrogen (H_2) consumption rate of 0.734. Lastly, the tri-serpentine configuration was analyzed, revealing a hydrogen (H_2) consumption rate of 0.796.

From all the results of the hydrogen (H_2) mass fraction at different voltages, it was observed that the tri serpentine flow channel has highest hydrogen (H_2) consumption rate compared to the single and bi serpentine flow channels. The high current is generated in tri serpentine flow channel because of its higher of consumption rate.

In the cell Reynolds number of the PEMFC at 0.25V (low), the value of single serpentine flow channel at the inlet is found to be 21.7, whereas at the outlet, it is 55. Next, the bi-serpentine PEMFC was simulated, with the Reynolds number at the inlet is found to be 14.2 and at the outlet has 39.4. Lastly, the tri-serpentine flow channel configuration was analyzed, revealing a Reynolds number of 10.1 at the inlet and 38.6 at the outlet.

In the cell Reynolds number of the PEMFC at 0.35V (medium), the value of single serpentine flow channel at the inlet is found to be 28.8, whereas at the outlet, it is 60.9. Next, the bi-serpentine PEMFC was simulated, with the Reynolds number at the inlet is found to be 17.3 and at the outlet has 43.9. Lastly, the tri-serpentine flow channel configuration was analyzed, revealing a Reynolds number of 11.9 at the inlet and 41.5 at the outlet.

In the cell Reynolds number of the PEMFC at 0.5V (high), the value of single serpentine flow channel at the inlet is found to be 31, whereas at the outlet, it

is 64. Next, the bi-serpentine PEMFC was simulated, with the Reynolds number at the inlet is found to be 22 and at the outlet has 49. Lastly, the tri-serpentine flow channel configuration was analyzed at 0.5V, revealing a Reynolds number of 13.2 at the inlet and 46.8 at the outlet.

In the cell Reynolds number of the PEMFC at 0.65V (very high), the value of single serpentine flow channel at the inlet is found to be 33.7, whereas at the outlet, it is 66.2. Next, the bi-serpentine PEMFC was simulated, with the Reynolds number at the inlet is found to be 23.7 and at the outlet has 50.5. Lastly, the tri-serpentine flow channel configuration was analyzed, revealing a Reynolds number of 15.1 at the inlet and 48.4 at the outlet.

In the cell Reynolds number of the PEMFC at 0.8V (extreme), the value of single serpentine flow channel at the inlet is found to be 35.3, whereas at the outlet, it is 67.8. Next, the bi-serpentine PEMFC was simulated, with the Reynolds number at the inlet is found to be 26.1 and at the outlet has 52.6. Lastly, the tri-serpentine flow channel configuration was analyzed, revealing a Reynolds number of 16.4 at the inlet and 49.6 at the outlet.

From these results from different voltages, it is observed that the Reynolds number of the cell varies between 10.1 to 67.8 for all the three flow channels which confirms that the flow range lies under laminar.

In chapter 8, the comparison between the flow channel designs of 1mm, 2mm, and 3mm flow channel width of PEMFC has been conducted at 373K (100°C). Additionally, the analysis of PEMFC similar to chapter 7 also done for the altered flow channel width at three different voltages. Based on the results obtained, the 3mm flow channel width has better performance because it provides more room to the reactants to flow than other flow channels. In the single serpentine PEMFC, the polarization curve indicates that the 1mm flow

channel width achieves a maximum peak power density of 0.539 W/cm^2 with a corresponding current density of 0.981 A/cm^2 generated at 0.55 V . Subsequently, the 3mm channel width exhibits a peak power density of 0.642 W/cm^2 and a current density 1.284 A/cm^2 at 0.5 V . In bi serpentine PEMFC, the peak power density with 1mm flow channel width is 0.575 W/cm^2 , accompanied by a corresponding current density of 1.15 A/cm^2 at 0.5V . Moreover, the 3mm flow channel width demonstrates a maximum power density of 0.6465 W/cm^2 with corresponding current density 1.293 A/cm^2 at 0.5V . For the tri serpentine flow channel PEMFC, the polarization curve indicates a maximum power density 0.6 W/cm^2 with a corresponding current density 1.2 A/cm^2 using the 1mm flow channel width at 0.5 V . Additionally, the 3mm flow channel width achieves a maximum power density of 0.715 W/cm^2 with corresponding current density 1.3 A/cm^2 at 0.55 V .

Additionally, chapter 8 contains the analysis work of PEMFC which comprises of pressure distribution, velocity magnitude, mass fraction of the hydrogen (H_2), and Reynolds number of the cell.

In the pressure distribution of 1mm flow channel width of the PEMFC at 0.25V (low), the initial pressure at the inlet of the single serpentine flow channel is 200 KPa , and at the outlet, it is 117 KPa . Therefore, the pressure drops across the single serpentine flow channel is 83 KPa . Next, the bi-serpentine PEMFC was simulated, with the initial pressure at the inlet of the bi serpentine flow channel being 200 KPa , and at the outlet, it is 133 KPa . Consequently, the pressure drops across the bi serpentine flow channel is 67 KPa . Lastly, the tri-serpentine configuration was analyzed, revealing an initial pressure at the inlet of 200 KPa , and at the outlet, it is 148 KPa . Therefore, the pressure drops across the tri serpentine flow channel is 52 KPa .

In the pressure distribution of 1mm flow channel width of the PEMFC at 0.35V (medium), the initial pressure at the inlet of the single serpentine flow channel is 200 KPa, and at the outlet, it is 127 KPa. Therefore, the pressure drops across the single serpentine flow channel is 73 KPa. Next, the bi-serpentine PEMFC was simulated, with the initial pressure at the inlet of the bi serpentine flow channel being 200 KPa, and at the outlet, it is 140 KPa. Consequently, the pressure drops across the bi serpentine flow channel is 60 KPa. Lastly, the tri-serpentine configuration was analyzed, revealing an initial pressure at the inlet of 200 KPa, and at the outlet, it is 153 KPa. Therefore, the pressure drops across the tri serpentine flow channel is 47 KPa.

In the pressure distribution of 1mm flow channel width of the PEMFC at 0.55V (high), the initial pressure at the inlet of the single serpentine flow channel is 200 KPa, and at the outlet, it is 138 KPa. Therefore, the pressure drops across the single serpentine flow channel is 62 KPa. Next, the bi-serpentine PEMFC was simulated at 0.5V, with the initial pressure at the inlet of the bi serpentine flow channel being 200 KPa, and at the outlet, it is 149 KPa. Consequently, the pressure drops across the bi serpentine flow channel is 51 KPa. Lastly, the tri-serpentine configuration was analyzed at 0.5V, revealing an initial pressure at the inlet of 200 KPa, and at the outlet, it is 161 KPa. Therefore, the pressure drops across the tri serpentine flow channel is 39 KPa.

In the pressure distribution of 1mm flow channel width of the PEMFC at 0.65V (very high), the initial pressure at the inlet of the single serpentine flow channel is 200 KPa, and at the outlet, it is 144 KPa. Therefore, the pressure drops across the single serpentine flow channel is 56 KPa. Next, the bi-serpentine PEMFC was simulated, with the initial pressure at the inlet of the

bi serpentine flow channel being 200 KPa, and at the outlet, it is 156 KPa. Consequently, the pressure drops across the bi serpentine flow channel is 44 KPa. Lastly, the tri-serpentine configuration was analyzed, revealing an initial pressure at the inlet of 200 KPa, and at the outlet, it is 162 KPa. Therefore, the pressure drops across the tri serpentine flow channel is 38 KPa.

In the pressure distribution of 1mm flow channel width of the PEMFC at 0.8V (extreme), the initial pressure at the inlet of the single serpentine flow channel is 200 KPa, and at the outlet, it is 153 KPa. Therefore, the pressure drops across the single serpentine flow channel is 47 KPa. Next, the bi-serpentine PEMFC was simulated, with the initial pressure at the inlet of the bi serpentine flow channel being 200 KPa, and at the outlet, it is 160 KPa. Consequently, the pressure drops across the bi serpentine flow channel is 40 KPa. Lastly, the tri-serpentine configuration was analyzed, revealing an initial pressure at the inlet of 200 KPa, and at the outlet, it is 167 KPa. Therefore, the pressure drops across the tri serpentine flow channel is 33 KPa.

In the pressure distribution of 3mm flow channel width of the PEMFC at 0.25V (low), the initial pressure at the inlet of the single serpentine flow channel is 200 KPa, and at the outlet, it is 125 KPa. Therefore, the pressure drops across the single serpentine flow channel is 75 KPa. Next, the bi-serpentine PEMFC was simulated, with the initial pressure at the inlet of the bi serpentine flow channel being 200 KPa, and at the outlet, it is 142 KPa. Consequently, the pressure drops across the bi serpentine flow channel is 58 KPa. Lastly, the tri-serpentine configuration was analyzed, revealing an initial pressure at the inlet of 200 KPa, and at the outlet, it is 149 KPa. Therefore, the pressure drops across the tri serpentine flow channel is 51 KPa.

In the pressure distribution of 3mm flow channel width of the PEMFC at 0.35V (medium), the initial pressure at the inlet of the single serpentine flow channel is 200 KPa, and at the outlet, it is 134 KPa. Therefore, the pressure drops across the single serpentine flow channel is 66 KPa. Next, the bi-serpentine PEMFC was simulated, with the initial pressure at the inlet of the bi serpentine flow channel being 200 KPa, and at the outlet, it is 151 KPa. Consequently, the pressure drops across the bi serpentine flow channel is 49 KPa. Lastly, the tri-serpentine configuration was analyzed, revealing an initial pressure at the inlet of 200 KPa, and at the outlet, it is 160 KPa. Therefore, the pressure drops across the tri serpentine flow channel is 40 KPa.

In the pressure distribution of 3mm flow channel width of the PEMFC at 0.5V (high), the initial pressure at the inlet of the single serpentine flow channel is 200 KPa, and at the outlet, it is 146 KPa. Therefore, the pressure drops across the single serpentine flow channel is 54 KPa. Next, the bi-serpentine PEMFC was simulated, with the initial pressure at the inlet of the bi serpentine flow channel being 200 KPa, and at the outlet, it is 155 KPa. Consequently, the pressure drops across the bi serpentine flow channel is 45 KPa. Lastly, the tri-serpentine configuration was analyzed at 0.55V, revealing an initial pressure at the inlet of 200 KPa, and at the outlet, it is 167 KPa. Therefore, the pressure drops across the tri serpentine flow channel is 33 KPa.

In the pressure distribution of 3mm flow channel width of the PEMFC at 0.65V (very high), the initial pressure at the inlet of the single serpentine flow channel is 200 KPa, and at the outlet, it is 159 KPa. Therefore, the pressure drops across the single serpentine flow channel is 41 KPa. Next, the bi-serpentine PEMFC was simulated, with the initial pressure at the inlet of the bi serpentine flow channel being 200 KPa, and at the outlet, it is 156 KPa.

Consequently, the pressure drops across the bi serpentine flow channel is 44 KPa. Lastly, the tri-serpentine configuration was analyzed, revealing an initial pressure at the inlet of 200 KPa, and at the outlet, it is 162 KPa. Therefore, the pressure drops across the tri serpentine flow channel is 38 KPa.

In the pressure distribution of 3mm flow channel width of the PEMFC at 0.8V (extreme), the initial pressure at the inlet of the single serpentine flow channel is 200 KPa, and at the outlet, it is 163 KPa. Therefore, the pressure drops across the single serpentine flow channel is 37 KPa. Next, the bi-serpentine PEMFC was simulated, with the initial pressure at the inlet of the bi serpentine flow channel being 200 KPa, and at the outlet, it is 170 KPa. Consequently, the pressure drops across the bi serpentine flow channel is 30 KPa. Lastly, the tri-serpentine configuration was analyzed, revealing an initial pressure at the inlet of 200 KPa, and at the outlet, it is 178 KPa. Therefore, the pressure drops across the tri serpentine flow channel is 22 KPa.

When analyzing pressure distributions in various flow channels under different voltages, it becomes evident that the single serpentine flow channel experiences a higher-pressure drop compared to the other channels. This difference can be linked to the increased number of bends in the single serpentine design. Conversely, the tri serpentine design shows minimal pressure drop thanks to its fewer bends, leading to enhanced cell performance.

In velocity magnitude of 1mm flow channel width of PEMFC at 0.25V (low), the velocity at the inlet and outlet of the single serpentine flow channel is 0.477 m/s and 1.10 m/s respectively. The difference in velocity magnitude from the inlet to the outlet of the single serpentine flow channel is 0.63 m/s. Next, the bi-serpentine PEMFC was simulated, with the velocities at the inlet and outlet of 0.283 m/s and 0.957 m/s respectively. The difference in velocity

magnitude from the inlet to the outlet of the bi serpentine flow channel is 0.674 m/s. Lastly, the tri-serpentine was analyzed, revealing velocities at the inlet and outlet of 0.191 m/s and 0.861 m/s respectively. The difference in velocity magnitude from the inlet to the outlet of the tri serpentine flow channel is 0.67 m/s.

In velocity magnitude of 1mm flow channel width of PEMFC at 0.35V (medium), the velocity at the inlet and outlet of the single serpentine flow channel is 0.493 m/s and 1.18 m/s respectively. The difference in velocity magnitude from the inlet to the outlet of the single serpentine flow channel is 0.691 m/s. Next, the bi-serpentine PEMFC was simulated, with the velocities at the inlet and outlet of 0.311 m/s and 0.974 m/s respectively. The difference in velocity magnitude from the inlet to the outlet of the bi serpentine flow channel is 0.663 m/s. Lastly, the tri-serpentine was analyzed, revealing velocities at the inlet and outlet of 0.216 m/s and 0.882 m/s respectively. The difference in velocity magnitude from the inlet to the outlet of the tri serpentine flow channel is 0.666 m/s.

In velocity magnitude of 1mm flow channel width of PEMFC at 0.55V (high), the velocity at the inlet and outlet of the single serpentine flow channel is 0.503 m/s and 1.24 m/s respectively. The difference in velocity magnitude from the inlet to the outlet of the single serpentine flow channel is 0.741 m/s. Next, the bi-serpentine PEMFC was simulated at 0.5V, with the velocities at the inlet and outlet of 0.369 m/s and 0.985 m/s respectively. The difference in velocity magnitude from the inlet to the outlet of the bi serpentine flow channel is 0.616 m/s. Lastly, the tri-serpentine was analyzed at 0.5V, revealing velocities at the inlet and outlet of 0.26 m/s and 0.921 m/s respectively. The

difference in velocity magnitude from the inlet to the outlet of the tri serpentine flow channel is 0.661 m/s.

In velocity magnitude of 1mm flow channel width of PEMFC at 0.65V (very high), the velocity at the inlet and outlet of the single serpentine flow channel is 0.519 m/s and 1.33 m/s respectively. The difference in velocity magnitude from the inlet to the outlet of the single serpentine flow channel is 0.811 m/s. Next, the bi-serpentine PEMFC was simulated, with the velocities at the inlet and outlet of 0.38 m/s and 0.997 m/s respectively. The difference in velocity magnitude from the inlet to the outlet of the bi serpentine flow channel is 0.617 m/s. Lastly, the tri-serpentine was analyzed, revealing velocities at the inlet and outlet of 0.282 m/s and 0.937 m/s respectively. The difference in velocity magnitude from the inlet to the outlet of the tri serpentine flow channel is 0.655 m/s.

In velocity magnitude of 1mm flow channel width of PEMFC at 0.8V (extreme), the velocity at the inlet and outlet of the single serpentine flow channel is 0.53 m/s and 1.43 m/s respectively. The difference in velocity magnitude from the inlet to the outlet of the single serpentine flow channel is 0.9 m/s. Next, the bi-serpentine PEMFC was simulated, with the velocities at the inlet and outlet of 0.4 m/s and 1.12 m/s respectively. The difference in velocity magnitude from the inlet to the outlet of the bi serpentine flow channel is 0.72 m/s. Lastly, the tri-serpentine was analyzed, revealing velocities at the inlet and outlet of 0.296 m/s and 0.945 m/s respectively. The difference in velocity magnitude from the inlet to the outlet of the tri serpentine flow channel is 0.649 m/s.

In velocity magnitude of 3mm flow channel width of PEMFC at 0.25V (low), the velocity at the inlet and outlet of the single serpentine flow channel is

0.505 m/s and 1.27 m/s respectively. The difference in velocity magnitude from the inlet to the outlet of the single serpentine flow channel is 0.765 m/s. Next, the bi-serpentine PEMFC was simulated, with the velocities at the inlet and outlet of 0.341 m/s and 1.03 m/s respectively. The difference in velocity magnitude from the inlet to the outlet of the bi serpentine flow channel is 0.689 m/s. Lastly, the tri-serpentine was analyzed, revealing velocities at the inlet and outlet of 0.231 m/s and 0.917 m/s respectively. The difference in velocity magnitude from the inlet to the outlet of the tri serpentine flow channel is 0.686 m/s.

In velocity magnitude of 3mm flow channel width of PEMFC at 0.35V (medium), the velocity at the inlet and outlet of the single serpentine flow channel is 0.519 m/s and 1.34 m/s respectively. The difference in velocity magnitude from the inlet to the outlet of the single serpentine flow channel is 8.21×10^{-01} m/s. Next, the bi-serpentine PEMFC was simulated, with the velocities at the inlet and outlet of 0.322 m/s and 1.07 m/s respectively. The difference in velocity magnitude from the inlet to the outlet of the bi serpentine flow channel is 0.748 m/s. Lastly, the tri-serpentine was analyzed, revealing velocities at the inlet and outlet of 0.244 m/s and 0.924 m/s respectively. The difference in velocity magnitude from the inlet to the outlet of the tri serpentine flow channel is 0.68 m/s.

In velocity magnitude of 3mm flow channel width of PEMFC at 0.5V (high), the velocity at the inlet and outlet of the single serpentine flow channel is 0.526 m/s and 1.40 m/s respectively. The difference in velocity magnitude from the inlet to the outlet of the single serpentine flow channel is 0.874 m/s. Next, the bi-serpentine PEMFC was simulated, with the velocities at the inlet and outlet of 0.399 m/s and 0.111 m/s respectively. The difference in velocity

magnitude from the inlet to the outlet of the bi serpentine flow channel is 0.711 m/s. Lastly, the tri-serpentine was analyzed at 0.55V, revealing velocities at the inlet and outlet of 0.271 m/s and 0.948 m/s respectively. The difference in velocity magnitude from the inlet to the outlet of the tri serpentine flow channel is 0.677 m/s.

In velocity magnitude of 3mm flow channel width of PEMFC at 0.65V (very high), the velocity at the inlet and outlet of the single serpentine flow channel is 0.561 m/s and 1.48 m/s respectively. The difference in velocity magnitude from the inlet to the outlet of the single serpentine flow channel is 0.919 m/s. Next, the bi-serpentine PEMFC was simulated, with the velocities at the inlet and outlet of 0.407 m/s and 1.18 m/s respectively. The difference in velocity magnitude from the inlet to the outlet of the bi serpentine flow channel is 0.773 m/s. Lastly, the tri-serpentine was analyzed, revealing velocities at the inlet and outlet of 0.306 m/s and 0.958 m/s respectively. The difference in velocity magnitude from the inlet to the outlet of the tri serpentine flow channel is 0.652 m/s.

In velocity magnitude of 3mm flow channel width of PEMFC at 0.8V (extreme), the velocity at the inlet and outlet of the single serpentine flow channel is 0.5 m/s and 1.59 m/s respectively. The difference in velocity magnitude from the inlet to the outlet of the single serpentine flow channel is 1.09 m/s. Next, the bi-serpentine PEMFC was simulated, with the velocities at the inlet and outlet of 0.419 m/s and 1.25 m/s respectively. The difference in velocity magnitude from the inlet to the outlet of the bi serpentine flow channel is 0.831 m/s. Lastly, the tri-serpentine was analyzed, revealing velocities at the inlet and outlet of 0.315 m/s and 0.974 m/s respectively. The

difference in velocity magnitude from the inlet to the outlet of the tri serpentine flow channel is 0.659 m/s.

When comparing the velocity magnitudes across all the flow channels, it is observed that the velocity is highest in the single serpentine flow channel, followed by the bi and tri serpentine flow channels. This higher velocity at the outlet can be attributed to the stoichiometric ratio of the anode.

In 1mm flow channel width of PEMFC, the mass fraction of hydrogen (H_2) at 0.25V (low) was analyzed. The consumption rate of hydrogen (H_2) at the single serpentine flow channel is 0.536. Next, the bi-serpentine PEMFC was simulated, showing a hydrogen (H_2) consumption rate of 0.583. Lastly, the tri-serpentine configuration was analyzed, revealing a hydrogen (H_2) consumption rate of 0.633.

In 1mm flow channel width of PEMFC, the mass fraction of hydrogen (H_2) at 0.35V (medium) was analyzed. The consumption rate of hydrogen (H_2) at the single serpentine flow channel is 0.574. Next, the bi-serpentine PEMFC was simulated, showing a hydrogen (H_2) consumption rate of 0.616. Lastly, the tri-serpentine configuration was analyzed, revealing a hydrogen (H_2) consumption rate of 0.67.

In 1mm flow channel width of PEMFC, the mass fraction of hydrogen (H_2) at 0.55V (high) was analyzed. The consumption rate of hydrogen (H_2) at the single serpentine flow channel is 0.622. Next, the bi-serpentine PEMFC was simulated at 0.5V, showing a hydrogen (H_2) consumption rate of 0.649. Lastly, the tri-serpentine configuration was analyzed at 0.5V, revealing a hydrogen (H_2) consumption rate of 0.696.

In 1mm flow channel width of PEMFC, the mass fraction of hydrogen (H_2) at 0.65V (very high) was analyzed. The consumption rate of hydrogen (H_2) at

the single serpentine flow channel is 0.669. Next, the bi-serpentine PEMFC was simulated, showing a hydrogen (H_2) consumption rate of 0.665. Lastly, the tri-serpentine configuration was analyzed, revealing a hydrogen (H_2) consumption rate of 0.696.

In 1mm flow channel width of PEMFC, the mass fraction of hydrogen (H_2) at 0.8V (extreme) was analyzed. The consumption rate of hydrogen (H_2) at the single serpentine flow channel is 0.682. Next, the bi-serpentine PEMFC was simulated, showing a hydrogen (H_2) consumption rate of 0.679. Lastly, the tri-serpentine configuration was analyzed, revealing a hydrogen (H_2) consumption rate of 0.710.

In 3mm flow channel width of PEMFC, the mass fraction of hydrogen (H_2) at 0.25V (low) was analyzed. The consumption rate of hydrogen (H_2) at the single serpentine flow channel is 0.555. Next, the bi-serpentine PEMFC was simulated, showing a hydrogen (H_2) consumption rate of 0.611. Lastly, the tri-serpentine configuration was analyzed, revealing a hydrogen (H_2) consumption rate of 0.661.

In 3mm flow channel width of PEMFC, the mass fraction of hydrogen (H_2) at 0.35V (medium) was analyzed. The consumption rate of hydrogen (H_2) at the single serpentine flow channel is 0.599. Next, the bi-serpentine PEMFC was simulated, showing a hydrogen (H_2) consumption rate of 0.632. Lastly, the tri-serpentine configuration was analyzed, revealing a hydrogen (H_2) consumption rate of 0.693.

In 3mm flow channel width of PEMFC, the mass fraction of hydrogen (H_2) at 0.5V (high) was analyzed. The consumption rate of hydrogen (H_2) at the single serpentine flow channel is 0.639. Next, the bi-serpentine PEMFC was simulated at 0.5V, showing a hydrogen (H_2) consumption rate of 0.671.

Lastly, the tri-serpentine configuration was analyzed at 0.55V, revealing a hydrogen (H_2) consumption rate of 0.727.

In 3mm flow channel width of PEMFC, the mass fraction of hydrogen (H_2) at 0.65V (very high) was analyzed. The consumption rate of hydrogen (H_2) at the single serpentine flow channel is 0.701. Next, the bi-serpentine PEMFC was simulated, showing a hydrogen (H_2) consumption rate of 0.721. Lastly, the tri-serpentine configuration was analyzed, revealing a hydrogen (H_2) consumption rate of 0.730.

In 3mm flow channel width of PEMFC, the mass fraction of hydrogen (H_2) at 0.8V (extreme) was analyzed. The consumption rate of hydrogen (H_2) at the single serpentine flow channel is 0.712. Next, the bi-serpentine PEMFC was simulated, showing a hydrogen (H_2) consumption rate of 0.708. Lastly, the tri-serpentine configuration was analyzed, revealing a hydrogen (H_2) consumption rate of 0.735.

Based on the results of the hydrogen (H_2) mass fraction at various voltages, it was noted that the tri serpentine flow channel exhibits the highest hydrogen (H_2) consumption rate compared to the single and bi serpentine flow channels. This higher consumption rate in the tri serpentine flow channel leads to the generation of high current.

In 1mm flow channel width of PEMFC at 0.25V (low), the cell Reynolds number value of single serpentine flow channel at the inlet is found to be 20.9, whereas at the outlet, it is 54.1. Next, the bi-serpentine PEMFC was simulated, with the Reynolds number at the inlet is found to be 13.7 and at the outlet has 38.5. Lastly, the tri-serpentine flow channel configuration was analyzed, revealing a Reynolds number of 10.1 at the inlet and 37.8 at the outlet.

In 1mm flow channel width of PEMFC at 0.35V (medium), the cell Reynolds number value of single serpentine flow channel at the inlet is found to be 28.1, whereas at the outlet, it is 59.4. Next, the bi-serpentine PEMFC was simulated, with the Reynolds number at the inlet is found to be 16.6 and at the outlet has 43.3. Lastly, the tri-serpentine flow channel configuration was analyzed, revealing a Reynolds number of 11.7 at the inlet and 41.1 at the outlet.

In 1mm flow channel width of PEMFC at 0.55V (high), the cell Reynolds number value of single serpentine flow channel at the inlet is found to be 30.3, whereas at the outlet, it is 63.1. Next, the bi-serpentine PEMFC was simulated at 0.5V, with the Reynolds number at the inlet is found to be 21.2 and at the outlet has 48.3. Lastly, the tri-serpentine flow channel configuration was analyzed at 0.5V, revealing a Reynolds number of 12.9 at the inlet and 43.9 at the outlet.

In 1mm flow channel width of PEMFC at 0.65V (very high), the cell Reynolds number value of single serpentine flow channel at the inlet is found to be 34.5, whereas at the outlet, it is 67.3. Next, the bi-serpentine PEMFC was simulated, with the Reynolds number at the inlet is found to be 24.3 and at the outlet has 52.3. Lastly, the tri-serpentine flow channel configuration was analyzed, revealing a Reynolds number of 13.7 at the inlet and 45.2 at the outlet.

In 1mm flow channel width of PEMFC at 0.8V (extreme), the cell Reynolds number value of single serpentine flow channel at the inlet is found to be 38.9, whereas at the outlet, it is 70.4. Next, the bi-serpentine PEMFC was simulated, with the Reynolds number at the inlet is found to be 26.2 and at the outlet has 53.4. Lastly, the tri-serpentine flow channel configuration was analyzed, revealing a Reynolds number of 14.5 at the inlet and 47.7 at the outlet.

In 3mm flow channel width of PEMFC at 0.25V (low), the cell Reynolds number value of single serpentine flow channel at the inlet is found to be 23.9, whereas at the outlet, it is 58.1. Next, the bi-serpentine PEMFC was simulated, with the Reynolds number at the inlet is found to be 14.9 and at the outlet has 40.5. Lastly, the tri-serpentine flow channel configuration was analyzed, revealing a Reynolds number of 10.8 at the inlet and 40.1 at the outlet.

In 3mm flow channel width of PEMFC at 0.35V (medium), the cell Reynolds number value of single serpentine flow channel at the inlet is found to be 29.6, whereas at the outlet, it is 63. Next, the bi-serpentine PEMFC was simulated, with the Reynolds number at the inlet is found to be 18.1 and at the outlet has 45.1. Lastly, the tri-serpentine flow channel configuration was analyzed, revealing a Reynolds number of 12.5 at the inlet and 42.7 at the outlet.

In 3mm flow channel width of PEMFC at 0.5V (high), the cell Reynolds number value of single serpentine flow channel at the inlet is found to be 31.7, whereas at the outlet, it is 65.5. Next, the bi-serpentine PEMFC was simulated at 0.5V, with the Reynolds number at the inlet is found to be 23.1 and at the outlet has 51.7. Lastly, the tri-serpentine flow channel configuration was analyzed at 0.55V, revealing a Reynolds number of 13.9 at the inlet and 48.5 at the outlet.

In 3mm flow channel width of PEMFC at 0.65V (very high), the cell Reynolds number value of single serpentine flow channel at the inlet is found to be 42.6, whereas at the outlet, it is 77.3. Next, the bi-serpentine PEMFC was simulated, with the Reynolds number at the inlet is found to be 28.4 and at the outlet has 55.7. Lastly, the tri-serpentine flow channel configuration was analyzed, revealing a Reynolds number of 15.3 at the inlet and 51.1 at the outlet.

In 3mm flow channel width of PEMFC at 0.8V (extreme), the cell Reynolds number value of single serpentine flow channel at the inlet is found to be 47, whereas at the outlet, it is 85.6. Next, the bi-serpentine PEMFC was simulated, with the Reynolds number at the inlet is found to be 31.2 and at the outlet has 60.6. Lastly, the tri-serpentine flow channel configuration was analyzed, revealing a Reynolds number of 17.9 at the inlet and 54.5 at the outlet.

From these results from different voltages, it is observed that the Reynolds number of the cell varies between 10.1 to 65.5 for all the three flow channels which confirms that the flow range lies under laminar.

CHAPTER 10

CONCLUSION

This thesis investigated three different flow field configurations across various cell temperatures and voltages. Additionally, it includes the validation of the data, analysis of pressure distribution, velocity magnitude, mass fractions of the hydrogen, Reynolds number of the cell and modified dimensional analysis of flow channel design. The findings of this work can provide valuable insights for fuel cell manufacturing industries seeking to optimum flow field designs. The major features of the study are summarized as follows:

(1). Among the three different flow field, the tri serpentine flow channel demonstrates superior performance compared to the single and bi serpentine flow channels. This finding is valuable for selecting the optimal configuration in applications where maximizing performance is crucial.

All the following simulations are done at 2 bar pressure.

(2). At 313K (40°C), the single serpentine flow channel achieved a maximum current density of 1.026 A/cm², resulting in a corresponding power density of 0.513 W/cm² at 0.5 V.

(3). At 313K (40°C), the bi serpentine flow channel achieved a maximum current density of 1.053 A/cm², resulting in a corresponding power density of 0.5265 W/cm² at 0.5 V.

(4). At 313K (40°C), the tri serpentine flow channel achieved a maximum current density of 1.071 A/cm², resulting in a corresponding power density of 0.5355 W/cm² at 0.5 V.

- (5). At 323K (50°C), the single serpentine flow channel achieved a maximum current density of 1.053 A/cm², resulting in a corresponding power density of 0.526 W/cm² at 0.5 V.
- (6). At 323K (50°C), the bi serpentine flow channel achieved a maximum current density of 0.981 A/cm², resulting in a corresponding power density of 0.539 W/cm² at 0.5 V.
- (7). At 323K (50°C), the tri serpentine flow channel achieved a maximum current density of 1.02 A/cm², resulting in a corresponding power density of 0.55 W/cm² at 0.55 V.
- (8). At 333K (60°C), the single serpentine flow channel achieved a maximum current density of 0.982 A/cm², resulting in a corresponding power density of 0.54 W/cm² at 0.55 V.
- (9). At 333K (60°C), the bi serpentine flow channel achieved a maximum current density of 1.007 A/cm², resulting in a corresponding power density of 0.554 W/cm² at 0.55 V.
- (10). At 333K (60°C), the tri serpentine flow channel achieved a maximum current density of 1.167 A/cm², resulting in a corresponding power density of 0.583 W/cm² at 0.5 V.
- (11). At 343K (70°C), the single serpentine flow channel achieved a maximum current density of 0.994 A/cm², resulting in a corresponding power density of 0.5467 W/cm² at 0.55 V.
- (12). At 343K (70°C), the bi serpentine flow channel achieved a maximum current density of 1.03 A/cm², resulting in a corresponding power density of 0.5665 W/cm² at 0.55 V.

(13). At 343K (70°C), the tri serpentine flow channel achieved a maximum current density of 1.142 A/cm², resulting in a corresponding power density of 0.6281 W/cm² at 0.55 V.

(14). At 353K (80°C), the single serpentine flow channel achieved a maximum current density of 1.131 A/cm², resulting in a corresponding power density of 0.5655 W/cm² at 0.5 V.

(15). At 353K (80°C), the bi serpentine flow channel achieved a maximum current density of 1.161 A/cm², resulting in a corresponding power density of 0.5805 W/cm² at 0.5 V.

(16). At 353K (80°C), the tri serpentine flow channel achieved a maximum current density of 1.198 A/cm², resulting in a corresponding power density of 0.599 W/cm² at 0.5 V.

(17). At 363K (90°C), the single serpentine flow channel achieved a maximum current density of 1.163 A/cm², resulting in a corresponding power density of 0.5815 W/cm² at 0.5 V.

(18). At 363K (90°C), the bi serpentine flow channel achieved a maximum current density of 1.194 A/cm², resulting in a corresponding power density of 0.597 W/cm² at 0.5 V.

(19). At 363K (90°C), the tri serpentine flow channel achieved a maximum current density of 1.152 A/cm², resulting in a corresponding power density of 0.6336 W/cm² at 0.55V.

(20). At 373K (100°C), the single serpentine flow channel achieved a maximum current density of 1.153 A/cm², resulting in a corresponding power density of 0.5765 W/cm² at 0.5V.

(21). At 373K (100°C), the bi serpentine flow channel achieved a maximum current density of 1.208 A/cm², resulting in a corresponding power density of 0.604 W/cm² at 0.5V

(22). At 373K (100°C), the tri serpentine flow channel achieved a maximum current density of 1.12 A/cm², resulting in a corresponding power density of 0.6655 W/cm² at 0.55V.

All the following simulations are done at 373K (100°C).

(23) The initial pressure at the inlet of the 2mm flow channel width of single serpentine PEMFC at 0.25 V is 199 KPa, and at the outlet, it is 120 KPa. Therefore, the pressure drops across the single serpentine flow channel is 79 KPa.

(24). The initial pressure at the inlet of the 2mm flow channel width of single serpentine PEMFC at 0.35 V is 199 KPa, and at the outlet, it is 128 KPa. Therefore, the pressure drops across the single serpentine flow channel is 71 KPa.

(25). The initial pressure at the inlet of the 2mm flow channel width of single serpentine PEMFC at 0.5 V is 199 KPa, and at the outlet, it is 139 KPa. Therefore, the pressure drops across the single serpentine flow channel is 60 KPa.

(26). The initial pressure at the inlet of the 2mm flow channel width of single serpentine PEMFC at 0.65 V is 200 KPa, and at the outlet, it is 152 KPa. Therefore, the pressure drops across the single serpentine flow channel is 48 KPa.

(27). The initial pressure at the inlet of the 2mm flow channel width of single serpentine PEMFC at 0.8 V is 200 KPa, and at the outlet, it is 157 KPa.

Therefore, the pressure drops across the single serpentine flow channel is 43 KPa.

(28). The initial pressure at the inlet of the 2mm flow channel width bi serpentine PEMFC at 0.25V is 199 KPa, and at the outlet, it is 136 KPa. Therefore, the pressure drops across the bi serpentine flow channel is 63 KPa.

(29). The initial pressure at the inlet of the 2mm flow channel width of bi serpentine PEMFC at 0.35V is 199KPa, and at the outlet, it is 142 KPa. Therefore, the pressure drops across the bi serpentine flow channel is 57 KPa.

(30). The initial pressure at the inlet of the 2mm flow channel width of bi serpentine PEMFC at 0.5V is 199 KPa, and at the outlet, it is 151 KPa. Therefore, the pressure drops across the bi serpentine flow channel is 48 KPa.

(31). The initial pressure at the inlet of the 2mm flow channel width of bi serpentine PEMFC at 0.65V is 200 KPa, and at the outlet, it is 161 KPa. Therefore, the pressure drops across the bi serpentine flow channel is 39 KPa.

(32). The initial pressure at the inlet of the 2mm flow channel width of bi serpentine PEMFC at 0.8V is 200 KPa, and at the outlet, it is 164 KPa. Therefore, the pressure drops across the bi serpentine flow channel is 36 KPa.

(33). The initial pressure at the inlet of the 2mm flow channel width of tri serpentine PEMFC at 0.25V is 200 KPa and at the outlet, it is 149 KPa. Therefore, the pressure drops across the tri serpentine flow channel is 51 KPa.

(34). The initial pressure at the inlet of the 2mm flow channel width of tri serpentine PEMFC at 0.35V is 200 KPa and at the outlet, it is 156 KPa. Therefore, the pressure drops across the tri serpentine flow channel is 44 KPa.

- (35). The initial pressure at the inlet of the 2mm flow channel width of tri serpentine PEMFC at 0.55V is 200 KPa and at the outlet, it is 163 KPa. Therefore, the pressure drops across the tri serpentine flow channel is 37 KPa.
- (36). The initial pressure at the inlet of the 2mm flow channel width of tri serpentine PEMFC at 0.65V is 200 KPa and at the outlet, it is 169 KPa. Therefore, the pressure drops across the tri serpentine flow channel is 31 KPa.
- (37). The initial pressure at the inlet of the 2mm flow channel width of tri serpentine PEMFC at 0.8V is 200 KPa and at the outlet, it is 173 KPa. Therefore, the pressure drops across the tri serpentine flow channel is 27 KPa.
- (38). The velocity at the inlet of the 2mm flow channel width of single serpentine PEMFC at 0.25V is 0.487 m/s, while at the outlet, it is 1.13 m/s. Consequently, the difference in velocity magnitude from the inlet to outlet of the single serpentine flow channel is 0.643 m/s.
- (39). The velocity at the inlet of the 2mm flow channel width of single serpentine PEMFC at 0.35V is 0.501 m/s, while at the outlet, it is 1.21 m/s. Consequently, the difference in velocity magnitude from the inlet to outlet of the single serpentine flow channel is 0.709 m/s.
- (40). The velocity at the inlet of the 2mm flow channel width of single serpentine PEMFC at 0.5V is 0.514 m/s, while at the outlet, it is 1.28 m/s. Consequently, the difference in velocity magnitude from the inlet to outlet of the single serpentine flow channel is 0.766 m/s.
- (41). The velocity at the inlet of the 2mm flow channel width of single serpentine PEMFC at 0.65V is 0.525 m/s, while at the outlet, it is 1.35 m/s. Consequently, the difference in velocity magnitude from the inlet to outlet of the single serpentine flow channel is 0.825 m/s.

(42). The velocity at the inlet of the 2mm flow channel width of single serpentine PEMFC at 0.8V is 0.530 m/s, while at the outlet, it is 1.38 m/s. Consequently, the difference in velocity magnitude from the inlet to outlet of the single serpentine flow channel is 0.85 m/s.

(43). The velocity at the inlet of the 2mm flow channel width of bi serpentine PEMFC at 0.25V is 0.289 m/s, while at the outlet, it is 0.977 m/s. Consequently, the difference in velocity magnitude from the inlet to outlet of the bi serpentine flow channel is 0.688 m/s.

(44). The velocity at the inlet of the 2mm flow channel width of bi serpentine PEMFC at 0.35V is 0.317 m/s, while at the outlet, it is 0.989 m/s. Consequently, the difference in velocity magnitude from the inlet to outlet of the bi serpentine flow channel is 0.672 m/s.

(45). The velocity at the inlet of the 2mm flow channel width of bi serpentine PEMFC at 0.5V is 0.374 m/s, while at the outlet, it is 0.998 m/s. Consequently, the difference in velocity magnitude from the inlet to outlet of the bi serpentine flow channel is 0.624 m/s.

(46). The velocity at the inlet of the 2mm flow channel width of bi serpentine PEMFC at 0.65V is 0.401m/s, while at the outlet, it is 1.06 m/s. Consequently, the difference in velocity magnitude from the inlet to outlet of the single serpentine flow channel is 0.659 m/s.

(47). The velocity at the inlet of the 2mm flow channel width of bi serpentine PEMFC at 0.8V is 0.423 m/s, while at the outlet, it is 1.10 m/s. Consequently, the difference in velocity magnitude from the inlet to outlet of the single serpentine flow channel is 0.677 m/s.

(48). The velocity at the inlet of the 2mm flow channel width of tri serpentine PEMFC at 0.25V is 0.197 m/s, while at the outlet, it is 0.886 m/s. Consequently, the difference in velocity magnitude from the inlet to outlet of the tri serpentine flow channel is 0.689 m/s.

(49). The velocity at the inlet of the 2mm flow channel width of tri serpentine PEMFC at 0.35V is 0.223 m/s, while at the outlet, it is 0.911 m/s. Consequently, the difference in velocity magnitude from the inlet to outlet of the tri serpentine flow channel is 0.688 m/s.

(50). The velocity at the inlet of the 2mm flow channel width of tri serpentine PEMFC at 0.55V is 0.267 m/s, while at the outlet, it is 0.946 m/s. Consequently, the difference in velocity magnitude from the inlet to outlet of the tri serpentine flow channel is 0.679 m/s.

(51). The velocity at the inlet of the 2mm flow channel width of tri serpentine PEMFC at 0.65V is 0.293 m/s, while at the outlet, it is 0.962 m/s. Consequently, the difference in velocity magnitude from the inlet to outlet of the tri serpentine flow channel is 0.669 m/s.

(52). The velocity at the inlet of the 2mm flow channel width of tri serpentine PEMFC at 0.8V is 0.303 m/s, while at the outlet, it is 0.99 m/s. Consequently, the difference in velocity magnitude from the inlet to outlet of the tri serpentine flow channel is 0.687 m/s.

(53). In the 2mm flow channel width of the single serpentine PEMFC at 0.25V, the consumption rate of mass fraction of hydrogen (H_2) at the gas diffusion layer (GDL) is 0.541.

(54). In the 2mm flow channel width of the single serpentine PEMFC at 0.35V, the consumption rate of mass fraction of hydrogen (H₂) at the gas diffusion layer (GDL) is 0.587.

(55). In the 2mm flow channel width of the single serpentine PEMFC at 0.5V, the consumption rate of mass fraction of hydrogen (H₂) at the gas diffusion layer (GDL) is 0.63.

(56). In the 2mm flow channel width of the single serpentine PEMFC at 0.65V, the consumption rate of mass fraction of hydrogen (H₂) at the gas diffusion layer (GDL) is 0.683.

(57). In the 2mm flow channel width of the single serpentine PEMFC at 0.8V, the consumption rate of mass fraction of hydrogen (H₂) at the gas diffusion layer (GDL) is 0.709.

(58). In the 2mm flow channel width of the bi serpentine PEMFC at 0.25V, the consumption rate of mass fraction of hydrogen (H₂) at the gas diffusion layer (GDL) is 0.601.

(59). In the 2mm flow channel width of the bi serpentine PEMFC at 0.35V, the consumption rate of mass fraction of hydrogen (H₂) at the gas diffusion layer (GDL) is 0.625.

(60). In the 2mm flow channel width of the bi serpentine PEMFC at 0.5V, the consumption rate of mass fraction of hydrogen (H₂) at the gas diffusion layer (GDL) is 0.662.

(61). In the 2mm flow channel width of the bi serpentine PEMFC at 0.65V, the consumption rate of mass fraction of hydrogen (H₂) at the gas diffusion layer (GDL) is 0.707.

(62). In the 2mm flow channel width of the bi serpentine PEMFC at 0.8V, the consumption rate of mass fraction of hydrogen (H_2) at the gas diffusion layer (GDL) is 0.734.

(63). In the 2mm flow channel width of the tri serpentine PEMFC at 0.25V, the consumption rate of mass fraction of hydrogen (H_2) at the gas diffusion layer (GDL) is 0.642.

(64). In the 2mm flow channel width of the tri serpentine PEMFC at 0.35V, the consumption rate of mass fraction of hydrogen (H_2) at the gas diffusion layer (GDL) is 0.676.

(65). In the 2mm flow channel width of the tri serpentine PEMFC at 0.55V, the consumption rate of mass fraction of hydrogen (H_2) at the gas diffusion layer (GDL) is 0.719.

(66). In the 2mm flow channel width of the tri serpentine PEMFC at 0.65V, the consumption rate of mass fraction of hydrogen (H_2) at the gas diffusion layer (GDL) is 0.765.

(67). In the 2mm flow channel width of the tri serpentine PEMFC at 0.8V, the consumption rate of mass fraction of hydrogen (H_2) at the gas diffusion layer (GDL) is 0.796.

(68). The Reynolds number of the 2mm flow channel of single serpentine PEMFC at 0.25V at the inlet is measured to be 21.7, while at the outlet, it is 55.

(69). The Reynolds number of the 2mm flow channel of single serpentine PEMFC at 0.35V at the inlet is measured to be 28.8, while at the outlet, it is 60.9.

- (70). The Reynolds number of the 2mm flow channel of single serpentine PEMFC at 0.5V at the inlet is measured to be 31, while at the outlet, it is 64.
- (71). The Reynolds number of the 2mm flow channel of single serpentine PEMFC at 0.65V at the inlet is measured to be 33.7, while at the outlet, it is 66.2.
- (72). The Reynolds number of the 2mm flow channel of single serpentine PEMFC at 0.8V at the inlet is measured to be 35.3, while at the outlet, it is 67.8.
- (73). The Reynolds number of the 2mm flow channel of bi serpentine PEMFC 0.25V at the inlet is measured to be 14.2, while at the outlet, it is 39.4.
- (74). The Reynolds number of the 2mm flow channel of bi serpentine PEMFC 0.35V at the inlet is measured to be 17.3, while at the outlet, it is 43.9.
- (75). The Reynolds number of the 2mm flow channel of bi serpentine PEMFC 0.5V at the inlet is measured to be 22, while at the outlet, it is 49.
- (76). The Reynolds number of the 2mm flow channel of bi serpentine PEMFC 0.65V at the inlet is measured to be 23.7, while at the outlet, it is 50.5.
- (77). The Reynolds number of the 2mm flow channel of bi serpentine PEMFC 0.8V at the inlet is measured to be 26.1, while at the outlet, it is 52.6.
- (78). The Reynolds number of the 2mm flow channel of tri serpentine PEMFC at 0.25V at the inlet is measured to be 10.1, while at the outlet, it is 38.6.
- (79). The Reynolds number of the 2mm flow channel of tri serpentine PEMFC at 0.35V at the inlet is measured to be 11.9, while at the outlet, it is 41.5.
- (80). The Reynolds number of the 2mm flow channel of tri serpentine PEMFC at 0.55V at the inlet is measured to be 13.2, while at the outlet, it is 46.8.

- (81). The Reynolds number of the 2mm flow channel of tri serpentine PEMFC at 0.65V at the inlet is measured to be 15.1, while at the outlet, it is 48.4.
- (82). The Reynolds number of the 2mm flow channel of tri serpentine PEMFC at 0.8V at the inlet is measured to be 16.4, while at the outlet, it is 49.6.
- (83). The 1mm single serpentine flow channel achieved a maximum current density of 0.981 A/cm^2 , resulting in a corresponding power density of 0.539 W/cm^2 at 0.55V.
- (84). The 3mm single serpentine flow channel achieved a maximum current density of 1.284 A/cm^2 , resulting in a corresponding power density of 0.642 W/cm^2 at 0.5V.
- (85). The 1mm bi serpentine flow channel achieved a maximum current density of 1.15 A/cm^2 , resulting in a corresponding power density of 0.575 W/cm^2 at 0.5V.
- (86). The 3mm bi serpentine flow channel achieved a maximum current density of 1.293 A/cm^2 , resulting in a corresponding power density of 0.6464 W/cm^2 at 0.5V.
- (87). The 1mm tri serpentine flow channel achieved a maximum current density of 1.2 A/cm^2 , resulting in a corresponding power density of 0.6 W/cm^2 at 0.5V.
- (88). The 3mm tri serpentine flow channel achieved a maximum current density of 1.3 A/cm^2 , resulting in a corresponding power density of 0.715 W/cm^2 at 0.55V.
- (89). The initial pressure at the inlet of 1mm width of the single serpentine flow channel at 0.25 V is 200 KPa, and at the outlet, it is 117 KPa. Therefore, the pressure drops across the 1mm width of single serpentine flow channel is 83 KPa.

(90). The initial pressure at the inlet of 1mm width of the single serpentine flow channel at 0.35 V is 200KPa, and at the outlet, it is 127 KPa. Therefore, the pressure drops across the 1mm width of single serpentine flow channel is 73 KPa.

(91). The initial pressure at the inlet of 1mm width of the single serpentine flow channel at 0.5 V is 200 KPa, and at the outlet, it is 138 KPa. Therefore, the pressure drops across the 1mm width of single serpentine flow channel is 62 KPa.

(92). The initial pressure at the inlet of 1mm width of the single serpentine flow channel at 0.65 V is 200 KPa, and at the outlet, it is 144 KPa. Therefore, the pressure drops across the 1mm width of single serpentine flow channel is 56 KPa.

(93). The initial pressure at the inlet of 1mm width of the single serpentine flow channel at 0.8 V is 200 KPa, and at the outlet, it is 153 KPa. Therefore, the pressure drops across the 1mm width of single serpentine flow channel is 47 KPa.

(94) The initial pressure at the inlet of 3mm width of the single serpentine flow channel at 0.25 V is 200 KPa, and at the outlet, it is 125 KPa. Therefore, the pressure drops across the 3mm width of single serpentine flow channel is 75 KPa.

(95). The initial pressure at the inlet of 3mm width of the single serpentine flow channel at 0.35 V is 200 KPa, and at the outlet, it is 134 KPa. Therefore, the pressure drops across the 3mm width of single serpentine flow channel is 66 KPa.

(96). The initial pressure at the inlet of 3mm width of the single serpentine flow channel at 0.5 V is 200 KPa, and at the outlet, it is 146 KPa. Therefore, the pressure drops across the 3mm width of single serpentine flow channel is 54 KPa.

(97). The initial pressure at the inlet of 3mm width of the single serpentine flow channel at 0.65 V is 200 KPa, and at the outlet, it is 159 KPa. Therefore, the pressure drops across the 3mm width of single serpentine flow channel is 41 KPa.

(98). The initial pressure at the inlet of 3mm width of the single serpentine flow channel at 0.8 V is 200 KPa, and at the outlet, it is 163 KPa. Therefore, the pressure drops across the 3mm width of single serpentine flow channel is 37 KPa.

(99). The initial pressure at the inlet of 1mm width of the bi serpentine flow channel at 0.25 V is 200 KPa, and at the outlet, it is 133 KPa. Therefore, the pressure drops across the 1mm width of bi serpentine flow channel is 67 KPa.

(100). The initial pressure at the inlet of 1mm width of the bi serpentine flow channel at 0.35 V is 200 KPa, and at the outlet, it is 140 KPa. Therefore, the pressure drops across the 1mm width of bi serpentine flow channel is 60 KPa.

(101). The initial pressure at the inlet of 1mm width of the bi serpentine flow channel at 0.5 V is 200 KPa, and at the outlet, it is 149 KPa. Therefore, the pressure drops across the 1mm width of bi serpentine flow channel is 51 KPa.

(102). The initial pressure at the inlet of 1mm width of the bi serpentine flow channel at 0.65 V is 200 KPa, and at the outlet, it is 156 KPa. Therefore, the pressure drops across the 1mm width of bi serpentine flow channel is 44 KPa.

(103). The initial pressure at the inlet of 1mm width of the bi serpentine flow channel at 0.8 V is 200 KPa, and at the outlet, it is 160 KPa. Therefore, the pressure drops across the 1mm width of bi serpentine flow channel is 40 KPa.

(104) The initial pressure at the inlet of 3mm width of the bi serpentine flow channel at 0.25 V is 200 KPa, and at the outlet, it is 142 KPa. Therefore, the pressure drops across the 3mm width of bi serpentine flow channel is 58 KPa.

(105). The initial pressure at the inlet of 3mm width of the bi serpentine flow channel at 0.35 V is 200 KPa, and at the outlet, it is 151 KPa. Therefore, the pressure drops across the 3mm width of bi serpentine flow channel is 49 KPa.

(106). The initial pressure at the inlet of 3mm width of the bi serpentine flow channel at 0.5 V is 200 KPa, and at the outlet, it is 155 KPa. Therefore, the pressure drops across the 3mm width of bi serpentine flow channel is 45 KPa.

(105). The initial pressure at the inlet of 3mm width of the bi serpentine flow channel at 0.65 V is 200 KPa, and at the outlet, it is 165 KPa. Therefore, the pressure drops across the 3mm width of bi serpentine flow channel is 35 KPa.

(105). The initial pressure at the inlet of 3mm width of the bi serpentine flow channel at 0.8 V is 200 KPa, and at the outlet, it is 170 KPa. Therefore, the pressure drops across the 3mm width of bi serpentine flow channel is 30 KPa.

(106). The initial pressure at the inlet of 1mm width of the tri serpentine flow channel at 0.25 V is 200 KPa, and at the outlet, it is 148 KPa. Therefore, the pressure drops across the 1mm width of tri serpentine flow channel is 52 KPa.

(107). The initial pressure at the inlet of 1mm width of the tri serpentine flow channel at 0.35 V is 200 KPa, and at the outlet, it is 153 KPa. Therefore, the pressure drops across the 1mm width of tri serpentine flow channel is 47 KPa.

(108). The initial pressure at the inlet of 1mm width of the tri serpentine flow channel at 0.5 V is 200 KPa, and at the outlet, it is 161 KPa. Therefore, the pressure drops across the 1mm width of tri serpentine flow channel is 39 KPa.

(109). The initial pressure at the inlet of 1mm width of the tri serpentine flow channel at 0.65 V is 200 KPa, and at the outlet, it is 162 KPa. Therefore, the pressure drops across the 1mm width of tri serpentine flow channel is 38 KPa.

(110). The initial pressure at the inlet of 1mm width of the tri serpentine flow channel at 0.8 V is 200 KPa, and at the outlet, it is 167 KPa. Therefore, the pressure drops across the 1mm width of tri serpentine flow channel is 33 KPa.

(111) The initial pressure at the inlet of 3mm width of the tri serpentine flow channel at 0.25 V is 200 KPa, and at the outlet, it is 151 KPa. Therefore, the pressure drops across the 3mm width of tri serpentine flow channel is 49 KPa.

(112). The initial pressure at the inlet of 3mm width of the tri serpentine flow channel at 0.35 V is 200 KPa, and at the outlet, it is 160 KPa. Therefore, the pressure drops across the 3mm width of tri serpentine flow channel is 40 KPa.

(113). The initial pressure at the inlet of 3mm width of the tri serpentine flow channel at 0.5 V is 200 KPa, and at the outlet, it is 167 KPa. Therefore, the pressure drops across the 3mm width of tri serpentine flow channel is 33 KPa.

(114). The initial pressure at the inlet of 3mm width of the tri serpentine flow channel at 0.65 V is 200 KPa, and at the outlet, it is 174 KPa. Therefore, the pressure drops across the 3mm width of tri serpentine flow channel is 26 KPa.

(115). The initial pressure at the inlet of 3mm width of the tri serpentine flow channel at 0.8 V is 200 KPa, and at the outlet, it is 178 KPa. Therefore, the pressure drops across the 3mm width of tri serpentine flow channel is 22 KPa.

(116). The velocity at the inlet of 1mm flow channel width of the single serpentine PEMFC at 0.25V is 0.477 m/s, while at the outlet, it is 1.10 m/s. Consequently, the difference in velocity magnitude from the inlet to outlet of the single serpentine flow channel is 0.63 m/s.

(117). The velocity at the inlet of 1mm flow channel width of the single serpentine PEMFC at 0.35V is 0.493 m/s, while at the outlet, it is 1.18 m/s. Consequently, the difference in velocity magnitude from the inlet to outlet of the single serpentine flow channel is 0.691 m/s.

(118). The velocity at the inlet of 1mm flow channel width of the single serpentine PEMFC at 0.5V is 0.503 m/s, while at the outlet, it is 1.24 m/s. Consequently, the difference in velocity magnitude from the inlet to outlet of the single serpentine flow channel is 0.741 m/s.

(119). The velocity at the inlet of 1mm flow channel width of the single serpentine PEMFC at 0.65V is 0.519 m/s, while at the outlet, it is 1.13 m/s. Consequently, the difference in velocity magnitude from the inlet to outlet of the single serpentine flow channel is 0.811 m/s.

(120). The velocity at the inlet of 1mm flow channel width of the single serpentine PEMFC at 0.8V is 0.53 m/s, while at the outlet, it is 1.43 m/s. Consequently, the difference in velocity magnitude from the inlet to outlet of the single serpentine flow channel is 0.9 m/s.

(121). The velocity at the inlet of 3mm flow channel width of the single serpentine PEMFC at 0.25V is 0.505 m/s, while at the outlet, it is 1.27 m/s. Consequently, the difference in velocity magnitude from the inlet to outlet of the single serpentine flow channel is 0.765 m/s.

(122). The velocity at the inlet of 3mm flow channel width of the single serpentine PEMFC at 0.35V is 0.519 m/s, while at the outlet, it is 1.34 m/s. Consequently, the difference in velocity magnitude from the inlet to outlet of the single serpentine flow channel is 0.821 m/s.

(123). The velocity at the inlet of 3mm flow channel width of the single serpentine PEMFC at 0.5V is 0.526 m/s, while at the outlet, it is 1.4 m/s. Consequently, the difference in velocity magnitude from the inlet to outlet of the single serpentine flow channel is 0.874 m/s.

(124). The velocity at the inlet of 3mm flow channel width of the single serpentine PEMFC at 0.65V is 0.516 m/s, while at the outlet, it is 1.48 m/s. Consequently, the difference in velocity magnitude from the inlet to outlet of the single serpentine flow channel is 0.919 m/s.

(125). The velocity at the inlet of 3mm flow channel width of the single serpentine PEMFC at 0.8V is 0.5 m/s, while at the outlet, it is 1.59 m/s. Consequently, the difference in velocity magnitude from the inlet to outlet of the single serpentine flow channel is 1.09 m/s.

(126). The velocity at the inlet of 1mm flow channel width of the bi serpentine PEMFC at 0.25V is 0.283 m/s, while at the outlet, it is 0.957 m/s. Consequently, the difference in velocity magnitude from the inlet to outlet of the bi serpentine flow channel is 0.674 m/s.

(127). The velocity at the inlet of 1mm flow channel width of the bi serpentine PEMFC at 0.35V is 0.311 m/s, while at the outlet, it is 0.974 m/s. Consequently, the difference in velocity magnitude from the inlet to outlet of the bi serpentine flow channel is 0.667 m/s.

(128). The velocity at the inlet of 1mm flow channel width of the bi serpentine PEMFC at 0.5V is 0.369 m/s, while at the outlet, it is 0.985 m/s. Consequently, the difference in velocity magnitude from the inlet to outlet of the bi serpentine flow channel is 0.616 m/s.

(129). The velocity at the inlet of 1mm flow channel width of the bi serpentine PEMFC at 0.65V is 0.38 m/s, while at the outlet, it is 0.997 m/s. Consequently, the difference in velocity magnitude from the inlet to outlet of the bi serpentine flow channel is 0.617 m/s.

(130). The velocity at the inlet of 1mm flow channel width of the bi serpentine PEMFC at 0.8V is 0.4 m/s, while at the outlet, it is 1.12 m/s. Consequently, the difference in velocity magnitude from the inlet to outlet of the bi serpentine flow channel is 0.72 m/s.

(131). The velocity at the inlet of 3mm flow channel width of the bi serpentine PEMFC at 0.25V is 0.341 m/s, while at the outlet, it is 1.03 m/s. Consequently, the difference in velocity magnitude from the inlet to outlet of the bi serpentine flow channel is 0.689 m/s.

(132). The velocity at the inlet of 3mm flow channel width of the bi serpentine PEMFC at 0.35V is 0.322 m/s, while at the outlet, it is 1.07 m/s. Consequently, the difference in velocity magnitude from the inlet to outlet of the bi serpentine flow channel is 0.748 m/s.

(133). The velocity at the inlet of 3mm flow channel width of the bi serpentine PEMFC at 0.5V is 0.399 m/s, while at the outlet, it is 1.11 m/s. Consequently, the difference in velocity magnitude from the inlet to outlet of the bi serpentine flow channel is 0.711 m/s.

(134). The velocity at the inlet of 3mm flow channel width of the bi serpentine PEMFC at 0.65V is 0.407 m/s, while at the outlet, it is 1.18 m/s. Consequently, the difference in velocity magnitude from the inlet to outlet of the bi serpentine flow channel is 0.773 m/s.

(135). The velocity at the inlet of 3mm flow channel width of the bi serpentine PEMFC at 0.8V is 0.419 m/s, while at the outlet, it is 1.25 m/s. Consequently, the difference in velocity magnitude from the inlet to outlet of the bi serpentine flow channel is 0.831 m/s.

(136). The velocity at the inlet of 1mm flow channel width of the tri serpentine PEMFC at 0.25V is 0.191 m/s, while at the outlet, it is 0.861 m/s. Consequently, the difference in velocity magnitude from the inlet to outlet of the tri serpentine flow channel is 0.67 m/s.

(137). The velocity at the inlet of 1mm flow channel width of the tri serpentine PEMFC at 0.35V is 0.216 m/s, while at the outlet, it is 0.882 m/s. Consequently, the difference in velocity magnitude from the inlet to outlet of the tri serpentine flow channel is 0.666 m/s.

(138). The velocity at the inlet of 1mm flow channel width of the tri serpentine PEMFC at 0.5V is 0.26 m/s, while at the outlet, it is 0.921 m/s. Consequently, the difference in velocity magnitude from the inlet to outlet of the tri serpentine flow channel is 0.661 m/s.

(139). The velocity at the inlet of 1mm flow channel width of the tri serpentine PEMFC at 0.65V is 0.282 m/s, while at the outlet, it is 0.937 m/s. Consequently, the difference in velocity magnitude from the inlet to outlet of the tri serpentine flow channel is 0.655 m/s.

(140). The velocity at the inlet of 1mm flow channel width of the tri serpentine PEMFC at 0.8V is 0.296 m/s, while at the outlet, it is 0.945 m/s. Consequently, the difference in velocity magnitude from the inlet to outlet of the tri serpentine flow channel is 0.649 m/s.

(141). The velocity at the inlet of 3mm flow channel width of the tri serpentine PEMFC at 0.25V is 0.231 m/s, while at the outlet, it is 0.917 m/s. Consequently, the difference in velocity magnitude from the inlet to outlet of the tri serpentine flow channel is 0.686 m/s.

(142). The velocity at the inlet of 3mm flow channel width of the tri serpentine PEMFC at 0.35V is 0.244 m/s, while at the outlet, it is 0.924 m/s. Consequently, the difference in velocity magnitude from the inlet to outlet of the tri serpentine flow channel is 0.68 m/s.

(143). The velocity at the inlet of 3mm flow channel width of the tri serpentine PEMFC at 0.5V is 0.271 m/s, while at the outlet, it is 0.948 m/s. Consequently, the difference in velocity magnitude from the inlet to outlet of the tri serpentine flow channel is 0.677 m/s.

(144). The velocity at the inlet of 3mm flow channel width of the tri serpentine PEMFC at 0.65V is 0.306 m/s, while at the outlet, it is 0.958 m/s. Consequently, the difference in velocity magnitude from the inlet to outlet of the tri serpentine flow channel is 0.652 m/s.

(145). The velocity at the inlet of 3mm flow channel width of the tri serpentine PEMFC at 0.8V is 0.315 m/s, while at the outlet, it is 0.974 m/s. Consequently, the difference in velocity magnitude from the inlet to outlet of the tri serpentine flow channel is 0.659 m/s.

(146). In the 1mm flow channel width of single serpentine PEMFC at 0.25 V, the consumption rate of mass fraction of hydrogen (H_2) at the gas diffusion layer (GDL) is 0.536.

(147). In the 1mm flow channel width of single serpentine PEMFC at 0.35 V, the consumption rate of mass fraction of hydrogen (H_2) at the gas diffusion layer (GDL) is 0.574.

(148). In the 1mm flow channel width of single serpentine PEMFC at 0.5 V, the consumption rate of mass fraction of hydrogen (H_2) at the gas diffusion layer (GDL) is 0.622.

(149). In the 1mm flow channel width of single serpentine PEMFC at 0.65 V, the consumption rate of mass fraction of hydrogen (H_2) at the gas diffusion layer (GDL) is 0.669.

(150). In the 1mm flow channel width of single serpentine PEMFC at 0.8 V, the consumption rate of mass fraction of hydrogen (H_2) at the gas diffusion layer (GDL) is 0.682.

(151). In the 3mm flow channel width of single serpentine PEMFC at 0.25 V, the consumption rate of mass fraction of hydrogen (H_2) at the gas diffusion layer (GDL) is 0.555.

(152). In the 3mm flow channel width of single serpentine PEMFC at 0.35 V, the consumption rate of mass fraction of hydrogen (H_2) at the gas diffusion layer (GDL) is 0.599.

(153). In the 3mm flow channel width of single serpentine PEMFC at 0.5 V, the consumption rate of mass fraction of hydrogen (H_2) at the gas diffusion layer (GDL) is 0.639.

(154). In the 3mm flow channel width of single serpentine PEMFC at 0.65 V, the consumption rate of mass fraction of hydrogen (H_2) at the gas diffusion layer (GDL) is 0.691.

(155). In the 3mm flow channel width of single serpentine PEMFC at 0.8 V, the consumption rate of mass fraction of hydrogen (H_2) at the gas diffusion layer (GDL) is 0.712.

(156). In the 1mm flow channel width of bi serpentine PEMFC at 0.25 V, the consumption rate of mass fraction of hydrogen (H_2) at the gas diffusion layer (GDL) is 0.583.

(157). In the 1mm flow channel width of bi serpentine PEMFC at 0.35 V, the consumption rate of mass fraction of hydrogen (H_2) at the gas diffusion layer (GDL) is 0.616.

(158). In the 1mm flow channel width of bi serpentine PEMFC at 0.5 V, the consumption rate of mass fraction of hydrogen (H_2) at the gas diffusion layer (GDL) is 0.649.

(159). In the 1mm flow channel width of bi serpentine PEMFC at 0.65 V, the consumption rate of mass fraction of hydrogen (H_2) at the gas diffusion layer (GDL) is 0.665.

(160). In the 1mm flow channel width of bi serpentine PEMFC at 0.8 V, the consumption rate of mass fraction of hydrogen (H_2) at the gas diffusion layer (GDL) is 0.679.

(161). In the 3mm flow channel width of bi serpentine PEMFC at 0.25 V, the consumption rate of mass fraction of hydrogen (H_2) at the gas diffusion layer (GDL) is 0.611.

(162). In the 3mm flow channel width of bi serpentine PEMFC at 0.35 V, the consumption rate of mass fraction of hydrogen (H₂) at the gas diffusion layer (GDL) is 0.632.

(163). In the 3mm flow channel width of bi serpentine PEMFC at 0.5 V, the consumption rate of mass fraction of hydrogen (H₂) at the gas diffusion layer (GDL) is 0.671.

(164). In the 3mm flow channel width of bi serpentine PEMFC at 0.65 V, the consumption rate of mass fraction of hydrogen (H₂) at the gas diffusion layer (GDL) is 0.693.

(165). In the 3mm flow channel width of bi serpentine PEMFC at 0.8 V, the consumption rate of mass fraction of hydrogen (H₂) at the gas diffusion layer (GDL) is 0.708.

(166). In the 1mm flow channel width of tri serpentine PEMFC at 0.25 V, the consumption rate of mass fraction of hydrogen (H₂) at the gas diffusion layer (GDL) is 0.633.

(167). In the 1mm flow channel width of tri serpentine PEMFC at 0.35 V, the consumption rate of mass fraction of hydrogen (H₂) at the gas diffusion layer (GDL) is 0.67.

(168). In the 1mm flow channel width of tri serpentine PEMFC at 0.5 V, the consumption rate of mass fraction of hydrogen (H₂) at the gas diffusion layer (GDL) is 0.696.

(169). In the 1mm flow channel width of tri serpentine PEMFC at 0.65 V, the consumption rate of mass fraction of hydrogen (H₂) at the gas diffusion layer (GDL) is 0.701.

(170). In the 1mm flow channel width of tri serpentine PEMFC at 0.8 V, the consumption rate of mass fraction of hydrogen (H_2) at the gas diffusion layer (GDL) is 0.710.

(171). In the 3mm flow channel width of tri serpentine PEMFC at 0.25 V, the consumption rate of mass fraction of hydrogen (H_2) at the gas diffusion layer (GDL) is 0.661.

(172). In the 3mm flow channel width of tri serpentine PEMFC at 0.35 V, the consumption rate of mass fraction of hydrogen (H_2) at the gas diffusion layer (GDL) is 0.693.

(173). In the 3mm flow channel width of tri serpentine PEMFC at 0.5 V, the consumption rate of mass fraction of hydrogen (H_2) at the gas diffusion layer (GDL) is 0.727.

(174). In the 3mm flow channel width of tri serpentine PEMFC at 0.65 V, the consumption rate of mass fraction of hydrogen (H_2) at the gas diffusion layer (GDL) is 0.73.

(175). In the 3mm flow channel width of tri serpentine PEMFC at 0.8 V, the consumption rate of mass fraction of hydrogen (H_2) at the gas diffusion layer (GDL) is 0.735.

(176). The Reynolds number of 1mm flow channel width of the single serpentine PEMFC at 0.25V at the inlet is measured to be 20.9, while at the outlet, it is 54.1.

(177). The Reynolds number of 1mm flow channel width of the single serpentine PEMFC at 0.35V at the inlet is measured to be 28.1, while at the outlet, it is 59.4.

(178). The Reynolds number of 1mm flow channel width of the single serpentine PEMFC at 0.5V at the inlet is measured to be 30.3, while at the outlet, it is 63.1.

(179). The Reynolds number of 1mm flow channel width of the single serpentine PEMFC at 0.65V at the inlet is measured to be 34.5, while at the outlet, it is 67.3.

(180). The Reynolds number of 1mm flow channel width of the single serpentine PEMFC at 0.8V at the inlet is measured to be 38.9, while at the outlet, it is 70.4.

(181). The Reynolds number of 3mm flow channel width of the single serpentine PEMFC at 0.25V at the inlet is measured to be 23.9, while at the outlet, it is 58.1.

(182). The Reynolds number of 3mm flow channel width of the single serpentine PEMFC at 0.35V at the inlet is measured to be 29.6, while at the outlet, it is 63.

(183). The Reynolds number of 3mm flow channel width of the single serpentine PEMFC at 0.5V at the inlet is measured to be 31.7, while at the outlet, it is 65.5.

(184). The Reynolds number of 3mm flow channel width of the single serpentine PEMFC at 0.65V at the inlet is measured to be 42.6, while at the outlet, it is 77.3.

(185). The Reynolds number of 3mm flow channel width of the single serpentine PEMFC at 0.8V at the inlet is measured to be 47, while at the outlet, it is 85.6.

(186). The Reynolds number of 1mm flow channel width of the bi serpentine PEMFC at 0.25V at the inlet is measured to be 13.7, while at the outlet, it is 38.5.

(187). The Reynolds number of 1mm flow channel width of the bi serpentine PEMFC at 0.35V at the inlet is measured to be 16.6, while at the outlet, it is 43.3.

(188). The Reynolds number of 1mm flow channel width of the bi serpentine PEMFC at 0.5V at the inlet is measured to be 21.2, while at the outlet, it is 48.3.

(189). The Reynolds number of 1mm flow channel width of the bi serpentine PEMFC at 0.65V at the inlet is measured to be 24.3, while at the outlet, it is 52.3.

(190). The Reynolds number of 1mm flow channel width of the bi serpentine PEMFC at 0.8V at the inlet is measured to be 26.2, while at the outlet, it is 53.4.

(191). The Reynolds number of 3mm flow channel width of the bi serpentine PEMFC at 0.25V at the inlet is measured to be 14.9, while at the outlet, it is 40.5.

(192). The Reynolds number of 3mm flow channel width of the bi serpentine PEMFC at 0.35V at the inlet is measured to be 18.1, while at the outlet, it is 45.1.

(193). The Reynolds number of 3mm flow channel width of the bi serpentine PEMFC at 0.5V at the inlet is measured to be 23.1, while at the outlet, it is 51.7.

(194). The Reynolds number of 3mm flow channel width of the bi serpentine PEMFC at 0.65V at the inlet is measured to be 28.4, while at the outlet, it is 55.7.

(195). The Reynolds number of 3mm flow channel width of the bi serpentine PEMFC at 0.8V at the inlet is measured to be 31.2, while at the outlet, it is 60.6.

(196). The Reynolds number of 1mm flow channel width of the tri serpentine PEMFC at 0.25V at the inlet is measured to be 9.7, while at the outlet, it is 37.8.

(197). The Reynolds number of 1mm flow channel width of the tri serpentine PEMFC at 0.35V at the inlet is measured to be 11.7, while at the outlet, it is 41.1.

(198). The Reynolds number of 1mm flow channel width of the tri serpentine PEMFC at 0.5V at the inlet is measured to be 12.9, while at the outlet, it is 43.9.

(199). The Reynolds number of 1mm flow channel width of the tri serpentine PEMFC at 0.65V at the inlet is measured to be 13.7, while at the outlet, it is 45.2.

(200). The Reynolds number of 1mm flow channel width of the tri serpentine PEMFC at 0.8V at the inlet is measured to be 14.5, while at the outlet, it is 47.7.

(201). The Reynolds number of 3mm width of the tri serpentine PEMFC at 0.25V at the inlet is measured to be 10.8, while at the outlet, it is 40.1.

(202). The Reynolds number of 3mm flow channel width of the tri serpentine PEMFC at 0.35V at the inlet is measured to be 12.5, while at the outlet, it is 42.7.

(203). The Reynolds number of 3mm flow channel width of the tri serpentine PEMFC at 0.5V at the inlet is measured to be 13.9, while at the outlet, it is 48.5.

(204). The Reynolds number of 3mm flow channel width of the tri serpentine PEMFC at 0.65V at the inlet is measured to be 15.3, while at the outlet, it is 51.1.

(205). The Reynolds number of 3mm flow channel width of the tri serpentine PEMFC at 0.8V at the inlet is measured to be 17.9, while at the outlet, it is 54.5.

(206). In the analysis of PEMFC, the pressure drop decreases as the channel width increases.

(207). The 3mm channel width has the lowest pressure drop among the three widths tested.

(208). The 1mm channel width has the highest pressure drop among the three widths tested.

(209). The 2mm channel width falls between the other two in terms of pressure drop, showing a gradual decrease from 1mm to 3mm.

(210). The velocity magnitude difference increases with increasing channel width, with the 3mm channel showing the highest difference and 1mm channel showing the lowest difference.

(211). The trend suggests that wider channels experience larger variations in velocity magnitude within the channel compared to narrower channels.

(212). There is a noticeable difference in velocity magnitude between all three channels, with a clear trend of increasing magnitude from 1mm to 3mm channels.

(213). The 2mm flow channel falls between the 1mm and 3mm channels, showing a gradual increase in velocity magnitude difference from narrow to wide channels.

(214). The hydrogen mass fraction consumption rates increase with channel width, with the 3mm channel showing the highest consumption rate, 1mm channel showing the lowest consumption rate whereas the 2mm channel width falls between the other two channels showing a gradual increase.

(215). Wider channels exhibit higher Reynolds number at both inlet and outlet points. There is a gradual increase in the inlet and outlet from 1mm channel to 3mm channel.

CHAPTER 11

FUTURE RESEARCH SCOPE

Building upon the findings and analysis presented in the thesis, there are several promising directions for future research that warrant exploration. These potential avenues for further investigation stem from the gaps identified in the existing literature, the limitations of the current study, and the implications of the research findings. By delving into these areas, researchers can deepen our understanding of the phenomenon under study and contribute to the advancement of knowledge in the field.

1. **Investigation of alternative flow field configurations:** Exploring additional flow field designs beyond the three studied in the thesis to further optimize performance and efficiency.
2. **Evaluation of novel materials:** Investigating the use of novel materials for the components of PEMFCs, such as catalyst layers and gas diffusion layers, to enhance durability and efficiency.
3. **Analysis of different operating conditions:** Extending the study to examine the performance of PEMFCs under various operating conditions such as temperature, pressures, and flow rates.
4. **Optimization of flow channel geometry:** Further optimize the geometry of flow channels to improve reactant distribution, minimize pressure drop, and enhance overall performance.
5. **Study of transient behavior:** Investigating the transient behavior of PEMFCs under dynamic operating conditions to better understand their response to changes in load and external factors.
6. **Development of advanced diagnostic techniques:** Developing and applying advanced diagnostic techniques for in-depth analysis of

PEMFC performance, such as tomographic imaging and electrochemical impedance spectroscopy.

7. **Assessment of system level performance:** Conducting comprehensive system level performance evaluations of PEMFCs in real world applications to validate laboratory findings and assess their practical feasibility.
8. **Designs inspired from nature:** Nature inspired designs can be incorporated in the design of flow channels to observe the diffusion process.

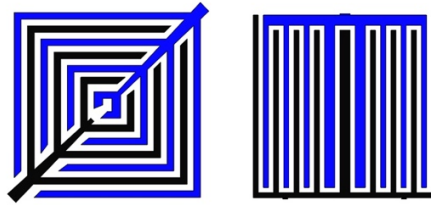


Figure 11.1 Naturally inspired design [87]

9. The angle of flow channel can be varied to see the effects occur in the performance of PEMFC.

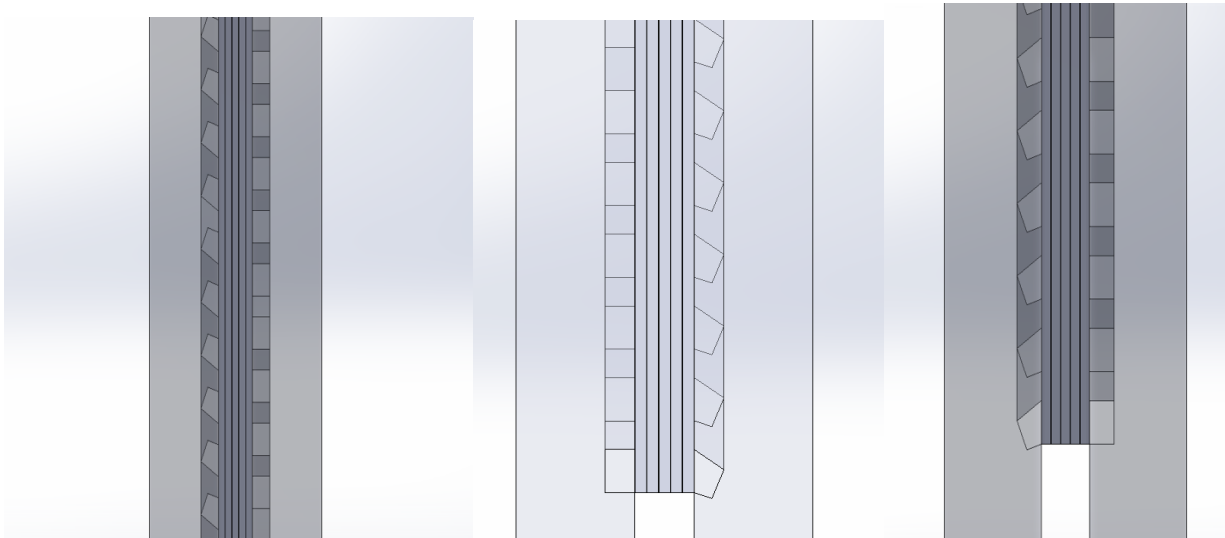


Figure 11.2 - Different fuel cell's flow channel angles

10. The flow channel type can be modified to see how the design affects the performance of the PEMFC.

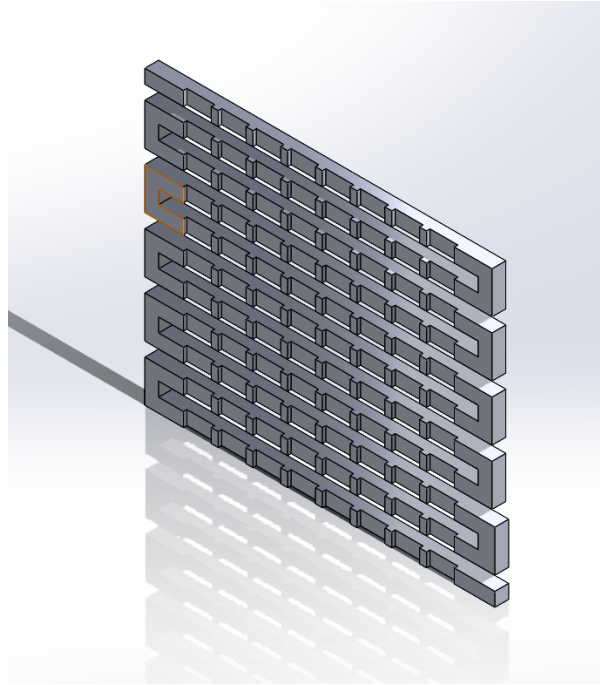


Figure 11.3 – Pinned configuration of single serpentine flow channel

BIBLIOGRAPHY

- [1] United Nations Article on Sustainability - <https://www.un.org/en/academic-impact/sustainability> - Accessed 27 Dec 2023
- [2] A. Kahan, "EIA projects nearly 50% increase in world energy usage by 2050, led by growth in Asia - Today in Energy - U.S. Energy Information Administration (EIA)," 2019. [Online]. Available: <https://www.eia.gov/todayinenergy/detail.php?id=41433>. Accessed 27 Dec 2023
- [3] Rob Stumpf, "How Many Cars are There in the World in 2023 | The Drive," <https://www.thedrive.com/guides-and-gear/how-many-cars-are-there-in-the-world>. Accessed 27 Dec 2023
- [4] Wang, Y. et al. (2020) 'Fundamentals, materials, and machine learning of polymer electrolyte membrane fuel cell technology', Energy and AI. Elsevier Ltd, 1, p. 100014.
- [5] Wolf Vielstich., 1970, Fuel Cells: Modern Processes for Electrochemical Production of Energy, Wiley.
- [6] Xianguo Li., 2003, Principles of Fuel Cells, Taylor & Francis
- [7] Gregor Hoogers., 2003, Fuel Cell Technology Handbook, CRC Press

- [8] Sheila, Samsatli. “Model-based design and operation of fuel cell systems”. (2012) <https://api.semanticscholar.org/CorpusID:64974828>
- [9] James Larminie., Andrew Dicks., 2003, Fuel Cell Systems Explained, Wiley
- [10] A.Bharti, R.Natarajan, “Proton Exchange Membrane Testing and Diagnostics” Pages 137-171, ISBN 9780128237083, <https://doi.org/10.1016/B978-0-12-823708-3.00007-9>.
- [11] Damien Chanal, Nadia Yousfi Steiner, Raffaele Petrone, Didier Chamagne, Marie-Cécile Péra, “Online Diagnosis of PEM Fuel Cell by Fuzzy C-Means Clustering”. Pages 359-393, ISBN 9780128197301, <https://doi.org/10.1016/B978-0-12-819723-3.00099-8>.
- [12] Baroutaji, Ahmad & Carton, James & Sajjia, Mustafa & Olabi, Abdul Ghani. (2015). Materials in PEM Fuel Cells. 10.1016/B978-0-12-803581-8.04006-6.
- [13] Kone J-P, Zhang X, Yan Y, Hu G, Ahmadi G. Three-dimensional multiphase flow computational fluid dynamics models for proton exchange membrane fuel cell: A theoretical development. *The journal of Computational Multiphase Flows*. 2017;9(1):3-25. <https://doi.org/10.1177/1757482X17692341>

- [14] B.-T. Tsai, C.-J. Tseng, Z.-S. Liu, C.-H. Wang, C.-I. Lee, C.-C. Yang, and S.-K. Lo, "Effects of flow field design on the performance of a PEM fuel cell with metal foam as the flow distributor," *Int. J. Hydrogen Energy*, vol. 37, no. 17, pp. 13060–13066, Sep. 2012.
- [15] A. Kumar and R. . Reddy, "Modeling of polymer electrolyte membrane fuel cell with metal foam in the flow-field of the bipolar/end plates," *J. Power Sources*, vol. 114, no. 1, pp. 54–62, Feb. 2003.
- [16] A. Kumar and R. G. Reddy, "Materials and design development for bipolar/end plates in fuel cells," *J. Power Sources*, vol. 129, no. 1, pp. 62–67, Apr. 2004.
- [17] J. G. Carton and A. G. Olabi, "Representative model and flow characteristics of open pore cellular foam and potential use in proton exchange membrane fuel cells," *Int. J. Hydrogen Energy*, vol. 40, no. 16, pp. 5726–5738, May 2015.
- [18] A. Baroutaji, J. Carton, J. Stokes, and A.-G. Olabi, "Design and development of proton exchange membrane fuel cell using open pore cellular foam as flow plate material," *Journal of Energy Challenges and Mechanics*. North Sea Conference & Journal LTD, 06-Sep-2014.

- [19] H. Wang, “Stainless steel as bipolar plate material for polymer electrolyte membrane fuel cells,” *J. Power Sources*, vol. 115, no. 2, pp. 243–251, Apr. 2003.
- [20] H. Wang and J. A. Turner, “Ferritic stainless steels as bipolar plate material for polymer electrolyte membrane fuel cells,” *J. Power Sources*, vol. 128, no. 2, pp. 193–200, Apr. 2004.
- [21] M. C. Li, C. L. Zeng, S. Z. Luo, J. N. Shen, H. C. Lin, and C. N. Cao, “Electrochemical corrosion characteristics of type 316 stainless steel in simulated anode environment for PEMFC,” *Electrochim. Acta*, vol. 48, no. 12, pp. 1735–1741, May 2003.
- [22] Y. Wang and D. O. Northwood, “Effects of O₂ and H₂ on the corrosion of SS316L metallic bipolar plate materials in simulated anode and cathode environments of PEM fuel cells,” *Electrochim. Acta*, vol. 52, no. 24, pp. 6793–6798, Aug. 2007.
- [23] D. P. Davies, P. L. Adcock, M. Turpin, and S. J. Rowen, “Bipolar plate materials for solid polymer fuel cells,” *J. Appl. Electrochem.*, vol. 30, no. 1, pp. 101–105, 2000.
- [24] A. Hermann, T. Chaudhuri, and P. Spagnol, “Bipolar plates for PEM fuel cells: A review,” *Int. J. Hydrogen Energy*, vol. 30, no. 12, pp. 1297–1302, Sep 2005

- [25] J.T. Gostick, M.A. Ioannidis, M.W. Fowler, M.D. Pritzker, Pore network modeling of fibrous gas diffusion layers for polymer electrolyte membrane fuel cells, *J. Power Sources*. 173 (2007) 277–290. doi:10.1016/j.jpowsour.2007.04.059.
- [26] J. Park, H. Oh, T. Ha, Y. Il, K. Min, A review of the gas diffusion layer in proton exchange membrane fuel cells: Durability and degradation, *Appl. Energy*. 155 (2015) 866–880. doi:10.1016/j.apenergy.2015.06.068.
- [27]. T. R. Ralph, “Low Cost Electrodes for Proton Exchange Membrane Fuel Cells,” *J. Electrochem. Soc.*, vol. 144, no. 11, p. 3845, Nov. 1997.
- [28] Y. Wang, K. S. Chen, J. Mishler, S. C. Cho, and X. C. Adroher, “A review of polymer electrolyte membrane fuel cells: Technology, applications, and needs on fundamental research,” *Appl. Energy*, vol. 88, no. 4, pp. 981–1007, Apr. 2011.
- [29] F.Y. Zhang, S. G. Advani, and A. K. Prasad, “Performance of a metallic gas diffusion layer for PEM fuel cells,” *J. Power Sources*, vol. 176, no. 1, pp. 293–298, Jan. 2008.
- [30] J. BENZIGER, J. NEHLSSEN, D. BLACKWELL, T. BRENNAN, and J. ITESCU, “Water flow in the gas diffusion layer of PEM fuel cells,” *J. Memb. Sci.*, vol. 261, no.1–2, pp. 98–106, Sep. 2005.

- [31] H. A. Gasteiger, N. Markovic, P. N. Ross, and E. J. Cairns, “Methanol electrooxidation on well-characterized platinum-ruthenium bulk alloys,” *J. Phys. Chem.*, vol. 97, no.46, pp. 12020–12029, Nov. 1993.
- [32] J. W. Long, R. M. Stroud, K. E. Swider-Lyons, and D. R. Rolison, “How To Make Electrocatalysts More Active for Direct Methanol Oxidation Avoid Pt-Ru Bimetallic Alloys,” *J. Phys. Chem. B*, vol. 104, no. 42, pp. 9772–9776, Oct. 2000.
- [33] S. M. Haile, “Fuel cell materials and components,” *Acta Mater.*, vol. 51, no. 19, pp.5981–6000, Nov. 2003.
- [34] B. Bahar, A. R. Hobson, J. A. Kolde, and D. Zuckerbrod, “Ultra-thin integral composite membrane,” US5547551 A, 20-Aug-1996.
- [35] B. Bahar, A. R. Hobson, and J. A. Kolde, “Integral composite membrane,” US5599614 A, 04-Feb-1997.
- [36] J. Gasa, H. Wang, R. DeSousa, and K. Tasaki, “Fundamental Characterization of Fullerenes and Their Applications for Proton-Conducting Materials in PEMFC,” in *ECS Transactions*, 2007, vol. 11, no. 1, pp. 131–141.
- [37] Y. Devrim, S. Erkan, N. Baç, and I. Eroglu, “Nafion/titanium silicon oxide nanocomposite membranes for PEM fuel cells,” *Int. J. Energy Res.*, vol. 37, no. 5, pp.435–442, Apr. 2013.

[38] S. Y. Chen, C. C. Han, C. H. Tsai, J. Huang, and Y. W. Chen-Yang, “Effect of morphological properties of ionic liquid-templated mesoporous anatase TiO₂ on performance of PEMFC with Nafion/TiO₂ composite membrane at elevated temperature and low relative humidity,” *J. Power Sources*, vol. 171, no. 2, pp. 363–372, Sep. 2007.

[39] N. H. Jalani, K. Dunn, and R. Datta, “Synthesis and characterization of Nafion®-MO₂ (M=Zr, Si, Ti) nanocomposite membranes for higher temperature PEM fuel cells,” *Electrochim. Acta*, vol. 51, no. 3, pp. 553–560, Oct. 2005.

[40] K. Kaneko, Y. Takeoka, M. Rikukawa, and K. Sanui, “FUEL CELL PERFORMANCE USING PROTON CONDUCTING POLYMERS BASED ON HYDROCARBON POLYMERS (II),” in *Abs. 189, 204th Meeting*, 2003.

[41] “Wikipedia - Fuel cell vehicle.” 2023.
https://en.wikipedia.org/wiki/Fuel_cell. Accessed 26 Dec 2023

[42] “2023 Toyota Mirai Hydrogen Fuel Cell Electric Vehicle | The Future of Everyday.” [Online]. Available: <https://www.toyota.com/mirai/fcv.html>. Accessed 27 Dec 2023

[43] Anna Hecht, “How rising car prices can hurt the average American,” Cnbc. Oct 2019, [Online]. Available: <https://www.cnbc.com/2019/10/22/car-prices-are-rapidly-increasing-heres-why-thats-bad-for-americans.html>. Accessed 27 Dec 2023

- [44] Mammar, K.; Chaker, A. Neural Network Based Modeling of PEM fuel cell and Controller Synthesis of a stand-alone system for residential. *Int. J. Comput. Sci.* 2012, 9, 13–15.
- [45].Yu, X.; Starke, M.; Tolbert, L.; Ozpineci, B. Fuel cell power conditioning for electric power applications: A summary. *IET Electr. Power Appl.* 2007, 1, 643.
- [46].Ansari, S.A.; Khalid,M.; Kamal, K.; Abdul Hussain Ratlamwala, T.; Hussain, G.; Alkahtani, M. Modeling and Simulation of a Proton Exchange Membrane Fuel Cell Alongside a Waste Heat Recovery System Based on the Organic Rankine Cycle in MATLAB/SIMULINK Environment. *Sustainability* 2021, 13, 1218.
- [47] E. Eker, I. Taymaz, “Akış kanalı genişliğinin pem tipi yakıt hücresi performansına etkisinin incelenmesi,”*Sakarya University Fen Bilimleri Dergisi*, 2013.
- [48].Wang X-D, Duan Y-Y, Yan W-M. Novel serpentine-baffle flow field design for proton exchange membrane fuel cells. *Journal of Power Source* 2007; 173:210-21
- [49].Liu, H, Li, P, Wang, K. Optimization of PEM fuel cell flow channel dimensions- Mathematic modeling analysis and experimental verification. *International Journal of Hydrogen Energy* 2013; 38: 9835–9846

- [50] Mohammad, H.A.; Behzad, R. Numerical investigation of flow field configuration and contact resistance for PEM fuel cell. *Renew. Energy* 2008, *33*, 1775–1783.
- [51].Khazaei, I, Ghazikhani, M & Mohammadiun, M, 'Experimental and thermodynamic investigation of a triangular channel geometry PEM fuel cell at different operating conditions', *Scientia Iranica*, vol. 19, no. 3, pp. 585-593, 2012.
- [52].Carcadea, E, Ismail, MS, Ingham, DB, Patularu, L, Schitea, D, Marinoiu, A, Ebrasu, DI, Mocanu, D, Varlam, M. Effects of geometrical dimensions of flow channels of a large-active-area PEM fuel cell: A CFD study. *International Journal of Hydrogen Energy* 2021; 46(25): 13572-13582
- [53] Um, S.; Wang, C.Y. Three-dimensional analysis of transport and electrochemical reactions in polymer electrolyte fuel cells. *J. Power Sources* 2004, *125*, 40–51.
- [54].Hashemi, F, Rowshanzamir, S & Rezakazemi, M, “CFD simulation of PEM fuel cell performance: effect of straight and serpentine flow fields,” *Mathematical and Computer Modelling*, vol. 55, no. 3, pp. 1540-1557, 2014.
- [55]. Zeng, X.; Ge, Y.; Shen, J.; Zeng, L.; Liu, Z.; Liu, W. The optimization of channels for a proton exchange membrane fuel cell applying genetic algorithm. *Int. J. Heat Mass Transf.* 2017, *105*, 81–89.
- [56]. Yoon, Y.-G.; Lee, W.-Y.; Park, G.-G.; Yang, T.-H.; Kim, C.S. Effects of channel and rib widths of flow field plates on the performance of a PEMFC. *Int. J. Hydrogen Energy* **2005**, *30*, 1363–1366.

- [57] A.D. Santamaria, N.J. Cooper, M.K. Becton, J.W. Park, Effect of channel length on interdigitated flow-field PEMFC performance: A computational and experimental study, *Int. J. Hydrogen Energy* 38 (36) (2013) 16253–16263.
- [58]. Yan, W.-M.; Mei, S.-C.; Soong, C.-Y.; Liu, Z.-S.; Song, D. Experimental study on the performance of PEM fuel cells with interdigitated flow channels. *J. Power Source* 2006, 160, 116–122.
- [59]. Atul Kumar, Ramana Reddy. G, Effect of flow channel dimensions and shape in the flow field distributor on the performance of polymer electrolyte membrane fuel cells, *J. Power Sources*, 113(2003) pp.11-18.
- [60].Jaruwasupant, N & Khunatorn, Y, “Effects of difference flow channel designs on Proton Exchange Membrane Fuel Cell using 3-D Model,” *Energy procedia*, vol. 9, pp. 326-337, 2011.
- [61]. Wang, X.-D.; Huang, Y.-X.; Cheng, C.-H.; Jang, J.-Y.; Lee, D.-J.; Yan, W.-M.; Su, A. An inverse geometry design problem for optimization of single serpentine flow field of PEM fuel cell. *Int. J. Hydrogen Energy* 2010, 35, 4247–4257.
- [62].Wan,Z.;Quan,W.;Yang,C.;Yan,H.;Chen,X.;Huang,T.;Wang,X.D.;Chan, S. Optimal design of a novel M-like channel in bipolar plates of proton exchange membrane fuel cell based on minimum entropy generation. *Energy Convers. Manag.* 2020, 205, 112386.
- [63]. Tüber, K.; Oedegaard, A.; Hermann, M.;Hebling, C. Investigation of fractal flow fields in portable proton exchange membrane and direct methanol fuel cells. *J. Power Source* **2004**, 131, 175–181.

- [64]. Chowdhury, M.Z.; Akansu, Y.E. Novel convergent-divergent serpentine flow fields effect on PEM fuel cell performance. *Int. J. Hydrogen Energy* **2017**, *42*, 25686–25694.
- [65]. Ahmed, D.H & Sung, HJ, “Effects of channel geometrical configuration and shoulder width on PEMFC performance at high current density,” *Journal of Power Sources*, vol. 162, no. 1, pp. 327-339, 2006.
- [66]. Seyhan, M.; Akansu, Y.E.; Murat, M.; Korkmaz, Y.; Akansu, S.O. Performance prediction of PEM fuel cell with wavy serpentine flow channel by using artificial neural network. *Int. J. Hydrogen Energy* **2017**, *42*, 25619–25629.
- [67]. Roshandel, R.; Arbabi, F.; Moghaddam, G.K. Simulation of an innovative flow-field design based on a bio inspired pattern for PEM fuel cells. *Renew. Energy* **2012**, *41*, 86–95.
- [68]. Lorenzini-Gutierrez, D.; Hernandez-Guerrero, A.; Ramos-Alvarado, B.; Perez-Raya, I.; Alatorre-Ordaz, A. Performance analysis of a proton exchange membrane fuel cell using tree-shaped designs for flow distribution. *Int. J. Hydrogen Energy* **2013**, *38*, 14750–14763.
- [69]. Liu, S.; Chen, T.; Xie, Y.; Zhang, J.; Wu, C. Numerical simulation and experimental study on the effect of symmetric and asymmetric bionic flow channels on PEMFC performance under gravity. *Int. J. Hydrogen Energy* **2019**, *44*, 29618–29630.

- [70]. Liu, H.; Tan, J.; Cheng, L.; Yang, W. Enhanced water removal performance of a slope turn in the serpentine flow channel for proton exchange membrane fuel cells. *Energy Convers. Manag.* **2018**, *176*, 227–235.
- [71]. Fontana, É.; Mancusi, E.; da Silva, A.; Mariani, V.C.; de Souza, A.A.U.; de Souza, S.M.G.U. Study of the effects of flow channel with non-uniform cross-sectional area on PEMFC species and heat transfer. *Int. J. Heat Mass Transf.* **2011**, *54*, 4462–4472
- [72]. Cai, G.; Liang, Y.; Liu, Z.; Liu, W. Design and optimization of bio-inspired wave-like channel for a PEM fuel cell applying genetic algorithm. *Energy* **2020**, *192*, 116670.
- [73]. .M.H. Akbari, B. Rismanchi, Numerical investigation of flow field configuration and contact resistance for PEM fuel cell performance, *Renew. Energy*. 33 (2008) 1775–1783. doi: 10.1016/j.renene.2007.10.009.
- [74]. Yousef, V.; Kurosh, S. Numerical investigation of a novel compound flow-field for PEMFC performance improvement. *Int. J. Hydrog. Energy* 2015, *40*, 15032–15039.
- [75]. Liu, H, Li, P, Juarez-Robles, D, Wang, K & Hernandez-Guerrero, A, “Experimental study and comparison of various designs of gas flow fields to PEM fuel cells and cell stack performance,” *Frontiers in Energy Research*, vol. 2, no. 2. 2014.
- [76]. Iranzo, A, Muñoz, M, Rosa, F & Pino, J, “Numerical model for the performance prediction of a PEM fuel cell. Model results and experimental

validation,” *International Journal of Hydrogen Energy*, vol. 35, no. 20, pp. 11533-11550, 2010.

[77]. T. Geneve, J. Regnier, C. Turpin, Fuel cell flooding diagnosis based on time-constant spectrum analysis, *Int. J. Hydrogen Energy* 41 (1) (2015) 516–523.

[78]. S. Shimpalee, S. Greenway, J.W.V. Zee, The impact of channel path length on PEMFC flow-field design, *J. Power Sources* 160 (1) (2006) 398–406.

[79]. N.J. Cooper, T. Smith, A.D. Santamaria, Experimental optimization of parallel and interdigitated PEMFC flow field flow field geometry, *Int. J. Hydrogen Energy* 41 (2) (2015) 1213–1223.

[80]. Santarelli, M & Torchio, M, “Experimental analysis of the effects of the operating variables on the performance of a single PEMFC”, *Energy Conversion and Management*, vol. 48, no. 1, pp. 40-51, 2007.

[81]. V. Velisala, G.N. Srinivasulu, Numerical Simulation and Experimental Comparison of Single, Double and Triple Serpentine Flow Channel Configuration on Performance of a PEM Fuel Cell, *Arab. J. Sci. Eng.* 43 (2018) 1225–1234. doi:10.1007/s13369-017-28137.

[82] J. Mahmoudimehr, A. Daryadel, “Influences of feeding conditions and objective function on the optimal design of gas flow channel of a PEM fuel cell”. *International Journal of Hydrogen Energy*, 2017.

- [83].Freire, LS, Antolini, E, Linardi, M, Santiago, EI & Passos, RR, “Influence of operational parameters on the performance of PEMFCs with serpentine flow field channels having different (rectangular and trapezoidal) cross-section shape', International Journal of Hydrogen Energy, vol. 39, no. 23, pp. 12052-12060, 2014.
- [84].Amirinejad, M, Rowshanzamir, S & Eikani, MH, “Effects of operating parameters on performance of a proton exchange membrane fuel cell,” Journal of Power Sources, vol. 161, no. 2, pp. 872-875, 2006.
- [85]. Vivek R, Muthukumar M (2018) Performance Improvement of Proton Exchange Membrane Fuel Cell. *Innov Ener Res* 7: 203.
- [86]. Wawdee P, et al., Water transport in a PEM fuel cell with slanted channel flow field plates, International Journal of Hydrogen Energy (2015)
- [87]. A. Arvay, J. French, J.-C. Wang, X. Peng, A. Kannan, *Open Electrochem. J.* **2015**, 6, 1–9.